PhD Thesis

CFD-Simulation of High Performance
2-Stroke Engines Applying
Multidimensional Coupling Methodologies

by

Dalibor JAJČEVIĆ

Institute for Internal Combustion Engines
and Thermodynamics
Graz University of Technology

submitted to

Graz University of Technology

for receiving a

doctor technicae

Graz, February 2011

1st Evaluator:
Ao.Univ.-Prof. Dipl.-Ing. Dr.techn. Raimund A. ALMBAUER
Graz University of Technology

2nd Evaluator:
Prof BSc MSAE PhD Roy DOUGLAS
Queen's University Belfast

Statutory declaration

I declare that I have authored this thesis independently, that I have not used other than the declared sources/resources, and that I have explicitly marked all material which has been quoted either literally or by content from the used sources.

Dalibor Jajčević

Graz, February 2011

"Most people do things because they have to …

…those that get ahead do things because they don't have to …"

– Anonymous

Acknowledgements

Abstract

Computational Fluid Dynamics has become an essential tool in the design and development process of IC-engines. Due to increasing computer hardware performances and steady decreasing costs it is to expect that simulation technology becomes an unavoidable tool for the analysis of many technical problems. In the development process of an engine the simulation results are required in short calculation time, so that the application of the 3D simulation is still limited - primary due to a high effort in the pre-processing step and a long computational time. The goal of this PhD thesis is to develop an efficient 3D CFD simulation method applicable in the development process of a 2-cylinder 2-stroke high performance engine. The method includes an especially developed work flow as well as a new type of boundary condition, which allows a reduction of the computational domain with a negligible influence on the simulation results.

In order to get efficient simulation results in a short computational time, two different ways can be employed; first "Simulation Strategy" and second "Computational Domain Reduction". In this work, the simulation strategy is developed in order to exploit resources already available in conventional CFD codes, such as meshing, dynamic mesh, and adjustment of the start conditions. The second method (Computational Domain Reduction) is based on the simulation of only the most important areas, where domains of less importance can be replaced by corresponding boundary conditions or simple models. This PhD thesis treats the basic methods and the solutions, such as the multidimensional coupling methodology and a new type of the cyclic/periodic boundary condition and their application in a real world 2-cylinder 2-stroke engine CFD simulation.

Kurzfassung

Im Lauf der letzten Jahre sind Computational Fluid Dynamics (CFD) Simulationen zu einem wichtigen Werkzeug im Forschungs- und Entwicklungsprozess von Verbrennungskraftmaschinen geworden. In Zukunft werden die Rechnenkapazitäten moderner Computer weiterhin steigen, während die Kosten signifikant abnehmen. Aus diesem Grund ist zu erwarten, dass Simulationstechniken verstärkt eingesetzt werden, um verschiedenste technische Probleme zu lösen. Im Entwicklungsprozess von Verbrennungskraftmaschinen werden kurze Berechnungszeiten gefordert, sodass die Anwendung von kompletten 3D CFD Simulationen noch immer eingeschränkt ist. Die Einschränkung ergibt sich aus dem aufwändigen Pre-processing und den langen Berechnungszeiten. Das Ziel dieser Dissertation ist die Entwicklung einer effizienten 3D CFD Simulationsmethodik für die Entwicklung eines 2 Zylinder 2-Takt Hochleistungsmotors. Die Simulationsmethodik beinhaltet neben einer speziellen Vorgehensweise auch eine neu entwickelte Randbedingung, die eine Reduktion des Berechnungsgebiets mit vernachlässigbarem Einfluss auf die Ergebnisgenauigkeit ermöglicht.

Um gute Simulationsergebnisse bei gleichzeitig kurzen Rechenzeiten zu bekommen stehen zwei Ansätze zur Verfügung: Der erste Ansatz betrifft die Simulationsstrategie, wo konventionelle Methoden (Netzgenerierung, bewegte Netze, Startbedingungen) verwendet werden. Der zweite Ansatz betrifft die Simulation eines reduzierten Berechnungsgebiets. Dabei werden Bereiche von untergeordneter Bedeutung durch entsprechende Randbedingungen oder einfache Modelle ersetzt. Diese Dissertation behandelt grundlegende Methoden und Lösungen wie beispielsweise multidimensionale Kopplungsmethoden und zyklische/periodische Randbedingung, die in der Simulation eines 2 Zylinder 2-Takt Motors angewendet werden.

Contents

List of Publications

The papers included in this PhD thesis are:

I. Jajcevic D., Almbauer R.A., Schmidt S. P., Glinser K., Fitl M., "CFD study of spray design for a GDI high performance 2-stroke engine", SAE Paper 2010-32-0014/20109014, 2010

II. Jajcevic D., Almbauer R.A., Schmidt S. P., Glinser K., "CFD Simulation of a Real World High-Performance Two Stroke Engine with Use of a Multidimensional Coupling Methodology", SAE Paper 2008-32-0042/20084742, 2008

III. Jajcevic D., Almbauer A., Lang W., Schmidt S., "A cyclic boundary condition for time delayed technical problems and its application for IC-engine simulation", Progress in Computational Fluid Dynamics, currently in print

IV. Jajcevic D., Almbauer R.A., Schmidt S. P., Glinser K., Fitl M., "Exhaust system simulation of a 2-cylinder 2-stroke engine including heat transfer effects", SAE Paper 2010-32-0035/20109035, 2010

V. Jajcevic D., Almbauer R.A., Schmidt S. P., Glinser K., Fitl M., "Reed valve CFD simulation of a 2-stroke engine using a 2D model including the complete engine geometry", SAE Paper 2010-32-0015, included in SAE International Journal of Engines, Vol. 3, No. 2, Pages 448-461, 2010

The author of this thesis is also the <u>first and lead</u> author of all papers this PhD thesis is based on.

Reference papers having emanated from this work are listed below.

1. Jajcevic D., Almbauer R.A., Schmidt S. P., Glinser K., "Symmetry and Time Delayed Boundary Condition for CFD Simulation and its Application in a Two-Cylinder Two-Stroke Engine", SAE Paper 2009-32-0046/20097046, 2009

2. Jajcevic D., Almbauer R.A., Schmidt S. P., Glinser K., "Simulation of Scavenging Process, Internal Mixture Preparation, and Combustion of a Gasoline Direct Injection Two-Cylinder Two-Stroke Engine", SAE Paper 2009-32-0046/20097046, 2009

3. Jajcevic D., Almbauer R.A., Schmidt S. P., Glinser K., "Simulation Strategy and Analysis of a Two-Cylinder Two Stroke Engine Using CFD Code Fluent", European Automotive Simulation Conference (EASC), 2009

4. Jajcevic D., Almbauer R.A., Schmidt S. P., "CFD Simulation of a High Performance Two Stroke Engine and Reduction of Computational Time Using Multidimensional Coupling Methodology", Int. Conf. on Accomplishments in Electrical and Mechanical Engineering and Information Technology, 2009

5. Lang W., Almbauer A., Jajcevic D., "Usage and validation of a fluid structure interaction methodology for the study of different suction valve parameters of a hermetic reciprocating compressor", Int. Journal of Multiphysics, Vol. 4, Nr. 1, 2010

6. Abart M., Schmidt S., Schoegl O., Trattner A., Kirchberger R., Eichlseder H., Jajcevic D., "Basic Investigations on the Prediction of Spray-Wall and Spray-Fluid Interaction for a GDI Combustion Process", SAE Paper 2010-32-0030/20109030, 2010

7. Schmidt, S., Abart, M., Schögl, O., Jajcevic, D., Trattner, A., Kirchberger, R.; Eichlseder, H., "Simulation and experimental investigations of a direct-injection combustion system for high speed - high performance engines", SAE Paper 2009-32-0045/20097045, 2009

Nomenclature

a	Accuracy
A, A_p, A_{flow}, A_{theo}	Area, Jacobian matrix, surface particle area, flow area, theoretical area
b_e	Specific fuel consumption
b_{width}	width of valve
c, c_{area}, $c_{sideflow}$	Speed of sound, correction factor, side flow coefficient
C, $C_{1\varepsilon}$, $C_{2\varepsilon}$, $C_{3\varepsilon}$	Model constants
C_D	Drag coefficient
$C_{i,s}$, $C_{i,\infty}$	Vapor concentration at the droplet surface and in the bulk gas
c_p, c_{p_p}, c_{p_g}	Heat capacity at constant pressure, particle heat capacity, gas heat capycity
c_v	Heat capacity at constant volume
c_q,	Flow coefficient
d_p	Particle diameter
E	Total energy
E_{imp}	Impact energy
$\overrightarrow{F_c}$, $\overrightarrow{F_v}$	Vector of convective fluxes, vector of viscous (diffusive) fluxes
F_D	Drag force
f_i	Mass force
F_x	Additional forces in the particle force balance
G_b	Production of turbulence kinetic energy due to buoyancy
g_i, g_x	Gravitational vector
H	Total enthalpy
h_0	Film thickness
h_{CHTC}	Convective heat transfer coefficient
h_{fg}	Latent heat
H_{pyrol}, $H_{lat_{ref}}$	Heat of pyrolysis as volatiles, latent heat at reference condition
H_u	Fuel calorific value
$h_{valvelift(\Delta p)}$	Height of valve lift in dependent on the pressure difference
Ma	Mach number

m_{air}	Air mass remaining from the previous cycle
m_E	Air mass
m_{EG}	Mass of exhaust gas
m_{exh}	Mass of rest exhaust gas
m_F	Fuel mass
m_{fuel}	Fuel mass
m_{IFM}	Injected fuel mass
k	turbulent kinetic energy
k_c	Mass transfer coefficient
L	Length
L_{st}	Stoichiometric air demand
$\dot{m}_p , m_{p_{in}} , m_{p_{out}}$	Mass flow rate of the particles, at inlet, at outlet
m_{RG}	Rest gas mass
$m_{th,DR}$	Reference air mass required to fill the swept cylinder volume
$m_{th,SR}$	Reference air mass required to fill the cylinder volume
m_{TR}	Trapped air mass
M_i	Indicated toraque, molecular weight
$n , \vec{n}$	Engine speed/rotation rate, normal vector
N	Number
N_i	Molar vapor flux
Nu	Nusselt number
p	Pressure
p_{at}	Atmospheric pressure
p_e	Mean effective pressure
p_i	Indicated Mean Effective Pressure
P_i	Indicated power
p_{in} , p_{out}	Pressure inside, outside
p_m	Mean pressure
P_k	Production of turbulence kinetic energy
Pr	Prandtl number
Pr_t	Turbulent Prandtl number

p_{sat}	Saturate vapor pressure
$q, \dot{q}_h$	Heat flux
$\vec{Q}$	Source vector
r	Radius, refinement or coarsening ratio
R	Gas constant
R_{at}	Gas constant of atmospheric condition
$\vec{R}_{CV}$	Residual of an individual control volume
Re	Reynolds number
Re_p	Relative Reynolds number of the particle
$\overline{R}_x$	Rotation matrix
s	Second
S, S_ϕ	Surface, mean rate of strain tensor
Sc	Schmidt number
S_{ij}	Strain-rate tensor
$S_c, S_M, S_E, S_{\phi_k}$	Source term of mass, momentum, energy, species k
S_k, S_ε	Source term of turbulent kinetic energy and dissipation
Sh	Sherwood number
t	Time
T, T_{bp}, T_{ref}	Temperature, boiling point temperature, reference temperature
$T_{at}, T_{p_{in}}$	Atmospheric temperature, particle temperature on the cell entry
T_∞, T_R, T_p	Local temperature of the continuous phase, radiation, particle temperature
$\vec{U}$	Vector of conservative variables
Q_F	Heat rate
u, u_i, u_p	Velocity, velocity components, particle velocity
V	Velocity normal to surface
V_c	Cylinder volume at top dead center
V_{CC}	Crankcase volume
V_{cyl}	Cylinder volume
V_{Exh}	Exhaust system volume
V_h	Swept volume
v_p, v_r, v_w	Particele velocity, relative velocity, wall velocity

W	Work
W_e	Effective work
We	Weber number
X_i	Local bulk mole fraction of species "i"
Y_{Fuel}	Mass fraction of fuel species
Y_M	Contribution of the fluctuating dilatation in compressible turbulence

Greek

α	Angle
β	Thermal expansion coefficient, parameter
γ	Heat capacity ratio
Γ_k	Diffusion coefficient
δ_{bl}	Boundary layer thickness
ε	Geometric compression ratio, dissipation rate
ε'	Trapped compression ratio
ε_p	Particle emissivity
η	Kolmogorov length scale
η_e	Effective engine efficiency
η_i	Indicated engine efficiency
η_m	Mechanical engine efficiency
λ	Thermal conductivity
λ_l	Laminar thermal conductivity
λ_t	Turbulent thermal conductivity
λ_∞	Thermal conductivity of the continuous phase
Λ_c	Velocity
μ	Dynamic viscosity
μ_l	Laminar viscosity
μ_t	Eddy viscosity
ν	Kinematic viscosity
ρ	Density

ρ_{at}, ρ_{out}	Density at atmospheric condition, density outside
ρ_p	Particle density
σ	Stefan-Boltzmann constant, surface tension
$\sigma_k, \sigma_\varepsilon$	Model constant
π	Mathematical constant
τ	Kolmogorov time scale
τ_{ij}	Stress tensor
ϕ	Fluctuating components
ϕ_k	Arbitrary scalar
ω	Parameter
Ω	Finite control volume

Acronyms

0D	Zero dimensional
1D	One dimensional
3D	Three dimensional
ADI	Alternating Direction Implicit
AFR	Air/fuel ratio
AMG	Algebraic Multigrid
AUSM	Advection Upstream Splitting Method
BRP	Bombardier Recreational Products
CDL	Christian Doppler Labor
CE	Charging efficiency
CFD	Computational Fluid Dynamics
CFL	Courant-Friedrichs-Lewy
CUSP	Convective Upwind Split Pressure
DDM	Discrete Droplet Method
DES	Detached-Eddy Simulation
DNS	Direct Numerical Simulation
DPM	Discrete Phase Model

DR	Delivery ratio
EG	Exhaust gas
ENO	Essentially Non-Oscillatory
ER	Equivalence ratio
FD	fuel distribution
FDM	Finite difference method
FDS	Flux-difference splitting
FEM	Finite element method
FS	Fluctuation-splitting
FTE	Fuel trapping efficiency
FVM	Finite volume method
FVS	Flux-vector splitting
GDI	Gasoline direct injection
IC-engine	Internal Combustion Engine
IFM	Injected fuel mass
IMEP	Indicated Mean Effective Pressure
IRS	Implicit Residual Smoothing
LES	Large Eddy Simulation
LIF	Laser-Induced Fluorescence
LL	Low-load
LU-SGS	Lower-Upper Symmetric Gauss-Seidel
LU-SSOR	Lower-Upper Symmetric Successive Overrelaxation
MUSCL	Monotone Upstream-Centred Schemes for Conservation Laws
PISO	Pressure Implicit with Splitting of Operators
QUB	Queen's University Belfast
QUICK	Quadratic Upstream Interpolation for Convective Kinematics
RANS	Reynolds Averaged Navier Stokes
RAVE	Rotax Adjustable Variable Exhaust
RG	Rest gas
SDL	Subdivision level
SE	Scavenging efficiency

SIMPLE	Semi-Implicit Method for Pressure-Linked Equations
SOI	Start of the injection
SR	Scavenging ratio
TE	Trapping efficiency
TOI	Time of ignition
TVD	Total variation diminishing
UDF	User defined function
WOT	Wide Open Throttle

1   Introduction

Computational Fluid Dynamics (CFD) has become an essential tool in the design and development process of engineering devices. In the beginning, it was mostly limited to high-technology engineering fields, e.g. aeronautics and astronautics, but in the last decades it has become a widely used tool for the analysis of complex technical problems in many modern engineering applications. Computer modelling allows virtual prototyping of a technical system in order to evaluate the performance of a new design and/or new technologies. This technique is used in the industry in order to reduce the development and retrofitting time and therewith the product costs.

The steady improvement of numerical methods together with the increase of computer power allows the simulation of more and more complex technical problems even for large calculation domains. The considered problems may involve complicated geometry and physically complex phenomena such as turbulence, phase change, chemical reactions, etc. In the last decades, CFD has also become a state of the art tool for the development of internal combustion engines (IC-engines). It offers the successful assessment of new technologies, e.g. new fuel preparation methods, new combustion concepts and/or alternative fuels. Furthermore, it successfully supports the prototyping phase on the engine test bench. Additionally, these new technologies require high standards of knowledge which can be partly acquired with the use of CFD simulation.

Currently, different CFD software packages are in use, such as ANSYS Inc. FLUENT® and CFX®, AVL-Fire®, STAR-CD®, KIVA®, CONVERGE® CFD, OPENFOAM® etc. Some of them are especially developed for the simulation of IC-engines (e.g. AVL-Fire®) and therefore provide all required models and mesh tools. Other software packages, e.g. ANSYS Inc. FLUENT®, can be applied to a wide array of industrial applications and are developed with a general purpose.

In the application for IC-engine simulation, the CFD tool can be used for the investigation of many processes inside the engine, such as scavenging, fuel injection, mixture preparation, combustion, heat transfer etc. There are many advantages in applying CFD in the development process of a new engine. CFD is focused on the solution of the governing equations and presents a perfect possibility to study the influence of specific terms on the flow inside an IC-engine in a detailed way. These investigations can only be realized with computational research and modelling. In addition, CFD supplements experimental studies by providing an alternative low cost analysis tool. Furthermore, it reduces the developing time of engine components – compared to the experimental studies – and offers the ability to solve a wide range of complicated physical problems. These advantages are realized through the increasing computer hardware performance and its steadily decreasing costs. Furthermore, CFD has the capacity of simulating flow conditions that are difficult reproducible in experimental tests or are coupled with huge invest costs in the engine test bench equipment. Finally, CFD can provide more detailed, visualized, and completed information, compared to experimental investigations and increases the level of understanding the processes inside an IC-engine.

Over a hundred years IC-engines have been most commonly used in mobile vehicles (automobiles, trucks, motorcycles etc.) due to advantages of high power-to-weight ratios together

with excellent fuel energy density. Generally, almost all vehicles use fossil fuel and in a modern world, economy and life cannot be imagined without IC-engines. Furthermore, with the first revolution of an IC-engine, over hundred years ago, the new polluting era of our environment with exhaust gases arising from the engine combustion process began. Due to growing production numbers and markets, the air quality becomes more and more important.

The exhaust gases of an IC-engine are the product of fuel-oxygen reaction, but they are not only caused by the combustion process itself. Starting with the analysis of the scavenging process, the fuel injection and mixture preparation processes, and finally the combustion process, exhaust gas emissions can be successfully improved. For the analysis of all these processes, CFD simulation presents an alternative and suitable tool.

First analyses of the flow inside an IC-engine applying computer technique were carried out in the 1960s using zero dimensional (0D) and one dimensional (1D) codes. Benson et al. [1] presented a 1D code, which was developed for the analysis of wave propagation in a single cylinder 2-stroke engine in the year 1964. Similar examples were presented which compared simulation results with normal graphical methods. DeHaller [2], Jenny [3], and Seifer [4], should be also mentioned as important pioneers in the development of graphical and numerical methods. Since the introduction of digital computer technique in the engineering world, the computer codes have been based on the method of characteristics have been used as a tool in the development process of specific engine parts, such as the exhaust system and intake ducts. Furthermore, the codes developed by Benson et al. [1] at the University of Manchester Institute of Science and Technology and by Blair and Goulburn [5] at The Queen's University of Belfast were widely used by many automotive companies. All these codes were developed as 1D-codes, as 3D simulation was unfeasible at that time, due to low computer power. Today, the 1D code is still a good approach to assist the development process of engines, primarily due to today's very low computational effort and satisfying accurateness, because the flow inside an exhaust system or an intake duct is very often close to one dimensional.

In the course of the last two decades the rapid increase of computer power made 3D simulation also realizable in a realistic computational time. In comparison to a 1D simulation, the 3D simulation is still too slow to completely replace 1D simulation in engineering departments; especially if the simulation results are required in very short calculation time (e.g. one or two days). Anyway, in many cases, 3D simulation is necessary; for instance a problem with strong 3D effects, such as an in-cylinder flow of an IC-engine. These effects would be also difficult and expensive to obtain experimentally.

The issues of each 3D simulation, according to Pope [6], are accuracy, level of description, completeness, computational costs, usability, and the range of applicability. The first three points could only be matched by the concept "Direct Numerical Simulation" (DNS). This method provides a very accurate description of the flow and does not require any empirical model modification to be applicable from all cases. Nevertheless, the computational costs and the range of applicability make the DNS concept inapplicable for most engineering calculations. An alternative increasingly popular approach, the "Large Eddy Simulation" (LES), can be basically viewed as an extension of the DNS with a wider range of applicability, the fifth of the above mentioned issues. Basically, LES concept provides a high level of completeness, resolves the motion of only large scales, but its computational cost is still too high for engineering relevant simulations. The unsteady boundary conditions are difficult to define, see Steiner [7]. Nonetheless, the LES concept has already become a very powerful tool in scientific research. For the relevant flows in industrial problems, the Reynolds Averaged Navier

Stokes (RANS) methods, based on the decomposition of the instantaneous flow variable into a time averaged and a fluctuating part, has been widely used until now. For Basara [8] the LES concept is only applicable for some genuine niches inaccessible for RANS methods. It seams to be obvious that the LES concept is too demanding considering mesh resolution, especially close to the wall. Furthermore, the author sees the RANS method as a main "tool" for solving practical industrial applications for a long time. Although the RANS methods are not computationally expensive, compared to the alterative DNS and LES methods, the 3D simulation still consumes a lot of computational resources, in comparison to 1D simulation. It is still very difficult to apply it in the development process of a new engine, where the results are required in a short calculation time including several variants. But in the engine concept phase, the 3D together with the 1D simulation is a very powerful tool. The specification of boundary conditions often represents a further open issue for each above mentioned concept and simulation. Previous 1D calculation results or measurement data are usually used as boundary conditions for the 3D simulation and the considered domain will be reduced as well as the time of calculation.

1.1   Motivation

The key for a successful application of CFD in the development process of an engine are accurate and complete boundary conditions. This allows the simulation of an isolated domain of importance for an engineer, concurrently with a negligible influence on the simulation accuracy. This strategy is already state of the art in the case of a 4 stroke engine simulation, see Goryntsev et al. [9], Rebhan et al. [10], Jajcevic [11], Korman [12], Trattner [13] etc. as well as Merker et al. [14] and Pischinger et al. [15], where the intake and exhaust systems are replaced by corresponding cyclic constant boundary conditions. In the case of a strong interaction between the IC-engine periphery parts and the cylinder volume, e.g. in 2-stroke engines, this strategy can cause a decrease of the simulation accuracy.

In the 1990s, the 3D 2-stroke engine simulation has become very popular, primarily due to growing computational power and availability of commercial 3D CFD codes on the market, which provide specialized tools for the IC-engine simulation. Authors, such as Raghunathan and Kenny [16], Cunningham et al. [17], and Corcione et al. [18], reduced the 2-stroke engine geometry to the cylinder volume and a short part of the intake and exhaust pipes. They employed transient boundary conditions obtained from measurements and/or previous 1D simulation, which were implemented via cyclic constant profiles.

In the early 2000s, the 3D simulation has also become applicable for bigger calculation domains; so that Meister [19], Kirchberger [20], and Schmidt [21] expand the considered domain of interest taking into account the exhaust system and the crankcase volume. This improved the simulation results considering the exhaust gas dynamic behavior calculation. Big calculation domains, which include the simulation of physically complex phenomena, increase the calculation time non-linearly, so the authors concluded, that the complete 3D simulation is improper for the development process of an engine. Primarily, due to the high pre-processing effort (mesh rebuild-up demand for new geometries, e.g. for variant studies) and a long computational time.

In order to reduce the computational effort and simultaneously to include the effect of engine periphery parts on the in-cylinder flow simulation, Chiavola [22] and Chiatti and Chiavola [23], used a multidimensional simulation method. It is based on the simultaneous use of a 1D model, which is applied for a good description of the phenomena inside the ducts, coupled with the 3D CFD code used for the domain of high interest. This technique can also be under-

stood as a method, where the domain of high interest and/or with a complex flow situation is solved 3 dimensionally and the 1D code is applied as a boundary condition exploiting the 1D code advantages, such as fast computation, high level of flexibility and adaptability of the IC-engine models etc. Riegler and Bargende [24] used this strategy for the simulation of a 4-stroke 8-cylinders IC-engine intake system with exhaust gas recirculation. In this case, the domain of interest was only the intake system, which was modeled with a 3D code, and the rest of engine geometry including all 8-cylinders and the complete exhaust system were replaced by a 1D code. Bozza et al. [25] also applied the multidimensional simulation method for a 2-stroke engine simulation; the cylinder volume was solved 3 dimensionally, including small parts of exhaust and intake pipes; the rest of the engine domains were calculated with a 1D code. Further, Zeng et al. [26] used this strategy for the simulation of a 2-cylinder 2-stroke engine considering the gas dynamic behavior of both cylinders in order to optimize the engine performance.

In all of the above mentioned cases, the authors clearly show that an accurate and fast CFD simulation, applicable in the development process, requires correct boundary conditions, which can successfully replace the IC-engine domains of smaller importance and therewith reduce the calculation time. The boundary conditions and their accuracy are and always will be an important issue for every CFD simulation.

1.2 Project description

The research work of Module 2 of the Christian Doppler Laboratory (CDL) for "Thermodynamics of Reciprocating Engines" was supported by the Christian Doppler Research Association (CDG) and BRP-Powertrain company. The CDG is named after the Austrian physicist and mathematician, Christian Andreas Doppler (1803-1853), famous for his discovery of the "Doppler Effect". It supports application-oriented fundamental research and enables member companies to have a direct access to new knowledge (source: http://www.cdg.ac.at/).

BRP-Powertrain, a subsidiary of Bombardier Recreational Products Inc. (BRP), is an international market leader in the development and production of 4-stroke and advanced 2-stroke ROTAX engines for motorized recreational products, like Ski-Doos and Lynx snowmobiles, Can-Am ATVs, Sea-Doo personal watercraft and sport boats, scooters, motorcycles, karts and aircrafts (source: http://www.rotax.com/).

Module 2 was established in the year 2004, together with the establishment of the CDL for "Thermodynamics of Reciprocating Engines". The core research work of Module 2, oriented on the requirements of the industry partner, was based on the methodology development for 2-stoke engine simulations in the development process. This methodology includes strategy and work flow as well as simulation tools and boundary conditions, which can accelerate the IC-engine simulation without a reduction of the level of simulation accuracy. Together with the industry partner, the developed simulation tool was successfully used in development process of a 2-cylinder 2-storke engine with fuel direct injection.

1.3 Starting basis

The basic investigation of a multidimensional coupling method is presented in Rothbauer [27]. The author investigated a coupling method between two completely separated 3D domains and validated this for some simple cases, such as a pipe-pipe, a pipe-volume and a cylinder-pipe coupling. The reference values for the validation are taken from a conventional simulation, where the above mentioned domains are already coupled together. In the valida-

tion case of a coupling between a moving cylinder and a pipe, the author used a conventional arbitrary interface technique as reference coupling method. In the case of a pipe-pipe coupling, an excellent agreement between the simulation results is shown. In other test cases, some differences between the results are visible. The author explained these deviations by the fact that in the case of a non-conformal interface coupling an exact flow area calculation is missing, e.g. coupling between a moving cylinder and an exhaust pipe, and that for an accurate coupling a further development of geometry code is required. However, a basic coupling technique was developed and validated for some simple cases and according to Rothbauer [27] the developed method could be used for the coupling between 3D-3D, 1D-3D, and 0D-3D domains. The last two coupling methods (1D-3D and 0D-3D) are only theoretically investigated and presented, so that for the application in the real world engine simulation an additional validation procedure and further code upgrades are needed. Nevertheless, these upgrades can be summarized as follows, also see Rothbauer [27]:

- An exact flow area calculation

- Upgrade for multiple coupling options

- Geometry code update for independency of cell types

- Possibility for the coupling between two faces instead of two cell threads

- Investigation and validation of 0D-3D and 1D-3D coupling methods

- Upgrade for multiprocessor ability

After these code upgrades, the developed multidimensional coupling method can be employed for the real world simulation of a 2-stoke engine and an evaluation of the used simulation strategy can be carried out as well.

1.4   Goal and working hypothesis

2-stroke internal combustion engines are widespread in market segments, in which a high power to weight ratio is essential, e.g. chainsaws, snowmobiles etc. But their disadvantages, especially high emissions and bad fuel economy, require further investigations and developments to reduce these negative effects. As these disadvantages are caused by mixture formation and the scavenging process, they can be analyzed with CFD simulation.

Due to 3D effects during the scavenging process inside the cylinder volume and a strong dependency of the results on the engine geometry, the application of a 0D/1D code is limited and a 3D CFD simulation of the in-cylinder process is required. The performance of a 2-stroke engine is extremely dependent on the design of the engine periphery parts (such as exhaust system, crankcase, reed valve etc.). For an efficient 2-stoke engine simulation these engine parts and their effects have to be included in the simulation as well as the second cylinder in the case of a 2-cylinder engine. Growing calculation domains increase the calculation time non-linearly and make them impracticable in the daily work of an engineer in the engine development process. The reduction of simulation time can be realized by the reduction of the calculation domain and/or by the simplification of the technical problem. The quality of the results depends on the completeness of the physical phenomena simulation. Potentially, sim-

plifications lead to incorrect results as well as the numerical evaluation of all relevant phenomena is usually the main focus to gain a better understanding of the investigated technical problem.

The goal of this work is to develop a simulation strategy which reduces the computational time in such a way that the 3D CFD simulation of a 2-stroke engine becomes applicable in the development process. The strategy includes a special developed work flow as well as a new type of boundary condition, which allows a computational domain reduction with a negligible influence on the simulation results and contributes to the reduction of computational time of an industrial relevant IC-engine simulation.

1.5 Procedure

Generally, two different ways, which are presented in Table 1, can be applied for the reduction of computational time; first "Simulation Strategy" and second "Computational Domain Reduction".

Table 1: Basic methods for the reduction of computational time

Simulation Strategy	Computational Domain Reduction
• Meshing strategy	• Boundary condition from previous 0D/1D simulation
• Case setup and start condition	• Multidimensional simulation
• Exploitation of used models	• Cyclic/periodic boundary conditions
• Moving mesh strategy	

A simulation strategy basically depends on the technical problem. The presented method "Simulation Strategy" has been especially developed for a 2-cylinder 2-stroke engine simulation, but some of its core objectives might also be applicable for 4-stroke IC-engine simulations as well as in combination with the second method "Computational Domain Reduction".

A CFD simulation starts with the grid build-up, followed by the case setup and the initialization of start conditions. Depending on the meshing techniques (e.g. hybrid mesh, cell type, number of generated 3D cells etc.) and the initialized start condition, the number of iterations and therewith the time of calculation can be influenced. Besides, a start with a simple simulation and a stepwise increasing of complexity leads to a faster convergence and a reduced number of calculated revolutions until cyclic steady conditions. The moving mesh technique is a powerful tool and is usually used in CFD simulations of piston and valve movement. This technique is able to take the change of the engine geometry during the simulation into account, whereas a mesh rebuild-up and case reset process is obsolete. So this advantage can be successfully applied in the engine design optimization.

The second method "Computational Domain Reduction" is only based on the simulation of the important domain, whereas the rest can be replaced by corresponding boundary conditions. The method can be divided into three subgroups, the boundary condition from a previous simulation, the multidimensional simulation, and the cyclic/periodic boundary condition,

which differ in the way how variables are provided at the boundary face. In the first one, the domain is replaced by a cyclic constant profile, so that the data exchange between the domains is missing. The second one, multidimensional simulation, allows a data exchange between a 3D and 0D/1D domain; both regions are still included in the simulation, in fact with different codes. Finally, the data for the cyclic/periodic boundary conditions are deduced from the 3D simulation itself and therefore do not need to come from another software or measurements.

In order to reduce the computational time and to make the CFD simulation appropriate for the development process of a 2-stroke engine, the above presented simulation techniques were evaluated. Starting with a conventional simulation, applying the presented simulation strategy, the calculation of a 2-cylinder 2-stroke engine including both cylinders was carried out. After this, a multidimensional coupling methodology, based on the work of Rothbauer [27], was advanced and applied for the simulation of a one cylinder 2-stroke engine. Finally, in order to make simulation applicable in the development process for 3D CFD 2-cylinder 2-stroke engines, a new type of cyclic boundary condition for time delayed technical problems was developed and investigated in a real world engine simulation.

2   Theoretical background

The theoretical background used for this research work can be split into two groups, the 2-stroke engine as test case and computational fluid dynamics as the used analysis tool. The following two chapters only show the basic background of these two scientific topics and are based on the works of Merker et al. [14], Pischinger et al. [15], Blair [28], Petermeier [31], Eichlseder et al. [38] etc. as well as Kundu and Cohen [32], Versteeg and Malalasekera [33], Blazek [45], Fluent [52] etc.

2.1   2-Stroke Engine

Due to its simple working principle, low production costs, and an excellent power to weight ratio the 2-stoke engine is widely used for motorization of recreational products as well as handheld products. But its disadvantages, especially high emissions and bad fuel economy, have led to an image loss in the last decades. Moreover, first emission regulations for small capacity engines were also introduced in the 1990s.

High emissions of a 2-stroke engine are caused by the working principle itself. In a 2-stroke engine, the complete thermodynamic cycle is realized within only two piston movements (only one revolution); in comparison to a 4-stroke engine, which needs two revolutions, four piston movements respectively. The reduced number of strokes increases the engine efficiency and often provides remarkable high specific power, but on the other side, the 2-stroke principle leads to a simultaneous exhaust gas exchange with the fresh incoming charge inside the cylinder volume. This process occurs in a very short time, when the intake and exhaust ports are simultaneously opened, so that a big part of the exhaust gas emissions are directly produced in this engine phase.

2.1.1   Working principle of 2-stroke engines
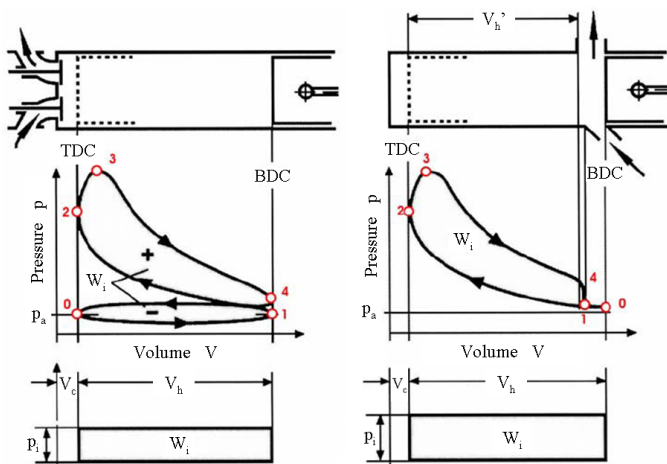
Figure 1:   Working principle 2-stroke vs. 4-stroke engine [21]

To clarify the processes taking place in a 2-stroke engine, following the gas movement through the engine and observing simultaneously the cylinder and crankcase volumes is a practicable way. Basically, a 2-stroke engine is a double-acting machine, so that above the piston the power process takes place and below the piston, inside the crankcase volume, the fresh charge is prepared for the transfer to the cylinder volume. Due to the piston movement, the pressure inside the crankcase decreases below the atmospheric value. During this phase, fresh air or fuel/air mixture (depending on the mixture formation system) is sucked in. Simultaneously, the *combustion process* inside the cylinder volume produces a rapid rise in pressure and temperature, which further moves the piston down in the power stroke, the so-called the *expansion process*. At the

8

same time, the sucked air or fuel/air mixture inside the crankcase volume is compressed due to the piston movement and concurrent closed intake ports. After this, the piston edge first reaches the exhaust port and the transmission of the exhaust gases into the exhaust duct is allowed. As the area of the exhaust port is increasing with time the cylinder pressure level is concurrently falling. In the exhaust system, the pressure wave moves through the duct and, due to specific exhaust system design, is reflected as well. Due to the piston movement, the piston edge next reaches the intake ports and compressed air or fuel/air mixture of the crankcase volume enters the cylinder volume. This phase is known as the *scavenging process* and, as mentioned before, the biggest part of the exhaust gas emissions are produced in this phase. For instance, if the intake ports are badly directed, the fresh charge can exit directly to the exhaust port. The cylinder volume will be filled with a lot of exhaust gas leading directly to a reduction of engine efficiency. Furthermore, in the case of a carbureted engine, the fuel/air mixture will be lost to the exhaust system with a consequential increase of hydrocarbon emissions. A fuel direct injection concept should reduce this emission rate and was widely investigated in a lot of works. The exhaust system supports the scavenging process inside the cylinder volume. Short before the piston edge closes the exhaust port, the reflected pressure wave returns and pushes the fresh charge back to the cylinder volume. This process also leads to a so-called *supercharging effect*. After this, the piston edge completely closes the exhaust port, approaching the point known as *trapping point*, and the scavenging process is completed. The cylinder volume is filled with the fresh fuel/air mixture and the extant exhaust gas. When the exhaust port is finally closed, the *compression process* begins until start of the combustion process which is started by the spark plug, so-called the *ignition process*.

2.1.2 Characteristics of the working process

Due to the specific 2-stroke engine design and a process control with the piston edge, the compression ratio is defined by the cylinder volume after exhaust port closure, so-called as the *trapped compression ratio* (see Blair [28]), in contrast to the 4-stroke compression ratio, which is known in literature as the *geometric compression ratio* based on the full swept volume (see Figure 1).

2-stroke engine, trapped compression ratio: $\qquad \varepsilon' = \dfrac{V_h' + V_c}{V_c} \; [-]$ (2.1)

4-stroke engine, geometric compression ratio: $\quad \varepsilon = \dfrac{V_h + V_c}{V_c} \; [-]$ (2.2)

The delivered work W related to the swept volume V_h represents the *mean pressure* p_m. Taking into account the effective work W_e the *mean effective pressure* p_e can be obtained. Likewise, the *indicated mean effective pressure* (IMEP) p_i is calculated from indicated work W_i and the swept volume V_h.

Mean pressure: $\qquad\qquad\qquad p_m = \dfrac{W}{V_h} \; [Pa]$ (2.3)

Mean effective pressure:
$$p_e = \frac{W_e}{V_h} \ [Pa]$$
(2.4)

Indicated mean effective pressure (IMEP):
$$p_i = \frac{W_i}{V_h} \ [Pa], \text{ with } W_i = \int p \, dV$$
(2.5)

The delivered power to the piston top is called the *indicated power output* and is given as

2-stroke indicated power:
$$P_i = n \cdot V_h \cdot p_i \ [KW]$$
(2.6)

4-stroke indicated power:
$$P_i = \frac{1}{2} n \cdot V_h \cdot p_i \ [KW]$$
(2.7)

Where n is the engine rotation rate given in revolutions per seconds. It can clearly be seen that a 4-stroke engine needs a double IMEP value for equal power output and equal swept volume compared to the 2-stroke engine. Likewise, the *indicated torque* is defined as follows:

2-stroke indicated torque:
$$M_i = \frac{V_h \cdot p_i}{2\pi} \ [Nm]$$
(2.8)

4-stroke indicated torque:
$$M_i = \frac{V_h \cdot p_i}{4\pi} \ [Nm]$$
(2.9)

Finally, the engine efficiencies and the specific fuel consumption can be calculated as follows:

Effective engine efficiency:
$$\eta_e = \frac{W_e}{Q_F} \ [-]$$
(2.10)

Indicated engine efficiency:
$$\eta_i = \frac{W_i}{Q_F} \ [-]$$
(2.11)

Mechanical engine efficiency:
$$\eta_m = \frac{W_e}{W_i} \ [-]$$
(2.12)

Specific fuel consumption:
$$b_e = \frac{1}{\eta_e H_u} \ \left[\frac{g}{KWh} \right]$$
(2.13)

Q_F is the rate of heat input and is calculated from $Q_F = m_F \cdot H_u$, where H_u is fuel calorific value given in $\left[\frac{KJ}{kg} \right]$.

2.1.3 Scavenging process of 2-stroke engines

The principle of exhaust gas exchange with the fresh incoming charge inside the cylinder volume is called scavenging process. Basically, *loop*, *cross*, and *uniflow* scavenging processes can be distinguished.

(a)   (b)   (c)
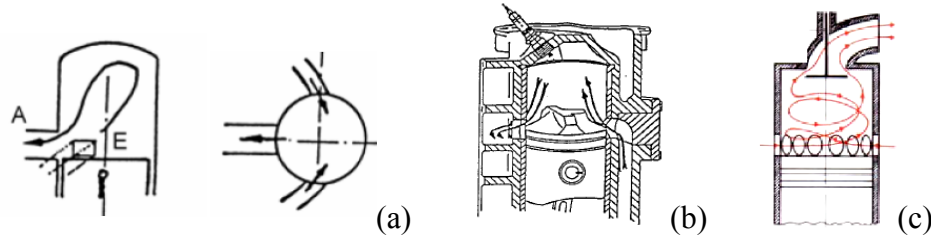
Figure 2:   Loop (a), cross (b), and uniflow scavenging process (c) according to Pischinger et al. [15]

The loop scavenging process was developed by Schnürle in Germany about 1926. The aim was to produce a scavenging process in a ported cylinder with several ports directed across the piston away form the exhaust port. An advantage of the loop scavenging process according to Blair [28] is the availability of a compact combustion chamber above the flat piston which permits a rapid and efficient combustion process. Therefore, this concept is widely used for high speed engines.

The cross scavenging process is proposed by Dugald Clerk [28] and is usually used for outboard motors. In this concept, the scavenging process is often supported by a specific piston design and Blair [28] shows that this has good characteristics at low throttle openings and low-power characteristics respectively. Due to a non-compact combustion chamber, the cross scavenged engine has rather unimpressive specific power and fuel economy characteristics during a high throttle opening. Nevertheless, some concepts, such as the QUB type (see Blair [28]), eliminate this disadvantage due to their specific intake ports and piston design.

The most efficient method of 2-stroke engine scavenging is the uniflow concept. The cylinder filling starts at one side and removes the exhaust gas from the cylinder on the other side. One of these ports is generally controlled by a valve system and during the scavenging process the flow is usually swirled. The swirling air motion is generally effective in promoting a good combustion process, especially for diesel engines. Therefore, this concept is widely used for the 2-stroke low-speed marine diesel engines with efficiencies in excess of 50%. For spark ignition engines, the uniflow concept advantages cannot be realized, primary due to increasing complexity and production costs in comparison to an insignificant power or efficiency advantage.

In order to desribe the scavenging process of a 4-stroke engine the characteristics of thermodynamic terms used in combination with engine design and testing are defined according to DIN 1940 [29]. Pischinger et al. [15] and Blair [28] took into account specific 2-stroke engine conditions by the definition of following characteristics.

The *delivery ratio* (DR) is a ratio of the air mass supplied during the scavenging period m_E and the reference air mass $m_{th,DE}$, which is required to fill the swept cylinder volume V_h

11

under atmospheric conditions calculated from the thermodynamic equation of state with the pressure p_{at}, temperature T_{at}, and the gas constant for air R_{at}.

Delivery ratio (DR): $\qquad DR = \dfrac{m_E}{m_{th,DR}}$, with $m_{th,DR} = \rho_{at} \cdot V_h$ and $\rho_{at} = \dfrac{p_{at}}{R_{at}T_{at}}$ $\qquad$ (2.14)

The *scavenge ratio* (SR) is a ratio between the air mass supplied during the scavenging period m_E and the reference air mass $m_{th,SR}$, which could fill the entire cylinder volume V_{cyl} under the atmospheric condition. In the case of a supercharged or turbocharged engine, the reference air mass $m_{th,SR}$ should be calculated from the state condition of pressure and temperature of the scavenge air supply.

Scavenge ratio (SR): $\qquad SR = \dfrac{m_E}{m_{th,SR}}$, with $m_{th,SR} = \rho_{at} \cdot V_{cyl} = \rho_{at} \cdot (V_c + V_h)$ $\qquad$ (2.15)

The *scavenging efficiency* (SE) is defined as the mass of delivered air that has been trapped m_{TR}, by comparison with the total mass of charge, that is retained at exhaust closure and represents the composition of fresh trapped charge m_{TR}, rest exhaust gas m_{exh} and any air remaining from the previous cycle m_{air}.

Scavenging efficiency (SE): $\quad SE = \dfrac{m_{TR}}{m_{TR} + m_{exh} + m_{air}}$ $\qquad$ (2.16)

The *trapping efficiency* (TE) is the ratio of delivered air mass that has been trapped m_{TR} to supplied m_E.

Trapping efficiency (TE): $\quad TE = \dfrac{m_{TR}}{m_E} = \dfrac{SE}{SR}$ $\qquad$ (2.17)

The *charging efficiency* (CE) formulates the ratio of the cylinder filling with air m_{TR}, compared to the perfect cylinder filling with air $m_{th,SR}$ at the onset of the compression stroke.

Charging efficiency (CE): $\quad CE = \dfrac{m_{TR}}{m_{th,SR}} = TE \cdot SR$ $\qquad$ (2.18)

The *rest gas* fraction (RG) is defined as the ratio between the rest gas mass inside the cylinder volume m_{RG} and the charge mass, which represents the composition of the trapped air mass m_{TR} and the rest gas mass m_{RG}.

Rest gas fraction (RG): $\qquad RG = \dfrac{m_{RG}}{m_{TR} + m_{RG}}$ $\qquad$ (2.19)

The *exhaust gas* fraction (EG) is the ratio between the exhaust gas mass m_{EG} and the mass composition of the trapped air m_{TR} and the exhaust gas mass m_{EG}. Attention should be paid to the fact that the exhaust gas mass m_{EG} becomes the rest gas mass m_{RG} after exhaust port closure.

Exhaust gas fraction (EG): $\quad EG = \dfrac{m_{EG}}{m_{TR} + m_{EG}}$ (2.20)
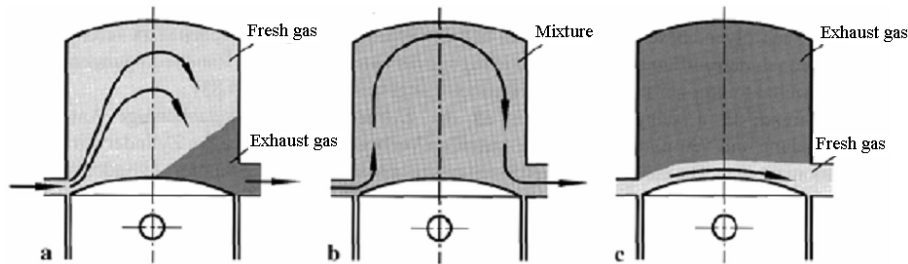
Figure 3: Perfect displacement (a), perfect mixing (b), and shorting scavenging process (c) according to Pischinger et al. [15]

By the analysis of the exhaust gas fraction inside the cylinder volume EG_{cyl} and the exhaust duct EG_{exh}, the following scavenging processes can be distinguished:

1. Perfect displacement scavenging: The fresh charge perfectly displaces the exhaust gas from the cylinder volume and therewith the exhaust gas fraction inside the exhaust duct is $EG_{exh} = 1$.

2. Perfect mixing scavenging: In this case, the entering charge does not have perfect displacement characteristics. The fresh charge is directly mixed with the exhaust gas, so that $EG_{exh} = EG_{cyl}$ can be obtained.

3. Shorting scavenging: This is the worst case. The fresh charge flows directly to the exhaust port and the complete exhaust gas remains inside the cylinder volume, therewith $EG_{exh} = 0$ and $EG_{cyl} = const$.

2.1.4 Mixture formation

During the development of the IC-engines, the real challenge is posed by mixture formation, in fact preparation and mixing of fuel and air. Basically, referring to gasoline engines, a distinction can be made between *external* and *internal* mixture formation.

2.1.4.1 External mixture formation

An essential solution of the mixture formation problem in gasoline engines was the Maybach spray carburetor invention in 1893 (see Basshuysen [36]). In this concept, the fuel was directed through an inlet tube with reduced cross-section, which accelerates the air flow and positively supports fuel atomization and fuel-air mixing. Furthermore, the mixture formation

occurs outside of cylinder, so that a good fuel-air homogenization can be successfully realized. In all engine operating points and loads a homogeneous mixture is available with a constant and, on demand, a stoichiometric equivalence ratio. In this case, the engine efficiency increases and allows an application of oxidation catalyst for the exhaust gas after treatment as well. In order to improve the exhaust gas emissions and the fuel consumption the carburetor can be replaced by an electronic controlled intake manifold fuel injection system. Due to a long transport of the injected fuel and a high level of turbulence in the valve gaps, well homogenized fuel-air mixture can be produced even with this system. The rail pressure of 4-5 bars can provide a homogenized mixture in all engine operating points (see Basshuysen and Schäfer [37]), e.g. due to rapid liquid fuel evaporation supported by a low air pressure in the intake manifold caused by a restricted operation with a closed throttle valve system. Both above mentioned concepts are still in use; the carburetor can primarily be found in small and low cost engines.

The mixture formation outside the cylinder has some disadvantages compared to the internal mixture formation. They are reflected in high fuel consumption and exhaust gas emissions independent on the working process, 2-stroke or 4-stroke. According to Petermeier [31], the scavenging losses of a modern 4-stroke engine are 3-4%, depending on the operating point and the duration of valve overlapping time. The scavenging losses of a 2-stroke engine are higher and rise up to 30% at high engine speed and full load. This effect can be explained by the fact that in a 2-stroke engine the gas exchange inside the cylinder occurs simultaneously, when the intake and exhaust ports are both open over a long period of the cycle. The load control of an engine with external mixture formation works with the control of the air/fuel mixture quantity inside the cylinder volume, so-called *quantity control*. It is realized through a fresh air mass restriction applying a throttle valve system, which further leads to an increase of the gas exchange work as well as a reduction of engine efficiency. Especially in low load engine operating points with very high throttling, the losses are higher. After fuel injection into the intake manifold, the control of the fuel is lost. The evaporated fuel will be mixed with the fresh air and is then transported to the cylinder volume. The unevaporated fuel forms a liquid fuel film on the intake manifold surfaces and will not be evaporated and transported to the cylinder volume within the next cycles. This effect presents a non-trivial problem in an engine with external mixture formation and rapid engine load changes, e.g. from full to low load. A rapid throttle closing causes a pressure decrease inside the intake manifold, which supports fuel evaporation. This evaporated fuel together with a low air concentration will be further transported to the cylinder volume. Due to a rich mixture the combustion process remains incomplete, so that hydrocarbon emissions rise. In the other case, the load change from low to full load, the problem is situated in a similar way. A rapid throttle opening causes a rapid pressure increase inside the intake manifold, which further leads to slow fuel evaporation, so that the sucked mixture will be leaner than desired and the unevaporated fuel again forms a fuel film. A well tuned motor control unit can partially resolve this problem of transient engine load changes.

2.1.4.2 Internal mixture formation

The idea of gasoline injection directly into the combustion chamber is almost as old as the carburetor history and was patented by Nikolaus August Otto in 1877 [36]. But in the early development period of the IC-engine the application of this system was unsuccessful, primarily due to lack of technological possibilities. First engines with fuel direct injection were aircraft engines by Daimler-Benz, which started series production in 1937, at almost the same time as the engines developed by Junkers and BMW [36]. This technology was first implemented due to the large potential of power increase of aircraft engines. With the good results

of aircraft engines with fuel direct injection in the 1930s the implementation of fuel direct injection technology in automotive engines became very popular. The aim was to combine the advantages of diesel and gasoline engines, i.e. a combination process with pure air compression, non-homogeneous mixture formation, spark ignition and mixture quality control at full load, part load and in low idle mode (see Basshuysen [36] and Eichlseder et al. [38]). In the 1930s, Daimler-Benz tested racing engines with fuel direct injection and the potential for the power increase compared to the carburetor engines was drastic. Development of engines with fuel direct injection was discontinued during World War II. After the war, the development was resumed mainly for 2-stroke engines for use in automobiles in close cooperation between Bosch and Gutbrod and between Bosch and Goliath. Based on the experiences with aircraft engines, the investigations were started very optimistically, but very soon results showed that this technique was more difficult than expected in the beginning. According to Basshuysen [36] the basic problems were related to the injection system, such as high pump speed required for 2-stroke engines, controlled injection pump over a large engine speed range, pump and injector nozzle etc. For a series production, a research team proposed an injector position in the cylinder head so that the injection spray was directed opposite to the scavenging flow, an increase of the engine compression, a determination of spark position so that the ignition process can be realized in a large engine speed range and load, and an adjument of the inlet and exhaust system. In the year 1959 Groth [39] published an investigation of a direct fuel injection into the cylinder of a 2-stroke engine and in his work he presented advantages and difficulties of the system application. All these concepts with fuel direct injection had the same problem, i.e. the coordination between injection, mixture formation and combustion, especially in dynamic engine operating mode with rapid load changes. It was not until the end of the 1980's that Plohberger and Miculic [40, 41] brought the gasoline direct injection into focus and showed the potential of this system with new technologies. Although the 2-stroke engine concept was not realized in series production, primarily due to general high exhaust gas emissions, the scientific background was formed for successful series introduction of the 4-stroke engine with direct injection system for passenger cars, e.g. Mitsubishi [42]. Today, the fuel direct injection concept with turbo-charging offers great potential for reducing the power to weight ratio and fuel consumption and will be widely used in the coming years [36, 38].

Generally, the gasoline direct injection (further: GDI) can be divided ino two different operating modes, *homogeneous* and *stratified*, which primarily differ in injection timing, throttle position, and mixture composition.

2.1.4.2.1 Homogeneous mixture

A homogeneous operating mode is usually used in the higher load range, a similar process to the external mixture formation. The fuel is injected directly inside the cylinder volume during the intake process (also so-called *early injection*) and is early mixed with moving fresh air with high velocity. During the compression stroke, enough time and air motion until the ignition point is still available for a homogenous mixture with an almost constant equivalence ratio inside the combustion chamber. Furthermore, in a GDI engine for homogeneous operating mode the droplet evaporation takes place inside cylinder and during the intake process. This further leads to a gas temperature reduction and causes an increase of volumetric efficiencies of GDI engines up to 9% in comparison to engines with external mixture formation. Moreover, this internal cooling effect will be also positively reflected on the knocking behavior [31, 36, and 38]. This advantage can be further used to increase the compression ratio by a geometrical reduction of the compression volume. According to Basshuysen [36] a rise in compression ratio from 1.5 to 2 can be assumed, which will be positively reflected in fuel

15

consumption up to 5%. With the compression volume changes, the surface/volume ratio (wall surface area to combustion chamber volume) will be also increase, which can cause a rise in hydrocarbon emissions due to uncompleted combustion and increasing wall influence [36]. Advantage of the compression ratio increase can be positively exploited by applying of super- or turbo-charging. Due to charge improvement with the same engine size an increase of engine power can be expected, or otherwise, the engine size can also be reduced, so-called *downsizing*, retaining the same engine power. Furthermore, the downsizing effect leads to a decrease in frictional losses up to 10% compared to the reference engine with intake manifold injection and without super-charging. This effect will be also directly reflected in fuel consumption.

In homogenous operating mode, the engine load is controlled by the throttle system, similar to the load control of engines with external mixture formation, so that the disadvantages of this system, such as restriction losses, cannot be avoided with a GDI strategy. But, in the case of a fully opened throttle valve, the boundary conditions are identical, compared to an engine with manifold fuel injection. However, in full load mode the GDI engines have higher volumetric efficiencies, primarily due to cylinder internal cooling effect. At high engine speeds the cylinder internal cooling advantages of a GDI engine can be neglected, because in an engine with external mixture formation and high speed the fuel evaporation also takes place inside the cylinder volume. However, in a GDI engine a reduced fuel film concentration on the intake manifold surfaces is presented with advantages that will be drastically visible in dynamic engine mode eliminating the above mentioned disadvantages of an intake manifold injection system.

2.1.4.2.2 Stratified mixture

At low engine speed and in part load operation the GDI engine is run in stratified mode with a big potential to improve the engine efficiency. In stratified mode the fuel will be injected during or towards the end of the compression phase, so-called *late injection* or *compression stroke injection*, see Basshuysen [36]. This strategy leads to a stratification of the charge in the combustion chamber, whereas an ignitable mixture around the spark plug at the point of ignition is required. In the wall area of the combustion chamber a very lean fuel/air mixture, or pure air, or pure exhaust gas can be found. The exhaust gas comes from a recirculation system in the case of a 4-stroke engine and/or from the previous cycle, e.g. due to an inefficient scavenging process, of a 2-stroke engine. Generally, the engine operation is very lean with large gradients of the fuel/air ratio. In the stratified operating mode the GDI engine should be operated with a fully open throttle, like a diesel engine, whereas the engine control is realized via the injected fuel amount, so-called *quality control*. This strategy has the advantage that the engine is operated with an unthrottled intake process, so that the gas exchange losses can be reduced, especially at low engine speed and in part load operation, where the throttling is extremely presented.

For an internal mixture formulation the fuel/air homogenization process takes place inside the cylinder volume, and in comparison to external mixture formulation process; it is realized in a clearly shorter time, especially in the case of a 2-stroke engine. A successful homogenization process depends on a range of parameters which must be considered with each other, e.g. intake flow, combustion chamber design, injector and spark plug positions, spray characteristics, injection parameters (rail pressure, start, duration, and end of injection etc.). For instance, in a 2-stroke GDI engine an early injection strategy can cause an increase of fuel losses as well as fuel wall wetting. Otherwise, a later fuel injection drastically reduces the scavenging losses, but simultaneously leads to a stratified mixture formulation and can cause a rise in

hydrocarbon emissions caused due to an inhomogeneous mixture at time of ignition as well as an incomplete combustion process. In a 4-stroke engine the piston design is also important for the mixture formation process as well as the spray interaction with the piston surface. The 2-stroke engine piston design should be rather kept compact and flat, due to a request for an efficient loop scavenging process and a compact combustion chamber design.

With regard to how the fuel is guided from the injector to the spark plug between three concepts of mixture formation processes, *wall-*, *air-*, and *spray-guided* concepts can be distinguished.

Wall-guided concepts are the first generation in the market of GDI engines. The mixture formation process takes place through an interaction between the injected fuel and the specially designed piston surface. The disadvantages of this concept are an increasing fuel concentration on the piston surface and increased hydrocarbon emissions. According to Basshuysen [36], a long way of injected fuel from the injector nozzle to the spark plug supports the mixture formation process, but requires specific, stable charge movement at each engine load and speed and precise determination of the injection and ignition points. A non-compact combustion chamber, due to requirement of a special piston design, has a negative influence on the knocking behavior, so that the full load potential of a GDI concept is reduced. In the heating engine phase, the engine is exclusively operated in homogeneous mode, due to strong affinity to fuel wall wetting, see Petermeier [31].

In the air-guided concept, the fuel transport from the injector nozzle to the spark plug occurs supported by charge movement generated by the intake manifold and supported by a specific piston design. The contact between spray and the combustion chamber wall should be avoided [36] in order to reduce the fuel film formation. The successful implementation of this concept primarily depends on the alignment and the interaction of the injected fuel and the generation of fluid flow in the cylinder volume. The general requirement is that the generated charge motion, e.g. tumble or swirl, should be sufficiently available during the compression phase in order to support the mixture formation and the transport to the spark plug.

The spray-guided concept is characterized by a very small distance between the spray and the spark plug, therefore the efficiency of this concept primarily depends on the spray characteristics and spark plug functionality. Experts, such as Pischinger et al. [15], Petermeier [31], and Basshuysen [36, 37], agree that only spray-guided concepts can exploit the potential of the stratified mode – the so called "direct injection of the second generation" concept. After a late fuel injection the stratification gradients are very high and only in the spray periphery an ignitable fuel/air mixture is situated, whereas a very rich mixture exists in the spray core. The spark plug should be positioned so that an ignitable mixture is available around of the ignition electrodes at the ignition point as well as in all engine operating points. Therewith, the spray-guided concept extremely depends on the spray characteristics and reacts very sensitive to fluctuations in this regard [36].

2.1.4.2.3 Characteristics of mixture formation of a 2-stroke GDI engine

In order to characterize the mixture formation efficiency inside a 2-stroke GDI engine, the transient characteristic of fuel distribution in different engine domains, e.g. cylinder, exhaust, and crankcase volumes, over a cycle was introduced and used in the evaluation process in this work. The total injected fuel mass m_{IFM} inside the considered domain can be presented as a sum of partial fuel masses inside separated domains and is given by:

Injected fuel mass *IFM* :
$$m_{IFM} = \int_{V_{Cyl}} \rho_t Y_{Fuel} dV + \int_{V_{CC}} \rho_t Y_{Fuel} dV + \int_{V_{Exh}} \rho_t Y_{Fuel} dV \qquad (2.21)$$

whereas, ρ_t is the total density, Y_{Fuel} is the mass fraction of fuel species, V_{Cyl} is the cylinder volume, V_{CC} is the crankcase volume and V_{Exh} the exhaust system volume. The ratio of fuel distribution *FD* in each considered domain can be obtained as follows:

Cylinder volume FD_{Cyl} :
$$FD_{Cyl} = \frac{\int_{V_{Cyl}} \rho Y_{Fuel} dV}{m_{IFM}} \qquad (2.22)$$

Crankcase volume FD_{CC} :
$$FD_{CC} = \frac{\int_{V_{CC}} \rho Y_{Fuel} dV}{m_{IFM}} \qquad (2.23)$$

Exhaust system volume FD_{Exh} :
$$FD_{Exh} = \frac{\int_{V_{Exh}} \rho Y_{Fuel} dV}{m_{IFM}} \qquad (2.24)$$

As mentioned before, these data are evaluated over an engine revolution, in fact from the start of injection until the ignition point. When the piston achieves the trapping point, the exhaust port is completely closed, so that the evaluated values from this point until the ignition point are constant. In this region, the evaluated characteristic in cylinder volume FD_{Cyl} represents the *fuel trapping efficiency*. In contrast to a 4-stroke engine, this transient data in a 2-stroke engine are used in order to determine the injector strategy efficiency, i.e. the start and the duration of injection as well as the injector position and the applicable spray characteristics to the existing scavenging typ.

The mixture quality estimation is obtained by the evaluation of the air/fuel ratio at the time of the ignition process, which is calculated as follows:

$$AFR = \frac{m_{air}}{m_{fuel} L_{st}} \qquad (2.25)$$

Where, m_{air} is the air mass, m_{fuel} is the fuel mass, and L_{st} the stoichiometric air demand in kg air per kg fuel. In this work, the so-called *equivalence ratio* is used, which is related to the air/fuel ratio as follows:

$$ER = \frac{1}{AFR} \qquad (2.26)$$

2.1.5 Combustion process

The combustion process in a gasoline engine is realized by the ignition process, which is locally started by an ignition source like a highly energetic plasma, generated by electrical

sparks between the electrodes of a spark plug. Inflammation of mixture takes place within the ignition volume, around the spark plug, and is continued by unsteady flame propagation into the unburnt fuel/air mixture. In an engine with external mixture formation for the stoichiometric mode, an ideal ignitable mixture composition is almost always situated around the spark plug (so-called *homogeneous combustion process*), so that the requirements on the ignition system are relatively low. In a GDI engine working in the homogeneous mode, a similar homogenous situation inside the cylinder is presented, so that the requirements on the ignition system are comparable to engines with external mixture formation. In contrast to this, a limited volume of ignitable mixture is available in the GDI engine in the stratified mode (also called *stratified combustion process*), due to a stratified mixture with local very lean and/or very rich fuel/air ratio. This situation provides a challenge for the ignition systems, which should allow an assured mixture inflammation over a large engine speed range. The high flow velocities, required for a good fuel/air mixing process, even complicate the flame kernel formation [43]. Furthermore, due to high stratification gradients in the stratified mode, the spark plug wetting with liquid fuel presents an additional problem related to the inflammation process and the spark plug durability. Further detailed discussion on this topic can be found in works of Pischinger et al. [15], Petermeier [31], Basshuysen [36, 37], Eichlseder et al. [38] and Kaiser and Hoffmann [43].

2.2   IC-engine flow characterization

Due to strong density dependency on the pressure and the temperature, the flow in an IC-engine is always taken as a *compressible flow*. In a compressible medium, infinitesimal changes of density cause propagation of pressure waves through the medium with a finite speed, so-called *speed of sound* and it is given by:

$$c^2 = \left(\frac{dp}{d\rho}\right)_s \quad \left[\frac{m}{s}\right] \qquad (2.27)$$

where, the subscript "s" signifies that the derivative is taken at constant entropy (see Kundu and Cohen [32]). The flow structure in a compressible medium is also depending on the flow velocity, so that a dimensionless number the *Mach number*, named after the Austrian physicist *Ernst Mach* (1838-1916), for the flow characterization can be defined by the ratio of flow velocity u and speed of sound c:

$$Ma = \frac{u}{c} \quad [-] \qquad (2.28)$$

Generally, the flow with $Ma < 0.3$ can be assumed as incompressible and the compressibility effects can be neglected as well. The flow with $Ma < 1.0$ is called *subsonic*, and in this case the propagation of the pressure wave created by a source is observable in all sides of the considered region. At a speed of sound of $c = u$, namely $Ma = 1$, the source creates a sound barrier, which is normal to the propagation direction, and this flow is also known as *sonic*. When the source exceeds the sound barrier $Ma > 1.0$ (so-called *supersonic* flow), a large pressure difference is created just in the source front. This abrupt rise of pressure is known as *shock wave*, which is also accompanied by an extremely rapid increase of temperature and density. With a rising Mach number the shock wave moves backward of the source and the propagation of the pressure wave is observable only behind the source located *Mach cone*, see Pischinger et al. [15] as well as Kundu and Cohen [32].

For an IC-engine the density change has an essential importance, primarily due to strong changes of pressure and temperature inside the cylinder volume as well as due to high pressure differences during the opening phase of the valve system in a 4-stroke engine and the intake and exhaust ports of a 2-stroke engine, where the flow exceeds a velocity of the speed of sound (see Pischinger et al. [15]).

Generally, the fluids can be distinguished as Newtonian and non-Newtonian fluids. The English physicist *Isaac Newton* (1642-1726) postulated a hypothesis where the shear stress of a Newtonian fluid between the layers in a straight, parallel, and uniform flow is proportional to the velocity gradient and the dynamic viscosity μ $[kg/ms]$ and it is given by:

$$\tau = \mu \frac{\partial u}{\partial y} \qquad (2.29)$$

According to Pischinger et al. [15] and Kundu and Cohen [32] the dynamic viscosity is basically depending on temperature and less on pressure; for gases it increases with a rising temperature. Taking into account the force independency, the kinematic viscosity can be calculated from the dynamic viscosity relating to fluid density:

$$\nu = \frac{\mu}{\rho} \left[\frac{m^2}{s} \right] \qquad (2.30)$$

For a non-Newtonian fluid the shear stress is a nonlinear function. Nevertheless, for fluids such as air and water the linear relationship is found to be accurate enough for most engineering applications (see Kundu and Cohen [32]).

The Reynolds number, named after the English mathematician and physicist Osborne Reynolds (1842-1912), is a dimensionless number and characterizes different flow regimes in the fluid mechanics, such as laminar or turbulent. The Reynolds number is defined by the ratio of inertial $\rho u^2 L^2$ and viscous forces $\mu u L$.

$$\mathrm{Re} = \frac{\rho \cdot u^2 \cdot L^2}{\mu \cdot u \cdot L} = \frac{\rho \cdot u \cdot L}{\mu} = \frac{u \cdot L}{\nu} \ [-], \text{ with } \nu = \frac{\mu}{\rho} \qquad (2.31)$$

where, ρ is fluid density, u is mean flow velocity, L is characteristic length, μ is dynamic fluid viscosity and ν is kinematic fluid viscosity.

The laminar flow occurs at low Reynolds numbers (<2300), where the viscous forces dominate. The laminar flow is also characterized by a smooth and constant motion, where the flow occurs in the layers with different velocities. In an IC-engine, these flow situations hardly ever exist, so that the flow can be characterized as turbulent with high Reynolds number (>4000), where inertial forces dominate.

The turbulent flow is characterized by chaotic fluid changes and tends to produce vortices which are variable in space and time, termed also *eddies*, in many different length scales. This flow also includes a fast variation of pressure and velocity with a dominant convection and a low level of momentum diffusion respectively. The dominant part of the kinetic energy of a

turbulent motion is embedded in large scale structures and their size is depending on the re-stricting external structure. The largest vortex structures are highly anisotropic and heavily flow dependent, due to their interaction with the mean flow. The large scale structures disag-gregate creating smaller and smaller structures with a decreasing level of turbulent kinetic energy, which form a hierarchy of the eddies and the energy cascade. At the end of this hierar-chy, the structures are small enough so that molecular diffusion dominates and the dissipation of kinetic energy in thermal energy takes place. The smallest eddies are highly isotropic, due to the reduction of scale and a loss of geometrical and directional information. The smallest possible eddies are described by the *Kolmogorov length scale* [30], proposed by the Russian mathematician *Andrey Kolmogorov* (1903-1987). According to Kolmogorov [30], the Rey-nolds number of the smallest eddy $\mathrm{Re}_\eta = u\eta/v$ is equal to one and the viscous forces domi-nate the flow. Based on this theory, Kolmogorov postulates following equations for the Kol-mogorov length and time scales, taking into account only two parameters, viscosity v and dissipation rate ε:

Kolmogorov length scale: $\eta = \left(\dfrac{v^3}{\varepsilon}\right)^{\frac{3}{4}}$ (2.32)

Kolmogorov time scale: $\tau = \left(\dfrac{v}{\varepsilon}\right)^{\frac{1}{2}}$ (2.33)

Both scales strongly depend on the Reynolds number and rise with an increasing Reynolds number.

As mentioned before, the flow inside an IC-engine is always turbulent and unsteady. Due to a pressure difference between different engine regions and their cyclic connections via the valve systems (4-stroke engine) or the intake/exhaust ports (2-stroke engine), a highly turbulent flow occurs accompanied by direction changes, rotations, and recirculation. In the case of a 4-stroke engine and after the valve system opening phase, the largest eddies are developed sup-ported by the specific 4-stroke engine intake duct design. Their structures have a length scale of about 10^{-2} m and achieve a length scale of about 10^{-1} m (cylinder bore) during the compres-sion phase, see Petermeier [31]. The velocity values get their maximum short after the open-ing phase of the valves. Due to a decreasing pressure difference between the cylinder and the intake duct volumes, the in-cylinder velocity decreases as well and declines to the value of mean piston velocity after valve system closure. Furthermore, Petermeier [31] also shows that the Reynolds number of the largest turbulence structures in the case of a 4-stroke engine is in the region from 10^4 to 10^5 and the smallest turbulence scales are from 10^{-4} to 10^{-5} m.

In contrast to a 4-stroke engine, a 2-stroke engine shows another form of flow inside the cyl-inder, primarily due to the specific 2-stroke engine design and working principle. In the ex-pansion phase, the in-cylinder velocity has the value of about the mean piston velocity, and the velocity vectors are oriented in the piston moving direction. Short before exhaust ports opening phase the pressure difference between the cylinder and the exhaust volumes is at a level of 1 bar to 9 bars, depending on the engine speed and operational point. For instance, at 9 bars pressure difference and an exhaust gas temperature of about 1400 K (e.g. 7900 rpm and wide-open throttle WOT), the flow inside the exhaust system achieves a supersonic condition with a Mach number up to 1.4. At the start of the intake ports opening phase the pressure dif-

ference is in the region between 0.1 and 0.6 bars. In contrast to a 4-stroke engine, a 2-stroke engine at high engine speed does not develop the largest eddies after the intake ports opening phase. Due to a specific intake port design the flow creates a "moving wall", which enables a good displacement of exhaust gas from the cylinder volume. The flow does not change its direction until the pressure wave comes back. Short before exhaust port closure, the flow changes its direction and develops the largest eddy inside the cylinder volume. Normally, its largest structure has a length scale smaller than the cylinder bore. At low engine speed the largest eddies are generated already at the beginning of scavenging process, similar to 4-stroke engines. Its rotation is supported by returning the pressure wave from the exhaust system. The Reynolds number of largest turbulence structure is in the region of 10^4 to 10^5 and the smallest turbulence scales of 10^{-4} to 10^{-5} m, similarly to a 4-stroke engine.

2.3   Governing equations of fluid flow and thermodynamics

The governing equations of fluid flow represent the mathematical description of the physical laws of conservation, which can be summarized as following [33]:

- The mass of fluid is conserved (*mass continuity equation*)

- The change rate of momentum is equal to the sum of the forces on a fluid particle applying Newton's second law (*Navier–Stokes equations*)

- Applying the first law of thermodynamics, the change rate of energy is the sum of the heat addition rate and the work rate on a fluid particle (*energy equation*)

2.3.1   Navier-Stokes equations

The Navier-Stokes equations were postulated by the French engineer and physicist *Claude-Louis Navier* (1785-1836) [34] and the English mathematician and physicist *George Gabriel Stokes* (1819-1903) [35] independent of each other. Together with the continuity and energy equations it describes the fluid motion of the Newtonian liquids and gases for a wide range of technical problems; therefore the name "Navier-Stokes equations" meaning all three above mentioned equations can often be found in literature. These equations couple a second order system of non-linear partial differential equations. For well formulated boundary conditions the fluid motion is described very accurately even for turbulent flows. The fluid is viewed as a *continuum* with length scales of 1 μm and larger. This means that the molecular structure of matter and molecular motions are neglected and the fluid behavior is described in terms of macroscopic properties, such as velocity, pressure, density and temperature, including their space and time derivates (cf. Versteeg and Malalasekera [33]). For the compressible flows and Newtonian fluids, where the time dependent density is included, the Navier-Stokes equations are given as follows:

Continuity:
$$\frac{\partial \rho}{\partial t} + \frac{\partial \rho u_i}{\partial x_i} = S_C \qquad\qquad (2.34)$$

Momentum:
$$\frac{\partial \rho u_i}{\partial t} + \frac{\partial \rho u_i u_j}{\partial x_j} = -\frac{\partial p}{\partial x_i} + \frac{\partial \tau_{ij}}{\partial x_j} + \rho f_i + S_M \qquad\qquad (2.35)$$

Energy:
$$\frac{\partial \rho E}{\partial t} + \frac{\partial \rho u_j E}{\partial x_j} = -\frac{\partial u_j p}{\partial x_j} + \frac{\partial u_i \tau_{ij}}{\partial x_j} - \frac{\partial q_j}{\partial x_j} + S_E$$
(2.36)

The stress tensor τ_{ij} of a Newtonian fluid with consideration of Stokes' hypothesis is defined by:

$$\tau_{ij} = 2\mu S_{ij} - \frac{2}{3}\mu \frac{\partial u_k}{\partial x_k}\delta_{ij}$$
(2.37)

where μ is the dynamic fluid viscosity. The strain-rate tensor S_{ij} is obtained with:

$$S_{ij} = \frac{1}{2}\left(\frac{\partial u_i}{\partial x_j} + \frac{\partial u_j}{\partial x_i}\right)$$
(2.38)

The term ρf_i in equation (2.35) represents the mass forces and is often irrelevant for gases. Relationships between the thermodynamic variables can be obtained through the thermodynamic equilibrium assumption. Although the fluid properties change rapidly in space and time, the fluid is always in a thermodynamic equilibrium. The only exceptions are strong shockwave flows, but still in these cases the equilibrium assumptions can be applied with a good approximation [33]. Terms, S_C, S_M, and S_E, present the source terms. Correlations between density ρ, pressure p, total energy E and temperature T for an ideal gas are given by the following equations:

Ideal gas law: $\quad p = \rho R T$
(2.39)

Total energy: $\quad E = c_v T + \frac{u_k u_k}{2} = \frac{1}{\gamma-1}\frac{p}{\rho} + \frac{u_k u_k}{2}$, with
(2.40)

$$\gamma = \frac{c_p}{c_v}, \ c_p - c_v = R \ \text{and} \ T = \frac{p}{\rho R}$$
(2.41)

where R is the gas constant, c_p the heat capacity at constant pressure, c_v the heat capacity at constant volume, and γ heat capacity ratio.

In equation (2.36), the q term presents the heat flux that goes through a surface. The heat flux is obtained with Fourier's law, proposed by the French mathematician and physicist *Jean Baptiste Joseph Fourier* (1768-1830), and is given as follows:

$$q_j = -\lambda \frac{\partial T}{\partial x_j}$$
(2.42)

The Fourier's law shows that the heat transfer through a surface is proportional to the negative local temperature gradient and the thermal material conductivity λ. The thermal conductivity is often treated as a constant, due to a small dependency on the temperature. Its behaviour is similar to the dynamic fluid viscosity μ, so that it can be obtained with *Prandtl number* and heat capacity as follows [44]:

$$\lambda = \frac{\mu c_p}{\text{Pr}} \tag{2.43}$$

The Prandtl number, named after the German physicist *Ludwig Prandtl* (1875-1953), presents the ratio between momentum- and heat diffusivity, $\text{Pr} = \mu c_p / \lambda$ [32].

For an arbitrary scalar ϕ_k, such as species mass fraction and/or user defined scalars, extra scalar transport equations are needed and can be defined as follows [52]:

$$\frac{\partial \rho \phi_k}{\partial t} + \frac{\partial}{\partial x_i} \left(\rho u_i \phi_k - \Gamma_k \frac{\partial \phi_k}{\partial x_i} \right) = S_{\phi_k} \quad k = 1, \ldots, N \tag{2.44}$$

where Γ_k is the diffusion coefficient and S_{ϕ_k} presents the source term for each of the N scalar transport equations.

In the case of species transport equation (2.44) is solved for $N-1$ species where N is the total number of fluid phase chemical species in the system. The mass fraction of species must sum up to unity, so that the Nth mass fraction can be determined as one minus the sum of the $N-1$ solved mass fractions. Furthermore, for calculation of diffusion coefficient between laminar and turbulent flows is to distinguish, see Fluent [52].

2.3.2 Turbulence modeling

Applying the above mentioned Navier-Stokes equations, the fluid motion for laminar or turbulent flow is completely described. A turbulent flow is characterized by a random fluctuation of the velocity field, whereas all transported quantities, such as momentum, energy, and species concentration, simultaneously fluctuate. These fluctuations can have very small scales and high frequencies making the concept *Direct Numerical Simulation* (DNS) computationally too expensive. Therefore, DNS is nowadays inapplicable for most of the engineering calculations. DNS plays a major role in the development and calibration process of turbulence models as well as for the understanding of turbulent structures and the laminar-turbulent transition (see Pecnik [44]).

An alternative approach, the *Large Eddy Simulation* (LES), can be basically viewed as an extension of the DNS. The idea is to accurately resolve only the large eddies, which transport the turbulent energy, and to approximate the effects of the small scales by *subgrid-scale models* [45]. The main advantage of this concept is to resolve only the large eddies which allow the use of a much coarser mesh and larger time steps than the DNS. LES computational costs are still high for the relevant simulations in engineering and the unsteady boundary conditions are more difficult, see Steiner [7]. Nonetheless, the LES concept has already become a very

powerful tool in scientific research, e.g. in the development and calibration process of turbulence models.

Today, the most important approach for the relevant simulation in engineering is the so-called *Reynolds Averaged Navier-Stokes* (RANS) concept, which was introduced by Reynolds in 1895. The basic idea is a decomposition of flow variables into mean and fluctuating parts by time or ensemble averaging [47].

$$u_i = \overline{u}_i + u_i' \text{ and } p = \overline{p} + p' \tag{2.45}$$

Time averaging: $$\overline{\phi} = \lim_{T \to \infty} \frac{1}{T} \int_t^{t+T} \phi \, dt \tag{2.46}$$

Ensemble averaging: $$\overline{\phi} = \lim_{N \to \infty} \frac{1}{N} \sum_{m=1}^{N} \phi_m \tag{2.47}$$

Whereas, ϕ presents fluctuating velocity components as well as pressure, energy, or species concentrations. In equation (2.46) it is clearly visible that the mean value does not vary in time, but only in space. This means that the time interval T should be very large. In equation (2.47), the mean value is a function of time and space. In the case of variable density, Favre [48, 49] supposed in 1965 a density weighted decomposition of the velocity components.

Favre averaging: $$\overline{\phi} = \frac{1}{\rho} \lim_{T \to \infty} \frac{1}{T} \int_t^{t+T} \rho \phi \, dt \tag{2.48}$$

Applying the Favre method, the equation becomes considerably more complicated - due to additional correlations involving density fluctuations [45] - so that only the Reynolds method is further explained. Taking into account time or ensemble averaging and setting the expressions from equation (2.45), the continuity and momentum equations are given in the following form:

Continuity: $$\frac{\partial \rho}{\partial t} + \frac{\partial \rho \overline{u}_i}{\partial x_i} = 0 \tag{2.49}$$

Momentum: $$\frac{\partial \rho \overline{u}_i}{\partial t} + \frac{\partial \rho \overline{u}_i \overline{u}_j}{\partial x_j} = -\frac{\partial \overline{p}}{\partial x_i} + \frac{\partial}{\partial x_j} \left[\mu \left(\frac{\partial \overline{u}_i}{\partial x_j} + \frac{\partial \overline{u}_j}{\partial x_i} - \frac{2}{3} \frac{\partial \overline{u}_k}{\partial x_k} \delta_{ij} \right) - \rho \overline{u_i' u_j'} \right] \tag{2.50}$$

In equation (2.50) an additional term $- \rho \overline{u_i' u_j'}$ appears; the so-called *Reynolds stress tensor*. In order to close the equation system this term must be modeled. The Reynolds stress tensor is a 3D tensor which consists of nine components assuming that the density is constant:

$$\overline{u_i' u_j'} = \begin{bmatrix} \overline{u_1'^2} & \overline{u_1' u_2'} & \overline{u_1' u_3'} \\ \overline{u_2' u_1'} & \overline{u_2'^2} & \overline{u_2' u_3'} \\ \overline{u_3' u_1'} & \overline{u_3' u_2'} & \overline{u_3'^2} \end{bmatrix} \tag{2.51}$$

Due to the interchange ability of the fluctuation components u_i' and u_j' the Reynolds stress tensor has six terms which have to be determined. The sum of normal stress components presents the *turbulent kinetic energy k* and is given as follows:

$$k = \frac{\overline{u_i' u_j'}}{2} = \frac{\overline{u_1'^2} + \overline{u_2'^2} + \overline{u_3'^2}}{2} \tag{2.52}$$

The basic problem of the turbulence modelling is to close the RANS equations, to find the influence of the six additional terms of the Reynolds stress tensor. The most used approach, especially for the industrial relevant flows, is the *Eddy-Viscosity Hypothesis* proposed by the French mathematician and physicist *Joseph Valentin Boussinesq* (1842–1929), see Boussinesq [50, 51]. The idea is that the momentum transfer in a turbulent flow is dominated by the mixing caused by large energetic turbulent eddies [45], whereas the turbulent shear stress is related linearly to the mean strain rate as in a laminar flow and can be written as:

$$-\rho \overline{u_i' u_j'} = \mu_t \left(\frac{\partial \overline{u}_i}{\partial x_j} + \frac{\partial \overline{u}_j}{\partial x_i} \right) - \frac{2}{3} \left(\rho k + \mu_t \frac{\partial \overline{u}_k}{\partial x_k} \right) \delta_{ij} \tag{2.53}$$

Where, k is the turbulent kinetic energy and μ_t presents the eddy viscosity. The eddy viscosity is not a physical characteristic of fluids, but it depends on the local flow condition and strongly on the flow history effects [45].

Applying the Boussinesq hypothesis, the dynamic viscosity μ in the momentum equation (2.50) is replaced by the sum of a laminar and a turbulent viscosity:

$$\mu = \mu_l + \mu_t \tag{2.54}$$

The laminar viscosity μ_l can be calculated from Sutherland formula [45]:

$$\mu_l = \frac{1.45 \cdot T^{\frac{3}{2}}}{T + 110} \cdot 10^{-6} \tag{2.55}$$

Analog to the viscosity calculation, the thermal conductivity can be obtained from:

$$\lambda = \lambda_l + \lambda_t = c_p \left(\frac{\mu_l}{\text{Pr}_l} + \frac{\mu_t}{\text{Pr}_t} \right) \tag{2.56}$$

c_p denotes the specific heat capacity and Pr_t is the turbulent Prandtl number, which is generally assumed to be constant over the flow field [45] (e.g. for air 0.9).

The eddy viscosity approach is widely used in most of the engineering calculations, primarily due to relatively low computational costs related to "only" the calculation of the turbulent viscosity μ_t. The disadvantage of this concept is the assumption that μ_t is an isotropic scalar quantity, which is not exactly true [52]. Furthermore, according to Blazek [45] and Wilcox [53] the limitations of Boussinesq hypothesis are caused by the assumption of equilibrium between the turbulence and the mean strain field and by the independence on the system rotation. Taking into account a non-linear eddy-viscosity model the accurateness of calculation can be significantly improved, see Craft et al. [54] and Basara [8, 55].

2.3.2.1 Turbulence models

As mentioned before, the basic problem of the turbulence modelling is to find the influence of the six additional terms of the Reynolds stress tensor. Therefore, a large variety of different turbulence models have been developed and the research work is still going on, but it is fact that there is no turbulence model, which can reliably predict all kinds of turbulent flows [45]. Generally, there are four principal turbulence model groups:

- Algebraic

- One- and multiple-equation - first order closure

- Reynolds stress models (RSM) - second order closure

- Detached-Eddy Simulation (DES) and Large Eddy Simulation (LES)

The first order closure group of turbulence models is the most important for engineering applications. They are based on the above explained eddy-viscosity concept as well as on the improved non-linear eddy viscosity formulations. This group includes the one-equation Spalart-Allmaras model and the two-equation $k-\varepsilon$ and $k-\omega$ models. In the case of two-equation turbulence models, two additional transport equations – first for the turbulent kinetic energy k and second for the turbulence dissipation rate ε or the specific dissipation rate ω – are solved. The turbulent viscosity μ_t is computed as a function of k and ε. In the following, the two-equation $k-\varepsilon$ model is explained in detail.

The alternative approach to the eddy-viscosity concept is the Reynolds stress model (RSM), which solves the transport equation for each of the terms in the Reynolds stress tensor and an additional equation for the turbulence dissipation rate ε. This means that seven equations have to be solved in order to close the RANS equations for a 3D case. The advantage of RSM is that it is clearly superior in situations in which the turbulence anisotropy has a dominant influence on the mean flow [52], but comparing it with two-equation models, the RSM requires additional calculation time due to the increased number of the solved transport equations. Furthermore, the RSM may take more iterations to converge due to the strong coupling between the Reynolds stresses and the mean flow [52]. Therefore, the RSM model is seldom used for engineering relevant calculation, primarily due approximately 50-60% increased CPU time and a decrease of calculation stability.

2.3.2.1.1 $k - \varepsilon$ turbulence model

The $k - \varepsilon$ turbulence model was proposed by Launder and Spalding [56] in 1972 and it is the simplest "complete model" of turbulence, a semi-empirical model based on two separate transport equations for the turbulence kinetic energy k and its dissipation rate ε. The model is only valid for fully turbulent flows and the effects of molecular viscosity are negligible, due to the assumptions in the model derivation [52]. The model characteristics are robustness and reasonable accuracy for a large range of applications, which explain its popularity in engineering relevant calculations.

In the conventional CFD code Fluent [52], the turbulent kinetic energy k and its dissipation rate ε of the standard $k - \varepsilon$ turbulence model are obtained as follows:

$$\frac{\partial \rho k}{\partial t} + \frac{\partial \rho k u_i}{\partial x_i} = \frac{\partial}{\partial x_j}\left[\left(\mu + \frac{\mu_t}{\sigma_k}\right)\frac{\partial k}{\partial x_j}\right] + P_k - \rho\varepsilon - G_b - Y_M + S_k \qquad (2.57)$$

$$\frac{\partial \rho \varepsilon}{\partial t} + \frac{\partial \rho \varepsilon u_i}{\partial x_i} = \frac{\partial}{\partial x_j}\left[\left(\mu + \frac{\mu_t}{\sigma_\varepsilon}\right)\frac{\partial \varepsilon}{\partial x_j}\right] + C_{1\varepsilon}\frac{\varepsilon}{k}\left(P_k + C_{3\varepsilon}G_b\right) - C_{2\varepsilon}\rho\frac{\varepsilon^2}{k} + S_\varepsilon \qquad (2.58)$$

Whereas, P_k presents the production of turbulent kinetic energy k due to the mean velocity gradients, G_b is the production of turbulent kinetic energy due to buoyancy, Y_M represents the contribution of the fluctuating dilatation in compressible turbulence to the overall dissipation rate, $C_{1\varepsilon}$, $C_{2\varepsilon}$, $C_{3\varepsilon}$, σ_k and σ_ε are the model constants, and S_k and S_ε represent the source terms [52]. The production of turbulent kinetic energy is defined as follows:

$$P_k = -\rho\overline{u_i' u_j'}\frac{\partial u_j}{\partial x_i} \qquad (2.59)$$

Taking into account Boussinesq's hypothesis, the production term is given:

$$P_k = -\mu_t S^2 \text{ with } S \equiv \sqrt{2S_{ij}S_{ij}} \qquad (2.60)$$

Whereas, S represents the mean rate of strain tensor. By the definition of a non-zero gravity field and a non-zero temperature gradient (or density), the production calculation of turbulent kinetic energy due to buoyancy effect occurs as follows:

$$G_b = \beta g_i \frac{\mu_t}{\Pr_t}\frac{\partial T}{\partial x_i} \qquad (2.61)$$

In equation (2.61) $\Pr_t$ is the turbulent Prandtl number (default value 0.85), g_i is the gravitational vector in i-th direction, and β is the thermal expansion coefficient defined as:

28

$$\beta = -\frac{1}{\rho}\left(\frac{\partial \rho}{\partial T}\right)_p \tag{2.62}$$

For ideal gases, the production of turbulent kinetic energy due to buoyancy is reduced to:

$$G_b = -g_i \frac{\mu_t}{\rho \operatorname{Pr}_t} \frac{\partial \rho}{\partial x_i} \tag{2.63}$$

In the equation (2.58) of turbulence dissipation rate the buoyancy term is determined by the model constant $C_{3\varepsilon}$, which is not specified, but it is calculated according to Henkes et al. [57] as follows:

$$C_{3\varepsilon} = \tanh\left|\frac{v}{u}\right| \tag{2.64}$$

Where, v is the velocity component parallel to the gravitational vector and u is the velocity component normal to the gravitational vector.

At high Mach-number flow, the compressibility influences the turbulence through so-called *dilatation dissipation*. In order to include this effect when the compressible form of the ideal gas law is applied, the conventional CFD code Fluent [52] adds an additionally dilatation dissipation term Y_M in equation (2.57) , which is modeled according to Sarkar and Balakrishnan [58]:

$$Y_M = 2\rho\varepsilon M_t^2 \text{ with } M_t = \sqrt{\frac{k}{c^2}} \text{ and } c = \sqrt{\gamma R T} \tag{2.65}$$

The model constants $C_{1\varepsilon} = 1.44$, $C_{2\varepsilon} = 1.92$, $C_\mu = 0.09$, $\sigma_k = 1.0$ and $\sigma_\varepsilon = 1.3$ were proposed by Launder and Spalding [56], which have been determined from experiments and work practically well for a wide range of technical applications.

2.4 Spray modeling

Applying the above presented RANS equations together with the turbulence modeling equations, the gas motion inside IC-engines is completely described. For the spray calculation, the Discrete Droplet Method (DDM) proposed by Dukowicz [59] –also called Discrete Phase Model (DPM) in the conventional CFD code Fluent [52] – is used, which follows the Euler-Lagrange approach. In contrast to fluid motion, which is treated as a continuum by solving the time averaged Navier-Stokes equations, the dispersed phase in a calculation domain is solved by tracking a large number of particles, bubbles, or droplets (further only *particles*), taking into account the momentum, mass, and energy exchange with the fluid phase as well. This method of droplet modeling requires a statistical problem formulation, whereas a spray is represented by a finite number of particles. Each computed particle is considered to represent a group of particles (particle *parcel*) with an exact number of particles and identical characteristics [59], such as size, position, velocity, temperature, density etc. This means that it is necessary to calculate only one representative particle of the particle group, which further reduces

the computational effort. According to Dukowicz [59], applying this method the problem of numerical diffusion and resolution in the vicinity of the injector is eliminated. Furthermore, the required particle number is not excessive in order to achieve acceptable accuracy and due to particle limitation to a part of the mesh, the computational effort is not time consuming.

At the beginning, it is assumed that the particle initial conditions are known, such as particle size, position, velocity etc. For instance, in the case of a liquid spray, the initial breakup or injector is not considered and the complete particle mass is presented in liquid form. In the course of time and dependent on the ambience condition, the mass and the energy exchange occurs between the fluid phase and the particle. The evaporated mass will be transferred to the continuum phase. Therefore, two sets of equations are individually solved, one set for the gas and the other for the particles. According to Dukowicz [59], the coupling between these equations will be realized applying two mechanisms, the gas displacement by the volume occupied by the particles and the momentum interchange between the particles and the gas.

2.4.1 Transport of droplets

The particle trajectory is written in a Lagrangian reference frame and it can be obtained by integration of force balance on a particle, i.e. the particle inertia with the forces acting on the particle. For the x direction in Cartesian coordinates is given [52]:

$$\frac{du_p}{dt} = F_D \cdot \left(u - u_p\right) + \frac{g_x\left(\rho_p - \rho\right)}{\rho_p} + F_x \qquad (2.66)$$

Where F_x presents any additional specific force term (force/unit particle mass), $F_D \cdot \left(u - u_p\right)$ is the drag force per unit particle mass, u is the fluid flow velocity, u_p is the particle velocity, μ is the molecular fluid viscosity, ρ is the fluid density, ρ_p is the particle density, and g_x is the gravity term in x direction. In the conventional CFD code Fluent [52], the drag force is given:

$$F_D = \frac{18\mu}{\rho_p d_p^2} \frac{C_D \, \text{Re}_p}{24} \qquad (2.67)$$

Here, d_p is the particle diameter, C_D is the drag coefficient, and Re_p is the relative Reynolds number of the particle defined as:

$$\text{Re}_p = \frac{\rho d_p \left|u_p - u\right|}{\mu} \qquad (2.68)$$

The drag coefficient C_D is a function of Reynolds number and it is obtained dynamically according to Schiller and Naumann [60] and Liu et al. [61]:

$$C_D = \begin{cases} \dfrac{24}{\text{Re}_p}\left(1 + \dfrac{1}{6}\text{Re}_p^{2/3}\right) & \rightarrow \quad \text{Re}_p \leq 1000 \\ 0.424 & \rightarrow \quad \text{Re}_p > 1000 \end{cases} \tag{2.69}$$

In equation (2.66), F_x represents additional forces in the particle force balance. The first is the so-called *virtual mass force,* which is needed to accelerate the fluid surrounding the particle [52] and it is given as:

$$F_x = \frac{1}{2}\frac{\rho}{\rho_p}\frac{d}{dt}\left(u - u_p\right) \tag{2.70}$$

Additional forces, which according to Fluent [52] can be also included in the additional force term F_x in the equation (2.66) are: the *particle rotation force* (the force which arises by flow modeling in rotating frames of reference), the *thermophoretic force* (a phenomenon where two small particles are subjected to the force of a temperature gradient), the *Brownian force* (the effect of Brownian motion is included, which presents a seemingly random particle movement in a fluid), and the *Saffman's lift force* (the lift due to shear).

2.4.2   Coupling method

The interaction between discrete and continuum phase is realized by a so-called *two-way* coupling. This coupling occurs by alternately solving the discrete and continuous phase equations until in both phases the exchange of the heat, the mass, and the momentum from the particle to the continuous phase and vice versa is in equilibrium [52].

2.4.2.1   Momentum exchange

The momentum exchange is obtained for each control volume and a particle which is situated inside by the following equation in the conventional CFD code Fluent [52]:

$$F = \sum\left(\frac{18\mu C_D \text{Re}_p}{\rho_p d_p^2 24}\left(u_p - u\right) + F_{other}\right)\dot{m}_p \Delta t \tag{2.71}$$

Here $\dot{m}_p$ presents the mass flow rate of the particles, F_{other} are other specific interaction forces (force/unit particle mass), and Δt is the time step. In the continuous phase, the momentum exchange appears as a momentum source, see equation (2.35).

2.4.2.2   Heat exchange

The heat exchange can be determined as the change in thermal energy of a particle which is situated in a cell volume and it occurs over the energy source, see equation (2.35). In Fluent [52], this change is obtained as follows:

$$Q = \left(m_{p_{in}} - m_{p_{out}}\right)\cdot\left[-H_{lat_{ref}} + H_{pyrol}\right] - m_{p_{out}}\int_{T_{ref}}^{T_{p_{out}}} c_{p_p} dT + m_{p_{in}}\int_{T_{ref}}^{T_{p_{in}}} c_{p_p} dT \tag{2.72}$$

Where $m_{p_{in}}$ is the particle mass on cell entry, $m_{p_{out}}$ on cell exit, c_{p_p} is the particle heat capacity, H_{pyrol} is the heat of pyrolysis as volatiles are evolved, $T_{p_{in}}$ is the particle temperature on cell entry, $T_{p_{out}}$ on cell exit, T_{ref} it the reference temperature for enthalpy and $H_{lat_{ref}}$ is latent heat at reference conditions. The latent heat at the reference condition is computed as the difference of the liquid and gas formation enthalpies [52], and related to the latent heat at the boiling point it can be calculated as follows:

$$H_{lat_{ref}} = H_{lat} - \int_{T_{ref}}^{T_{bp}} c_{p_g} dT + \int_{T_{ref}}^{T_{bp}} c_{p_p} dT \qquad (2.73)$$

Here is c_{p_g} the heat capacity of gas product species, T_{bp} the boiling point temperature, and H_{lat} the latent heat at the boiling point temperature.

2.4.2.3 Mass exchange

The mass exchange is calculated as the source mass S_c in the continuous phase continuity equation (2.34) and simultaneously as the chemical species source S_{ϕ_k} in the species transport equations (2.45). The mass source is given as follows:

$$S_C = \frac{\Delta m_p}{m_{p,0}} \dot{m}_{p,0} \qquad (2.74)$$

The indices p and 0 indicate the particle and the start condition respectively.

2.4.2.4 Droplet inert heating or cooling

In the case when the particle temperature is less than the vaporization temperature T_{vap} the inert particle heating or cooling effect is started. In order to determine the particle temperature $T_p(t)$, the heat balance, taking into account the convective heat transfer and the radiation absorption or emission at the particle surface, is obtained as:

$$m_p c_p \frac{dT_p}{dt} = h_{CHTC} A_p (T_\infty - T_p) + \varepsilon_p A_p \sigma (T_R^4 - T_p^4) \qquad (2.75)$$

Here is A_p the surface particle area, T_∞ the local temperature of the continuous phase, h_{CHTC} the convective heat transfer coefficient, ε_p particle emissivity, σ Stefan-Boltzmann constant and T_R the radiation temperature. The radiation heat transfer is taken into account only in the case when the radiation model is used, e.g. for the combustion process simulation. The convective heat transfer coefficient is calculated from the Nusselt number, named after the German engineer *Ernst Kraft Wilhelm Nusselt* (1882-1957), which presents the ratio of convective to conductive heat transfer across a boundary. According to Ranz and Marshall [62] the convective heat transfer coefficient for a droplet can be obtained from following relation:

$$Nu = \frac{h_{CHTC}\, d_p}{\lambda_\infty} = 2.0 + 0.6\, \text{Re}_p^{1/2}\, \text{Pr}^{1/3} \qquad (2.76)$$

Where, λ_∞ presents the thermal conductivity of the continuous phase, d_p is the particle diameter, Re_p is the relative Reynolds number of the particle, and Pr is Prandtl number of the continuous phase.

Finally, the calculated heat loss or increase of a particle is transferred to the continuous phase as a source term in the energy equation.

2.4.2.5 Droplet vaporization

The vaporization process of a droplet is onset in the case when the droplet (particle) temperature T_p reaches the vaporization temperature T_{vap} and takes on until it reaches the boiling temperature T_{bp} (so-called boiling point). When the vaporization process is started, the vaporization takes place even if the droplet temperature falls below the vaporization temperature and the process will be stopped only if the droplet temperature falls below the dew point [52]. In the case when the droplet temperature reaches the boiling temperature, the droplet vaporization is controlled by the boiling rate, see chapter 2.4.2.6.

In the conventional model of the CFD code Fluent [52] the vaporization rate is defined by the gradient diffusion of the droplet vapor flux into the gas phase related to the gradient of the vapor concentration between the droplet surface and the bulk gas:

$$N_i = k_c \left(C_{i,s} - C_{i,\infty} \right) \qquad (2.77)$$

Here is N_i the molar vapor flux in [kmol/m²-s], k_c is the mass transfer coefficient in [m/s], $C_{i,s}$ is the vapor concentration at the droplet surface in [kmol/m³], and $C_{i,\infty}$ is the vapor concentration in the bulk gas in [kmol/m³]. The vapor concentration at the droplet surface is obtained from the ideal gas law assuming that the partial vapor pressure at the interface is equal to the saturated vapor pressure p_{sat} at the droplet temperature T_p, and that the vapor concentration in the bulk gas is calculated likewise. Taking into account the local bulk mole fraction of species X_i obtained from the equation solution for species i, $C_{i,s}$ and $C_{i,\infty}$ are given as follows:

$$C_{i,s} = \frac{p_{sat}(T_p)}{R T_p} \quad \text{and} \quad C_{i,\infty} = X_i \frac{p}{R T_\infty} \qquad (2.78)$$

Where R is the universal gas constant, p is the local absolute pressure, and T_∞ is the local bulk gas temperature. The mass transfer coefficient k_c is obtained from the Sherwood number (also called the mass transfer Nusselt number), named after the American chemical engineer *Thomas Kilgore Sherwood* (1903–1976), see Ranz and Marshall [62]:

$$Sh = \frac{k_c d_p}{D_{i,m}} = 2.0 + 0.6 \, \text{Re}_p^{1/2} \, Sc^{1/3} \tag{2.79}$$

Whereas, $D_{i,m}$ presents the bulk vapor diffusion coefficient in [m²/s] (mass diffusivity) and Sc the dimensionless *Schmidt number*, named after the German engineer *Ernst Heinrich Wilhelm Schmidt* (1892-1975), which is defined as the ratio of the viscous diffusion rate and the mass diffusion rate:

$$Sc = \frac{\mu}{\rho D_{i,m}} \tag{2.80}$$

Finally, the reduced droplet mass due to vaporization process is obtained as follows:

$$m_p^{n+1} = m_p^n - N_i A_p M_i \Delta t \tag{2.81}$$

Here M_i presents the molecular weight of species i and m_p^{n+1} the new droplet mass at time $t + \Delta t$. The evaporated droplet mass is transported to the continuous phase as the source in the species transport equation.

2.4.2.6 Droplet boiling

When the droplet temperature T_p reaches the boiling temperature T_{bp} (boiling point), the change of droplet diameter d_p is obtained according to Kuo [63] with following equation:

$$\frac{d(d_p)}{dt} = \frac{4\lambda}{\rho_p c_{p,\infty} d_p} \left(1 + 0.23\sqrt{\text{Re}_p}\right) \cdot \ln\left[1 + \frac{c_{p,\infty}\left(T_\infty - T_p\right)}{h_{fg}}\right] \tag{2.82}$$

Where $c_{p,\infty}$ present the gas heat capacity and h_{fg} the latent heat in [J/kg]. When the radiation process is included in the calculation, equation (2.82) will be accordingly modified, see Fluent [52]. Furthermore, when the boiling process takes place, the droplet temperature is set to a constant value, the boiling temperature T_{bp}. The required vaporization energy appears as a negative source in the energy equation of the continuous phase and the evaporated liquid is transported to the gas phase as a source of species in the species transport equation.

2.4.3 Droplet break-up

Generally, regarding the droplet break-up a primary and a secondary break-up can be distinguished. The primary break-up process occurs directly after the liquid exits the injector nozzle. In this phase, the spray still has the form of liquid ligaments, which further break up to droplets. The form of the spray during the primary break-up basically depends on the properties, which the spray already gets inside the nozzle, e.g. concerning turbulence and cavitation. According to Merker et al. [14] the primary break-up is irrelevant in a gasoline direct injection system, due to a low level of turbulence and cavitation in contrast to diesel injection systems, which clearly have higher rail pressure during the injection process. Therefore, for a

GDI injector the primary break-up is not modeled, but it is replaced by a nozzle model adapted to the injector typ. A nozzle model requires the spray start condition, such as temperature, velocity, penetration, droplet diameter, position, direction etc. Some of these start condition data, such as droplet diameter and penetration, should be taken from measurement data, in order to model the injection process correctly. Other data, e.g. velocity, can be calculated from the data of the liquid media and the pressure difference Δp applying the Bernoulli equation:

$$v_p = c_q \sqrt{\frac{\Delta p}{\frac{1}{2}\rho_p}}$$

(2.83)

Where c_q is the flow coefficient and, according to Stanciu [64], can be described as a function of the Reynolds number and the pressure difference.

After the primary break-up, where the spray has a form of liquid ligaments and a high liquid concentration, the secondary break-up occurs. This process already takes place very close to the nozzle attached to the liquid core. The break-up process is mainly caused by the interaction between liquid and gas phases. In this phase, the aerodynamic forces, the angle of joint, the impulse and the droplet collision have an important influence on the droplet atomization. Prime liquid ligaments and droplets are further atomized until the acting forces are stabilized. Due to a decreasing liquid concentration, the droplet collision becomes irrelevant and the aerodynamic forces have a dominant influence on the droplet atomization. In the course of time, the droplets get a spherical form caused by surface tension. In order to characterize the interaction between liquid and gas phase and the droplet atomization, the dimensionless *Weber number*, named after the German mechanics professor *Moritz Gustav Weber* (1871-1951), is useful. The Weber number is defined by the ratio of the inertia force $\rho \cdot d_p \cdot v_p^2$ and the surface tension σ and it is given as follows:

$$We = \frac{\rho \cdot d_p \cdot v_p^2}{\sigma}$$

(2.84)

Here is ρ the gas density, d_p the droplet diameter, and v_p the droplet velocity. The force, which causes the droplet atomization, quadratically increases with the relative velocity between the droplet and the gas, whereas the surface tension has a damping effect [64]. Furthermore, the liquid medium viscosity has an influence on the droplet stability, due to the damping effect of droplet vibration and droplet deformation. The Weber number is an important characteristic for the description of droplet atomization and it is used for the droplet break-up modeling, as the critical Weber number describes the limit below which the droplets will not be atomized anymore. A dependence of the Weber number and the type of atomization mechanism can be found in [37] and [64].

In conventional CFD codes several droplet atomization models can be found which are applicable for different criteria, such as injection systems and rail pressure levels. They are the Chu-Break-up model [65], the GM-model proposed by Reitz and Diwakar [66], the WAVE-model of Reitz [67] and Liu and Reitz [68], the TAB-model of O'Rourke and Amsden [68], the FIPA-model of Baritaud [70], the Huh-Gosman [71] and the KH-RT model of Patterson

and Reitz [72]. According to Stanciu [64], AVL Fire [73], and Petermeier [31], the well suitable break-up models for the GDI spray modeling are Chu, TAB, WAVE, FIPA and Huh-Gosman. In the conventional CFD code Fluent [52], which is used in this work, <u>only</u> the TAB and the WAVE break-up models are integrated, so that these two models are further taken into consideration. Nevertheless it secures that the Huh-Gosman break-up model is best suitable for a multi-hole nozzle injector used in this work, see Stanciu [64] and AVL Fire [73].

The Taylor Analogy Breakup model (TAB model) of O'Rourke and Amsden [68] is based on Taylor's analogy between an oscillating and distorting droplet and a spring mass system given in time. For instance, with growing droplet oscillations up to a critical value, the droplet will break up into a smaller number of droplets. The new small droplets are named the "child" droplets, whereas the primal droplets are named "parent". The TAB model is usually used for low Weber number sprays, whereas according to Fluent [52], the Weber number should be smaller than hundred (We<100).

An alternative model to the TAB model, suitable for high Weber number sprays (We>100) is the WAVE break-up model of Reitz [67] and Liu and Reitz [68]. Generally, the Weber number is a reliable indicator for the atomization of the spray and it is helpful for the choice of the atomization models. According to Basshuysen [37] the Weber number greater than hundred indicates a "catastrophic droplet atomization", which appears in the flow where aerodynamic forces dominate and essentially influence the breakup of droplets. Exactly these effects are taken into account by the WAVE break-up model, where the breakup of the droplet is induced by the relative velocity between the gas and the liquid phase of the injected fuel. Furthermore, the model also assumes that the break-up time and the resulting droplet size are related to fast growing Kelvin-Helmholz instability, whereas the wavelength and growth rate of this instability are used to predict the details of the newly formed droplets [52].

2.4.4   Droplet wall interaction

Spray-wall interaction is an important part of the mixture formation process in an internal combustion engine. Basically, two different spray-wall interaction models can be distinguished in simulation, the *wall-jet* and the *wall-film*. The wall-jet model takes into account that the wall is warm and dry, whereas the wall-film model considers a warm wall which can be wetted with a liquid medium.

In the wall-film model, the impinging droplets are used to model the thin wall-film over a surface. It is assumed that the film thickness is less than 500 microns due to the assumption of a linear velocity profile in the film. This model was originally devolved for intake manifold fuel injection engines with low pressure injection systems and low Weber numbers respectively. For the calculation of the wall-film the CFD code Fluent [52] takes following major topics into account: the initial droplet impact with the wall boundary, subsequent droplet tracking on the boundary surface, calculation of additional film variables (e.g. film thickness), and the coupling with the gas phase. The initial droplet impact on the wall modeling is based on the work of Stanton and Rutland [74] and O'Rourke and Amsden [75], where four different regimes depending on the impact of dimensionless energy and the wall temperature (see Figure 4) can be distinguished: stick, rebound, spread, and splash.
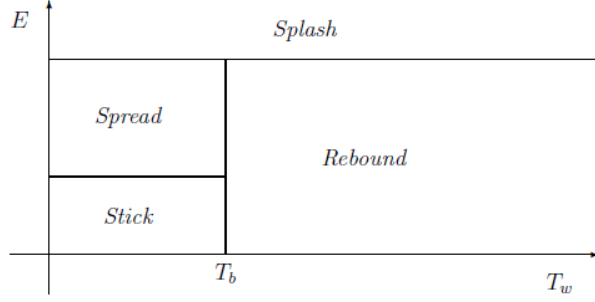
Figure 4: **Wall interaction criterion according to Fluent [52]**

In Figure 4 it can be seen that below the boiling temperature T_b, the impinging liquid droplet can stick, spread or splash, and above T_b rebound or splash. The impact energy E, which is required in order to determinate the regime, is calculated from equation (2.85), where ρ_p is the droplet density, v_r is the particle relative velocity in the frame to the wall ($v_r = v_p - v_w$), d_p is the droplet diameter, σ is the surface tension, δ_{bl} is the boundary layer thickness defined by $\delta_{bl} = d_p / \sqrt{\text{Re}}$ (whereas, the Reynolds number is calculated with relative velocity v_r) and h_0 is the film thickness.

$$E^2 = \frac{\rho_p v_r^2 d_p}{\sigma} \left(\frac{1}{\min(h_0 / d_p) + \delta_{bl} / d_p} \right) \tag{2.85}$$

In cases where the dimensionless energy is less than 16 [52], the sticking regime is applied, where the droplet velocity is set to the wall velocity. In the spreading regime, the initial direction and velocity of the droplet are defined using the wall-jet model, so that the moving droplet has a particular velocity along the boundary surface (see description of wall-jet model). In cases with a droplet energy above 57.7 [52], the splashing regime is active. The impinging droplet splashes on the surface and the new droplets are created. The number of new parcels (particle group) is defined by the user and it ranges between zero (no-splashing effect) and ten. The properties of the newly created droplets are taken from the experimental data integrated in the wall-film model. For wall temperatures above the liquid boiling temperature, the impinging droplets are rebound from the wall. As mentioned before, in the CFD code Fluent [52] the wall film covering a surface is created with the impinging droplets and for each droplet group (parcel), the conservation equations for mass, momentum, and energy are solved according to the method proposed by O'Rourke and Amsden [76].

For the modeling of a spray interaction with a hot wall (e.g. warm engine simulation) applying a high pressure injection system with a high Weber number, the second spray-wall interaction model "wall-jet" is more appropriate. This model was originally devolved for diesel injection systems with high rail pressures and high Weber numbers respectively. In this model, it is assumed that the impinging droplet responds according to its Weber number, whereas, according to Petermeier [31], the critical Weber number is 80. For Weber numbers below 80, the impinging droplet is rebound from the wall whereas above 80 the droplet slides over the boundary surface. The droplet direction and droplet velocity after the droplet-wall interaction are given by the resulting momentum flux as a function of the impingement angel and the Weber number [52].

In Petermeier [31] an evaluation of these two spray-wall interaction models can be found together with a comparison between CFD simulation results and measurement data obtained from a spectroscopic method - Laser-Induced Fluorescence (LIF) - in the case of a 4-stroke GDI engine with a wall-guided concept. The presented results show that the wall-film model tends to a strong dissipation of the droplet impulse so that the droplet transport over the sur-

face is clearly slower compared to the wall-jet model and the measurement results. The author views the advantage of the wall-film model as a possibility to calculate the heat transfer between the liquid film and the surface. Trattner [13] also shows a comparison of different spray-wall interaction models and experimental data. The author clearly shows that the wall-jet model is more appropriate for high pressure injection systems with high Weber numbers. An impressive depiction of the droplet moving over the piston surface is presented as well. In the case of a low Weber number, e.g. from reflected droplets of the piston to the cylinder wall, it can be stated that the wall-jet model fails, especially in the case of a low wall temperature (e.g. cool engine simulation). In this case, the wall-jet model should be used for the spray-wall interaction prediction with the piston surface and the wall-film model for the interaction with the cylinder wall. In contrast to 4-stroke engines, the spray-wall interaction in a 2-stroke engine is less important, primary due to a stronger interaction between spray and flow caused by the air-guided concept. The injected fuel inside the cylinder volume can be also transported to the crank case volume in the closing phase of the intake ports. Due to relative small droplet velocities and low Weber numbers the droplets inside the crank case volume can form the fuel film, so that the wall-film model should be used for the crank case surfaces. Due to high Weber numbers and engine simulations in warm conditions, the wall-jet model is chosen for all cylinder volume surfaces. For higher liquid droplet concentrations inside the crank case volume, the wall-film model is used for the crank case surfaces in this work.

2.5 Computational fluid dynamics

Computational fluid dynamics (CFD) uses numerical methods to calculate the fluid flows with computer techniques. The considered spatial domain of interest is discretised into a finite number of small cells (volumes), which altogether form the computational mesh (grid), and the motion equations are solved for each cell.
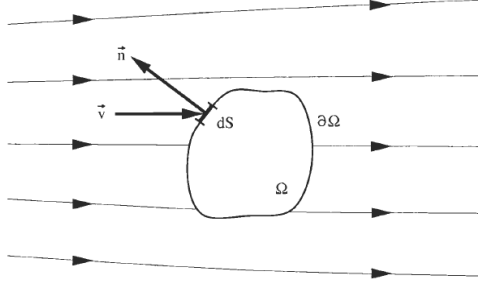
Figure 5: **Finite control volume [45]**

A practicable way to describe the physical properties inside a volume is to define a so-called *finite control volume* Ω, which is defined as an arbitrary finite region of the flow bounded with the closed surface $\partial\Omega$ fixed in space [45], see Figure 5. The closed surface $\partial\Omega$ consists of a finite number of surface elements dS with outward pointing unit normal vectors $\vec{n}$. The conservation law of a transported quantity inside this volume can be obtained by balancing the quantity crossing the boundary surfaces the so-called *fluxes*, any internal sources and the temporal gradient of the quantities. Generally, for the flux transport over a surface the *convective* and the *diffusive* fluxes can be distinguished. Taking into account the integral formulation of the Navier-Stokes equations, the general conservation law of a vector quantity can be written as follows:

$$\frac{\partial}{\partial t}\int_{\Omega}\vec{U}\,d\Omega + \oint_{\partial\Omega}\left(\vec{F_c}-\vec{F_v}\right)dS = \int_{\Omega}\vec{Q}\,d\Omega \tag{2.86}$$

The vector $\vec{U}$ is the vector of *conservative variables*, which consists of three dimensions for the velocity and altogether has five components; the vectors $\vec{F_c}$ and $\vec{F_v}$ present the two flux vectors, namely the *vector of convective fluxes* and the *vector of viscous (diffusive) fluxes*, see equation (2.87). Where V presents the velocity normal to the surface element dS obtained from the scalar product of the velocity vector and the unit normal vector, see equation (2.88) and H is the total enthalpy given by equation (2.89). In the definition of the vector of viscous fluxes, τ_{ij} and Θ_i describe the work of the viscous stresses and the heat conduction in the fluid, see equation (2.90). Finally, $\vec{Q}$ is the source vector with $\vec{f_e}$ external force vector, e.g. mass forces, and $\dot{q_h}$ the heat flux, e.g. radiation, chemical reaction etc.

$$\vec{U} = \begin{bmatrix} \rho \\ \rho u \\ \rho v \\ \rho w \\ \rho E \end{bmatrix}, \ \vec{F_c} = \begin{bmatrix} \rho V \\ \rho u V + n_x p \\ \rho v V + n_y p \\ \rho w V + n_z p \\ \rho H V \end{bmatrix}, \vec{F_v} = \begin{bmatrix} 0 \\ n_x\tau_{xx}+n_y\tau_{xy}+n_z\tau_{xz} \\ n_x\tau_{yx}+n_y\tau_{yy}+n_z\tau_{yz} \\ n_x\tau_{zx}+n_y\tau_{zy}+n_z\tau_{zz} \\ n_x\Theta_x+n_y\Theta_y+n_z\Theta_z \end{bmatrix} \text{ and } \vec{Q} = \begin{bmatrix} 0 \\ \rho f_{e,x} \\ \rho f_{e,y} \\ \rho f_{e,z} \\ \rho\vec{f_e}\cdot\vec{v}+\dot{q_h} \end{bmatrix} \tag{2.87}$$

$$V = \vec{v}\cdot\vec{n} = n_x u + n_y v + n_z w \tag{2.88}$$

$$H = h + \frac{|\vec{v}|^2}{2} = E + \frac{p}{\rho} \tag{2.89}$$

$$\begin{aligned}
\Theta_x &= u\tau_{xx} + v\tau_{xy} + w\tau_{xz} + \lambda\frac{\partial T}{\partial x} \\
\Theta_y &= u\tau_{yx} + v\tau_{yy} + w\tau_{yz} + \lambda\frac{\partial T}{\partial y} \\
\Theta_z &= u\tau_{zx} + v\tau_{zy} + w\tau_{zz} + \lambda\frac{\partial T}{\partial z}
\end{aligned} \tag{2.90}$$

As explained in chapter 2.3.1, the Navier-Stokes equations describe the behavior of a viscous fluid, but in some cases, such as high Reynolds number flows, the viscous stresses and heat flux can be neglected, so that equation (2.86) can be reduced to:

$$\frac{\partial}{\partial t}\int_\Omega \vec{U}d\Omega + \oint_{\partial\Omega}\vec{F}_c dS = \int_\Omega \vec{Q}d\Omega \tag{2.91}$$

Equation (2.91) is known in literature as *Euler equations*, named after the Swiss mathematician and physicist *Leonhard Euler* (1707-1783), which describe pure convective flow of an inviscid fluid and convective transport of quantities. The Euler equations are able to describe important phenomena such as shocks and expansion waves, but due to increasing computer power and due to growing requirements on the simulation result quality these equations are seldom used for 3D simulation at low Mach numbers. However, according to Blazek [52] and Toro [77], today these equations are still widely used as the basis for the development of discretisation methods and boundary conditions as well as for 1D CFD simulations.

In the case of a 1D CFD simulation, such as simulation of ducts, pipes, shock tubes and nozzles, only one dimension is considered, whereas the area variations are included as a quasi two dimensional system with a geometric source term as a function of space. According to Toro [77], the most common case is that the cross-sectional area depends only on the considered direction, for which the conservative variable vector $\vec{U}$, the convective flux vector $\vec{F}_c$, and the source vector $\vec{Q}$ (where the external force and the heat flux is not included) can be written as follows:

$$\vec{U} = \begin{bmatrix} \rho A \\ \rho u A \\ \rho E A \end{bmatrix}, \quad \vec{F}_c = \begin{bmatrix} \rho u A \\ (\rho u^2 + p)A \\ (E + p)\rho u A \end{bmatrix}, \text{ and } \vec{Q} = \begin{bmatrix} 0 \\ p\frac{dA}{dx} \\ 0 \end{bmatrix} \tag{2.92}$$

This means that the equations, which describe the 1D flow through the ducts and pipes with area variation, can be interpreted as the usual one dimensional equation of gas dynamics with an additional source term. Today, the 1D code is still a good approach to assist the development process of engines, primary due to fast computation, high level of flexibility and a satisfying accurateness, as the flow inside pipes and ducts is very close to one dimensional.

2.5.1 Solution of governing equations

An analytical solution of the Navier-Stokes equations is only possible for some simplified flow problems. Therefore these equations have to be solved numerically for almost all industrially relevant applications, whereas today a huge number of solution methodologies exist. First of all, the considered domain of interest is divided into a large number of geometrical elements (so-called *cells*); a process well known as *computational grid or mesh build-up*. In the case of three dimensions, the mesh consists of tetrahedra, hexahedra, pentrahedra, or polyhedra; in two dimensions of triangles or quadrilaterals; and in one dimension of volume with two neighbours. For each cell the discretized governing equations are applied and in almost all CFD codes the discretisation in space and in time occurs separately. The generated cells are used to evaluate the integral of the fluxes. In the following chapters, the spatial and temporal discretisation is discussed as well as same solving methods for the governing equations.

2.5.1.1 Spatial discretisation

Generally, for spatial discretisation schemes *finite difference*, *finite volume* and *finite element* methods can be distinguished. These methods are used to discretise the above mentioned governing equations on a computational grid. These grids can be further divided into *structured* and *unstructured* grids. The advantage of the structured grid is that it has a particular ordering, e.g. a neighbor cell can be easy identified by their indices (like i-1 or i+1), which clearly reduces the programming effort. The disadvantages are that the grid build-up becomes very expensive in the case of complex geometries. The unstructured grid overcomes this problem and today it is widely used for engineering relevant simulations. A so-called *hybrid grid* is a mix of all cell types, e.g. in the case of a 3D computational grid: tetrahedral, hexahedra, prisms and pyramids, and offers the largest flexibility in the treatment of complex industrially relevant geometries.

2.5.1.1.1 Finite difference method

The first method, which applied the numerical solution of governing equations, is the finite difference method (FDM) employed by Euler already in 1768 [45]. In this method, the Taylor series expansion, named after the English mathematician *Brook Taylor* (1685-1731), is used for the discretisation of derivatives of the variables. Essential advantages are its simplicity and the possibility to easily obtain higher order approximation and accuracy. Otherwise, the disadvantage is that this method needs a structured grid, so that the application is strongly limited for industrially relevant simulations. More details about FDM can be found in Anderson et al. [79].

2.5.1.1.2 Finite element method

The finite element method (FEM) was first employed for structural analysis. In the 1990s the FEM became popular for solving Navier-Stokes equations and fluid flow. In this method the physical space is divided into tetrahedral (3D case) or into triangular (2D case) elements, so that the FEM can only be used for unstructured grids. Furthermore, solving the Navier-Stokes equation applying the FEM, the equations are transformed from a differential into an equivalent integral form, see Blazek [45]. This integral form of the governing equation and the application for the unstructured grid make the FEM applicable for flow around complex forms, but due to high numerical effort in comparison with finite volume method (FVM), this method is seldom used in the conventional CFD codes. However, according to Blazek [45] some methods are taken from the FEM and are applied in the FVM, such as the treatment of the boundaries and the discretisation of viscous fluxes.

2.5.1.1.3 Finite volume method

The finite volume method is used in almost all CFD codes, primary due to the employment of the conservation law, the integral formulation of the Navier-Stokes equations, the flexibility for application for the structured and unstructured grids, as well as due to its feature that under certain conditions, the FVM is equivalent to the FDM or to the low order FEM [45]. The finite volume method was first proposed by McDonald [80] in 1971 applying this method for the simulation of a 2D inviscid flow. First, the considered physical space is divided into a finite number of arbitrary control volumes taking into account following requirements: the considered physical space is completely covered by the grid, no free space between the cells, and no overlapping cells. The control volume is introduced in order to evaluate the integrals of the convective and viscous fluxes as well as the source term. Considering another form of the time derivative of the conservative variable $\vec{U}$, the equation (2.86) can be written as follows:

$$\frac{\partial \vec{U}}{\partial t} = -\frac{1}{\Omega}\left[\oint_{\partial\Omega}\left(\vec{F}_c - \vec{F}_v\right)dS - \int_{\Omega}\vec{Q}\,d\Omega\right] \tag{2.93}$$

On the right side of equation (2.93), two integrals are visible; a surface integral which is approximated by a sum of the fluxes crossing the control volume faces and a source term integral. Taking into account an individual volume Ω_{CV}, whereas the index CV references the control volume, equation (2.93) can be transformed:

$$\frac{\partial \vec{U}_{CV}}{\partial t} = -\frac{1}{\Omega_{CV}}\left[\sum_{n=1}^{N_F}\left(\vec{F}_c - \vec{F}_v\right)_n \cdot \Delta S_n - \vec{Q}_{CV}\cdot\Omega_{CV}\right] = -\frac{1}{\Omega_{CV}}\vec{R}_{CV} \tag{2.94}$$

Where, N_F is the number of control volume faces and ΔS_n is the area of the face n. In literature can often be found that the fluxes and the source terms in the square bracket are called the *residual* and for an individual control volume is written in the vector form as $\vec{R}_{CV}$.

Solving equation (2.94), the first appearing problem is the storage location of the flow variables regarding the computational grid. According to Blazek [45], following strategies, which are still in use in the conventional CFD codes, can be distinguished for the finite volume schemes:

- Cell-centre scheme – all flow variables are stored in the cell center.

- Cell-vertex scheme with *median-dual* control volume – the flow variables are stored in grid vertices or nodes and the control volumes are defined connecting the surrounding elements, namely face-centroids and edge-midpoints.

In both above mentioned cases, all flow variables are stored on the same location, namely the conservative variable vector $\vec{U}$ as well as the dependent variables (p, T, c, etc.). This method is known in literature as the *co-located* grid scheme, see Blazek [45], Patankar [78], Anderson et al. [79] etc. An older method (the so-called *staggered* grid scheme) is the variable storage on different locations, whereas the pressure and the velocity components are saved on different locations; in order to damp oscillations and to prevent a decoupling of pressure and velocity.

The second appearing problem is the choice of the convective $\vec{F_c}$ and diffusive $\vec{F_d}$ fluxes evaluation method. The basic problem is related to the fact that the flow variables are not known on the face centroid locations, where the flux values have to be evaluated. Therefore, the fluxes or the flow variables have to be interpolated to the faces of a control volume. Generally, there are two possibilities to execute this interpolation:

- *Central* discretisation scheme – a method of arithmetic averaging.

- *Upwind* discretisation scheme – a method which includes the characteristics of the flow.

The central discretisation scheme has an advantage for the viscous flux calculation due to its physical nature. Applying this method on the structured Cartesian grid is simple. For unstructured grids, the viscous fluxes are best approximated using the Galerkin finite element method [45], even if the finite volume method is used. The convective flux calcualtion can also be carried out applying the central averaging method in order to evaluate the conservative variable and thus to calculate the flux on the face centroid position. Unfortunately, this method can lead to an odd-even decoupling (a generation of two independent solutions of the discretised equations) and an oscillation at the shocks [45]. Therefore, the upwind schemes are more appropriate for the convective flux calculation of physical properties of the Euler equations and are identical for structured and unstructured grids. The upwind schemes consider the wave propagation direction and can distinguish between upstream and downstream domain. In contrast to the central scheme, the upwind schemes are more accurate for the discontinuity description and for the boundary layer calculation, but go with a higher numerical effort respectively. In order to interpolate the flow variable on the face centroid location, higher order accuracy methods, such as *Quadratic Upstream Interpolation for Convective Kinematics* (QUICK) or *Monotone Upstream-Centred Schemes for Conservation Laws* (MUSCL), can be applied. The disadvantage is that the extension to second- or higher order accuracy is complex and implementation of limiter functions is necessary in order to damp the solution oscillations, which further can cause convergence problems with a high numerical effort. However, in the chapter 2.5.1.1.4 only upwind schemes are discussed including several variants.

2.5.1.1.4   Convective flux discretisation applying upwind schemes

According to Blazek [45], the upwind schemes for the convective flux calculation can be divided into four main groups:

- Flux-vector splitting (FVS)

- Flux-difference splitting (FDS)

- Total variation diminishing (TVD)

- Fluctuation-splitting (FS)

These schemes are developed in order to solve the one-dimensional Euler equations and they are also applicable for the 3D simulations, due to the rotational invariance of the Euler and Navier-Stokes equations, see Trescher [81]. This rotation is required only for the velocity vector, whereas density, total energy, and other scalar quantities are not affected.

2.5.1.1.4.1   Flux-vector splitting (FVS)

The FVS schemes are based on the decomposition of the convective fluxes in two parts. There are two groups of flux decomposition schemes. The first group is a decomposition according to the sign of characteristic variables introduced by Van Leer [82] and the second group a decomposition into a convective and a pressure part, such as *Advection Upstream Splitting Method* (AUSM) of Liou and Steffen [83] as well as a similar approach to the *Convective Upwind Split Pressure* (CUSP) of Jameson [84] etc.

For instance, Van Leer [82] proposed a method where the convective flux is split into a positive and a negative part according to the Mach number normal to the control volume face:

$$\vec{F}_c = \vec{F}_c^+ + \vec{F}_c^- \tag{2.95}$$

The second group proposed by Liou and Steffen [83] assume that the convective flux of the AUSM scheme consists of two physical parts, the convective and the pressure part:

$$\vec{F}_c = V\vec{U} + \begin{bmatrix} 0 \\ n_x p \\ n_y p \\ n_z p \\ 0 \end{bmatrix} \tag{2.96}$$

Where, V is the velocity component normal to the surface. Jameson [84] introduced an approach where the convective flux of the CUSP scheme is approximated as the average flux on both sides of the interface minus a stabilizing dissipation vector $\vec{D}$:

$$\vec{F}_c = \frac{\vec{F}_c(\vec{U}_R) + \vec{F}_c(\vec{U}_L)}{2} - \vec{D} \tag{2.97}$$

The stabilizing dissipation vector is obtained as a linear combination of the state vector differences $\vec{U}_R - \vec{U}_L$ and the flux vector differences $\vec{F}_{c_R} - \vec{F}_{c_L}$. The indices L and R describe the state of the left und the right side of the interface, whereas i (for the left) and $i+1$ (for the right) notation as well as $i+1/2$ for the interface position is also used in the literature.

2.5.1.1.4.2 Flux-difference splitting (FDS)
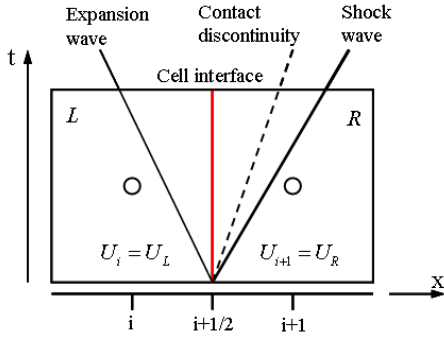
Figure 6: **Schematic illustration of the Riemann problem between two cells**

The FDS scheme was first proposed by Godunov [85] in the year 1959 leading to the introduction of the basic idea of the modern finite volume method. The basic idea of this approach is that the convective flux at an interface is calculated from the left and the right state by solving the Riemann problem. In this case, the information of the wave direction propagation (similar to the FVS scheme) as well as the waves themselves are also taken into consideration. In order to reduce the numerical effort and the scheme accuracy Roe [86] introduced in 1981 a solver which offers an exact solution of the Riemann problem between two cells, which contains two initial gas states at different pressures and densities separated by a contact discontinuity, see Figure 6. This solver is characterized by a high accuracy for boundary layers and a good resolution of shocks [45], so that it is presented for the 1D case in the next section in detail. The equation notation in this work is taken from Sanz [87].

The flux vector $\overrightarrow{F_c}$ at the cell interface position "i+1/2" (see Figure 6) can be calculated from one of three following equations:

$$\overrightarrow{F}_c = \frac{\overrightarrow{F}_{c,i} + \overrightarrow{F}_{c,i+1}}{2} - \frac{1}{2}|A| \cdot \left(\overrightarrow{U}_{i+1} - \overrightarrow{U}_i\right), \text{ or} \tag{2.98}$$

$$\overrightarrow{F}_c = \overrightarrow{F}_{c,i} + \left(R\frac{\Lambda - |\Lambda|}{2}L\right)_{i+1/2} \cdot \left(\overrightarrow{U}_{i+1} - \overrightarrow{U}_i\right), \text{ or} \tag{2.99}$$

$$\overrightarrow{F}_c = \overrightarrow{F}_{c,i+1} - \left(R\frac{\Lambda + |\Lambda|}{2}L\right)_{i+1/2} \cdot \left(\overrightarrow{U}_{i+1} - \overrightarrow{U}_i\right) \tag{2.100}$$

In equation (2.98), A represents the Jacobian matrix and can be written for the one-dimensional case as:

$$A = \frac{\partial F_c}{\partial U} = L^-\Lambda L, \tag{2.101}$$

with $R = L^-$ the Jacobian matrix is given by:

$$A^+ = R\Lambda^+L = R\frac{\Lambda + |\Lambda|}{2}L, \text{ respectively } A^- = R\Lambda^-L = R\frac{\Lambda - |\Lambda|}{2}L \tag{2.102}$$

The matrix $\Lambda^{\pm}$ is a diagonal matrix defined as:

$$\Lambda^{\pm} = \begin{vmatrix} \dfrac{|V \pm |V||}{2} & & \\ & \dfrac{(V+c) \pm |V+c|}{2} & \\ & & \dfrac{(V-c) \pm |V-c|}{2} \end{vmatrix} \tag{2.103}$$

The matrixes R and L are described as:

$$L = \begin{bmatrix} 1 - \dfrac{\gamma-1}{2} Ma^2 & (\gamma-1) \cdot \dfrac{V}{c^2} & -\dfrac{\gamma-1}{c^2} \\ \dfrac{c}{\rho} \cdot \left(\dfrac{\gamma-1}{2} Ma^2 - \dfrac{V}{c} \right) & \dfrac{1}{\rho} - \left(\dfrac{\gamma-1}{\rho} \cdot \dfrac{V}{c} \right) & \dfrac{\gamma-1}{\rho \cdot c} \\ \dfrac{c}{\rho} \cdot \left(\dfrac{\gamma-1}{2} Ma^2 + \dfrac{V}{c} \right) & -\dfrac{1}{\rho} - \left(\dfrac{\gamma-1}{\rho} \dfrac{V}{c} \right) & \dfrac{\gamma-1}{\rho \cdot c} \end{bmatrix} \tag{2.104}$$

$$R = \begin{bmatrix} 1 & \dfrac{\rho}{2c} & \dfrac{\rho}{2c} \\ V & \dfrac{\rho}{2c} \cdot (V+c) & \dfrac{\rho}{2c} \cdot (V-c) \\ \dfrac{V^2}{2} & \dfrac{\rho}{2c} \cdot \left(\dfrac{c^2}{\gamma-1} + \dfrac{V^2}{2} + V \cdot c \right) & \dfrac{\rho}{2c} \cdot \left(\dfrac{c^2}{\gamma-1} + \dfrac{V^2}{2} - V \cdot c \right) \end{bmatrix} \tag{2.105}$$

Where, Ma is the Mach number and c is speed of sound. In order to calculate the variables at the cell interface position "i+1/2" in equations (2.103), (2.104), and (2.105) the density ρ, the velocity V (the velocity component normal to the surface), and the speed of sound c are replaced by averaged weighted values. These particular mean values are built by using the square root of the densities $R_{i+1/2} = \sqrt{\rho_{i+1}/\rho_i}$:

$$\overline{\overline{\rho}}_{i+1/2} = \sqrt{\rho_{i+1}\rho_i} = R_{i+1/2} \cdot \rho_i \tag{2.106}$$

$$\overline{\overline{V}}_{i+1/2} = \frac{R_{i+1/2} \cdot V_{i+1} + V_i}{R_{i+1/2} + 1} \tag{2.107}$$

$$\overline{\overline{H}}_{i+1/2} = \frac{R_{i+1/2} \cdot H_{i+1} + H_i}{R_{i+1/2} + 1} \tag{2.108}$$

$$\overline{\overline{c}}_{i+1/2} = \sqrt{(\gamma - 1) \cdot \left(\overline{\overline{H}} - \frac{\overline{\overline{V}}^2}{2}\right)}, \text{ with the total enthalpy defined as: } H = \frac{\gamma}{\gamma - 1}\frac{p}{\rho} + \frac{V^2}{2} \tag{2.109}$$

Applying the above presented Roe's method for the solving the Riemann problem for a case when the expansion wave achieves $Ma \geq 1$, the linearised approximation via discontinuous jumps is incorrect. This arises in the form of unphysical, entropy violating discontinuous waves, see Toro [77]. A technique to avoid the expansion shock is so-called *entropy fix* modification proposed by Harten and Hyman [102]. This method includes a local expansion fan in the approximate Riemann solution when an expansion is detected through a sonic point, so that a modification of the eigenvalue $|\lambda|$ is realized as follows:

$$\left|\overline{\overline{\lambda}}\right|_{\text{mod}} = \begin{cases} \left|\overline{\overline{\lambda}}\right|_{i+1/2} & if & \left|\overline{\overline{\lambda}}\right|_{i+1/2} \geq \varepsilon \\ \varepsilon & if & \left|\overline{\overline{\lambda}}\right|_{i+1/2} < \varepsilon \end{cases}, \text{ where} \tag{2.110}$$

$$\varepsilon = \max\left(0, (\overline{\overline{\lambda}}_{i+1/2} - \lambda_i), (\lambda_{i+1} - \overline{\overline{\lambda}}_{i+1/2})\right) \tag{2.111}$$

In equation (2.111), the zero value eliminates this modification for the compression shock, see Sanz [87].

2.5.1.1.4.3 Total variation diminishing (TVD)

The TVD scheme allows an accurate shock wave resolution without any oscillation of the solution. The scheme was first introduced in the year 1983 by Harten [88]. The basic idea is that the maxima must be non-increasing, minima non-decreasing, and new extrems must not be created [45]. The total variation of the solution is defined as:

$$TV \equiv \sum |U_{i+1} - U_i| \tag{2.112}$$

In order to fulfill the above mentioned restrictions the total variation of the next time step must be equal or lower for convection cases without sources:

$$TV^{n+1} \leq TV^n \tag{2.113}$$

The TVD fluxes are calculated as a convective average flux including a dissipation term (so-called *flux-limited dissipation* [45]). When this dissipation term depends on the characteristic speed, the TVD scheme is called *symmetric*, otherwise it is an *upwind* scheme. According to Blazek [45], the upwind scheme tends to higher accuracy, better shock and boundary layer resolution. The TVD scheme can easily be extended to second order spatial accuracy applying so-called *limiter* or *limiter functions*, but it is difficult to extend to a higher order. Therefore, in the practice for higher order spatial accuracy requirements the *Essentially Non-Oscillatory* (ENO) scheme proposed by Harten et al. [89] is often applied.

2.5.1.1.4.4 Fluctuation-splitting (FS)

The fluctuation-splitting scheme is provided for true multidimensional upwinding, which resolves the flow accurately taking into account the grid cells orientation during the equations splitting [45]. Due to a high numerical effort and complexity as well as convergence problems, this scheme is only used in research codes. A short introduction to this scheme is presented in Blazek [45] as well as a detailed description in the work of Roe [90].

2.5.1.1.5 Viscous fluxes discretisation

Due to an elliptic nature of the viscous fluxes, the values required for the calculation (such as the velocity components, the dynamic viscosity, and the heat conduction coefficient) are simply averaged at the face applying following equation:

$$\phi_{i+1/2} = \frac{\phi_{i+1} + \phi_i}{2}$$
(2.114)

Where ϕ denotes any of the above mentioned variables. In order to evaluate the gradients of the velocity components and of the temperature distinguishing between structured and unstructured grids according to Blazek [45] following methods are available:

- Finite difference or Green's theorem (for the structured grid discretisation)

- Element based gradients or average of gradients (for the unstructured grid discretisation)

The viscous fluxes calculation applying the finite difference method can be used for the structured grids and is based on a local transformation from Cartesian coordinates (x, y, z) to the curvilinear coordinate (ξ, η, ζ), for instance:

$$\frac{\partial \phi}{\partial x} = \frac{\partial \phi}{\partial \xi}\frac{\partial \xi}{\partial x} + \frac{\partial \phi}{\partial \eta}\frac{\partial \eta}{\partial x} + \frac{\partial \phi}{\partial \xi}\frac{\partial \xi}{\partial x}$$
(2.115)

Whereas, the derivatives ϕ_ξ, ϕ_η, and ϕ_ζ are calculated applying the finite difference approximation.

The second method (Green's theorem) is also applicable for the structured grid and uses an additional cell construction for the computation of the derivatives, i.e. an auxiliary control

volume. This method can be used for the cell-centered as well as the cell-vortex schemes, whereas in the following explanation only the cell-centered scheme is taken into consideration. The new auxiliary control volume is created by the connection of the edges midpoints defining an adjacent grid cell at the face (a similar method to the staggered grid). The flow variable ϕ is integrated over the boundary face of the new control volume and according to Blazek [45] the first derivative in the x-direction (such as the velocity components of the temperature) can be calculated as follows:

$$\frac{\partial \phi}{\partial x} = \frac{1}{\Omega'} \int_{\partial \Omega'} \phi \, dS'_x \approx \frac{1}{\Omega'} \sum_{m=1}^{N_F} \phi_m S'_{x,m} \tag{2.116}$$

Where, N_F is the number of the control volume faces, Ω' is the volume and $\vec{S'_m} = \begin{bmatrix} S'_{x,m} & S'_{y,m} & S'_{z,m} \end{bmatrix}^T$ is the face vector, whereas the superscript ' denotes the new auxiliary control volume. The value ϕ_m at the face midpoint is simply averaged using the data of all neighbor cells.

The element based gradient method is used for unstructured grids, whereas the most common used methods are: *face-centered control volume*, *approximate Galerkin finite element approach* and *average on nodal values*. The first method, face-centered control volume, is based on above described Green's theorem applying an auxiliary control volume. The approximate Galerkin finite element approach transforms the integration of gradients over the surface of the control volume into an evaluation of the Hessian matrix (second derivatives) at the central node [45]. The last approach is based on an average of the values taking into account three nodes which define the cell face and the quantities at the cell centroids [45]. The last two approaches are only developed for triangular or tetrahedral grids, whereas the Galerkin method can be extended for the elements, such as prisms and hexahedra with an increase of numerical effort.

Finally, the average of gradients approach uses already calculated gradients inside each control volume, e.g. obtained applying the piecewise linear reconstruction proposed by Barth and Jespersen [91], to determine the gradient at the face midpoint by a simple average [45]:

$$\nabla \phi_{IJ} = \frac{1}{2} \left[\nabla \phi_I + \nabla \phi_J \right] \tag{2.117}$$

Taking into account the distance between the cell centroids, the accuracy and the tendency of the solution decoupling on hexahedral grids can be significantly improved, see Blazek [45].

2.5.1.2 Temporal discretisation

On the left side of the equation (2.94) the time dependent term is presented, which describes how the conservative variable vector $\vec{U}$ changes with time. Considering that the cell volume is constant over time, for each control volume CV equation (2.94) can be written as follows:

$$\Omega_{CV} \frac{\partial \vec{U}_{CV}}{\partial t} = -\vec{R}_{CV} \tag{2.118}$$

According to Hirsch [92] as well as Blazek [45], the time derivative of the vector $\vec{U}$ can be approximated applying the following non-linear scheme:

$$\frac{\Omega_{CV}}{\Delta t} \left(\vec{U}_{CV}^{n+1} - \vec{U}_{CV}^{n} \right) = -\frac{\beta}{1+\omega} \vec{R}_{CV}^{n+1} - \frac{1-\beta}{1+\omega} \vec{R}_{CV}^{n} + \frac{\omega \cdot \Omega}{(1+\omega)\Delta t} \vec{R}_{CV}^{n-1} \tag{2.119}$$

Where, the superscript n denotes the time level and Δt the time step. In dependence on the parameter β and ω, the temporal discretisation scheme is either *explicitly* or *implicitly* defined.

2.5.1.2.1 Explicit scheme

By setting the parameters $\beta = 0$ and $\omega = 0$ equation (2.119) is reduced to the following form:

$$\frac{\Omega_{CV}}{\Delta t} \left(\vec{U}_{CV}^{n+1} - \vec{U}_{CV}^{n} \right) = -\vec{R}_{CV}^{n} \text{, respectively } \vec{U}_{CV}^{n+1} = \vec{U}_{CV}^{n} - \frac{\Delta t}{\Omega_{CV}} \vec{R}_{CV}^{n} \tag{2.120}$$

In this case, the explicit scheme is applied and the calculation of the vector $\vec{U}$ at the new time level $n+1$ is realized using only already known variables at old time level n.

An explicit scheme is stable only up to a certain value of the time step and in order to get a stable solution, the scheme has to fulfill the *Courant-Friedrichs-Lewy* (CFL) condition, which is defined for a 1D case [45]:

$$\Delta t = CFL \cdot \frac{\Delta x}{|\Lambda_c|} \tag{2.121}$$

Where Λ_c is the velocity and Δx is the distance the information is transported across. The CFL condition of the explicit scheme shows that the time step Δt should be smaller or equal to the time required to transport the information across the distance Δx given by spatial discretisation.

2.5.1.2.2 Implicit scheme

Applying an implicit scheme the variables at the new time level $n+1$ are already used for the calculation of the vector $\vec{U}$ at the same time level. Therefore, the parameter β in equation (2.120) is positive. Furthermore, it can be seen that the combinations of the parameters β and ω in equation (2.120) do not only select the temporal discretisation scheme but also the order of accuracy in time. For instance, by setting the parameters $\beta = 1$ and $\omega = 1/2$ equation (2.119) is transformed to:

$$\frac{\Omega'_{CV}}{\Delta t}\left(\vec{U}_{CV}^{n+1} - \vec{U}_{CV}^{n}\right) = -\frac{2}{3}\vec{R}_{CV}^{n+1} + \frac{\Omega}{3\Delta t}\vec{R}_{CV}^{n-1} \text{ , respectively} \tag{2.122}$$

$$\vec{U}_{CV}^{n+1} = \vec{U}_{CV}^{n} + \frac{\Delta t}{\Omega'_{CV}}\left(-\frac{2}{3}\vec{R}_{CV}^{n+1} + \frac{\Omega}{3\Delta t}\vec{R}_{CV}^{n-1}\right) \tag{2.123}$$

Equation (2.123) is 2nd order accurate in time applying the 3-point implicit backward differencing scheme. On demand, for a more robust scheme, the parameters β and ω can be set to 1 and 0 respectively, whereas equation (2.123) results in a 1st order accurate temporal discretisation:

$$\frac{\Omega'_{CV}}{\Delta t}\left(\vec{U}_{CV}^{n+1} - \vec{U}_{CV}^{n}\right) = -\vec{R}_{CV}^{n+1} \text{ , respectively } \vec{U}_{CV}^{n+1} = \vec{U}_{CV}^{n} - \frac{\Delta t}{\Omega'_{CV}}\vec{R}_{CV}^{n+1} \tag{2.124}$$

2.5.1.2.3 Explicit vs. implicit

According to Blazek [45] an essential advantage of the implicit scheme, in contrast to the explicit one, is that significantly larger time steps Δt can be used without a decrease of simulation stability, as well as its superior robustness and convergence speed in the case of stiff equation system and/or present source terms (e.g. real gas and combustion process simulation, turbulence, as well as user defined source terms). Nevertheless, the implicit scheme needs higher computational effort, therefore applying the multi-grid method the explicit scheme can be also equal or more efficient. Furthermore, the implicit scheme is more complex to parallelize than the explicit one. Further details about these schemes can be found in Blazek [45], Hirsch [92], Tucker [93] etc.

2.5.1.3 Treatment of the source term

In the case of a combustion process or turbulent flow simulation, the source terms appear with a dominant influence on the flow variables. The source term causes rapid changes of the flow variables, in fact with smaller time scales than the time scale of the flow field. According to Blazek [45], this significantly increases the *stiffness* of the governing equations, where the stiffness is defined as the ratio of the largest to the smallest eigenvalue of the Jacobian matrix, namely $\partial\vec{R}/\partial\vec{U}$. Furthermore, the stiffness can also be seen as the ratio of the largest to smallest time scale. In the case of different time scales, the time step should be reduced in order to stabilize the calculation. Moreover, a slower convergence behavior will be presented. In order to solve this problem, Curtiss and Hirschfelder [94] proposed a method in 1952 in which the source term is treated in an implicit way. Due to the fact that the source term is unknown at the time level $n+1$, the requested value is interpolated applying following equation:

$$\vec{Q}^{n+1} = \vec{Q}^{n} + \frac{\partial\vec{Q}}{\partial\vec{U}}\Delta\vec{U}^{n} \tag{2.125}$$

In equation (2.125) $\vec{Q}^{n}$ is the explicit part of the source term and $\frac{\partial\vec{Q}}{\partial\vec{U}}\Delta\vec{U}^{n}$ is the implicit part.

By setting the implicit part to zero, the source term is treated explicitly; otherwise in order to increase the stability of the solution and the convergence, an implicit part should be defined.

In Fluent [95] the source terms with their explicit and implicit parts can be set by the user, i.e. the *real* source term $\vec{Q}^n$ and the implicit term $\frac{\partial \vec{Q}}{\partial \vec{U}}$. In the case of a known source term function - such as in the turbulent kinetic energy k equation (2.57) and in the dissipation rate ε equation (2.58) - the explicit and the implicit parts are obtained as functions. Otherwise, when the source term is calculated, such as the convective flux transfer as source term in the work of Rothbauer [27], only the explicit part is obtained. Therefore, the author defined a small negative value as the implicit source part in order to improve the solution stability and the convergence. Even though this value is not obtained from physical reasons, the calculation achieves a converged solution. Due to the fact that Rothbauer [27] has only investigated several simple cases, this treatment of the implicit source term part is not satisfying for the simulation of engineering relevant technical problems. Therefore, in this work the implicit source term part, which is transferred to the Fluent-solver, is obtained by following equation:

$$\frac{\partial \vec{Q}}{\partial \vec{U}} = \frac{\left(\vec{Q}^{n+1} - \vec{Q}^n\right)/\Delta t}{\left(\vec{U}^{n+1} - \vec{U}^n\right)/\Delta t} = \frac{\vec{Q}^{n+1} - \vec{Q}^n}{\vec{U}^{n+1} - \vec{U}^n} \tag{2.126}$$

During the iteration process, the values at the time level n are kept constant, whereas the required values at time level $n+1$ are set a new with each iteration.

2.5.1.4   Initial and boundary conditions

At the start of a calculation, the *initial* and *boundary* conditions must be defined. The initial conditions determine the state of the fluid at time level zero (unsteady simulation) or at the start of an iterative scheme (steady simulation). Due to the fact that initial data are unknown in the majority of cases - especially in the case of the spatial distribution of the flow field as well as the turbulence start conditions - it is important that the assumed initial conditions satisfy the governing equations and the thermodynamics relations. Generally, it can be expected that the better the assumed initial conditions are, the faster the converged solution can be obtained. Furthermore, the wrong assumed initial conditions do not only cause convergence problems but can also lead to a breakdown of the numerical calculation process.

CFD-simulation usually considers only a part of the physical domain of interest, whereas the rest or all surrounding domains are replaced with corresponding boundary conditions. The specification of boundary conditions often represents a non-trivial problem, which requires particular care. The quality of the results depends on the type and the completeness of the boundary, so that simplifications can lead to incorrect results as well as to a decrease of stability and of convergence speed.

In conventional CFD codes, such as Fluent [52], Kiva [96], AVL Fire [97], Star-CD [98], Converge [99], OpenFOAM [100] etc., the following boundary conditions can be found:

- Inlet/Outlet: pressure, velocity, mass flow

- Wall, periodic (cyclic) and pole: wall, symmetry, periodic, axis etc.

2.5.1.4.1   Inlet/outlet boundary conditions

In literature inlet/outlet boundary conditions are also referred to as *open* boundary conditions [45]. Generally, several boundary conditions can be found in the conventional CFD codes, which allow the flow to enter and/or to exit the calculation domain. Their application primary depends on the technical problem as well as on the available data. According to Blazek [45], the boundary condition has to fulfill the following basic requirement. The boundary condition, which replaces a domain, should not have a wrong influence on the flow solution, e.g. any outgoing annoyance must not be reflected back into the flow field. This requirement is specifically related to so-called *far-field* boundary conditions; see Blazek [45] and Fluent [52]. Due to the elliptic nature of the Navier-Stokes equations, the subsonic and transonic flows are sensitive on the far-field boundary conditions. An inaccurate boundary condition can negatively influence the accuracy of the solution and the convergence behavior. Several concepts have been developed for the non-reflecting boundary conditions, which are able to absorb the outgoing waves. One of them is the concept of *characteristic variables*; see Blazek [45] and Sanz [87]. In this concept, the information is transported in or out of the computational domain according to the characteristics. For this concept, the following boundary conditions, considering the Mach number [45], can be distinguished:

- Supersonic inflow: The variables at the boundary face are only taken form the freestream values of the entering flow of the computational domain.

- Supersonic outflow: The variables at the boundary face are only taken from the domain interior of the leaving flow of the computational domain.

- Subsonic inflow: In this case, four characteristic variables (based on the free-stream values) enter and one (which is extrapolated from the domain interior) leaves the computational domain.

- Subsonic outflow: In this case, four characteristic variables (e.g. ρ, u, v and w) are extrapolated form the domain interior and one is taken from the outlet boundary condition definition.

A detailed discussion about inlet/outlet boundary conditions can be found in Versteeg and Malalasekera [33], Blazek [45], Fluent [52], Toro [77], Patankar [78], Anderson et al. [79], Sanz [87], Hirsch [92], Tucker [93] etc.

2.5.1.4.2   Symmetry plane/line boundary condition

In cases where the flow is very close to be symmetrical in respect to a plane and/or to a line, the symmetry boundary condition can be applied in order to reduce the computational domain and therewith the calculation time. In this case, the flux across the boundary face must be equal to zero and therewith the normal velocity component. According to Blazek [45], following relations concerning the gradients have to be assumed as well:

- Considering the gradient normal to the boundary of a scalar quantity ϕ: $\vec{n} \cdot \vec{\nabla}\phi = 0$

- Considering the gradient normal to the boundary of a tangential velocity: $\vec{n} \cdot \vec{\nabla}(\vec{v} \cdot \vec{t}) = 0$

- Considering the gradient along the boundary of the normal velocity: $\vec{t} \cdot \vec{\nabla}(\vec{v} \cdot \vec{n}) = 0$

Where, $\vec{t}$ is the vector tangential and $\vec{n}$ normal to the symmetry boundary face.

2.5.1.4.3 Periodic/cyclic boundary conditions

The periodic/cyclic boundary conditions (further P-BC) allow the reduction of the computational domain where the solution has a periodically repeating nature regarding one or multiple coordinate directions. In this work, a periodic/cyclic boundary condition is developed which has a cyclic repeating nature regarding the coordinate directions and additionally cyclic repeating nature in time. A detailed discussion about this new P-BC can be found in chapter 5, so that following descriptions are only related to the conventional P-BC.
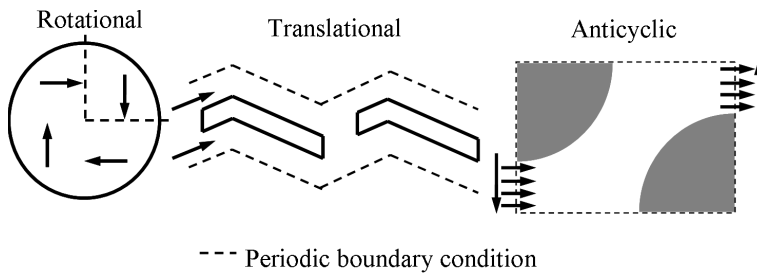
Figure 7: Application of rotational, translational, and anti-cyclical P-BC

P-BC can also be seen as the inlet/outlet boundary conditions, which are additionally periodic or cyclic regarding to the velocity components as well as the pressure, the temperature and the scalar quantities. All P-BC are always used in pairs. The conventional CFD-codes Fluent [52] and Star-CD [98] provide two types of P-BC, with and without pressure drop option. In dependence on the geometry and the technical problem, *rotational* or *translational* P-BC can be distinguished (see Figure 7).

The rotational P-BC is used when the flow across two opposite planes are identical. A good example is an axis-symmetric cylinder flow with a swirl, where the periodicity is based on the coordinate system rotation. This means that all vector quantities have to be transformed according to following rotation matrix when the rotation axis is parallel to the x-axis [45]:

$$\overline{R}_x = \begin{bmatrix} 1 & 0 & 0 \\ 0 & \cos\alpha & -\sin\alpha \\ 0 & \sin\alpha & \cos\alpha \end{bmatrix} \qquad (2.127)$$

Where α is the angle between two rotational periodical boundary faces. The scalar quantities (e.g. pressure, density etc.) remain unchanged regarding the coordinate transformation. The velocity vector is obtained from the following relation:

$$\vec{v}_2 = \overline{R}_x \vec{v}_1 \qquad (2.128)$$

The second translational P-BC can be used with and without the pressure drop function. For a technical problem with pressure drop, the boundary condition can be executed for "fully-developed" or "stream-wise" periodic flow, see Fluent [52]. The "fully-developed flow" is a flow with a flow pattern repeating in successive cycles along the direction of the flow. The "stream-wise flow" includes the fully-developed flow in pipes and ducts and is applicable when the entrance length is long enough. The application also depends on the Reynolds num-

ber and the geometry. Figure 7 shows an example of the translational P-BC in the vertical direction. In this case, the same relation is valid for the vector quantities as well as for all scalar quantities, so that for the translational P-BC a correction of the vector variables is not required.

The conventional CFD code Star-CD [98] allows a symmetry periodic boundary condition, defined as *anticyclic*, where the direction for variable matching is reversed. E.g. a 2D case of heat transfer from tube bundles in cross flow. A small symmetry segment of this anti-cyclical example is shown in Figure 7. In this case, two boundaries at which the flow is entering and leaving the calculating domain are matched in an anti-cyclical way by reversing one of the boundary local coordinate directions.

An impressive analysis of the periodic boundary conditions for the relevant technical engineering problems is shown in the work of Tucker [93]. The author presents the P-BC in the case of a cyclic annular cavity flow, where the annulus consists of discs connected by concentric cylinders and rotates at an angular velocity. The flow is similar to the earth's atmosphere which sometimes consists of cyclonic and anticyclonic flows. Furthermore, some examples of cyclic moving boundary flows are discussed in detail.

The conventional periodic/cyclic boundary conditions, mentioned here, are not feasible for the simulation of a 2-cylinder 2-stroke engine, so that a new type of the P-BC has been developed and is presented in this work.

2.5.1.4.4 Interface between grid blocks

In some simulations, it is not possible to create a single grid block inside a complex physical domain – e.g. due to technical requirements for the multi-block domains such as 2-stroke engines and/or a complex geometry – so that the *multi-block* technique is applied. The coupling between the blocks occurs applying a so-called *grid interface* in Fluent [52], *arbitrary interface* in AVL Fire [97], *sliding interface* in OpenFOAM [100] technique etc. In this work, the *3D-3D coupling methodology* notation is used, due to the fact that two 3D-blocks are coupled together, even if they are physically separated. If the solution depends on the flow in multiple neighboring blocks an information exchange between these blocks must be provided as well as in the case of a multi-processor calculation ability. Applying the above mentioned technique a mathematical connectivity between the blocks is realized.

Basically, each of the above mentioned techniques consists of two parts. First, for the overlapping surfaces of the coupled blocks the *intersection* must be calculated. This section includes all geometrical data required for the flux calculation. In the second step, the convective and diffusive fluxes are computed using the intersection faces obtained in the first step. For instance, the CFD code Fluent [52] provides two approaches in order to obtain the intersection faces, namely the *triangular face* and the *virtual polygon* approach. In the first, the overlapping face is divided into triangular faces including the node movement as well as the water tight cells. The second approach stores area vectors and centroids of the polygon faces, whereas the node moving and the water tight cells are not needed, so that gradients correction is applied in order to take into account the missing face area.

In Rothbauer [27], the basic investigation of the 3D-3D coupling methodology is presented. The author investigated a coupling method between two completely separated 3D-blocks and validated it for some simple cases, such as a pipe-pipe, a pipe-volume and a cylinder-pipe

coupling including a moving piston surface. The reference values for the validation are taken from a conventional simulation, where the above mentioned blocks are already physically coupled together. In the validation case of a coupling between a moving cylinder and a pipe, the author used the above mentioned grid interface technique of Fluent [52] as the reference coupling method. In contrast to a conventional coupling method, the author uses the source term in order to transport the computed fluxes, instead of the flux transport over the coupling intersection faces. A detailed discussion about Rothbauer's coupling method can be found in chapter 4.

2.5.1.5 Solution of linear equations

Starting with initial start conditions, the time-dependent equations are solved taking into account the calculated fluxes and the source terms. Generally, for the solving process two basics methods are available, namely either a *direct* or an *iterative* method. Due to an extremely high computational effort, the direct methods (such as *Gaussian elimination*, see Press at el. [101]) are seldom used for the solving process of 3D problems. Therefore the iterative methods (e.g. *Alternating Direction Implicit* ADI scheme, *Jacobi* or *Gauss-Seidel* relaxation scheme, *Lower-Upper Symmetric Gauss-Seidel* LU-SGS, *Lower-Upper Symmetric Successive Overrelaxation* LU-SSOR etc.) are applied in almost all CFD codes. A detailed description of the above mentioned numerical schemes can be found in the work of Press at el. [101].

In the case of a steady state calculation, usually an iterative method is applied until a non-changing solution (steady state solution) is reached. In the Navier-Stokes equations, the density is considered as an independent variable, due to the time dependent term in the continuity equation. In the momentum equations, there is a coupling between the time evolution of density and of pressure [45]. A solver, which simultaneously solves the governing equations of continuity, momentum, energy and species transport, is called a *density-based or coupled* solver. According to Blazek [45], additional problems applying this solver occur for steady state simulations. The time dependent density term in the continuity equation disappears and usually the equations become increasingly stiff and hard to solve. In order to overcome this problem, a so-called *pressure-based or segregated* solver is applied, which solves a *Poisson equation* for the pressure derived from momentum equations; see Patankar [78] and Anderson et al. [79]. For almost all engineering relevant calculations, the pressure-based solver is applied, so that in the next chapter only this solving method is discussed.

2.5.1.5.1 Pressure-velocity coupling

The Navier-Stokes equations couple the second order system of non-linear partial differentials equations in three directions. The solving process of the momentum equations is difficult as the pressure field is unknown. A separate conservation equation for the pressure field is not given, so that a new pressure equation (Poisson equation) taking into account the continuity equation is derived and solved in order to close the equation system. The well knows solving procedure is proposed by Patankar [78], the so-called *Semi-Implicit Method for Pressure-Linked Equations* SIMPLE method. This method is based on a predictor-corrector procedure and consists of following steps:

1. Guessing an initial pressure field p^*

2. Obtaining of u^*, v^*, and w^* by solving the momentum equations using the guessed pressure field p^*

3. Solving the Poisson equation in order to obtain p'

4. Calculation of the pressure field from $p = p^* + p'$

5. Calculation of the corrected velocity components u, v, and w

6. Solving the other equations, such as energy, turbulence, scalar etc.

7. The corrected pressure p is treated as a new guessed pressure p^* and the steps from 2 to 7 are repeated until a converged solution is reached.

The SIMPLE method is an iterative procedure for the calculation of the pressure and velocity fields and it is implemented in almost all CFD codes. Other variations of the SIMPLE algorithm, such as SIMPLER (SIMPLE-Revised), SIMPLEC (SIMPLE-Consistent), Pressure Implicit with Splitting of Operators (PISO) etc., can improve the convergence and therewith can reduce the computational time, but according to Versteeg and Malalasekera [33] it is not clear which of these variants is the best for general purpose.

2.5.1.6 Acceleration techniques

In order to accelerate the solution of a CFD simulation several acceleration techniques can be applied, see Blazek [45]. Some of them, such as local-time stepping, residual smoothing and multigrid are shortly discussed.

2.5.1.6.1 Local-time stepping

The local-time stepping method applies the largest possible time step for each control volume. The convergence to the steady state solution can be significantly accelerated, whereas this method can only be successfully used for steady state simulation. For transient simulation the temporal inaccuracy is often a problem.

2.5.1.6.2 Residual smoothing

According to Blazek [45], the residual smoothing technique is introduced in order to increase the CFL number of the explicit scheme as well as to improve the damping of the high frequency error components of the residual, which is important for the successful application of the multigrid method. Today, this acceleration technique can be used in explicit as well in implicit schemes. The very popular Implicit Residual Smoothing (IRS) technique is discussed in detail in [45].

2.5.1.6.3 Multigrid

The multigrid technique is applied in order to reduce the number of iterations. The acceleration of the solver convergence is gained with the computation of the solution on a series of different grid resolutions. Starting with a coarse grid solution, it is successively interpolated on the next finer grid, whereby the finer grid solution achieves the converged result definitely faster. The essential advantage is that the work for determining the new solution is distributed mainly over the coarser grid so that the high frequency components must be only obtained over the finer grid. This means that the low frequency components on the finest grid become

high frequency components on the coarser grid, which are successively damped applying the multigrid technique [45].

An alternative method to the geometrical multigrid is the *Algebraic Multigrid* (AMG), which controls directly the system matrix [45]. Generally, the purpose of this technique is to generate a coarse matrix in order to reduce the dimension. The coarse matrix is newly constructed in such a way that the equations with strong coupling are added together [45], so that the matrix reduction occurs according to the flow and not to the grid. The essential advantage is that the coarse grid must not be generated and stored.

2.5.1.7 Consistency, accuracy and stability

The governing equations are discretised in space and applied for each control volume. An approximation of the fluxes on the boundary faces of each control volume causes a so-called spatial *discretisation error*, so that the discretised equations differ from the exact equations by the discretisation error [45]. The topics *consistency*, *accuracy*, and *stability*, analyze the above mentioned problems.

A discretisation scheme is *consistent*, if the discretised equations converge to the exact differential equation for the time step $\Delta t \to 0$ and the grid size $\Delta x \to 0$. The consistency can be also viewed as the *verification* that the governing equations are solved considering the quantification of the *numerical* errors (also called *truncation* error) [45]. The numerical error should go to zero with decreasing time step Δt and grid size Δx.

The *accuracy* is coupled with the numerical error. If the leading term of the numerical error is proportional to grid size Δx, the scheme is 1st order accurate in space, or if the leading term is proportional to $(\Delta x)^2$, the scheme is 2nd order accurate, etc. A numerical scheme must not be less than 1st order accurate in order to be consistent; otherwise the numerical error cannot be reduced for the time step $\Delta t \to 0$ and the grid size $\Delta x \to 0$ [45]. When the exact physical solution is known, the numerical error can easily be obtained taking into account a series of different grid sizes, whereas the rate of the numerical error decrease determines the discretisation accuracy. In the case when the exact solution is not known, the order of accuracy can be obtained using following equation [45]:

$$a = \frac{\ln\left(\dfrac{f_3 - f_2}{f_2 - f_1}\right)}{\ln(r)} \tag{2.129}$$

Where a is the accuracy, r is the refinement or coarsening ratio, and $f_{1,2,3}$ are the numerical solutions on different grid sizes, e.g. the index 1 indicates the finest and 3 the coarsest grid.

The stability analysis is carried out in order to determine the influence of the numerical scheme on the stability and convergence behavior of the scheme which is applied on a computational grid. Several methods are presented and discussed in the work of Blazek [45], such as the Neumann method of stability analysis, which is based on the decomposition of the solution into a Fourier series. However, a condition which should be fulfilled in order to get a stable numerical scheme is the *Courant-Friedrichs-Lewy* (CFL) condition, see equation (2.121),

wherefrom the required time step Δt can be obtained. More details about the stability analysis methods can be found in the work of Blazek [45].

3 Strategy and work flow for efficient simulation

In order to get efficient simulation results in a short computational time, two different ways can be employed; first "Simulation Strategy" and second "Computational Domain Reduction". A simulation strategy basically depends on the technical problem. The presented strategy has been especially developed for a 2-cylinder 2-stroke engine simulation, but some of its core objectives might also be applicable for 4-stroke IC-engine simulations, eventually even in combination with the second method "Computational Domain Reduction". Generally, the simulation strategy is developed in order to exploit the resources which are already available in the conventional CFD codes. The techniques, such as meshing, dynamic mesh, and adjustment of the start conditions, are discussed in the following sub-chapters. On the other hand the second method (Computational Domain Reduction) is based on the simulation of only the most important areas, where domains of less importance can be replaced by corresponding boundary conditions or simple models. The basic methods and the solutions, such as the multidimensional coupling methodology and the cyclic/periodic boundary condition, are discussed in the chapters 4 and 5.

3.1 Simulation strategy
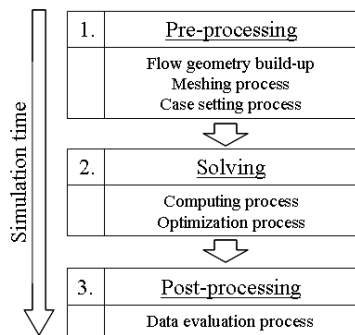
Figure 8: Basic steps of a CFD simulation

In order to analyze the efficiency of a CFD simulation and the possibilities to reduce the computational time, an evaluation of all simulation steps beginning with the flow geometry build-up until the data evaluation process is a practicable way. Basically, a CFD simulation consists of the following three basic steps: *pre-processing*, *solving*, and *post-processing* (see Figure 8).

In the "pre-processing" step the geometrical flow model and the computational grid are created. In addition, the injector model has to be calibrated for distinct spray chamber geometry in order to be able to compare it to experimental data. The last step in this phase is the case setting process, where the boundaries, the initial conditions are defined as well as the simulation models and the numerical schemes. The pre-processing phase does not offer a lot of possibilities to reduce its duration. It mainly depends on the engine geometry and the availability of the required data. Furthermore, it is also recommended to carry out a very detailed analysis of the available data and the aim of the simulation. A mistake in this phase usually becomes evident not before the post-processing phase. This can cause a considerable increase of simulation time due to a simulation re-run and a return to the pre-processing step. Therefore, a return to the pre-processing step should be avoided.

The duration of the second simulation step "solving" depends on the model size, the settings, and the strategy, e.g. the number of 3D cells, selection of physical models etc. The user of the CFD software chooses the models, determines the strategy, and therewith directly influences the success and the duration of a simulation. However, this step provides a lot of possibilities to increase the simulation speed as well as to avoid a return to the pre-processing step. This is, for instance, possible by applying some grid manipulation techniques, which are discussed in

the following chapters taking into account the considerable complex CFD simulation of a 2-cylinder 2-stroke engine.

The final step of the simulation is the "post-processing", specifically the analysis of the results. This phase can only be accelerated by the use of automatic evaluation procedures, such as macros in the conventional CFD codes as well as in the data evaluation tools (e.g. Excel, Open Office etc.). The data evaluation process, due to its strong dependency on the user and the applied software, is not discussed in this work.

3.1.1 Simulation of a 2-cylinder 2-stroke engine
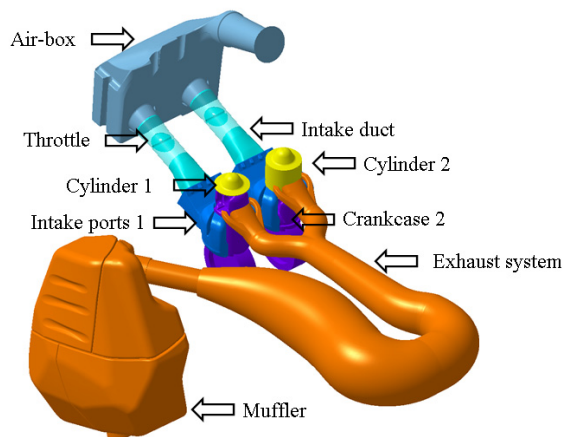
Figure 9: **Flow geometry of the 2-cylinder 2-stroke engine**

The experimental engine is a 2-cylinder 2-stroke engine from the BRP-Powertrain Company, applying loop scavenging via five intake ports (see Figure 9). The displacement of one cylinder is approximately 300 cm³. The engine can also be classified as a 2-stroke engine with reed valve controlled sucked air mass, crank case charge, Schnürle loop scavenging, variable exhaust port (RAVE – Rotax Adjustable Variable Exhaust), tuned exhaust pipe and high pressure gasoline direct injection (GDI) system. The intake ports are located symmetrically around the cylinder with the same opening time. The exhaust port consists of three ports, one central and two small lateral ports. In order to reduce the scavenging losses and to widen the speed range, the RAVE system controls the exhaust port opening/closing timing for an effective exhaust tuning. Furthermore, its use and position depends on the engine speed (low engine speed = RAVE system closed, high engine speed = RAVE system open). Due to a well-tuned exhaust system the reflected pressure wave reduces the scavenging losses. The engine has two separated intake ducts as well as two separate throttles. These intake ducts are further connected to an air-box volume.

The investigation of a 2-cylinder 2-stroke engine requires the simulation of the complete geometry including both cylinders and the complete exhaust system (see Figure 9). In this engine, the cylinders are coupled together in a so-called "two-into-one" exhaust system. Furthermore, the intake and the exhaust ports are open simultaneously over a long period of the cycle and the gas dynamic behaviour inside the exhaust pipe has a dominant influence on the scavenging process and on the mixture formation inside the cylinder. The simulation of only one cylinder causes an incorrect gas dynamic behaviour inside the exhaust pipe and leads to unrealistic results. In addition, the simulation of different engine operating points requires modifications of simulation settings and a grid rebuild-up, namely a return to the pre-processing phase. In order to investigate different fuel injection strategies, the simulation of several variants is generally required, resulting in an increased simulation effort. The main challenge is to achieve a cyclic steady condition inside the engine in a short calculation time acceptable for the application of CFD simulation in the development process. In contrast to a 4-stroke engine, the calculation of only one or two cycles is not enough to smooth out wrong initial conditions. Taking into account all processes inside the engine, their calculation can cause an additional time delay due to complex physics and convergence problems. However, with an appropriate strategy these simulations can be successfully realized in an acceptable

time. Applying a detailed analysis of the pre-processing and solving steps the requirements for the simulation in the engine development process and simultaneously the potentials for the reduction of the computational time are discussed in the following chapters.

3.1.1.1 Pre-processing

The pre-processing step consists of the *flow geometry build-up*, the *meshing* and the *case setting process*.

3.1.1.1.1 Flow geometry build-up process

The build-up of the flow geometry from 3D engine parts, as presented in Figure 9, can be carried out with the conventional 3D-CAD software packages, such as CATIA, Pro-E, etc. Additional difficulties can be expected by the build-up of the naturally complex geometries, such as intake ports, metal sheet parts, exact reed petal geometries etc. Furthermore, the poor quality of the 3D-CAD data itself can additionally decelerate the build-up time, so that it should be implicitly considered for the time evaluation.

3.1.1.1.2 Meshing process

The construction of the computational mesh is heavily depending on some techniques, such as automatic meshing, multi-block domains and arbitrary mesh interface. Almost every conventional CFD code provides a meshing tool, e.g. Gambit [103] for the CFD-code Fluent. In Figure 9 it is clearly visible that the 2-stroke engine geometry consists of several block domains, such as cylinder, intake ports, crankcase, intake duct, air-box and exhaust system. Applying the multi-block domain technique each of these domains can be further divided into sub-blocks (e.g. the muffler is a sub-block domain of the exhaust system). The block domains are treated in Fluent as *cell-thread* selections, which are clearly identified with an ID-number as well as with a name. Theoretically, the coupling between the blocks can be realized either applying the grid interface technique - in the case when the blocks are physically decoupled (see chapter Interface between grid blocks 2.5.1.4.4 as well as chapter 3D-3D Coupling 4.1) - or using a very simple method, namely an interior face. In the second method, the mesh build-up occurs in such a way that a volume is split into two domains. The shared contact face is defined as an interior face, whereas the numerical effort applying this method does not increase in contrast to the grid interface technique. The disadvantage is that the coupling between two moving blocks cannot be realized, e.g. coupling between cylinder and exhaust/intake port volumes of a 2-stroke engine, in contrast to the grid interface technique. Even though the multi-domain technique clearly decelerates the meshing process and causes an additional time delay, the method has some essential advantages which are visible in the solving step of a CFD simulation as well as in the meshing process. These advantages in the meshing process can be summarized as follows:

- Due to a partition of the domain into sub-blocks a hybrid mesh can be created, so that for each block individual mesh setting parameters and cell types can be defined. This technique can drastically reduce the number of 3D cells and therewith the calculation duration as well.

- In the case of geometry variations, only one computational grid block must be replaced. For instance, for the investigation of several muffler designs, only the muffler volume must be newly meshed and replaced instead of the complete exhaust system.

During the meshing process and the domain partition into sub-blocks the moving grid technique should be taken into consideration. The conventional CFD-code Fluent [52] provides two moving mesh techniques applicable for the simulation of a 2-stroke engine, i.e. the *layering* and the local *re-meshing* methods. The layering method uses the dynamic layering to add or remove layers of cells next to a selected plane, in which the layer height is used as the criterion. This dynamic mesh technique can only be used in prismatic (hexahedral and/or wedge) mesh domains. In contrast, the Fluent re-meshing method marks cells of a moving boundary that violate the set "skewness" or size criteria and locally re-meshes the marked cells or faces. As soon as the cells or faces do not satisfy the skewness criterion, the mesh is locally updated with new cells. This method can only be used in the domains with tetrahedral cells. In contrast to the layering method the re-meshing process is time consuming and is thus not applied for the piston movement in this work.

The size of cells in a domain directly determines the number of 3D cells and therewith the duration of the solving step. First of all, the cell size must be chosen in a way that the surface geometry is accurately discretized and reproduced. In addition, the initial mesh should contain sufficient cells in order to capture the essential features of the flow field. After that, the criteria (such as accuracy and stability, discussed in the chapter 2.5.1.7) should be taken into consideration. In the development process of an IC-engine the method of different grid sizes is not appropriate; especially due to a long computational time of a 2-stroke engine CFD simulation. However, the above mentioned criteria must be met. In chapter 3.1.1.2 some methods for the grid improvement are discussed in detail.

3.1.1.1.3   Case setting process

In the case setting process, boundary conditions, material properties, models and numerical scheme settings are defined. Usually, the case settings can be taken from old simulations, if the boundary and the volume selection names are not changed from case to case. However, in the CFD code Fluent some boundary conditions (such as the grid interfaces) cannot be taken from old simulation settings and have to be newly defined in each new case setting process.

3.1.1.2   Solving

In the solving step of a CFD simulation the governing equations are solved by a high performance computer. Theoretically, the user should only control the solving process, but in this step there are many possibilities to optimize the simulation in order to increase the simulation speed and accuracy as well as to avoid a return to the pre-processing step. Exactly this simulation phase is the key for an efficient and fast CFD simulation in the development process of a new 2-stroke engine. The calculation time can be considerably reduced by the use of a stepwise simulation strategy. Based on our experience the calculation time, until a cyclic steady condition is reached, can be reduced up to 50% applying a reasonable strategy. Generally, the solving phase can be divided into the two following steps:

1. Simulation of a cyclic converged (steady) scavenging process

2. Simulation with injection and combustion process

3.1.1.2.1   Simulation of a cyclic converged scavenging process

The first step can be understood as the step in which the initial conditions for the fuel injection and the combustion process simulation are obtained. The calculation is started with a

minimal computational effort. This means with a minimal number of 3D cells, taking only gas dynamic simulation into account, with a simple and stable turbulence model (e.g. standard $k - \varepsilon$ model), a simulation without fuel injection and combustion process. The gas dynamic simulation is realized in a way that at a selected position of the piston (just before the exhaust port opens) the thermodynamic condition in the cylinder is initialized each cycle with reasonable values of pressure, temperature, and accordant composition of exhaust gases. This data can be taken from test bench data or from preceding simulation results. On the one hand, this strategy significantly accelerates the calculation, as injection and combustion process simulations are missing. On the other hand, the gas dynamic behaviour inside all parts of the engine achieves a steady condition within three or four revolutions. In the next step, the simulation accuracy can be improved by applying a mesh refining technique for special areas.
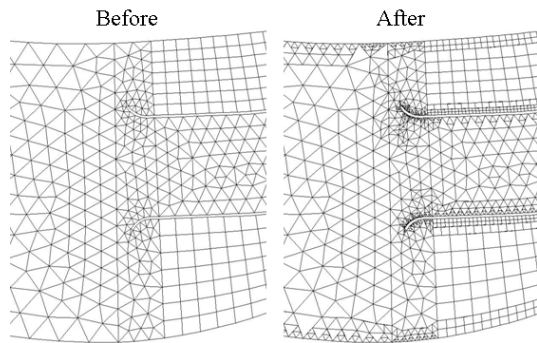
Figure 10: **Application of the local refining technique**

As mentioned before, the computational grid is generated in such a way that an accurate reproduction of the surface geometry as well as of the internal flow field is provided. The reduced number of the 3D cells allows a relative fast calculation of the gas dynamic simulation also taking the above mentioned criteria with satisfying calculation accuracy into account. However, the grid quality and therewith the calculation accuracy can be improved by applying the local re-meshing technique. After completed gas dynamic simulation the regions, where the local grid improvement is required, can be subsequently refined (this method is known as the *static adaption*). The data calculated in the first step are automatically mapped on the new created cells, so that usually only the calculation of one or two additional revolutions is needed to get a cyclic steady condition including improved result accuracy. Figure 10 shows an example inside the exhaust system where the boundary layer grid is improved by applying the local re-meshing technique in CFD code Fluent [52]. This technique can also be applied for the refinement process of the interior cells inside a domain. An important advantage of the described method is a grid improvement without a return to the pre-processing step which considerably shortens the calculation time.

In addition to the static grid adaption, a fully automated *dynamic adaption* process can also be used, see Fluent [52] as well as Converge [99]. This technique is usually applied together with the gradient adaption function, where the cells for the adaption are marked on the basis of the gradients of a predefined field variable. The basic idea of this technique is to improve the resolution of the flow features without a drastic increase of the computational effort. Assuming that the maximum error occurs in the high gradient regions, the already available physical features inside the flow field can be used for a local grid refinement. Due to the fact that a determination of the numerical error is difficult and a time consuming process, this technique represents a reasonable solution for the improvement of the simulation accuracy; especially in the case of industry relevant calculations where the results are required in a short calculation time. However, it should be taken into consideration that the computational effort is increased in any case, but with clearly improved results. In the conventional CFD code Converge [99], this technique is optimized and widely used for IC-engine simulations.

In the first step of the simulation strategy applicable in the development process of a 2-stroke engine not only the number of the 3D cells has to be reduced but also the numerical scheme

settings and the used models are set with the focus on computational speed. Therefore, the standard two equations $k - \varepsilon$ turbulence model is used and the discrete phase model (DPM) and the combustion model are switched off in order to accelerate the calculation speed. When the initial conditions are calculated once, the simulation duration of the first step of the presented strategy can be reduced or completely avoided. Explicitly, taking into account the engine speed and the operating point data already calculated in the previous investigation can be mapped on the new geometry as initial conditions, so that a calculation of only one or two additional revolutions is needed. After that, the above mentioned mesh improvement strategy as well as the more accurate turbulence model can be applied in order to improve the simulation accuracy.

3.1.1.2.2 Simulation with fuel injection and combustion process

The second step of the simulation strategy includes the fuel injection and the combustion process. In this case, the DPM and the combustion model are switched on and the injector properties are defined as well. This simulation is comparable with a conventional 4-stroke engine simulation where only one revolution has to be calculated in order to investigate the mixture preparation process (see Jajcevic [11]). Thereafter the combustion process simulation can be carried out as well. In the development process of a new engine the simulation of only one revolution is needed for the fuel injection and the mixture preparation investigation. In order to verify this assumption, a calculation of additional four revolutions including fuel injection and the combustion has been carried out.
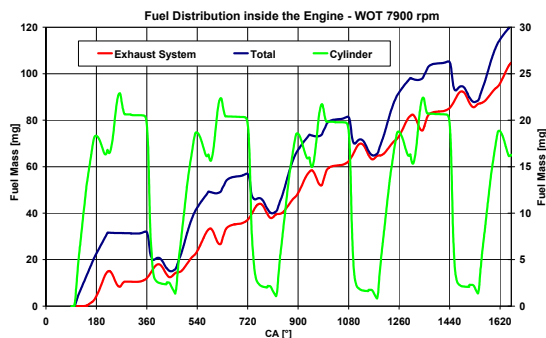
Figure 11: Fuel distribution inside the engine

Figure 11 shows the fuel distribution in different regions of the engine at 7900 rpm and wide open throttle (WOT). The green curve shows the fuel mass inside cylinder 1 over the crank angle for four revolutions and four fuel injections respectively. The red curve represents the fuel mass inside the exhaust system and the blue curve the total mass of the injected fuel inside the calculation domain. The fuel mass inside the cylinder shows an almost periodical steady behavior without big changes. This confirms the correctness of the simulation strategy, e.g. the initialization of the cylinder volume with the corresponding condition short before the exhaust pipe opening leads to a fast convergence of the simulation. Concerning the second simulation phase, Figure 11 shows that already the first cycle results in the same fuel distribution inside the engine as the following do. This means that for an evaluation of different injection strategies in the development process already the first injection can be used for a suitable estimation of the fuel trapping efficiency (FTE). The averaged FTE over four revolutions is 0.64 with a deviation of ±0.01. The red curve presents the fuel mass inside the exhaust system and shows an increasing fuel concentration from cycle to cycle caused by the scavenging losses and by unburned fuel after the combustion process. Therefore, the fuel concentration inside the complete calculation domain (blue curve) increases as well.

3.1.1.2.3 Summary of the simulation strategy

Summarized, the essential advantage of this sophisticated strategy is an accelerated simulation in which the initial conditions for the second step are obtained. Trescher [81] used a similar

strategy for the scavenging process simulation without fuel injection and the combustion process simulation. Moreover, the author neither included fuel injection nor combustion process into his investigations. However, the advantages of the presented simulation strategy can be summarized in the following points:

- The simulation of the gas dynamic behaviour and therewith the scavenging process can be carried out without time consuming fuel injection and combustion process. This strategy leads to a faster convergence of the simulation, especially for the determination of initial condition for the simulation of mixture formation and the combustion processes.

- The first fuel injection generates almost the same fuel distribution inside the engine as the following injections of the subsequent revolutions. For the analysis of different injection strategies already the first injection can be used for a suitable evaluation.

3.1.2 Geometry variations
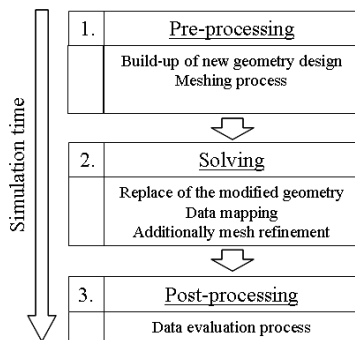
Figure 12: **Workflow for geometry variations**

For geometry variations the simulation is again started with the pre-processing step followed by the above mentioned simulation steps. In the development process of an engine the results are required in a very short time, so that only necessary steps should be repeated. Figure 12 shows a workflow for a changed engine design that has to be investigated with CFD, e.g. a modification of the combustion chamber design.

Assuming that the simulation results from a previous investigation are available, the simulation process is started with the flow field geometry build-up process of the modified engine part applying 3D-CAD software. Next, the meshing process can be carried out, but the cell selections as wells as the face selections should keep the same names as the old geometry selections. Taking the old simulation case and data file, only the modified engine part is replaced by the new one (e.g. only combustion chamber), without a new case setting process. The start conditions are taken from the previous investigation and are mapped on the complete engine domain. This if followed by only one/two additional revolutions calculation of the scavenging process as well as an additionally mesh refinement process. Finally, the calculation including fuel injection and combustion process completes the solving phase and the data evaluation process can take place.

Summarized, starting with known data from a previous investigation a simulation with the new engine design needs the calculation of only one/two additional revolutions and a small effort in the pre-processing phase.

3.1.3 Intake ports opening time variations

The intake ports opening time has an importance influence on the scavenging process and the scavenging ratio. Due to the fact that the scavenging process is strongly accompanied by 3D flow effects, 1D simulation is not appropriate for this investigation. Therefore, the 3D simulation applying the above described geometry variation strategy can be employed (see chapter 3.1.2). The simulation starts with the flow field geometry modification and the meshing proc-

ess. These two steps can be replaced by the moving mesh strategy - in the pre-processing phase the computational grid of the intake ports is generated in such a way that an interior surface is selected and the hexahedral or wedge mesh block - required for the layering mesh strategy - is created on this face.
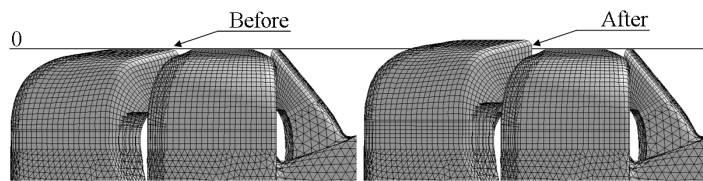
Figure 13: **Moving mesh strategy for the intake port timing**

When the intake ports are closed, the selected interior face together with the cell block can be moved as required, so that the intake ports opening time is automatically changed. This can be employed for only one or all intake ports. The essential advantage of this strategy is that the complete pre-processing as well as the above mentioned steps in the solving phase is avoided. Figure 13 shows the movement of only one intake port leading to a changed opening time.

3.1.4 Different engine speeds and operating points
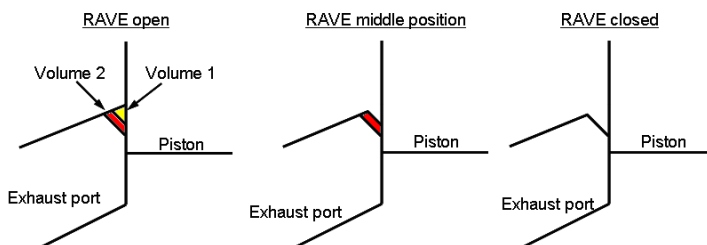
Figure 14: **RAVE system positions**

A new mesh build-up process is time consuming and would lead to a simulation rerun, i.e. a return to the pre-processing step. Therefore, it is very important that the simulation of all engine speeds and operating points can be carried out with only one computational mesh. A good tool to meet this challenge is the RAVE system (RAVE – Rotax Adjustable Variable Exhaust), which controls the opening time of the exhaust port. The position of the RAVE inside the exhaust system depends on the engine speed and the engine operating point. This means that for the new RAVE position an exhaust mesh rebuild is required. In order to get a fast simulation result in the development process of an engine, a new mesh build-up is inappropriate. Therefore, a simulation strategy has been developed allowing for the simulations with only one mesh for all engine operating points and RAVE positions respectively. Figure 14 shows three different RAVE positions: RAVE open, RAVE middle position and RAVE closed. At the start of the mesh build-up two volumes (cell blocks) are selected (see Figure 14, Volume 1 and Volume 2 selections). These cell blocks are coupled to the rest of the grid over interior surfaces and in case of an open RAVE system, the flow is able to enter both volumes. For the RAVE middle position, the marked "Volume 1" is deleted. Fluent [52] automatically creates a surface wall condition instead of an interior wall, where the wall properties can be defined, such as wall temperature, spray-wall interaction model etc. For the third RAVE position, both marked volumes are deleted. Therewith the opening time of the exhaust port is also changed and the RAVE position in the simulation can be included without a mesh rebuild-up and a case reset process.

A second difficulty for the simulation of the different engine operating points is related to the throttle position which appears in the case when the reed valve system and the intake ducts are included in the simulation. The throttle position depends on the engine operating point, so that for the new position a mesh rebuild-up is also required. Figure 15 shows two different throttle positions for two engine operating points - 7900 rpm at wide open throttle (WOT) and

6800 rpm at low-load (LL). Usually, in order to include other throttle positions, a return to the pre-processing process is needed. But applying a rotational function the throttle geometry can be moved around its rotation axis to the correct position already during the simulation.
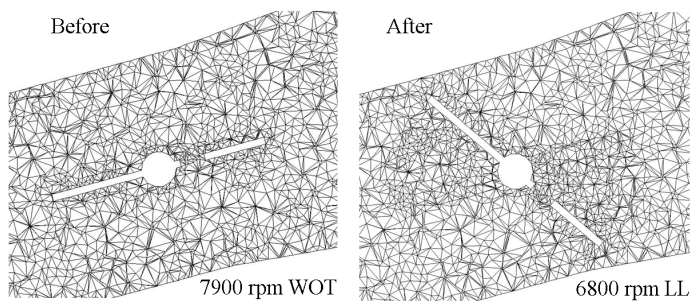
Figure 15: **Throttle position for two engine operating points**

This rotational function is implemented in Fluent [52] via a user defined function (UDF) [95] and can be started on demand. The ideal timing for the throttle movement is a closed reed valve system. Therewith, a correct throttle position in the simulation of the different engine operating points can be included without a mesh rebuild-up process, i.e. without a return to the pre-processing step. The time required for the simulation case setting is also reduced to the minimum, due to the fact that only the engine speed and the injection parameters must be changed.

3.1.5 Spray investigations

A successful homogenization process depends on a range of parameters which must be considered interdependent, e.g. intake flow, combustion chamber design, injector and spark plug positions, spray characteristics, injection parameters (rail pressure, start, duration, and end of injection etc.). Applying the above described methods and strategy, an investigation of different injection parameters does not need a return to the pre-processing step and offers a possibility to change the data directly during the solving step. Taking the initial conditions obtained in the first step of the simulation strategy, the fuel injection simulation begins with the start of the injection (SOI) and lasts until the time of ignition (TOI), i.e. less than a complete revolution. Furthermore, every next spray variation begins at the same starting point and with the same initial conditions. The purpose of this strategy is to get the same boundary conditions for every injection strategy. However, this methodology allows a realistic comparison of different injector positions, spray designs, and injection strategies, such as rail pressure, start, end, and duration of the injection etc. A detailed analysis of a spray design investigation can be found in the enclosed Paper I, see chapter 3.2.

3.2   Paper I

CFD study of spray design for
a GDI high performance 2-stroke engine

SAE *International*®

CFD Study of Spray Design for a GDI High Performance 2-Stroke Engine

Dalibor Jajcevic, Raimund Almbauer and Stephan Schmidt
Graz University of Technology

Karl Glinsner and Matthias Fitl
BRP-Powertrain GmbH & Co KG

ABSTRACT

The advantages of 2-stroke engines, high power and low weight, are in conflict with their disadvantages, high emissions and bad fuel economy. As these disadvantages are caused by the scavenging process, a reason for the problem can be analyzed by using three dimensional computational fluid dynamics simulation (3D CFD simulation). The scavenging losses can be dramatically reduced with a high pressure fuel injection strategy. The purpose of this strategy is to prevent a fuel concentration in the incoming charge and to reduce the fuel concentration inside the exhaust system. These advantages can only be successfully exploited with the application of an optimal injection strategy.

This paper covers a spray study for a gasoline direct injection (GDI) high performance 2-stroke engine using the commercial CFD Code Fluent. The simulations were conducted for four different engine operating points and the test bench results of the fired engine were used for the validation of the gas dynamic behavior simulation inside the engine. The main focus of the present paper lies on the simulation methodology used for the fuel injection simulation. The used injection settings and their validation results are presented and discussed in detail. The assessment and definition of the best injection strategy for a 2-stroke engine at high engine speed is a demanding task and presented in this paper.

INTRODUCTION

2-stroke internal combustion engines are widespread in market segments where a high power to weight ratio is essential, e.g. chainsaws, snowmobiles etc. But their disadvantages - especially high emissions (primarily hydrocarbon emission) and bad fuel economy in contrast to 4-stroke engines - require further investigations to reduce these negative effects. As the disadvantages are caused by mixture formation and the scavenging process (a process of exhaust gas exchange with the fresh incoming charge inside the cylinder volume), they can be analyzed with 3D CFD simulation. CFD simulation has been widely used to predict flow inside the 2-stroke engine over the past twenty years. The constant improvement of numerical methods together with the increase of computer power allows the simulation of more and more demanding technical problems. Even physically complex processes inside the internal combustion engine can be analyzed. The numerical investigation of these processes offers an array of information on the engine and provides a state of the art tool for the development of a new engine. For the development of a GDI 2-stroke engine, the use of 3D CFD simulation is particularly recommended due to strong 3D effects inside the cylinder, such as a tumble interaction with incoming flow and geometry, fuel/air mixing effects etc.
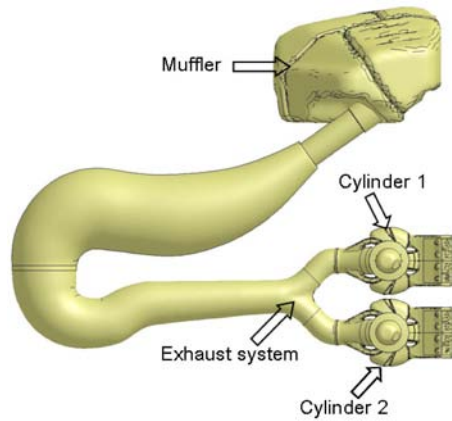
Figure 1. Design of a 2-cylinder 2-stroke engine

The investigation of a 2-cylinder 2-stroke engine requires the simulation of the complete geometry including both cylinders and the complete exhaust system (see Figure 1). In this engine, the cylinders are coupled together in a so-called "two-into-one" exhaust system. Furthermore, the intake and the exhaust ports are open simultaneously over a long period of the cycle and the gas dynamic behavior inside the exhaust pipe has a dominant influence on the scavenging process and on the mixture formation inside the cylinder. The simulation of only one cylinder causes an incorrect gas dynamic behavior inside the exhaust pipe and further leads to unrealistic results. In addition, the simulation of different engine operating points requires modifications of simulation settings and a grid rebuild and therefore causes time loss. In order to investigate different fuel injection strategies the simulation of several variants is generally required, resulting in an increased simulation effort. The main challenge is to achieve a cyclic steady condition inside the engine in a short calculation time acceptable for application of CFD simulation in the development process. In contrast to a 4-stroke engine, the calculation of only one or two cycles is not enough to smooth out wrong initial conditions in a 2-stroke engine simulation. Taking into account all processes inside the engine, the calculation can cause additional time delay, due to complex physics calculation and convergence problems. Anyway, with an appropriate strategy these simulations can be successfully realized in an acceptable time, which is presented and discussed in this work. The used injection settings and injector validation strategy are also presented and discussed. Finally, three spray designs are exemplarily investigated with a real engine simulation taking into account four different engine operating points. These simulation results are presented and discussed in details.

SIMULATION STRATEGY

In general, CFD simulations consist of the following three basic steps: pre-processing, solving, and post-processing. In the pre-processing step, the geometrical flow model and the grid are created. In addition, the injector modeling has to be calibrated for distinct spray chamber geometry in order to be able to compare it to experimental data. The calibration of the injector is carried out for each engine operating point, due to different rail pressures. This phase of the simulation does not offer a lot of possibilities to reduce its duration. It mainly depends on the engine geometry and the availability of the required data. The duration of the second simulation phase "solving" depends on the model size, settings, and strategy, e.g. the number of 3D cells, interaction, and selection of physical models. A good example for the importance of the strategy is the investigation of a 2-cylinder 2-stroke engine. The main challenge is to achieve a steady cyclic condition of the gas dynamic behavior. This has to include all processes - fluid flow, heat transfer, fuel injection, mixture preparation and finally combustion - inside the engine as well. Some of these processes are not at equilibrium after one cycle. Therefore, to smooth out wrong initial conditions is nontrivial. The effects are self energizing as in the first several revolutions bad initial conditions lead to wrong results for the combustion process. These incorrect results lead to a wrong pressure difference between cylinder and exhaust port during the opening phase, which again leads to improper conditions for the scavenging and the combustion process simulation in the next cycle. In this case, the time for calculation to achieve steady cyclic conditions in the whole engine increases significantly. Hence, the straightforward simulation of the 2-cylinder 2-stroke engine is time consuming. The calculation time in this phase of the simulation can be considerably reduced by the use of a sophisticated simulation strategy; based on our experience, the time of calculation until a cyclic steady condition is reduced by 50%. This strategy can be divided into two following steps:

1. Simulation of a cyclic converged (steady) scavenging process

2. Simulation of injection and combustion processes

In the first step of this strategy the discrete phase model (DPM) and the combustion model are switched off. At a selected position of the piston (before the exhaust port opens) the volume of the cylinder is initialized every cycle with the pressure, the temperature, and the accordant composition of the exhaust gases. This data can be taken from test bench or from old simulation results. On the one hand, this strategy significantly accelerates the time of calculation, as injection and combustion process simulations are missing. On the other hand, the gas dynamic behavior inside all parts of the engine achieves a steady condition within three or four revolutions. In the second phase, the DPM and the combustion model are switched on and the fuel injection and combustion process simulations can be carried out.

Trescher [1] uses a similar strategy for the scavenging process simulation, without fuel injection and the combustion process simulation. Moreover, the influence on the fuel

injection and combustion process results is not investigated. The previous investigation [2] shows the discussion of the results of a 2-stroke engine simulation using the before mentioned simulation strategy including fuel injection and combustion process. The advantage of the presented simulation strategy can be summarized in the following points:

1. The gas dynamic behavior simulation and therewith the scavenging process simulation can be carried out without time consuming fuel injection and combustion process.

2. This strategy leads to a faster convergence of simulation, especially for the simulation of the injection, the mixture formation, and the combustion processes.

3. The previous investigation [2] shows that the first fuel injection generates almost the same fuel distribution inside the engine as the following injections of the subsequent revolutions.

4. For the analysis of different injection strategies already the first injection can be used for a suitable evaluation.

ENGINE DESIGN

The experimental engine is a 2-cylinder 2-stroke engine from BRP-Powertrain Company, applying loop scavenging via five intake ports. The displacement of each cylinder is approximately 300 cm^3. The engine can be also classified as a 2-stroke engine with reed valve controlled sucked air mass, crank case charge, Schnürle loop scavenging, variable exhaust port (RAVE - Rotax Adjustable Variable Exhaust), tuned exhaust pipe and high pressure gasoline direct injection (GDI). The intake ports are located symmetrically around the cylinder with the same opening time. The position of these ports causes the fresh charge to be directed upwards into the cylinder to avoid the exhaust port, in order to increase the efficiency of the scavenging process. The exhaust port consists of three ports, one main and two small ports. In order to reduce the scavenging losses and to widen the speed range for effective exhaust tuning, the RAVE system controls the exhaust port opening/closing time. Furthermore, its use and position depends on the engine speed (low engine speed = RAVE system closed, high engine speed = RAVE system open). Due to a well-tuned exhaust system the reflected pressure wave reduces the scavenging losses. It reaches the cylinder just before the piston closes the exhaust port and charges the lost fuel-air mixture back to the cylinder.

A direct fuel injection into the cylinder of a 2-stroke engine is not a new topic. In the year 1959 Groth [3] had already used a direct fuel injection into the cylinder and in his work he presented advantages and difficulties of the system application. Also Schmidt et al. [4] and Basshuysen [5] show an analysis of GDI system with a high performance 2-cylinder 2-stroke engine. Winkler [6] shows in his work that the GDI strategy has a potential to reduce fuel consumption

and exhaust gas emission of a 50 cm^3 two-wheeler engine. Johnson et al. [7] and Harker et al. [8] show an application of a GDI system in the case of a snowmobile 2-stroke engine, similar to the engine investigated in this work. However, all these investigations with gasoline direct injection show the same problems, i.e. coordination between injection, mixture formation and combustion, especially in dynamic engine operating mode with fast load changes. Today, the GDI systems work with rail pressure up to 200 bar and an electronic controlled injection, which offers more flexibility to overcome these disadvantages.

A GDI injector injects the fuel directly into the cylinder as late as possible with a major part or even the whole mass after exhaust port closing (EC). The purpose of this strategy is to prevent a fuel concentration in the incoming charge and to reduce the fuel concentration in the exhaust port (late injection, stratified charge). This strategy can be successfully used when the time for fuel injection and evaporation after EC is sufficiently long, usually at low engine speed. For WOT (wide open throttle), an early fuel injection during the scavenging process has to be chosen (early injection, homogeneous charge), which may cause high fuel losses. The advantages of a GDI system can only be successfully exploited with the application of an optimal injection strategy. The development of this strategy also has to take other engine operating points into account. In order to reduce the number of prototypes and therewith the costs, CFD has to be employed in the development process of a new GDI 2-stroke engine, although the engineer is faced with a very complex task.

The presented simulations in this work conducted at four engine speeds: 7900 rpm with wide-open throttle (WOT), 6800 rpm low-load condition, 5200 rpm low-load condition and 1200 rpm idle. General injection settings for these engine speeds are presented in Table 1.
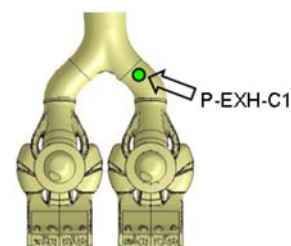
Figure 2. Measurement point in the exhaust port

Figure 2 shows the measurement point in the exhaust port. The indicated pressure values (further P-EXH-C1) for four engine speeds are presented in the following chapter together with simulation results. The data are used for the validation of the gas dynamic behavior simulation inside the exhaust system.

Table 1. Used injection settings

Test bench data		7900	6800	5200	1200
Rail pressure	bar	200	125	85	28
Start of injection (ATDC)	°CA	100	160	190	338
Duration of injection	°CA	140	70	30	10

MODEL BUILD-UP AND SIMULATION SETTINGS

The build-up of the flow geometry was carried out using the conventional CAD software package CATIA V5R16. The construction of the computational mesh (grid) is heavily dependent on some techniques, such as automatic meshing, multi-block domain and arbitrary mesh interface. A detailed description of these techniques can be found in Ansys [9] and Ansys[10]. In order to simulate the moving piston, a hexahedral mesh inside the cylinder and inside the moving part of the crank case was created using the software Ansys [9]. For the coupling methodology between the multi-block domains the standard arbitrary mesh interface technology of Ansys [10] was applied. The mesh build-up process is time consuming and a mesh change leads to the simulation rerun and often doubles the simulation duration. Therefore, it is very important that the simulation of all engine operating points can be carried out with only one mesh build-up. A good example for this problem is the RAVE system. The position of the RAVE inside the exhaust system is depending on the engine speed. This means that for the new RAVE position an exhaust mesh rebuild is required. In order to get a fast simulation result in the development process of an engine, the mesh rebuild is often inappropriate. Therefore, a simulation strategy was developed allowing for the simulations with only one mesh for all engine operating points and RAVE positions respectively. Figure 3 shows three different RAVE positions: RAVE open, RAVE middle position and RAVE closed. At the start of the mesh build-up two volumes are selected (see Figure 3, Volume 1 and Volume 2 selections). These volumes are coupled together over interior surfaces and in case of an open RAVE system, the flow is able to enter both volumes and the complete exhaust port remains undisturbed. For the RAVE middle position, the marked "Volume 1" is deleted. Fluent [10] automatically creates a surface wall condition instead of an interior wall, where the wall properties can be defined, such as wall temperature, spray-wall interaction model etc. For the third RAVE position, both marked volumes are deleted. Therewith the opening time of the exhaust port is also changed and the RAVE position in the simulation can be included without a mesh rebuild and a case reset.
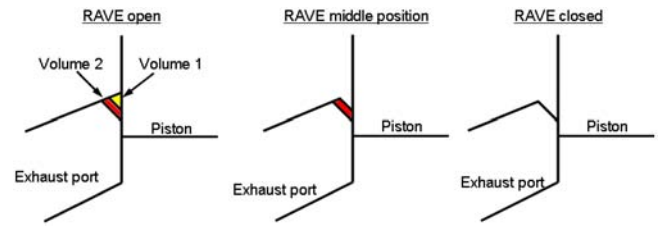
Figure 3. RAVE system positions

The applied injector is a standard automotive high pressure injector with six streams, capable for rail pressures up to 200 bar. The injector is mounted in the cylinder head coaxially to the cylinder axis. Due to an asymmetric spray axis offset of 17°, compared to the injector axis, the fuel spray is directed to the side opposite to the exhaust port.

The spray model was calibrated with experimental data from the injector test bench. The measurements are carried out for four different rail pressure variations, adapted for the four investigated engine speeds and operating points. These measurements included timing of the spray, spray angle and penetration of the injected fuel. The injector calibration in the CFD simulation consists of the following three basic steps: spray classification, model settings, and comparison with measurement data. The Weber number (We), a reliable indicator for the atomization of the spray, is helpful for the choice of the atomization models and is defined by the ratio of the inertia force and the surface tension σ:

$$We = \frac{\rho \cdot d_d \cdot v_d^2}{\sigma}$$

(1)

Where ρ is the gas density, d_d the droplet diameter, and v_d the droplet velocity. E.g. We > 100 indicates a catastrophic atomization of the droplets. Further information about the classification of the droplet atomization in dependence on the Weber number can be found in Basshuysen [5], Winkler [6],

Petermeier [12], and Eichlseder et al. [13]. For instance, "Catastrophic atomization" appears in the flow where aerodynamic forces dominate and essentially influence the breakup of the droplets (We>100). This means that the breakup of the droplet is induced by the relative velocity between the gas and the liquid phase of the injected fuel. For this condition, the WAVE model is well applicable for the droplet break-up calculation, namely by We>100. An alternative to the WAVE model is the TAB model, which is appropriate for low-Weber number flows (We < 100). This model is based on Taylor's analogy between an oscillating and distorting droplet and a spring mass system. A detailed description of these models can be found in Ansys [10]. Table 2 shows the calculated We-number for four different engine operating points and the used breakup model.

Table 2. We-number and used breakup model

	7900	6800	5200	1200
Rail pressure [bar]	200	125	85	28
We - number	210	130	91	29
Breakup model	Wave	Wave	Wave	Tab

During the injection of a GDI system the mass flow and the velocity of the injected droplets are not constant. For a realistic simulation of an injection process a variable rate for the mass flow and velocity was implemented, as the change of the velocity gradients has an important influence on the penetration of the spray and therewith directly on the results of the simulation. The mean velocity is calculated from the Bernoulli equation in dependence of the pressure difference Δp and the fuel density ρ_{fuel}:

$$v = c_q \sqrt{\frac{2\Delta p}{\rho_{fuel}}}$$

(2)

The flow coefficient c_q for this calculation was taken from Stanciu [14 Figure 4 shows the comparison of the simulation results and the measurement data for three different rail pressures of 30, 75, and 100 bar and 1 ms after start of injection. Generally, regarding spray angle and penetration, the results show a satisfying agreement. Anyway, it can be seen that the spray penetration of the same streams differ and that the penetration distance of the same streams is deeper in the measured data. Basically, the droplet penetration depends on the initial droplet velocity, which is calculated from the above mentioned Bernoulli equation. According to Merker et al. [17], the initial droplet velocity should not be larger than the calculated value, even though this might improve the results. Furthermore, in a previous investigation [2], the

difficulties of a fuel injection simulation using CFD code Fluent have been discussed in detail, with the same problems of defining the injection rate, being possibly responsible for a deviation in spray penetration. However, for the validation process of spray penetration, an averaged penetration distance of all six streams is taken into account. For the required rail pressures of 28, 85, 125, and 200 bar for the simulation purpose, the data were extrapolated. After the calibration of the injector, the corresponding spray settings can be implemented into the simulation case.
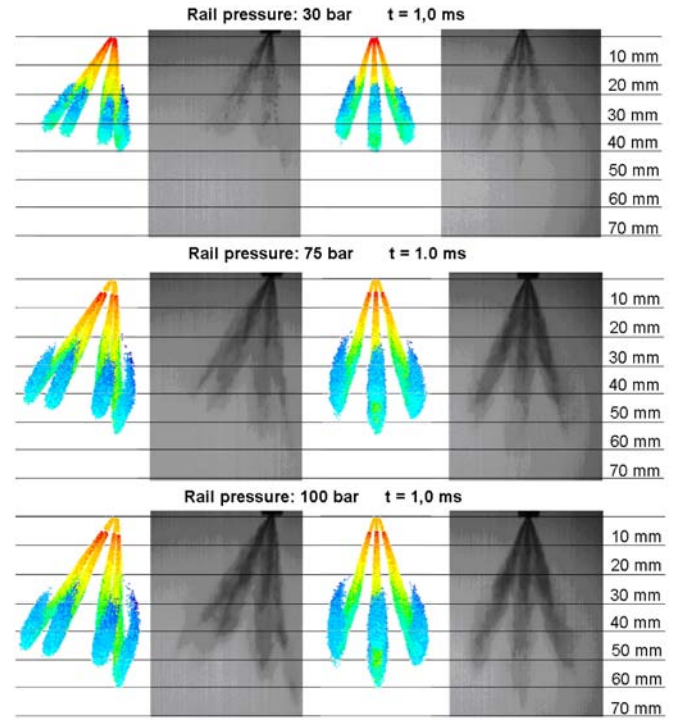
Figure 4. Spray validation for 30, 75, and 100 bar rail pressure

Spray-wall interaction is an important part of the mixture formation process in an internal combustion engine simulation. An impinging droplet on the surface responds according on its properties (especially on the We-number) as well as on the wall boundary condition (e.g. wall temperature). Therefore, the choice of spray-wall interaction model has an important influence on the quality of simulation results. The conventional CFD-code Fluent [10] provides two different models. The first model is a "wall-film" model, where additional equations for the fuel film over the surface are solved. This model is applicable for intake port fuel injection engines with low pressure injection systems and low We-number respectively. For the modeling of a spray interaction with a hot wall (warm engine simulation) applying a high pressure injection system with a high We-number, the second Fluent model "wall-jet" is more appropriate. Trattner [15] shows a comparison of different spray-wall interaction models and experimental data. It is clearly visible that the

wall-jet model is more appropriate for high pressure injection systems with a high We-number. An impressive depiction of the droplet moving over the piston surface is shown as well. In the case of a low We-number, e.g. from reflected droplets of the piston to the cylinder wall, it can be stated that the wall-jet model fails, especially in the case of a low wall temperature (cool engine simulation). In this case, the wall-jet model should be used for the spray-wall interaction prediction with the piston surface and the wall-film model for the interaction with the cylinder wall. Due to a high We-number and a warm engine simulation, the wall-jet model was chosen for the simulations presented in this work.

For the simulation the pressure-based solver with an implicit formulation for unsteady flow is used. For the coupling of pressure and velocity the Pressure Implicit with Splitting of Operators (PISO) scheme has been chosen, as recommended for transient flow calculations. The variation of density is calculated with the ideal gas law (p=ρRT). The standard k- ε turbulence model was used to model the turbulent flow. The standard values for the parameters of turbulent kinetic energy k and the dissipation rate ε models were taken from Ansys [10]. Further, the standard wall function for the near wall modeling of the turbulent boundary layer was selected.

The simulation of a 2-stroke engine requires a reed valve model as boundary condition and for this purpose an adaptive boundary condition is generated. The basic idea is to change the mass flow rate during the simulation depending on the pressure difference between the crank case volume and the section upstream the reed valve. This leads to a quasi self-control of the sucked air mass. The pressure upstream the reed valve is set to constant and has been taken from the measurement upstream the reed valve as an averaged value according to the engine speed. The basic investigation of the reed valve model can be found in [16]. The disadvantage of this methodology is that the gas dynamic behavior in the region upstream the reed valve is not included and that the sucked air mass rate is required from test bench measurements or a 1D simulation in order to validate the simulation.

GAS DYNAMIC BEHAVIOR SIMULATION

As mentioned before, the gas dynamics simulation is carried out without fuel injection and combustion process. Before the exhaust port opens, the volume of the cylinder is initialized every cycle with correct values of pressure, temperature, and the accordant composition of exhaust gases. This simulation is run until a cyclic steady condition inside the engine is achieved. This is the case when the pressure trends inside the exhaust system and the crankcase volume plus the sucked air mass do not differ over at least the last two cycles. In addition, the pressure trends must show a good agreement with the test bench data.

The results are evaluated with "very good" when the cyclic averaged relative deviation RD between the measurement and the simulation data in the measurement points ranges between 0 and 5% and with "good" between 5% and 10% respectively. The cyclic averaged relative deviation is calculated as follows:

$$RD = \frac{\sum_{i=1}^{n} \left| \left(\frac{x_{s_i}}{x_{m_i}} - 1 \right) \cdot 100 \right|}{n}$$

(3)

Where, n is the number of points inside a cycle, x_{s_i} are the simulation values and x_{m_i} are the measurement values.

Figure 5, Figure 6, Figure 7, and Figure 8 show a comparison of the pressure trends of the test bench and the simulation results inside the exhaust pipe for four different engine operating points. The presented simulation results show a good prediction of the pressure trend at 7900 rpm with a relative deviation of 8.9%, and a very good at 6800 and 5200 rpm with a relative deviation of 3.8 and 1.8% respectively (see Figure 9). At 1200 rpm (idle) the prediction of the trend can be seen as well, even though not all pressure vibrations are visible. Probably, these vibrations stem from the mechanical engine parts, which are not included in the simulation. Nevertheless, the relative deviation in this engine operating point is about 1% (see Figure 9). Furthermore, it is clearly visible that at 1200 rpm only a weak fluid motion occurs inside the exhaust system.
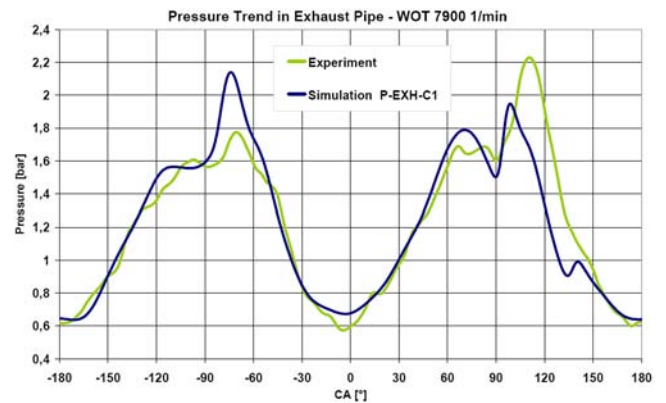
Figure 5. Pressure trend exhaust pipe at 7900 rpm
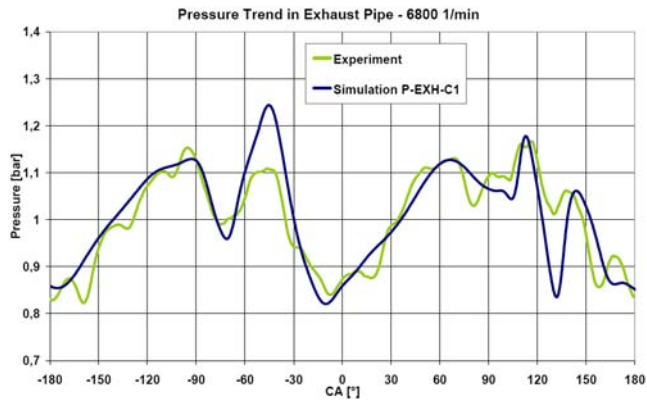
Figure 6. Pressure trend exhaust pipe at 6800 rpm
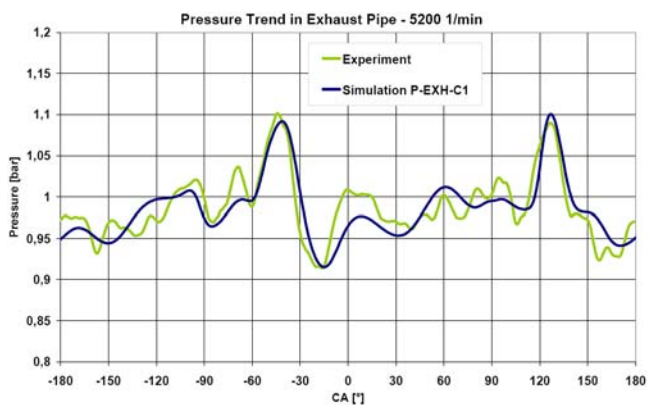
Figure 7. Pressure trend exhaust pipe at 5200 rpm
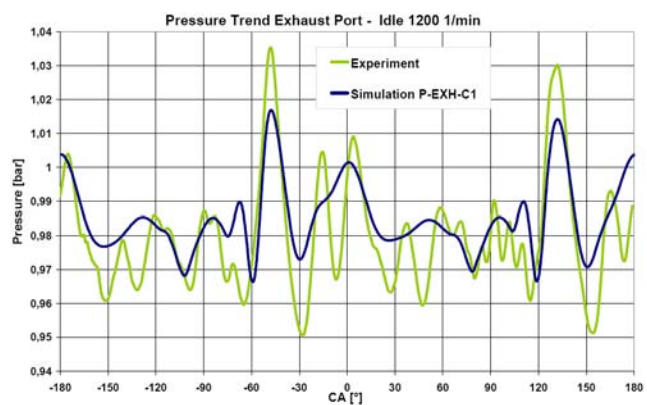
Figure 8. Pressure trend exhaust pipe at 1200 rpm
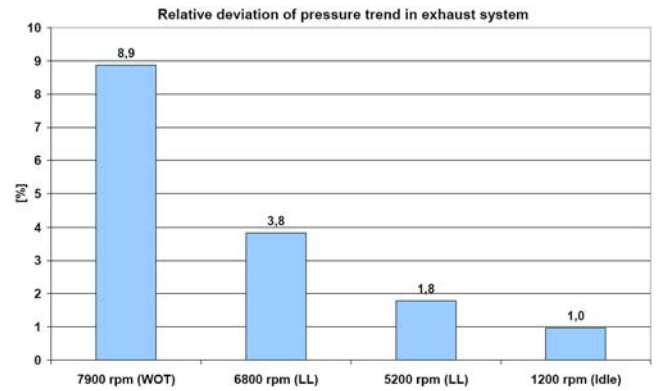
Figure 9. Relative deviation of pressure trend in exhaust system

SPRAY DESIGN

After the gas dynamic behavior simulation the calculation of the fuel injection can be started. This means that the first simulation is only carried out in order to get a good start condition inside the engine for this next simulation step. Furthermore, every next spray variation is started at the same starting point and with the same initial conditions. The purpose of this strategy is to get the same boundary conditions for every injection strategy. In any case, this methodology allows a realistic comparison of the investigated spray design variants.

Figure 10 shows a sketch of three investigated spray geometries. Spray variant 1 (further SV-1) is the original spray geometry of a conventional high pressure injector. Spray variant 2 (further SV-2) is the first modified spray design. In this case, the spray is rotated around its spray axis. This can actually be realized with another injector position or with an injector spray correction on the injector itself. The second investigated modification (further SV-3) applies an increased spray angle but this is only possible with a new injector. The injector position is retained in all investigated cases. The settings for each engine speed, such as start of injection, duration of injection, injected fuel mass etc., are kept constant for all spray variations. Therewith, the influence of the spray design can be successfully investigated. The used injection settings are presented in Table 1.

Spray variant 1 (SV-1)

Spray variant 1 is the original spray design of a conventional high pressure injector which has six streams (see Figure 10). The injector is mounted in the cylinder head coaxially to the cylinder axis. Due to an asymmetric spray axis offset the fuel spray is directed to the side opposite of the exhaust port. The streams 1&4 are exactly situated on the cylinder symmetry plane. The streams 2&6 are symmetric to each other and the streams 3&5 respectively.

Figure 10. Investigated spray variants

Spray variant 2 (SV-2)

Spray variant 2 retains the original injector design. The spray is rotated around its axis by 30° in order to move the streams 1&4 out of the cylinder symmetry plane. In this case, the streams 1&6, 2&5 and 3&4 are symmetric to each other.

Spray variant 3 (SV-3)

In order to get a good homogenized mixture inside the cylinder, the spray angle was modified. A larger spray angle than the original one (see Figure 10, SV-1 and SV-2) should offer a better fuel distribution inside the cylinder and therewith produce a better mixture quality. The spray angle is adjusted to the actual injector position and the combustion chamber geometry.

RESULTS OF SPRAY INVESTIGATION

The goal of this investigation was to find out the influence of the spray design on the mixture quality and the scavenging losses. Therefore, a detailed analysis of the fuel distribution inside the engine after start of injection until start of ignition and for every engine operating point was carried out. For the estimation of the mixture quality for each investigated spray variant, the equivalence ratio contour in the combustion chamber had to be evaluated as well.

Figure 11, Figure 12, and Figure 13 show the fuel distribution in [%] compared to the totally injected fuel mass inside the engine after start of injection until start of ignition. The presented data include three engine operating points, i.e. 7900, 6800, and 5200 rpm. For 1200 rpm (idle) the results of the fuel distribution are not presented, due to the late start of injection (see Table 1), when the exhaust port is already closed. Therewith, the completely injected fuel remains in the cylinder.

At 7900 rpm, the start of injection occurs at approximately 100 °CA ATDC and lasts approximately 140 °CA. In the time span between 100 and 150 °CA the entire fuel resides in the cylinder volume only. After that, the first scavenging losses occur and increase the fuel mass inside the exhaust system volume. At approximately 225 °CA, the pressure wave returns and reduces the scavenging losses. During the closing phase of the exhaust port and the rise of the pressure inside the cylinder a new fuel loss occurs. The fuel mass inside the crank case volume is less than 1.1% for all fuel injection strategies. The spray variation SV-2 shows an increase of the scavenging losses by approximately 1%, in comparison to the spray variant SV-1. For the spray variation SV-3, it is clearly visible that the scavenging losses increase by approximately 4%. Explicitly, an increase of the spray angel causes a better droplet distribution inside the cylinder, but simultaneously some droplets are positioned very close to the exhaust port and due to the scavenging process they are already transported into the exhaust system in the early scavenging phase (see Figure 11, region between 180 and 230 °CA).

At 6800 rpm, the two modified spray variants (SV-2 and SV-3) show similar fuel distributions inside the engine over the complete speed range as well as the same fuel losses, In comparison with spray variant SV-1 the fuel losses increase by approximately 4%. This effect is caused by a spray rotation around its axis.

At 5200 rpm, CFD simulations show that the spray modifications do not influence the scavenging losses. In this case, the fuel is injected late (see Table 1), and the scavenging losses occur only in the closing phase of the exhaust port.

Figure 11. Fuel distribution inside the engine at 7900 rpm, WOT

Figure 12. Fuel distribution inside the engine at 6800 rpm

Figure 13. Fuel distribution inside the engine at 5200 rpm

Summarized, the presented results show that a spray rotation around its axis and a modification of the spray angle cause an increase of scavenging losses. The influence on the scavenging losses of the rotated spray angle can be well explained with an analysis of the droplet distribution. Figure 14 shows the injected liquid fuel droplets inside the cylinder

at 55 °CA after start of injection (7900 rpm, WOT) and a comparison between the spray variants SV-1 and SV-2. In the case of SV-1, the streams 1&4 are positioned in the cylinder symmetry plane. For SV-2, the spray is rotated in order to move the streams 1&4 out of the cylinder symmetry plane. The simulation result of SV-1 shows that the droplets of stream 1 reach the exhaust system already at the start of the scavenging process. In case of SV-2, the streams 1&6 cause scavenging losses, so that the transported fuel mass to the exhaust system is bigger than in the case of SV-1. This effect is clearly visible in Figure 12 in the area between 190 and 210 °CA. The losses at the start of the scavenging process should be avoided, as the fuel penetrates deeply inside the exhaust system and cannot be transported back to the cylinder volume - not even with gas dynamics.
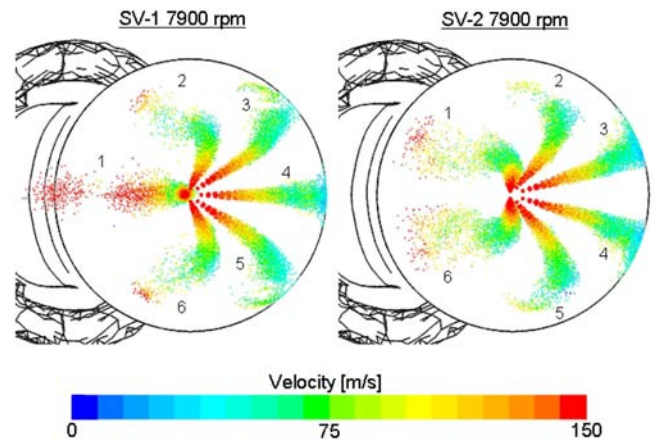
Figure 14. Spray variants SV-1 and SV-2, 55 °CA after start of injection

Figure 15 shows the equivalence ratio contours at start of ignition of four engine operating points for the three different spray variants from three different points of view - the top, the piston (viewing from the cylinder head towards the piston), and the symmetry view.

7900 rpm

For this engine speed, the difference between spray variants SV-1 and SV-2 is hardly visible. In both cases, a similar equivalence ratio contour inside the cylinder can be seen. Higher fuel concentrations are visible on the piston surface. The concentration for SV-2 is generally smaller, as in this spray variant approx. 1.1% less fuel remains in the cylinder. For the spray variant SV-3, the fuel concentration around the symmetry plane is clearly bigger.
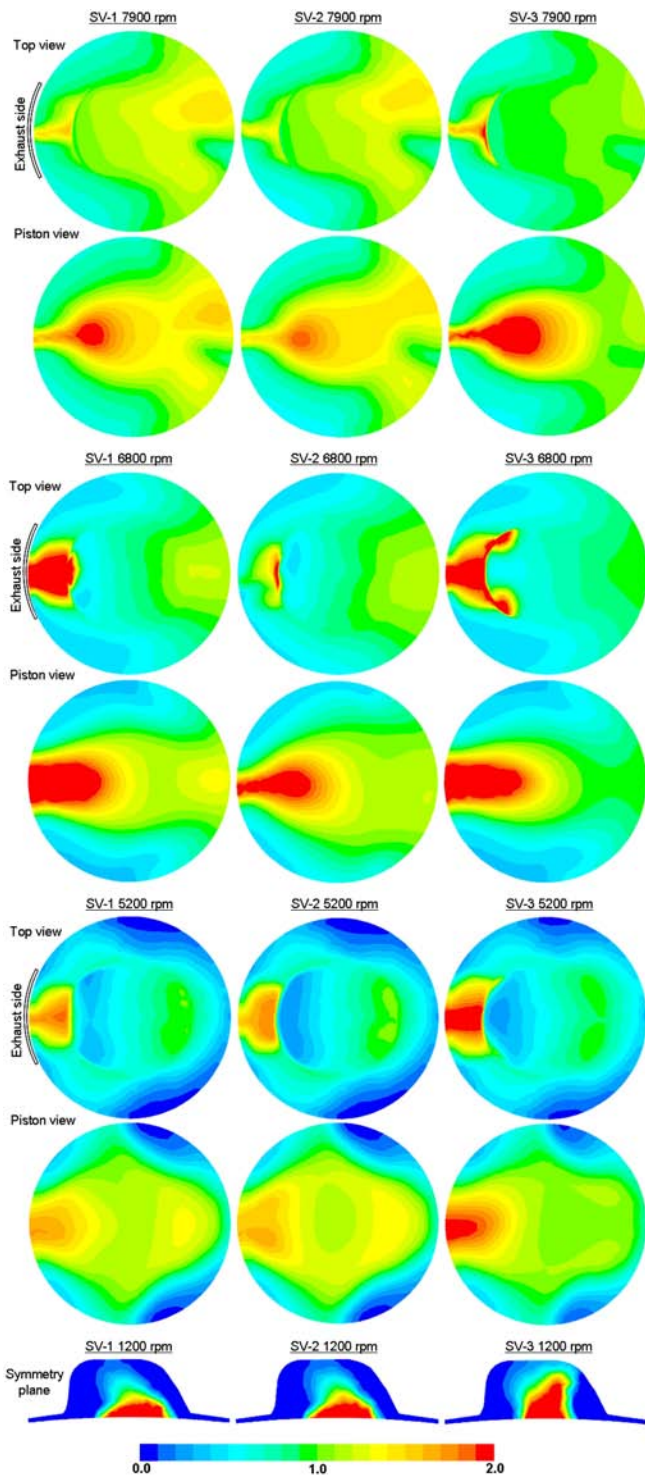
Figure 15. Equivalence ratio at start of ignition

6800 rpm

At 6800 rpm, the CFD simulation clearly shows a stratified situation inside the cylinder volume with lean and fat zones. In comparison to spray variant SV-1, SV-2 shows a reduction of fuel concentration around the cylinder symmetry plane.

This effect cannot be found in SV-3 and thus the stratified situation is even more distinct.

5200 rpm

This engine operating point is also characterized by a stratified situation. A poor fuel concentration is clearly situated around the cylinder wall. In this case, the CFD simulation shows that the spray-wall contact is reduced to a minimum. An ignitable mixture can only be found inside the cylinder volume. The spray variants, SV-1 and SV-2, show a similar equivalence ratio contour. In the case of SV-3, a bigger fuel concentration around the symmetry plane can be seen. This effect is also visible at 7900 rpm as is caused by the increase of the spray angle.

1200 rpm - Idle

The last comparison of the spray variation investigation is the equivalence ratio at 1200 rpm. At this engine speed, an extreme stratified situation can be seen. Due to a late start of injection and a weak fluid motion inside the cylinder, the injected fuel does not mix with the fresh air. Therefore, a very small zone with an ignitable mixture is achieved. In this case, the spray geometry must be designed in a way that the ignitable mixture reaches the spark plug. An alternative injection strategy would be an early fuel injection, leading to increased fuel consumption, due to an increased injected fuel mass and the requirement for an ignitable mixture in every region of the cylinder volume respectively.

Summarized, the presented equivalence ratio contours inside the cylinder show a very similar shape for all investigated spray variants. This means that the mixture quality inside the cylinder volume primarily depends on the scavenging process itself and the flow situation respectively. The spray variant SV-2 shows a reduced fuel concentration over the piston surface only at 6800 rpm, but with increased scavenging losses. At other engine speeds, the mixture quality improvement is not visible. The spray variant SV-3 causes an increase of scavenging losses at all investigated engine speeds as well as a decrease of the mixture quality.

CONCLUSION

This paper covers the discussion about the simulation methodology for the spray design investigation of a GDI injector for 2-stroke engines using the commercial CFD Code Fluent. The used settings for the simulation are presented and discussed in detail. Test bench results of the fired engine at four different engine operating points were used for the validation of the gas dynamic behavior simulation.

The employed simulation strategy consists of two steps. In the first step, the gas dynamic behavior simulation is carried out without the time consuming fuel injection and combustion process simulations. Nevertheless, this

calculation is still time consuming, due to the request for a calculation of several revolutions until a cyclic steady condition inside the engine is reached. Based on our experience, the time of calculation until a cyclic steady condition applying this simulation strategy can be reduced up to 50%. After this first step, good start conditions are available inside the engine and fuel injection simulation can be carried out as second step. Every spray variation is started from the same starting point as well as with the same initial conditions. This strategy allows a fast investigation of the different spray designs without a big computational effort. Generally, the presented gas dynamics results show a good agreement with the measurement data, indicating the applicability of the employed simulation strategy and settings. Thus, the simulation strategy can be used for investigation of all injection data, such as start and duration of injection, injector position, multiple injection strategy etc.

The results of the spray investigation show that the mixture quality inside the cylinder volume primarily depends on the scavenging process itself and the flow situation inside the cylinder volume. An increase of the spray angle (spray variant SV-3) causes a raise of the scavenging losses at all investigated engine speeds as well as a decrease of the mixture quality. A spray rotation around its spray axis has an influence on the scavenging losses and only shows an improvement of the mixture quality at 6800 rpm. For other engine speeds, the equivalence ratio contour of SV-2 is very similar to the original spray design SV-1. Furthermore, the spray investigation results show that the mixture quality is not improved by these spray modifications, so that further research work will have to focus on the injection strategy, such as start, end, and duration of injection, rail pressure variations, multiple injection strategy etc. The authors presume that there is a greater improvement potential in mixture quality applying the above mentioned injection strategy in contrast to spray design modifications.

REFERENCES

1. Trescher, D., "Development of an Efficient 3-D CFD Software to Simulate and Visualize the Scavenging of a Two-Stroke Engine", Archives of Computational Methods in Engineering, page 67-111, DOI 10.1007/s11831-007-9014-6, 2007

2. Jajcevic, D., Almbauer, R.A., Schmidt, S. P., Glinser, K., "Simulation Strategy and Analysis of a Two-Cylinder Two Stroke Engine Using CFD Code Fluent", European Automotive Simulation Conference (EASC), 2009

3. Groth, K., "Das Betriebsverhalten des schnellaufenden Zweitakt-Ottomotors mit Einspritzung und seine Entwicklungsmöglichkeiten", VDI-Verlag Düsseldorf, 1959

4. Schmidt, S., Winkler, F., Schoegl, O., and Pontoppidan, M., "Development of a Combustion Process for a High Performance 2-Stroke Engine with High Pressure Direct Injection," SAE Technical Paper 2004-01-2942, 2004.

5. Basshuysen, R., "Ottomotor mit Direkteinspritzung"; ATZ/MTZ-Fachbuch, Vieweg Germany, 2007

6. Winkler, F., "Untersuchungen zur Reduktion von Spülverlusten bei kleinvolumigen Zweitaktmotoren", PhD thesis, Graz University of Technology, 2009

7. Johnson, J. and Braven, K.R.D., "Comparison of Homogeneous, Stratified and High-Squish Stratified Combustion in a Direct-Injected Two-Stroke Engine," SAE Technical Paper 2008-32-0030, 2008, doi: 10.4271/2008-32-0030.

8. Harker, N., DenBraven, K.R., Johnson, J., and Findlay, A., "University of Idaho's Clean Snowmobile Design Using a Direct-Injection Two-Stroke Engine," SAE Technical Paper 2008-32-0031, 2008, doi: 10.4271/2008-32-0031.

9. ANSYS Fluent: "Gambit User's Guide"; Fluent Inc, 2005

10. ANSYS Fluent: "Fluent 6.3 User's Guide"; Fluent Inc, 2005

11. ANSYS Fluent: "UDF Manual"; Fluent Inc, 2005

12. Petermeier, L., "Simulation der Gemischbildung wandgeführter Otto - DE Brennverfahren unter besonderer Berücksichtigung der Strahl-Wandinteraktion", Dissertation, TU Graz, 2001

13. Eichlseder, H., Klüting, M., Piok, W.F., "Grundlagen und Technologien des Ottomotors", Springer, 2008

14. Stanciu, A.S.: "Gekoppelter Einsatz von Verfahren zur Berechnung von Einspritzhydraulik, Gemischbildung und Verbrennung von Ottomotoren mit Kraftstoff-Direkteinspritzung", Dissertation, TU Berlin, 2005

15. Trattner, A., "Experimentelle Untersuchungen und thermodynamische Analyse eines Brennverfahrenskonzepts für 4-Takt Hochleistungsmotoren mit Direkteinspritzung", Diploma thesis, Graz University of Technology, 2009

16. Schmidt, S., Schoegl, O., Rothbauer, R.J., Eichlseder, H. et al. "An Integrated 3D CFD Simulation Methodology for the Optimization of the Mixture Preparation of 2-Stroke DI Engines," SAE Technical Paper 2007-32-0029, 2007.

17. Merker, G., Schwarz, C, Stiesch, G., Otto, F., "Verbrennungsmotoren, Simulation der Verbrennung und Schadstoffbildung", B. G Teubner Verlag, ISBN-10 3-8351-0080-7, 2006

CONTACT INFORMATION

Dipl.-Ing. Dalibor Jajcevic
Christian Doppler Laboratory for "Thermodynamics of Reciprocating Engines"
Graz University of Technology
Inffeldgasse 25C
8010 Graz-Austria
Phone: +43 316 873 4586
FAX: +43 316 873 8080
jajcevic@ivt.tugraz.at
www.tugraz.at

ACKNOWLEDGMENTS

DEFINITIONS/ABBREVIATIONS

1D
one-dimensional

3D
three-dimensional, three dimensions

CA
crank angle

CFD
computational fluid dynamics

DPM
discrete phase model

EXH
exhaust

EC
exhaust close

EO
exhaust open

GDI
gasoline direct injection

LL
low load

PISO
pressure Implicit with Splitting of Operators

P-EXH-C1
pressure trend exhaust pipe cylinder 1

RAVE
Rotax Adjustable Variable Exhaust

RD
relative deviation

rpm
revolutions per minute

SV-1
spray variant 1

SV-2
spray variant 2

SV-3
spray variant 3

We
Weber number

WOT
wide open throttle

*SAE*International

4 Multidimensional coupling methodology

In order to reduce the computational effort and simultaneously include the effect of the engine periphery parts in the in-cylinder flow simulation the multidimensional simulation strategy can be employed. The basic idea is that the domain of smaller interest can be replaced by corresponding boundary conditions considering that the applied boundary condition does not influence the calculation accuracy. This technique can be understood as well as a method, where the domain of high interest and/or with a complex 3D flow is solved three dimensionally and the 0D/1D code is applied as a boundary condition exploiting the 0D/1D code advantages, such as fast computation, high level of flexibility and adaptability of the IC-engine models etc.

The data exchange between coupled domains (e.g. a 3D and 0D/1D domains) must be provided and is realized with the multidimensional coupling methodology. The basic investigation is presented in Rothbauer [27]. The author investigated a coupling method between two completely separated 3D domains and validated it for some simple cases, such as a pipe-pipe, a pipe-volume and a cylinder-pipe coupling. A further improvement step in the accuracy and in the application for the coupling between 3D and 0D/1D domains in the real world 2-stroke engine simulation is presented in the following sub-chapters.

4.1 3D-3D Coupling

The 3D-3D coupling is applied in cases where the data exchange between two completely separated cell blocks is needed. A good example is a 2-stroke engine simulation, where a coupling between the cylinder and the exhaust port as well as the cylinder and the intake ports is required. The state-of-the-art method is the so-called grid interface coupling methodology in Fluent [52], arbitrary interface in AVL Fire [97], sliding interface in OpenFOAM [100] etc. The basic difference between the conventional methods and the method used in this work is the exchange of variables. In contrast to conventional coupling methods, the computed fluxes are transported as source terms instead of the flux transport over the coupling intersection faces. The reason for this choice of data exchange is that the input value for the user defined source term of all governing equations is available in almost all conventional CFD codes, so that a direct access to the solving equations is possible as well as its implementation in all conventional CFD codes. In the following chapters the theoretical background of the 3D-3D coupling method is discussed as well as the required modifications for 1D-3D and 0D-3D coupling methods.

4.1.1 Theoretical background of the 3D-3D coupling methodology

The coupling algorithm consists of the geometry, the flux, and the source calculation, see Figure 16. At the beginning of the algorithm the coupling faces and the boundary cells are identified. The coupling flow area is divided into interface sections (in Figure 16 represented with pink and green colors). The number of sections is arbitrary and can be chosen at the beginning of the calculation. A section can include more than one cell, e.g. a cell group, but it should be considered that the coupling accuracy decreases with a decreasing section number. Otherwise, a section may not be smaller than the cell face itself. The flow area subdivision in the section is introduced by Rothbauer [27]. The advantage lies in the low programming ef-

fort, but the disadvantage is the inaccuracy caused by the introduction of a "third geometry" between the coupling faces and a double variable averaging on both sides.
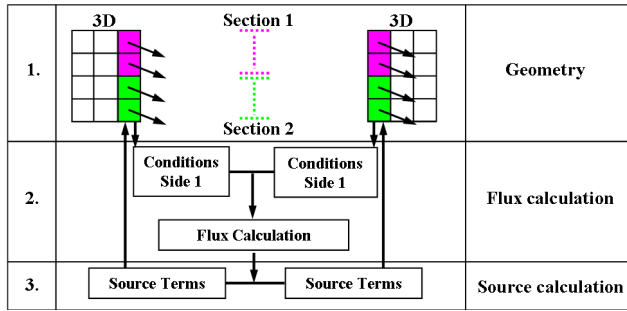
Figure 16:   3D-3D coupling methodology

In the CFD code Fluent [52] the grid interface coupling method is based on only one averaging. The geometry of one coupling face is used as predefined sections, whereas the values of the opposite face are mapped. However, Rothbauer's method is followed up in this work, due to already available functions and macros. Furthermore, flow area subdivision into sections is not required for the 0D-3D and 1D-3D coupling methods, see chapters 4.2 and 4.3. The geometry part is finished when the flow area and the section normal vector are obtained. The flux calculation part begins with the reading of cell conditions. In a next step, the cell values are mapped to the related section. After that, the fluxes can be calculated, e.g. applying the ROE-solver (see chapter 2.5.1.1.4). Finally, the well-adjusted flux values are submitted to the CFD-code as source terms and are implemented in every cell respectively. As the 3D-3D coupling procedure is already available in almost all important commercial CFD-codes, it is not necessary to apply the developed method in standard cases. Thus the focus has to be put on the advantages of 0D-3D and 1D-3D coupling methodologies (see chapters 4.2 and 4.3) and the application of the new cyclic boundary conditions (see chapters 5, 6, and 7).

4.1.2   Flow area calculation
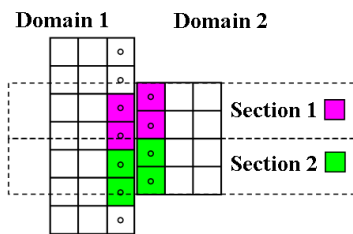
Figure 17:   Allocation problem of non-conformal grids

In the 3D-3D coupling method of Rothbauer [27] the exact flow area calculation of the sections for the case of non-conformal grids is missing. The problem is caused by the cell position in a section, see Figure 17. A cell is allocated to a section when the cell centroid is situated inside the section area. Otherwise, the cell belongs to the neighbor section or is not included in the calculation even if an overlapping surface region exists, see Figure 17 allocation problem of section 1. In order to calculate the exact flow area of the sections, a further code development is required. One possibility is to subdivide the coupling face into a finite number of triangles defined by the user at the start of calculation. Taking into account the triangle centroids instead of the cell centroids, the allocation accuracy of each cell and each section is evaluated. This method is further used for the calculation of the condition of all conserved variables of each section as well as source term of the each cell.

In order to evaluate the face area subdivision and the allocation factor, the calculation face geometry of a real world unstructured grid is used, see Figure 18. On the left side of the figure the cell face consists of four nodes and its centroid point is presented. Furthermore, an arbitrary subdivision in two sections is chosen, see dashed line. Applying Rothbauer's method the complete flow area is clearly allocated to section-1. On the right side of the figure a face subdivision into triangles is presented, where a subdivision level (SDL) of 5 is applied. The subdivision level is defined by the user at the beginning of simulation and defines the number of discretized points N on an edge with $N = SDL - 1$. After the face area subdivision into trian-

gles the allocation of every new triangle centroid to the corresponding section is determined. From these data the corresponding area division related to each section can be obtained as well as the allocation factors. In this case the allocation factor to section-1 is 0.809 and to section-2 0.191 respectively.
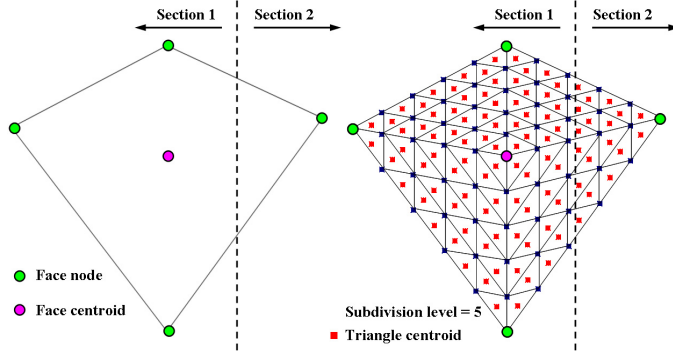
Figure 18: Face area subdivision into triangles   **Figure 19:** Relative error vs. SDL
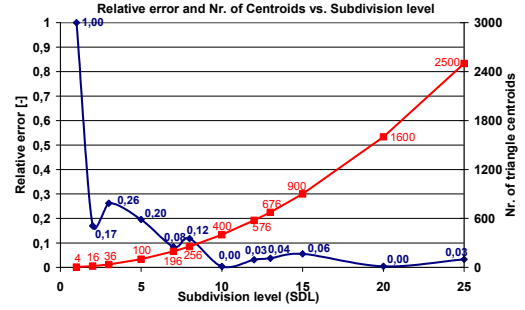
A very important fact is that the allocation factor accuracy depends on the predefined subdivision level. It should be also taken into account that the numerical effort increases non-linearly with the increasing subdivision level. Therefore, an analysis of the relative error in dependence of the subdivision factor was carried out, see Figure 19. The diagram shows that for an SDL greater than 10 the relative error is lower than 0.06. In this work the SDL is set to 10, due to the fact that for an SDL of 20 the numerical effort increases by the factor 4. In the case of moving faces, the algorithm has to be executed every time step in order to determine the new flow areas.

4.1.3 Flux and source calculations

The convective flux $\vec{F_c}$ is calculated by the Approximate Riemann Solver of Roe discussed in chapter 2.5.1.1.4.2 and is given for a 1D case as follows:

$$\vec{F_c} = \begin{bmatrix} f_1 \\ f_2 \\ f_3 \end{bmatrix} = \begin{bmatrix} \rho V A_{\text{sec}} \\ (\rho u V + p) \cdot A_{\text{sec}} \\ \rho H V A_{\text{sec}} \end{bmatrix} \tag{4.1}$$

After the flux vector calculation all required data are available and the source S_ϕ can be calculated as follows:

Continuity source: $S_C = f_1$ (4.2)

Momentum source: $S_M = f_2 - p \cdot A_{\text{sec}}$ (4.3)

Energy source: $S_E = f_3$ (4.4)

Turbulent kinetic energy source: $S_k = f_1 \cdot k$ (4.5)

Turbulent dissipation rate source: $S_\varepsilon = f_1 \cdot \varepsilon$ (4.6)

Species/scalar source: $S_{S_i} = f_1 \cdot Y_i$ (4.7)

Where, Y_i is the mass fraction of the chemical species "i" and/or the user defined passive scalars, A_{sec} is the section flow area, and V is the velocity component normal to the section face. Whereas it must be also considered that the units of all source terms are given in the form generation-rate per volume. For example, a source term for the continuity equation would have units of kg/(m³s). More details about the definition and the transport of the source term via user defined functions can be found in Fluent [95] as well as in the work of Rothbauer [27].

4.2 1D-3D Coupling

Generally, the 1D-3D coupling methodology is realized in almost the same way as the above described 3D-3D coupling. The basic difference is the variable transport to the 1D domain, whereas the data transfer to the 3D domain occurs similar to the 3D-3D coupling. This methodology allows a simultaneous application of both coupling methodologies. The cylinder and the exhaust domain can for instance be coupled by the 3D-3D coupling and simultaneously a part of the exhaust system can be replaced by the fast calculating 1D code (where the data transfer between 3D and 1D domains is realized by applying the 1D-3D coupling methodology). In the following sub-chapters the state-of-the-art and the theoretical background of the 1D-3D coupling methodology is discussed in detail.

4.2.1 State-of-the-art

Various coupling methods can be found in literature and user guides of commercial CFD codes. As mentioned before, the methods differ in the way of variable transport, but the fundamentals behind are quite similar. In this work the coupling methods between commercial codes such as AVL Fire/AVL BOOST [104], GT-Power/Star-CD [98], and GT-Power/Fluent [105] are shortly discussed.

The AVL Fire-Boost coupling method is based on an overlapping region idea. First, when the Boost model is initialized, an additional pipe consisting of one cell is automatically created [104]. In the Fire model a 3D region (cell selection) should be selected in order to define the overlapping region; otherwise the first cell layer at the coupling interface is used as overlapping region. At the beginning of the calculation the averaged values of density, momentum and temperature of the 3D domain are obtained and sent to the Boost pipe, so that the additional created pipe can be initialized. For the 3D domain the average mass flow and the flows of momentum and energy over the coupling face are set as boundary conditions.

In the coupling method between GT-Power and Star-CD the boundaries at the interface between the 1D and 3D domain can be defined as either inlet or pressure boundary conditions. In case of the inlet boundary condition, the velocity value is sent to the 3D domain, otherwise it is the pressure value respectively. The quantities are averaged, projected normal to the interface, and provided in a way that the 1D code can solve the governing equations on a staggered

grid [105]. An overlapping region for the averaging of transported values must also be selected.

The coupling between GT-Power and Fluent is realized in such a way that GT-Power is dynamically linked to Fluent via user defined functions (UDFs). The control over the GT-Power simulation is done inside Fluent by a direct call of the GT-Power engine model. The data exchange is realized in a similar way as described above. Two methods - the mass-flow inlet or the pressure inlet boundary condition - can be applied. The 1D code is used in order to define the boundary condition for the 3D domain. In the case of the mass-flow inlet boundary condition the mass flux rate and other quantities such as the density, the total energy, and the species concentrations are sent to Fluent at the beginning of each time step. Otherwise, instead of the mass-flow rate the pressure data are sent to Fluent. In order to initialize the 1D code the volume averaged data over the boundary face are sent to GT-Power.
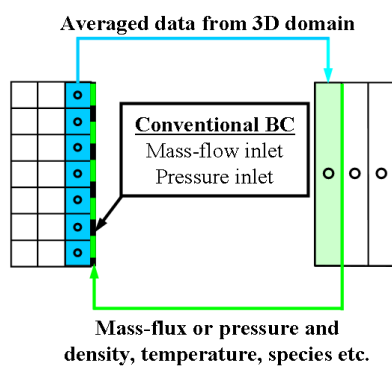
Figure 20: **Conventional 1D-3D coupling methods**

Summarizing, each of above described coupling method includes an overlapping region, see Figure 20 (domains marked with blue and green colors). From the 3D domain the volume averaged data are sent to the 1D domain in order to initialize the overlapping cells of the 1D domain. Dependent on the coupling strategy, the mass-flux or the pressure and other required quantities are sent to the 3D domain. In all above mentioned cases, the conventional boundary conditions are used for the data transfer to the 3D domain. The data from the 1D domain are input parameters for the CFD boundary conditions. The required fluxes are obtained by the boundary condition itself. The 1D domain is considered as a tool which is used in order to determine more accurate inlet/outlet data, whereas the domain of lower interest is replaced by the fast calculating 1D code.

4.2.2 Theoretical background of 1D-3D coupling methodology
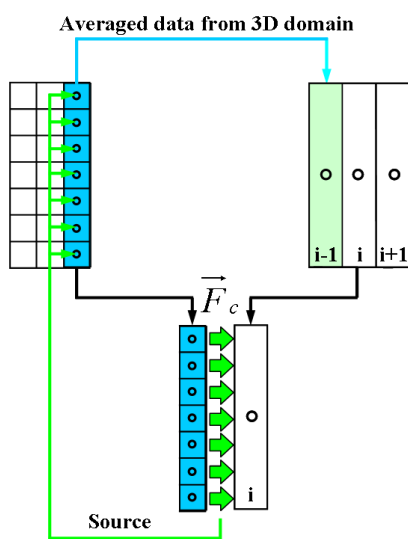
Figure 21: **1D-3D coupling method**

The scheme of the 1D-3D coupling methodology applied in this work is presented in Figure 21. The first step is the data transfer from 3D to 1D domain. The first cell at position "i-1" of the 1D code is initialized with the conserved variables which are averaged over all cells of the blue marked domain in the 3D region. The cell at position "i-1" and time step "n" can be seen as prescribed variables at the boundary of the 1D code. The 1D code has now all required data for the calculation at the time step "n+1". Concurrently, the cell at position "i" and at time step "n" is used for the calculation of fluxes for the sections of the 3D region. In the next step, the calculated fluxes are transferred into the 3D domain as source terms. Therefore, the coupling methodology between 1D and 3D domains is the same as the coupling between two 3D domains. The only difference is that cell "i" of the 1D code consists of only 1 section, respectively the sections of these regions have the same conserved variables as cell "i". The flow area for the 1D side is received from the 3D region and the correspond-

ing sections. Due to the fact that the 1D domain consists of only one cell, which is connected to the 3D domain, the division into subsection is obsolete. This means that every cell in the 3D domain can be viewed as a section and that for each cell the fluxes and the sources can be obtained.
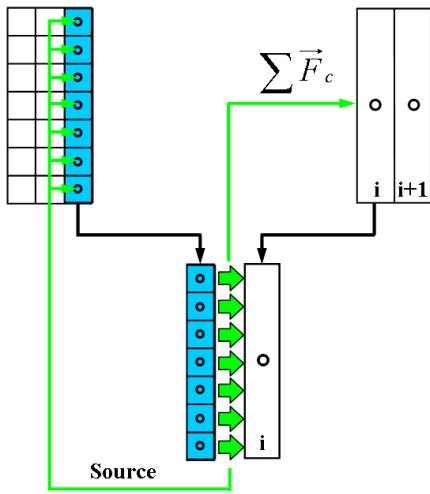
Figure 22: **1D-3D coupling method without overlapping region**

The basic difference between the used 1D-3D coupling method and the above mentioned conventional methods is that the calculated fluxes are transported to the 3D domain via source terms instead of the definition of the properties for the conventional inlet/outlet boundary conditions. However, in both methods as well as in some cases it can occur that the fluxes for the same boundary face differ due to separate flux calculation for each domain. This problem can be avoided by applying the scheme presented in Figure 22. In this case the initialization of the 1D cell "i-1" is avoided. The calculated fluxes for the 3D domain are used for the flux definition of the cell "i" inside the 1D domain and are obtained as a sum. An important advantage of the proposed method is the consistency of the fluxes of the individually conserved variables as well as the avoidance of the overlapping region.

The benefit of the presented 1D-3D coupling method can be summarized as follows:

- Due to the fact that the data transfer to the 3D domain occurs by applying the source terms, a boundary specification is not required. Therefore, the 3D domain is not sensitive to the flow direction and the conventional boundary scheme is eliminated.

- Due to a direct calculation of fluxes both coupling areas are coupled in the strongest possible way.

- The consistency of the fluxes is always provided and an overlapping region can be avoided.

4.2.3 Validation of the 1D-3D coupling method
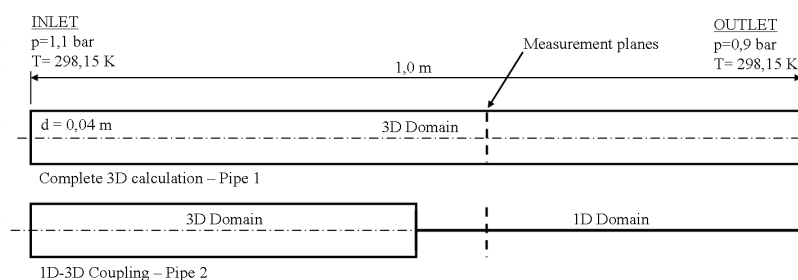
Figure 23: **Validation of the 1D-3D coupling method**

For the validation of the 1D-3D coupling method, a simulation of two simple pipe flows is carried out, see Figure 23. The pipes have a length of 1 meter and a diameter of 0.04 meter. The 1D-3D coupling is placed exactly in the middle of pipe 2 (0.5 meter). In the region where the 1D

code is applied the measurement planes are set in both pipes, see dashed line. The evaluated data inside pipe 1 are used as reference values for the validation without the influence of any coupling. These data are compared with the values inside pipe 2, which include the influence of the coupling and the 1D code. For both pipes identical inlet and outlet boundary conditions are defined, see Figure 23. The fluid in the model is defined as air with constant properties. The variation of density is calculated from the ideal gas law ($p = \rho RT$). At the inlet face the pressure value of 1.1 bar and the temperature of 298.15 K are set and 0.9 bar and 298.15 K at the outlet face respectively. The calculation is carried out until a steady condition along complete pipe length is reached. The in-house developed 1D code, which uses the second order accurate TVD solver, is applied in this simulation for the flux calculation inside the 1D region. In the previous paper [106] the 1D code and the TVD solver are discussed in detail.
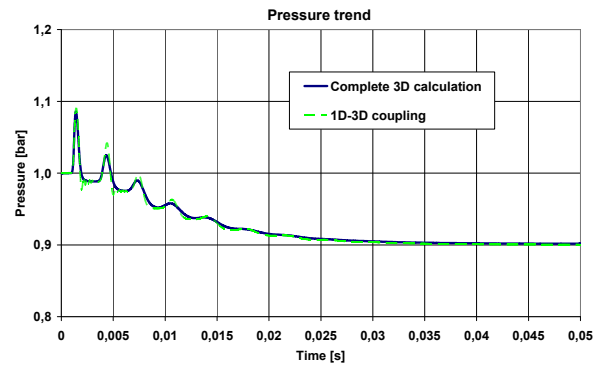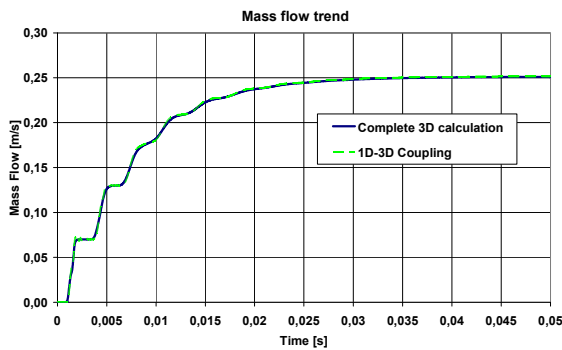
Figure 24:   1D-3D coupling – Mass flow trend   **Figure 25:   1D-3D coupling – Pressure trend**

Figure 24 and Figure 25 show the comparison of the mass flow and the pressure trend between the complete 3D pipe 1 simulation and the simulation where half of pipe 2 is replaced with the 1D code. In general, a good agreement between both results is visible; especially in the comparison of the mass flow trend. In the pressure trend comparison and in the region between 0 and 0.01 seconds, the pressure trend inside the 1D code shows an oscillating trend, which can be neglected for industry relevant simulations. This deviation occurs due to a discontinuity between the 3D and 1D domain, e.g. due to a friction coefficient deviation.

4.3   0D-3D Coupling
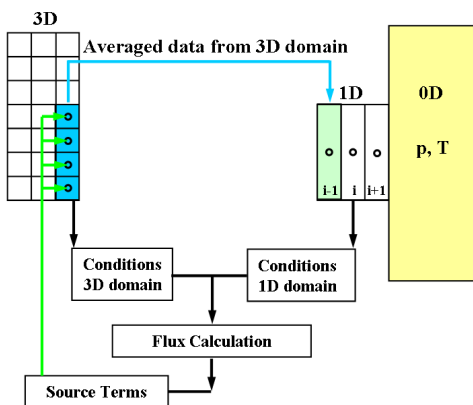
Figure 26:   0D-3D coupling method

Figure 26 represents a scheme of the 0D and the 3D coupling methodology used in this work. This model consists of 0D, 1D and 3D domains that are coupled together. Between the crank case (in Figure 26 the 0D domain is presented with yellow color) and the 3D domain a short pipe is modeled using the 1D code with the same diameter as the connecting area in the 3D region. Pressure and temperature as total properties of the gas inside the crank case are taken as the outlet boundary condition of the 1D pipe. The first cell "i-1" of the 1D code is initialized as already described in the 1D-3D coupling methodology. Therewith the 1D code has all required data for the calculation of the next time step "n+1". The data transfer to the 3D domain is realized analogue to the above described 1D-3D coupling methodology.

89

The crank case volume is modeled using a 0D code considering the conservation of mass, energy, heat transfer and variability of the volume, see Rothbauer [106]. The condition of the gas in the crank case is obtained by solving the First Law of Thermodynamics, see equation (4.8) and the continuity equation.

$$\frac{d(m \cdot e)}{dt} = -p\frac{dV}{dt} + \sum \frac{dQ}{dt} + \sum \frac{dm_i}{dt} \cdot h_i - \sum \frac{dm_e}{dt} \cdot h_e \qquad (4.8)$$

Where, m is mass, e is specific internal energy, p is pressure, V is volume, Q is heat flux, h is specific enthalpy, t is time, subscript i is inlet and e is exit. The crank case volume is calculated by the motion and the position of the piston and therefore is a function of the crank angle. The total mass inside the crankcase is calculated from the sum of the inflow and outflow masses of the connected ports of the 3D domain.

4.4   Limitation of the multidimensional coupling methodology and simulation

The multidimensional coupling methodology can be used for the coupling between two completely separated 3D domains as well as for the coupling between 0D/1D and 3D domains. Due to the fact that the 3D-3D coupling methodology is already integrated in almost all CFD codes, the presented coupling method is normally not used in the development process of a new engine. For the coupling between 0D/1D and 3D domains the coupling method is applied as well as in the development of the new cyclic boundary condition presented in chapter 5. However, the 3D-3D coupling methodology is the core of all coupling methods and of the boundary condition applied in this work.

The basic idea of the multidimensional simulation is that the domain of smaller interest can be replaced by fast calculating 0D/1D codes in order to reduce the number of 3D cells and therewith the duration of the calculation. The application of this method is strongly limited by the position of the coupling face. In regions with recirculation zones or zones of non-uniform flow profiles the application of this method causes a decrease of the simulation accuracy, due to the fact that the 0D/1D codes do not provide information of the flow profile. The data from the 0D/1D codes are generally approximated to be constant in space over the complete face. Therefore, the coupling face has to be placed far from the interesting domain in order to avoid a negative influence on the 3D domain; unfortunately this directly increases the calculation time due to the increase of the 3D calculation domain. The next problem when applying the multidimensional simulation is directly related to the 0D/1D tools and their limitations in a simulation of complex geometries and strong 3D physical effects, such as recirculation, turbulence, fuel injection process, mixture preparation, combustion process etc. However, this limitation should be taken into consideration for the definition of the coupling positions and for the region which is replaced by the 0D/1D codes.

4.5 Paper II

CFD Simulation of a Real World High-Performance Two Stroke Engine with Use of a Multidimensional Coupling Methodology

SAE *International*®

CFD Simulation of a Real World High-Performance Two Stroke Engine with Use of a Multidimensional Coupling Methodology

Dalibor JAJCEVIC, Raimund A. ALMBAUER
Christian Doppler Laboratory "Thermodynamics of Reciprocating Engines", Graz University of Technology

Stephan P. SCHMIDT
Institute for Internal Combustion Engines and Thermodynamics, Graz University of Technology

Karl GLINSNER
BRP Rotax

ABSTRACT

CFD simulation (Computational Fluid Dynamics) is a state of the art tool for the development of internal combustion engines, especially for internal mixture preparation, scavenging process and combustion. Simulation offers an array of information in the early development phase without the need of building a prototype engine. It shortens the development time, reduces the number of prototypes and therewith test bench costs.

In previous investigations [SAE 2005-32-0099] and [SAE 2007-32-0030] a new coupling methodology which bases on the combination of three-dimensional (3D), one-dimensional (1D), and zero-dimensional (0D) CFD calculation has been presented. This methodology uses a new multidimensional interface technology and is able to handle 3D-0D, 3D-1D and 3D-3D connections. The special feature of this methodology is the capability of being placed on any position in the 3D CFD mesh. For instance, reed valve and crankcase are replaced by a 0D model, exhaust pipe by a 1D model and finally all these models are connected with the new interface technology in the 3D CFD mesh. Therefore, this methodology allows the replacement of regions with a high number of 3D cells by fast-calculating 0D or 1D models and therewith reduces computational time.

This paper covers the detailed discussion of the above mentioned coupling methodology and its application on a real-world high-performance two-stroke engine. The validation of the methodology is based on a simulation with the CFD-Code FLUENT 6.3. This analysis of a high-performance two stroke engine will be carried out to demonstrate the working of this coupling methodology and it will be compared with a conventional 3D CFD calculation. The main focus lies on the accurateness of results with 3D-3D, 3D-1D and 3D-0D coupling models, their computational time, and handling of the coupling methodology. Also the use of the methodology for a real world development task like the optimization of two-stroke engines will be demonstrated.

INTRODUCTION

The new emission standards demand the further development of two stroke engines by the implementation of new technologies respectively new methods. The use of CFD simulation (Computational Fluid Dynamics) offers an array of information in the early development phase. It should offer the R&D team a success assessment of new technologies, e.g. new fuel preparation methods, new combustion concepts and/or alternative fuels, and furthermore support the prototyping phase on the engine test bench. Additionally, these new technologies require high standards of knowledge and high testing efforts on the engine test-bench. This knowledge can be partly acquired with the use of new fast-calculating simulations tools in combination with the 3D CFD simulation.

The 3D CFD simulation of two stroke engines is required to calculate the processes of scavenging, in-cylinder charge motion, spray formation, mixture preparation and combustion. The drawback of full 3D CFD simulation is the required time for grid generation and calculation. The difficulties in the simulation of two stroke engines arise due to the open scavenging process of two stroke specific parts (exhaust port/intake ports and cylinder). The exhaust pipe and the two stroke crankcase predominantly affect the scavenging process. The 3D region of the exhaust system can be replaced by a fast-calculating 1D model and the 3D region of the crankcase

by a 0D model. The difficulty with the two stroke simulation is that conventional 0D/1D models cannot provide the requested quality and cannot be used for the simulation of specific parts of the two stroke engine. A possibility to combine the advantages of the 0D/1D and 3D approach offers an array of information in shorter calculation time and therewith increases the number of investigated cases in the early development phase of a new engine. The time-consuming 3D simulation is only used in engine regions where 3D dissolved results are required.

The fast-calculating models (0D or 1D), appropriate for two stroke engines, require a new multidimensional interface coupling technology to be able to handle connections with 3D regions. The connection between 3D regions is a technical basis for other coupling methods and furthermore is used for simulation of two stroke engines between the intake ports and the cylinder. The special feature of this interface coupling methodology is the capability of being placed on any face of the 3D CFD mesh. The coupling allows a connection between a conformal and a non-conformal grid. In previous investigations [SAE 2005-32-0099] [1] and [SAE 2007-32-0030] [3] a new coupling interface methodology has been presented and discussed in detail. In this paper the geometry of a real world two stroke engine is used and the results will be compared with a conventional 3D CFD calculation.

INTERFACE COUPLING STRUCTURE
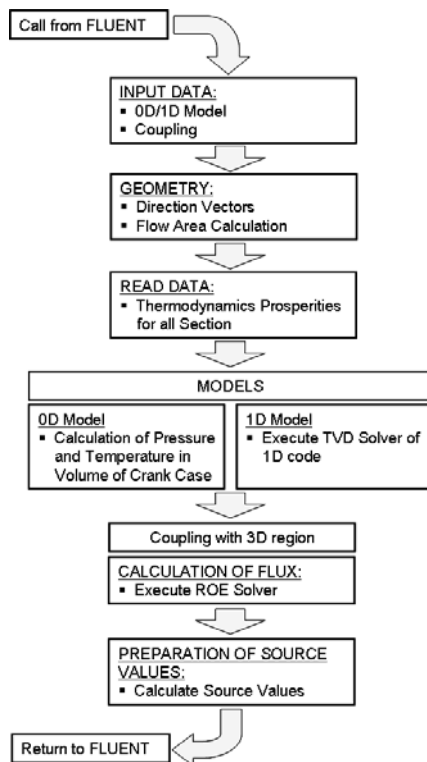
Figure 1: Flowchart of the coupling methodology

The coupling code and the models (0D and 1D code) are written in the C programming language as a user-defined function (UDF) and can be dynamically loaded with the FLUENT solver. The source code containing UDFs is directly compiled in FLUENT and uses additional macros and functions that are supplied by Fluent. Detailed description of UDFs can be found in [16].

Figure 1 presents a flowchart of the new coupling methodology and models. The code consists of six main blocks - i.e. input data, geometry, read data, models, calculation of fluxes, and preparation of source values. The code is executed every time step/iteration from FLUENT. The block "Input Data" includes all required geometries and condition data which have been defined at the start of the simulation. The "Geometry" code is able to calculate the flow area for conformal and non-conformal grids in dependency of the piston position. The current flow area is divided into interface sections and for each section the appropriate area and normal vector are calculated. In the next step, for each interface section, thermodynamic properties from the marked 3D region, and/or the corresponding model, are read and saved (code "Read Data"). Therewith, all required data for the calculation of fluxes between two coupling regions are available and are calculated separately for each coupling methodology (code "Calculation of fluxes"). Finally, the well-adjusted values are submitted to the CFD-code Fluent (code "Preparation of source values"). The 0D and 1D models are executed after the function "Read data" and work independent from the coupling code - after reading data from the 3D coupling region, the 0D or 1D code has all required data for the calculation of the next time step "n+1".

APPLICATION OF THE MODELS AND COUPLING

In the first phase of simulation and development of a new engine a minimum amount of data and time is available. The total 3D CFD simulation requires the maximum effort in modeling and computational time, but provides high quality predictive results. When a region of 3D flow geometry is replaced by 0D/1D models, the simulation offers almost the same information about the new engine in short calculation time. In this paper the crankcase is replaced by a 0D model and the exhaust by a 1D model. Finally, all these models are connected with the new interface technology in the 3D CFD model. A technical basis for 0D-3D and 1D-3D coupling methods is the 3D-3D coupling methodology.

3D-3D COUPLING - The coupling flow area is divided into interface sections (see Figure 2). An interface flow between the coupling cells of each interface sections is calculated from mass, velocity, energy, turbulence, transported species and droplets. The fluxes are calculated by the approximate Riemann Solver of Roe, according to Toro [9]. Finally, the calculated values are

submitted as a source to the 3D CFD solver. A typical example of the 3D-3D coupling method for the simulation of two stroke engines is used between the cylinder and intake/exhaust ports. In this paper this has been used in both cases.
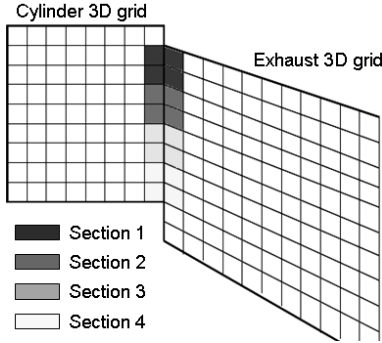
Figure 2: 3D-3D coupling methodology

1D-3D COUPLING - A 1D code is well suited to be used for exhaust simulation of two stroke engines and has been developed for a good description of the area changes. The second order accurate TVD (Total Variation Diminishing) solver is used in this model for the calculation of fluxes of pipes with varying diameter. In the previous paper [SAE 2007-32-0030] [3], this model and the TVD solver were discussed in detail. The simultaneous use of 1D and 3D CFD calculations requires overlapping regions of the geometry. These regions in conventional codes are calculated simultaneously in the 1D and the 3D solver (see [6], [15]).

The governing equation (1) for the 1D simulation with an additional term due to the cross-section variation is formulated:

$$\frac{\partial U}{\partial t} + \frac{\partial F(U)}{\partial x} + B + S = 0 \tag{1}$$

$$U = \begin{pmatrix} U_1 \\ U_2 \\ U_3 \end{pmatrix} = \begin{pmatrix} \rho A \\ \rho u A \\ E A \end{pmatrix}, F = \begin{pmatrix} F_1 \\ F_2 \\ F_3 \end{pmatrix} = \begin{pmatrix} \rho u A \\ (\rho u^2 + p) A \\ u A (E + p) \end{pmatrix}, S = \begin{pmatrix} S_1 \\ S_2 \\ S_3 \end{pmatrix},$$

$$B = \begin{pmatrix} 0 \\ p \dfrac{dA}{dx} \\ 0 \end{pmatrix}$$

with ρ=density, u=velocity, p=pressure, E=energy, S=source vector, U=state vector, F=flux vector, t=time, A=area, x=length.

In this coupling methodology between 1D and 3D regions, a first cell at position "i-1" (see Figure 3) of the 1D code is initialized with a conserved variable $\overline{\Phi}$ (see equation (2)) which is averaged over all cells of a marked domain in the 3D region.

$$\overline{\Phi} = \frac{\int \Phi \, dV}{V} \tag{2}$$

The cell at position "i-1" and at time step "n" can be seen as prescribed variables data at the boundary of the next cell at position "i" of the 1D code. The 1D code now has all required data for the calculation at the time step "n+1". Concurrently, this cell at position "i" and at time step "n" is used for the calculation of fluxes for the sections of the 3D region. In the next step calculated fluxes are transferred into the 3D domain as source terms. Therefore, the coupling methodology between 1D and 3D domains is the same as the coupling between 3D and 3D domains. The only difference is the cell "i" without sections, respectively, the sections of these regions have the same conserved variable Φ as the cell "i". The flow area for the 1D side is received from the 3D region and the corresponding section.
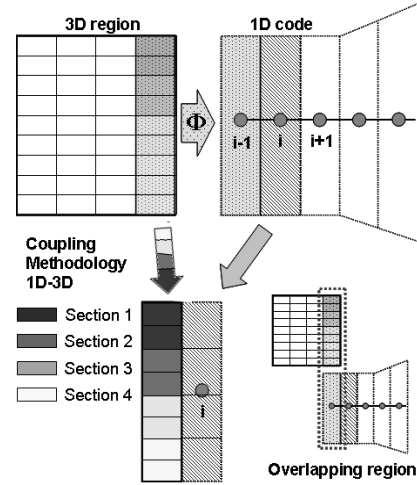
Figure 3: 1D-3D coupling methodology

0D-3D COUPLING - The crank case volume is modeled using a 0-dimensional code considering the conservation of mass, energy, heat transfer and variability of the volume. The condition of gas in the crank case is obtained by solving the First Law of Thermodynamics (see equation (3)), with m=mass, e=specific internal energy, p=pressure, V=volume, Q=heat release, h=specific enthalpy, t=time, subscript i=inlet, e=exit and the continuity equation.

$$\frac{d(m \cdot e)}{dt} = -p \frac{dV}{dt} + \sum \frac{dQ}{dt} + \sum \frac{dm_i}{dt} \cdot h_i - \sum \frac{dm_e}{dt} \cdot h_e \tag{3}$$

The crank case volume is calculated by the motion and the position of the piston and therefore this is a function of the crank angle. Total mass inside the crankcase is calculated from the sum of the inflow and outflow masses of connected ports of the 3D domain. For the calculation of the heat transfer between the gas inside the crank case and its surfaces the *Adair* model [13] was used.

Figure 4 represents a scheme of the 0D and the 3D coupling methodology. This model consists of 0D, 1D and 3D domains that are coupled together. Between the crank case (0D domain) and the 3D domain a short pipe is modeled using the 1D code with the same diameter as the connecting area in the 3D region. Pressure and temperature as total properties of the gas inside the crank case are taken as the boundary condition of the 1D pipe. The first cell "i-1" of the 1D code is initialized as already described in the 1D-3D coupling methodology. Therewith the 1D code has all required data for the calculation of the next time step "n+1". The coupling with the 3D domain occurs analog to the described 1D-3D coupling methodology.
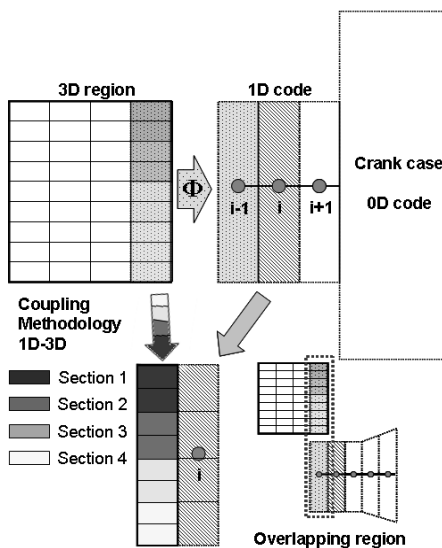
Figure 4: 0D-3D coupling methodology

MODEL BUILD-UP

The modeling of the real geometry of two stroke engines requires a lot of time and data. Additional difficulties could be attributed to the mesh generation of a naturally complicated geometry like intake ports. The construction of the mesh is heavily dependent on some techniques, such as automatic meshing, multi-block domain and arbitrary mesh interface [11]. The focus of this paper was mainly to explore the feasibility of the above mentioned coupling methodology, its handling and the accurateness of results for the simulation of real world two stroke engines. The simulations were conducted at only one engine speed of 5000 rpm.

GRID GEOMETRY - The grid geometry was based on a single-cylinder of a two stroke engine from BRP Rotax Company, with loop scavenging via five intake ports and a stroke volume of 500 cm³. The simulation took advantage of the symmetrical layout by modeling only one half of the geometry. This method reduces the time required to generate the mesh and consequently the computational time of the total simulation. The grid structure contains approximately 150000 cells at top

dead center of the piston and is composed of four main blocks - the cylinder, the crank case, the intake ports, and the exhaust (see Figure 5).
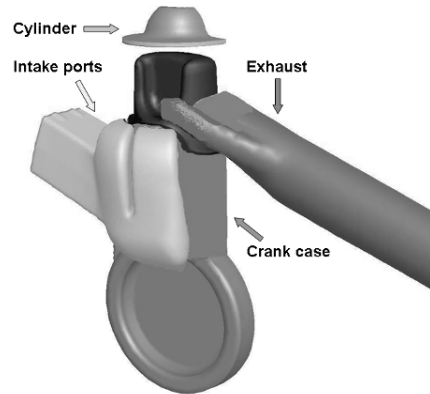
Figure 5: Grid geometry of the investigated two stroke engine

The coupling between these blocks occurs with the use of a 3D-3D coupling methodology. The first alternative is the use of the standard coupling tool of the CFD-Code FLUENT 6.3 [11] (further in the text: 3D-3D-FLUENT) which was used for the total 3D CFD simulation. The second alternative is the above mentioned new 3D-3D coupling methodology (further in the text: 3D-3D).

The piston geometry, cylinder, intake ports, crank case and exhaust, were generated exactly as the real engine geometry. This was necessary to check how the geometry code of the new interface coupling methodology works for the different cell geometries and for the very complex geometry of a two stroke engine. During the validation it emerged that the real geometry requires more complicated program solutions of the coupling than the simple geometry with a structured grid. However, the above mentioned coupling methodology was programmed for any type of cells, the tetrahedron or the hexahedron cells, as well as the conformal or non-conformal grids and every direction.

Table 1: Technical data of the investigated two stroke engine

Engine type	Rotax SDI 995 – 2 Cylinder		
Power	P[kW]	120	
Bore	[mm]	88	
Stroke	[mm]	82	
Connecting rod	[mm]	145	
Cylinder volume	[cm³]	498	
Compression ration	[-]	11.66	
Exhaust port 1 open	°CA	78	mm	38.00
Exhaust port 2 open	°CA	80	mm	40.00
Intake ports open	°CA	115	mm	63.00
Exhaust port 1 close	°CA	282	mm	38.00
Exhaust port 2 close	°CA	280	mm	40.00
Intake ports close	°CA	245	mm	63.00

The mesh was constructed using an automatic meshing tool of the software code GAMBIT [12] for all blocks of the geometry. Other major dimensions are presented in Table 1. The mesh movements on both sides of the piston are carried out with the use of the layering methodology of the software tools ANSYS FLUENT 6.3. The mesh motion was executed for every time step and for both motions. Detailed description of this mesh moving methodology can be found in FLUENT [11].

BOUNDARY CONDITIONS - The boundary conditions were specified using data from the engine tests on a test bench [8] and from a simulation [4]. The five main boundary types are used in the model, i.e. pressure, velocity, wall, symmetry and interface. The pressure was defined only at the outlet of the exhaust and set to atmospheric conditions of 100000 Pa and 300 K. The velocity is used as boundary condition for the reed valve and was calculated with the 1D code analogous to [3]. The velocity is calculated from the data of mass flow with the constant density at the atmospheric conditions 100000 Pa and 300 K. The Mach number is very small (Ma << 1) and the influence of the compressibility can be neglected. Figure 6 represents a velocity plot of only one inlet face from the total of four faces.
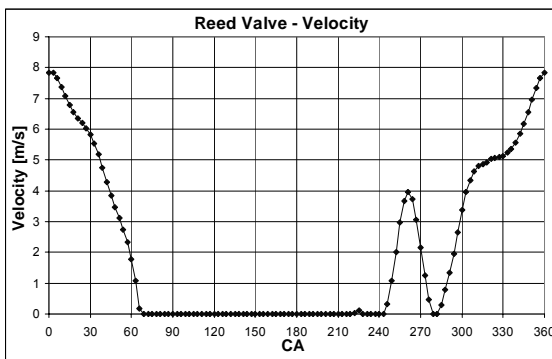
Figure 6: Reed valve – velocity

The temperature at the wall of the crank case and the intake ports was set to a constant value of 313 K, the wall of the cylinder to 450 K, the piston to 550 K and the wall of the exhaust to 943 K. The default wall temperature was set to 313 K. The boundary type interface is used for the connection between two 3D regions, for instance, between the cylinder and the intake ports or the exhaust. This is used only in the calculation without the above described 3D-3D coupling methodology.

INITIAL CONDITIONS - Fluid in the model is defined as air with starting conditions for temperature of 313 K and pressure of 100000 Pa. The variation of density is calculated from the ideal gas law (p=ρRT). The standard k- ε turbulence model was used to model the turbulent flow. The standard values for the turbulent kinetic energy k and the dissipation rate ε were taken from the settings of software ANSYS FLUENT 6.3 [11].

At the top dead center of the piston, the cylinder was initialized with the temperature of 2800 K and the pressure of 4600000 Pa. The crank case and the intake ports are initialized with the temperature of 313 K and the pressure of 87500 Pa. The total exhaust region is initialized with the temperature of 943 K and the pressure of 100000 Pa. The data stem from the simulation described by [4] and [8].

SIMULATION OF THE COMPLETE ENGINE

The validation of the models and the new multidimensional interface technology is carried out by separate simulations of each coupling methodology (see Table 2). All these calculations are compared with the conventional 3D CFD calculation of the scavenging process, namely without an injection and a combustion. At the top dead center of the piston (0 °CA) and for every next revolution, the 3D region of the cylinder is initialized with the pressure of 4600000 Pa and the temperature of 2800 K.

Table 2: Investigated cases

Case	Description	Comment
1.	3D-3D Coupling	Coupling between 3D regions of the cylinder and exhaust/intake ports
2.	1D-3D Coupling	The 3D region of the exhaust was replaced with the 1D code
3.	0D-3D Coupling	The 3D region of the crank case was replaced with the 0D code
4.	0D-1D-3D Coupling	The simulation with the simultaneous coupling of the 0D, 1D and 3D coupling methodology

The first simulation is the validation of the 3D-3D interface coupling methodology and was used for the coupling of the 3D region of the cylinder and 3D regions of the intake ports and the exhaust. The second validation was carried out by the simulation where the 3D region of the exhaust was replaced with the fast-calculating 1D code. The third simulation is the validation of the 0D model of the crank case. In the final simulation the exhaust and the crank case 3D region were replaced with corresponding fast-calculating models and compared with the total 3D CFD calculation of the two stroke engine.

The required data for the validation are calculated on predefined faces. On these faces the averaged area values - pressure, mass flow and temperature - are evaluated. In the 3D regions of the cylinder, the intake ports and the crank case the averaged volume values of the pressure and the temperature are calculated as well. The results are evaluated with "good agreement" when the deviation of the averaged values in the measurement faces ranges within ±5%. Further, for the validation of the above mentioned coupling methodology, the figures with a passive scalar and a velocity in the symmetry plane are compared with the 3D-3D Fluent results. At the top dead center of the piston (0 °CA) and for each of the five revolutions, the

3D region of the intake ports and the crank case are initialized with the passive scalar with the value of zero (0), the 3D region of cylinder with the value of one (1) and the 3D region of exhaust with the value of two (2).

The position and the name of the measurement faces are displayed in Figure 7. The exhaust port consists of the main and the side pipe. In this 3D region of the exhaust four measurement faces are set. The measurement faces "EXH 0" and "EXH 0a" are designed with the diameter of 90 mm (diameter of the cylinder is 88 mm) and the measurement faces "EXH 1" and "EXH 1a" with the diameter of 130 mm, measured from the axis of the cylinder. In the 3D region of intake ports three measurement faces are set, "IN 1", "IN 2" and "IN 3". They are also designed with the diameter of 90 mm just as the measurement faces of the exhaust.
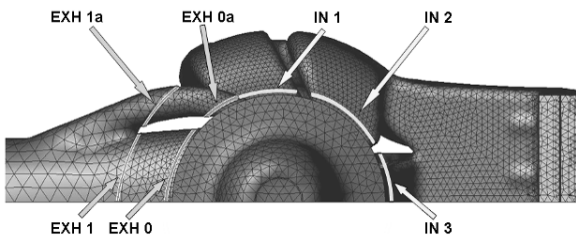
Figure 7: Measurement faces in the 3D region

VALIDATION OF THE 3D-3D COUPLING METHODOLOGY - The 3D-3D coupling methodology is automated and does not require a lot of data for a start of the calculation. It is enough to define an ID number of the coupling faces and all other data are calculated from the code itself. In this case five couplings between 3D regions are necessary, namely two for the coupling on the side of the exhaust and three on the side of the intake ports. In this code it is possible to couple only one face with one or more opposite faces. This option was used in the validation; namely two faces, small exhaust pipe and intake port "IN 1", are coupled with one face of the cylinder.
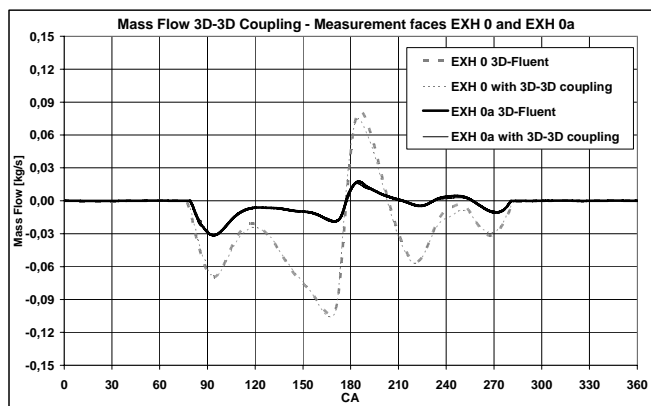
Figure 8: Mass flow 3D-3D coupling, EXH 0 and 0a
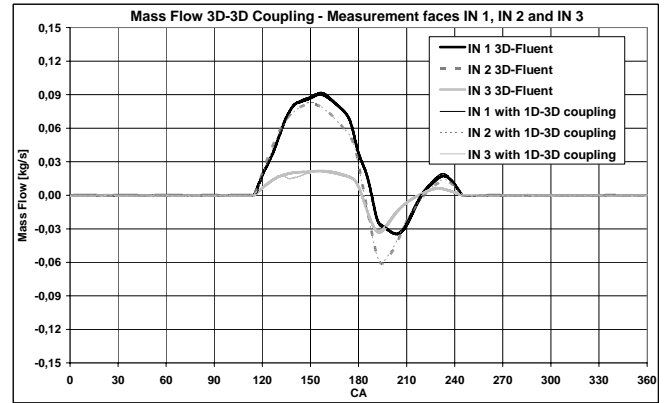
Figure 9: Mass flow 3D-3D coupling, IN 1, 2 and 3

Results after five cycles of the simulation with the 3D-3D coupling are presented in Figure 8 - Figure 13. Mass Flow: Figure 8 shows the comparison of the mass flow in the measurement faces of the exhaust (EXH 0 and EXH 0a) and Figure 9 shows the comparison of the mass flow in the region of intake ports (IN 1, IN 2 and IN 3). A good correlation between the simulation with the 3D-3D coupling methodology and the 3D-3D-FLUENT coupling is visible. In the region between 130°CA and 150°CA a small deviation in the trend of curve (IN 3) is visible.

Pressure: Figure 10 shows the comparison of the pressure in measurement faces "EXH 0" and "EXH 0a" and Figure 11 in faces "IN 1", "IN 2" and "IN 3". Plots of the pressure in the intake ports and in the exhaust port show a good correlation over the complete revolution of 360°CA.
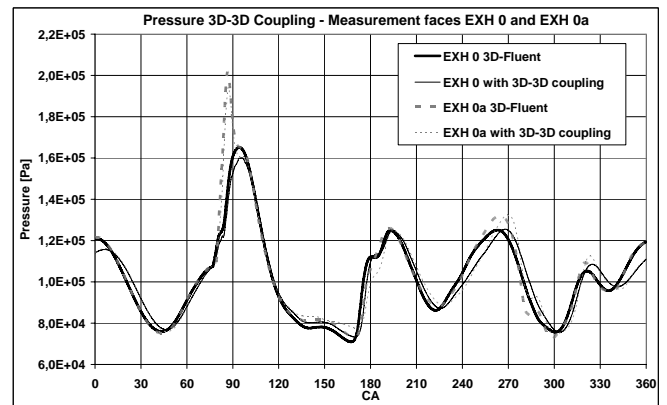
Figure 10: Pressure 3D-3D coupling, EXH 0 and 0a
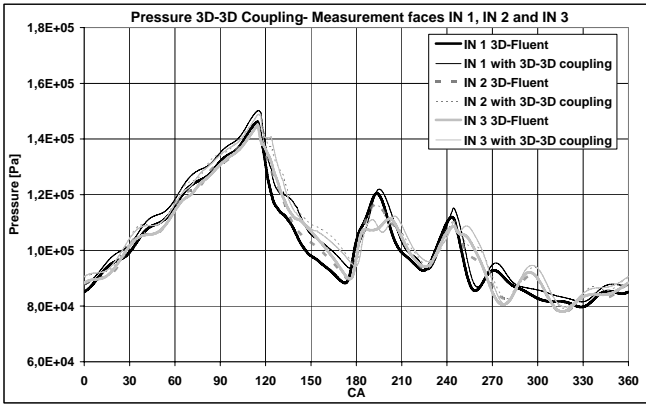
Figure 11: Pressure 3D-3D coupling, IN 1, 2 and 3

Temperature: The temperature trend in the exhaust shows a good agreement (Figure 12). The deviation can only be seen in the region between 220°CA and 260°CA. In the measurement faces "IN 2" and "IN 3" the difference is smaller than the difference in the "IN 1" face (see Figure 13). The biggest deviation can be seen in the region between 0°CA and 120°CA with 37 K.
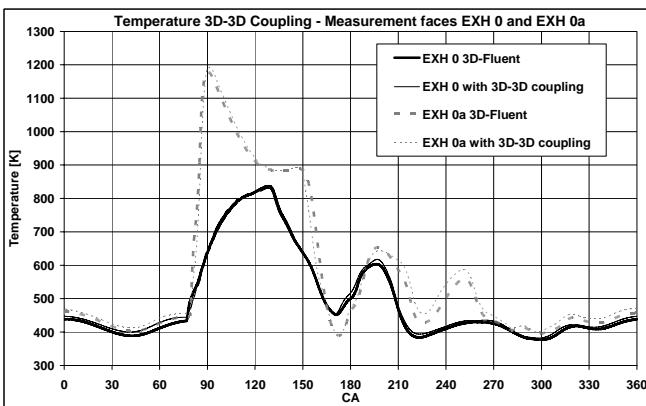
Figure 12: Temperature 3D-3D coupling, EHX 0 and 0a
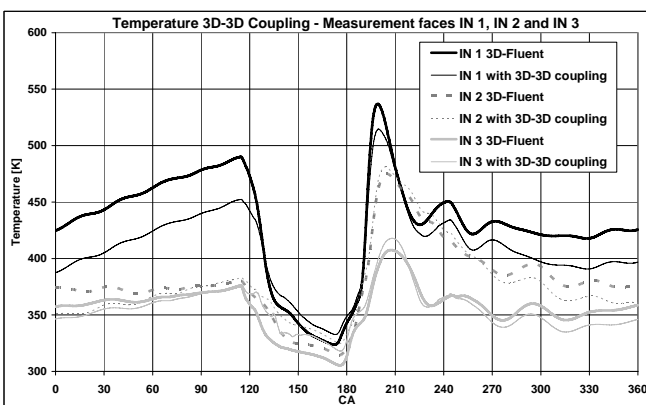
Figure 13: Temperature 3D-3D coupling, IN 1, 2 and 3
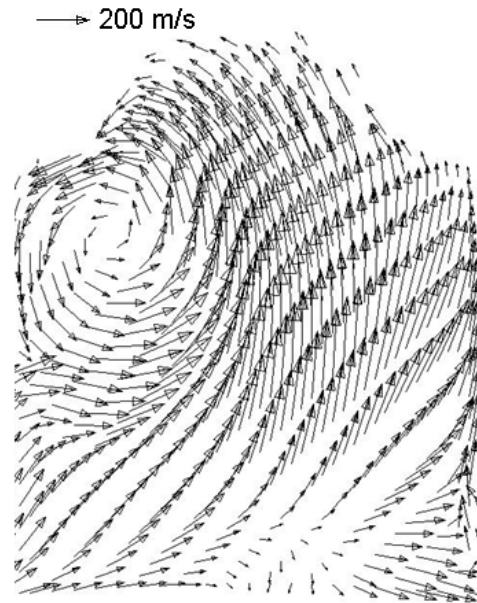
Figure 14: Velocity at 180 °CA (BDC), 3D-3D Fluent
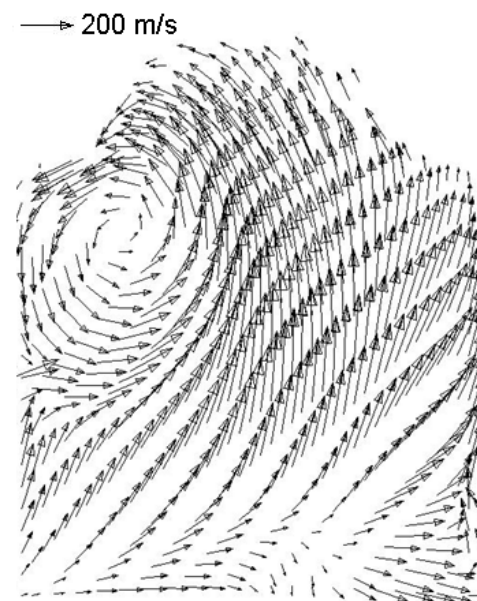
Figure 15: Velocity at 180 °CA (BDC), 3D-3D coupling methodology

Figure 14 shows the velocity field inside the cylinder at 180°CA (BDC) and the symmetry plane with the 3D-3D Fluent simulation and Figure 15 the result of the simulation with the 3D-3D coupling methodology. Both figures illustrate that the tumble flow has the same center of rotation. The flow situation in both figures shows a good agreement in terms of the velocity vector direction. The difference is only visible in the coupling region between the exhaust port and the cylinder.
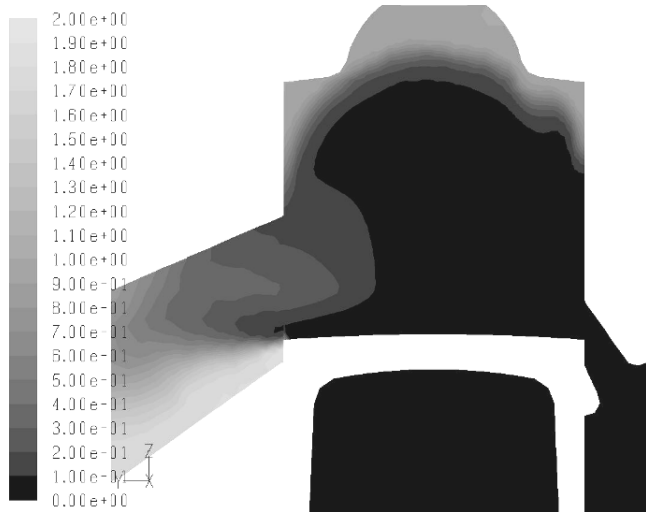
Figure 16: Passive scalar at 140 °CA, 3D-3D Fluent
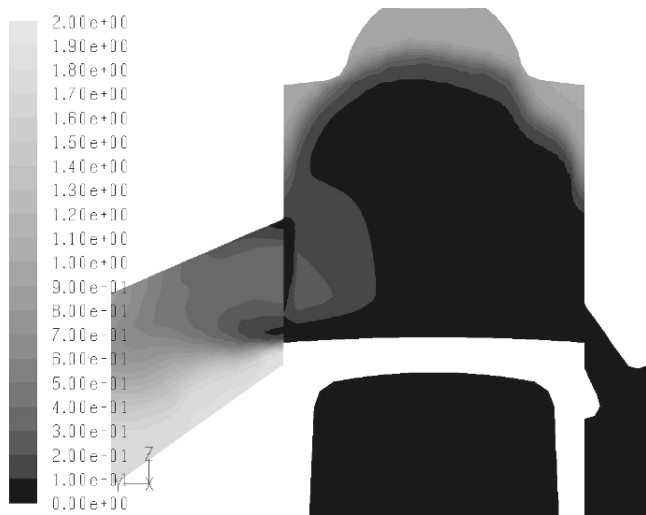
Figure 17: Passive scalar at 140 °CA, 3D-3D coupling methodology

Figure 16 and Figure 17 show the passive scalar at 140 °CA in the symmetry plane. The difference is only noticeable between the cylinder and the exhaust port. This draws the conclusion that the deviation partly depends on the post processing and partly on the 3D-3D coupling methodology, where the number of sections in the coupling face is constant. The failure is generated in the post processing as Fluent does not have the information about the coupling between the two 3D regions.

The 3D-3D coupling methodology in general is characterized by the division of the interface area into constant (small) number of sections, for which the fluxes of all conservative variables are averaged from all attaching cells. The accurateness of the coupling methodology predominantly depends on the number of interface sections. In the 3D-3D Fluent areas and numbers of the sections are not constant and are

composed for each individual cell surface. The flow area of this zone is calculated from the nodes of both overlapping faces [11]. In both coupling methodologies the fluxes are calculated in dependence of the status on both sides. Further, Fluent transports the flux as surface flux and not as source term as already described in the 3D-3D methodology. In addition, the surface definition for the coupling area is "wall" due to the fact that Fluent does not have the information about the coupling of the two adjacent 3D regions.

VALIDATION OF THE 1D-3D COUPLING METHODOLOGY – The 3D mesh of the exhaust was replaced with the fast-calculating 1D code. The typical two stroke exhaust system consists of the following parts [10]:

- Power section: connecting pipe, cone and counter cone
- Muffler: damping volume

This simulation was carried out in consideration of the power section, without the modeling of the muffler. The replaced region of the 3D exhaust region consisted of approximately 15000 cells and a total length of 1.1 m. Other major dimensions are presented in Figure 18. In this case only one coupling face in the 3D region is necessary. The pressure at the outlet of the exhaust is defined in the 1D model and set to atmospheric conditions of 100000 Pa and 300 K.
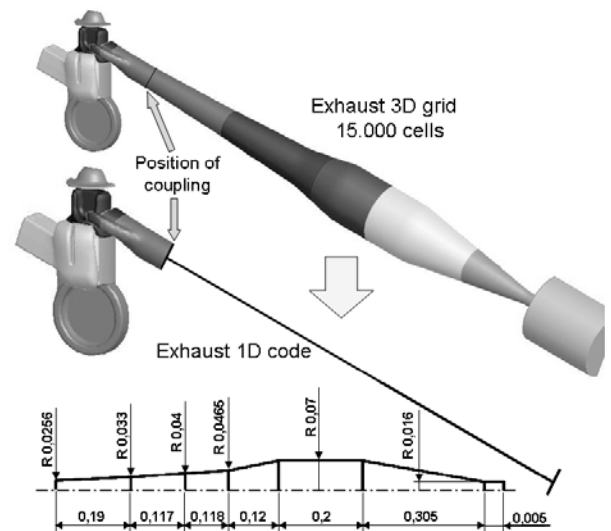
Figure 18: Geometry of the exhaust and replaced 3D region

Results after five cycles of the simulation with the 1D-3D coupling methodology are presented in Figure 19-Figure 24 and are compared with the total 3D simulation.

Mass Flow: Figure 19 shows the comparison of the mass flow in the measurement faces of the exhaust (EXH 0 and EXH 0a). In the opening phase of the exhaust port a good correlation between the calculation with 1D code and the calculation with the 3D-CFD code

can be seen. The plot shows a small deviation in the region between 180°CA and 285°CA. The plot of the mass flow in "EXH 0a" shows a good correlation over the complete revolution of 360°CA. Figure 20 shows the comparison in the measurement faces of intake ports (IN 1, IN 2 and IN 3). It is evident that the 1D code has a small influence on the mass flow in intake ports.
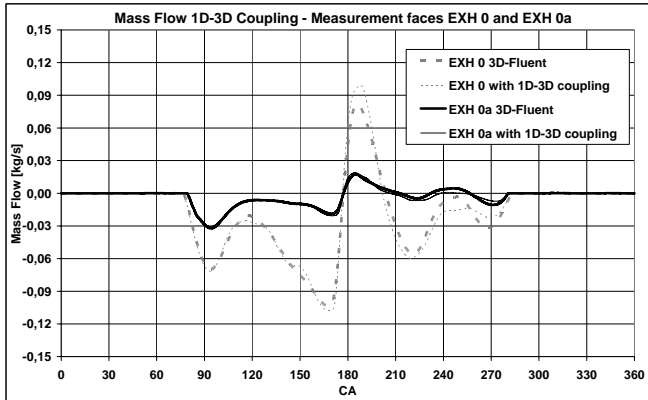
Figure 19: Mass flow 1D-3D coupling, EXH 0 and 0a
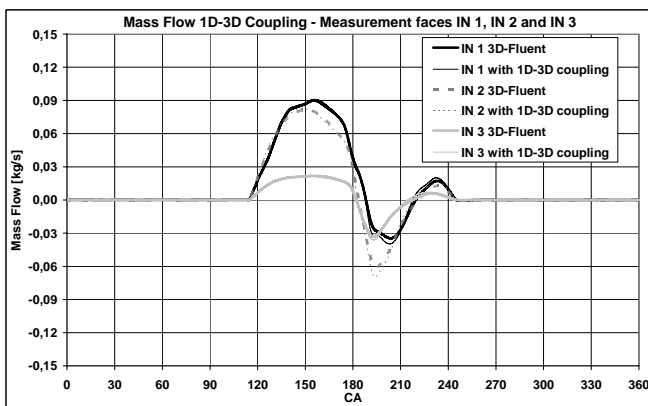
Figure 20: Mass flow 1D-3D coupling, IN 1, 2 and 3

Pressure: Figure 21 shows the comparison of the pressure in the measurement faces "EXH 0" and "EXH 0a" and Figure 22 in faces "IN 1", "IN 2" and "IN 3". Plots of the pressure in the intake ports show a good agreement and that the 1D code has no influence on the pressure. The extreme influence of the 1D code in the 3D region of the exhaust can be seen between 300°CA and 360°CA, especially in extreme points of curves.
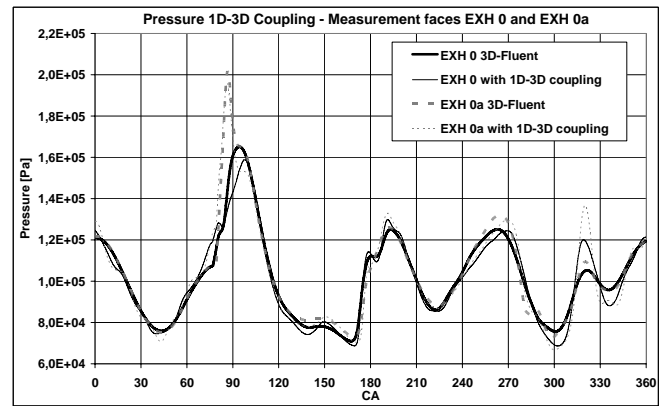

**Figure 21: Pressure 1D-3D coupling, EXH 0 and 0a**
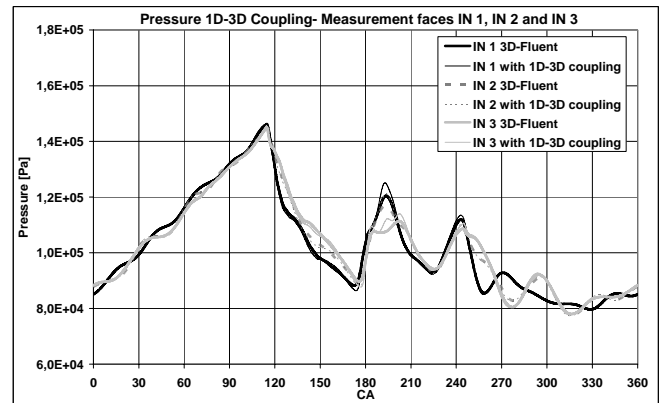
Figure 22: Pressure 1D-3D coupling, IN 1, 2 and 3

Temperature: Figure 23 and Figure 24 show the temperature curves in the measurement faces of the exhaust and intake ports. The temperature trend in the exhaust shows a good correlation. Another situation can be seen in the intake ports - the temperature in face "IN 1" is higher than the calculated temperature of the total 3D simulation. The other two curves show the temperature in measurement faces "IN 2" and "IN 3", which are lower than the calculated temperature of the total 3D-simualtion.
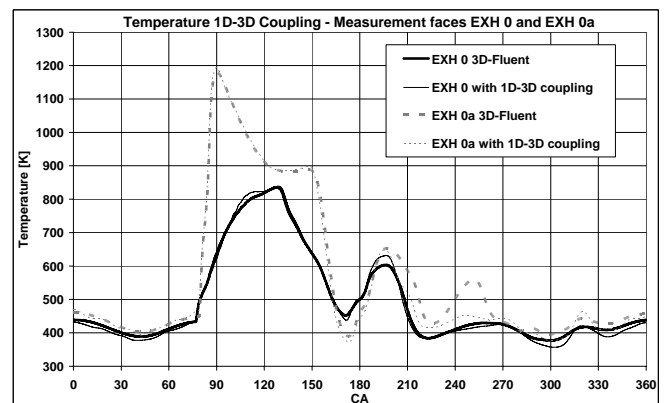
Figure 23: Temperature 1D-3D coupling, EXH 0 & 0a
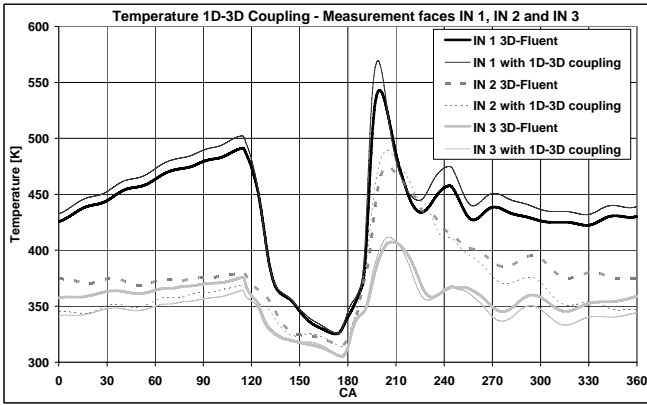
Figure 24: Temperature 1D-3D coupling, IN 1, 2, and 3

Figure 25: Velocity 195 °CA, 3D-3D Fluent

Figure 26: Velocity 195 °CA, 1D-3D coupling methodology

Figure 25 (3D-3D Fluent) and Figure 26 (1D-3D coupling) show the velocity at 195 °CA in the symmetry plane. 195 °CA was selected because the difference in the mass flow is visible in the range between 180 °CA and 210 °CA (see Figure 20) and therewith the influence of the back flow from 1D code. The tumble flow has the same center of rotation and the flow situation in both figures shows a good correlation regarding the velocity vector direction. In the region of the intake port and the exhaust port the difference in the velocity gradients is clearly visible. The flow inside the exhaust, calculated with 1D code, shows a higher mass flow than the one calculated with 3D code. A possible explanation for this deviation is the laminar and frictionless flow in the 1D code with missing friction and loss coefficients.

Figure 27: Passive scalar at 195 °CA, 3D-3D Fluent

Figure 28: Passive scalar at 195 °CA, 1D-3D coupling methodology

Figure 27 and Figure 28 show the passive scalar in the symmetry plane at 195 °CA. The difference can be seen

in the 3D region of exhaust and therewith the influence of the 1D code inside the cylinder. From the back flow (the flow from 1D code to the 3D region) is only one velocity information available. The velocity profile is constant over the coupling face, which explains the differences in the flow situation inside the cylinder.

In the 1D code turbulent kinetic energy and turbulent dissipation are not calculated, moreover, as they are not transported into the 3D region via the back flow, explaining the deviation between the results. Additionally, the values in the 1D code are only calculated for one flow direction and hence the simulation of a recirculation or turbulence is not possible. This information is not available in the 1D code.

VALIDATION OF 0D-3D COUPLING METHODOLOGY – In this case the 3D mesh of the crank case geometry is replaced with the fast-calculating 0D code. The 0D model of the crank case is connected with three faces to the 3D region. Two faces have a varying area in dependence of the piston position and one face has a constant area (see Figure 29).
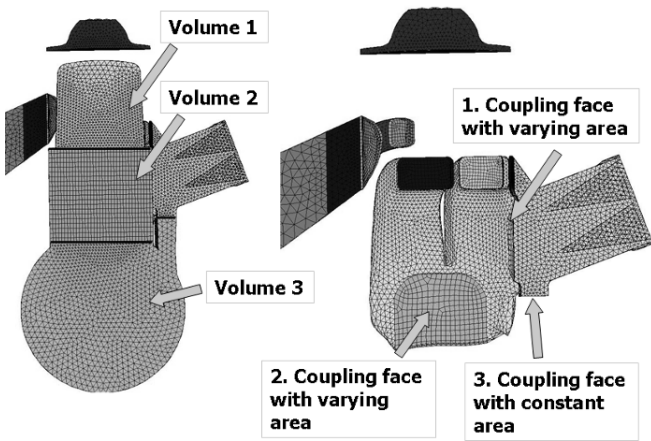
Figure 29: Geometry of the crank case and replaced 3D region

The volume of the crank case has been calculated in dependence of the piston position and the major dimensions for this calculation are presented in Table 3. The replaced 3D region of the crank case has approximately 45000 cells.

Table 3: Data for the 0D model of the crank case

Data crank case		
Cylinder bore	[m]	0.088
Connecting rod	[m]	0.145
Volume 1	[m³]	0.0002511958
Volume 2	[m³]	Calculated
Volume 3	[m³]	0.0003723492
Initial pressure	[Pa]	87500
Initial temperature	[K]	313

Results after five cycles of the simulation with the 0D-3D coupling are presented in Figure 30-Figure 37.

Mass Flow: Figure 30 shows the comparison of the mass flow in the measurement faces of the exhaust (EXH 0 and EXH 0a). In the region between 0°CA and 180°CA a good correlation between the simulation with the 0D code of the crank case and the total 3D calculation is visible. After 180°CA a small difference representing the influence of the 0D model can be seen. Figure 31 shows the comparison of the mass flow in the measurement faces of intake ports "IN 1", "IN 2", and "IN 3". In the region between 205°CA and 245°CA the deviation between these curves is small and therewith the influence of the 0D code on the mass flow in the measurement faces.
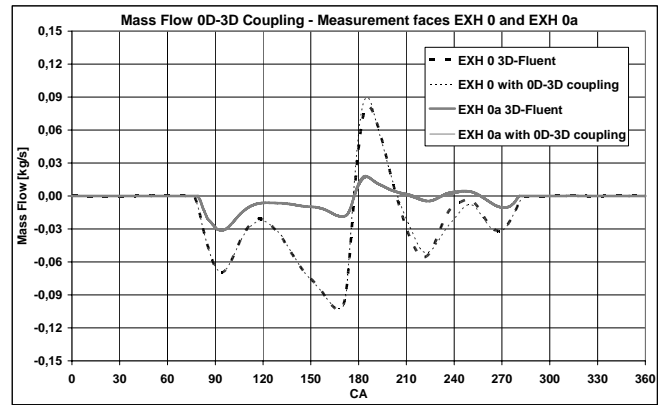
Figure 30: Mass flow 0D-3D coupling, EXH 0 & 0a
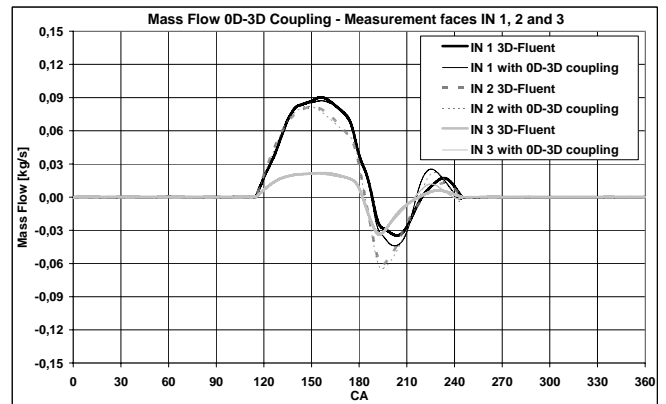
Figure 31: Mass flow 0D-3D coupling, IN 1, 2 and 3

Pressure: Figure 32 shows the comparison of the pressure in the measurement faces "EXH 0" and "EXH 0a" and Figure 33 in faces "IN 1", "IN 2" and "IN 3". In Figure 32 a good correlation can be seen over the complete fifth revolution of 360°CA. The influence of the 0D code in the 3D region of the exhaust is hardly visible. In the intake ports, a good agreement in the region between 0°CA and 180°CA is visible. After that, the curves have an entirely different pressure trend and the influence of the 0D code is visible.
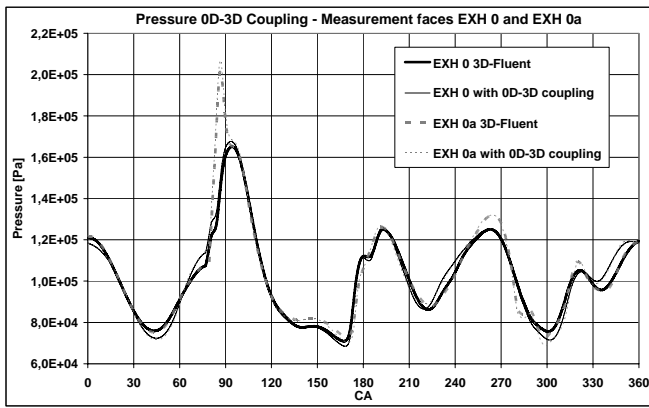
Figure 32: Pressure 0D-3D coupling, EXH 0 & 0a
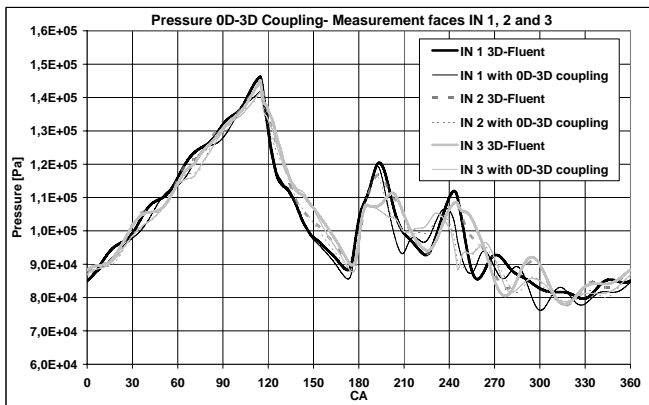
Figure 33: Pressure 0D-3D coupling, IN 1, 2 & 3

<u>Temperature:</u> Figure 34 and Figure 35 show the temperature in the measurement faces of the exhaust and the intake ports. The measurement faces "EXH 0" and "EXH 0a" in Figure 34 show a good correlation between the calculation with the 0D model and the total 3D calculation. In Figure 35, after approximately 200°CA, the difference in the trend of the temperature for all three measurement faces is visible. This trend is comparable with the calculation for the 1D model of the exhaust.
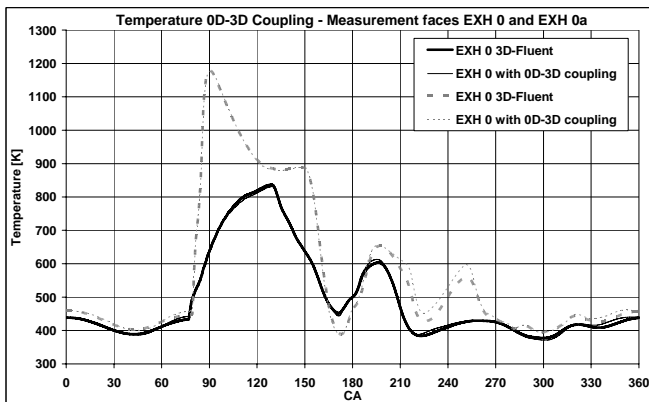
Figure 34: Temperature 0D-3D coupling, EXH 0 & 0a
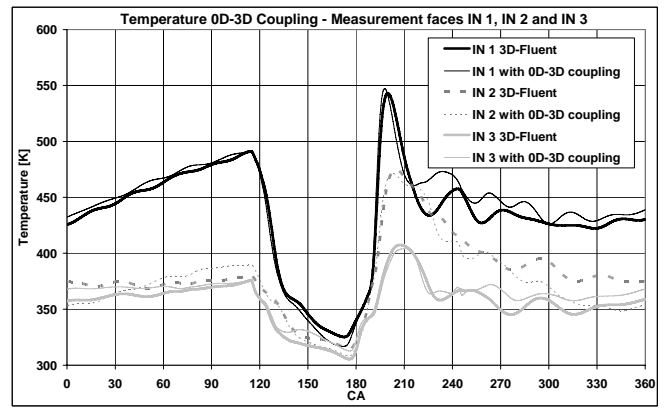
Figure 35: Temperature 0D-3D coupling, IN 1, 2 &3

<u>Crank case and Intake ports:</u> Figure 36 shows the comparison of the pressure in the volume of the crank case and intake ports. This direct comparison reveals the trend of the pressure in the crank case with and without the 3D geometry. After five revolutions and in the region between 0°CA and 210°CA a good correlation is visible. The biggest difference can be seen between 210°CA and 315°CA and is almost 5%. The second curve in Figure 36 shows the comparison of the pressure in the volume of intake ports and the influence of the 0D model on this 3D region. In the region between 0°CA and 190°CA a good agreement with a negligible influence of the 0D model on 3D region of the intake ports can be seen. After 190°CA a deviation in the pressure trend occurs. The temperature trend in the 3D region of intake ports and the crank case shows a good correlation, especially between 0°CA and 205°CA (see Figure 37). After 205°CA this trend differs in the 3D region of the intake ports. The biggest difference in the 3D region of intake ports is visible at 220°CA with approximately 10 K. The temperature in the crank case at 360°CA, calculated with the 0D model, is approximately 4 K lower than the temperature calculated with the total 3D simulation.
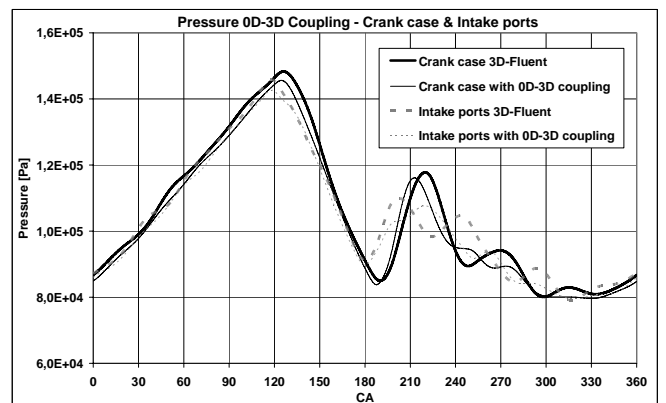
Figure 36: Pressure 0D-3D coupling, crank case and intake ports
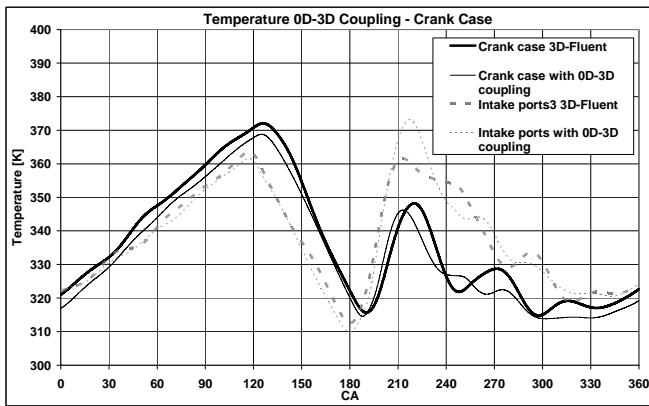
Figure 37: Temperature 0D-3D coupling, crank case and intake ports

The difference between the results can be explained by the fact that the 0D model does not describe the design of geometry, but only the volume. The differences between inlet and outlet regions are not dissolved, because the 0D model consists of only one cell. The volume of the crank case has a perfect mixed condition after only one time step. Further, the condition of the gas in the crank case is obtained by solving only the First Law of Thermodynamics; momentum, turbulent kinetic energy and turbulent dissipation are also neglected.
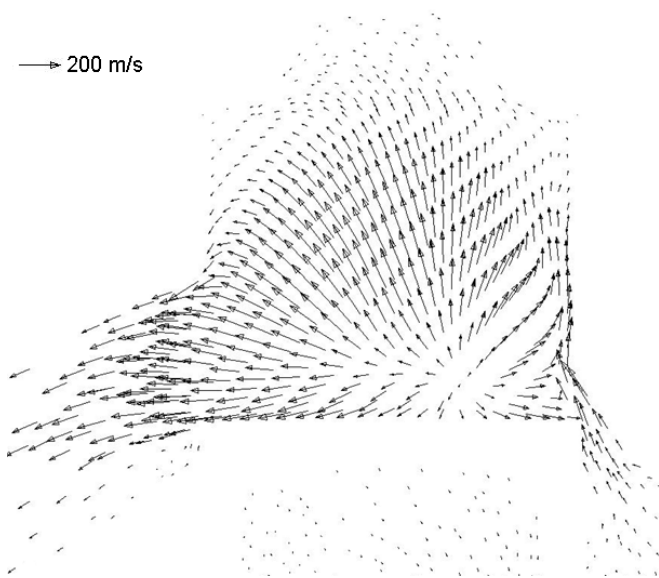
Figure 38: Velocity field at 135 °CA, 3D-3D Fluent

Figure 38 (3D-3D Fluent) and Figure 39 (0D-3D coupling methodology) show the velocity field in the cylinder at 135 °CA. These results point up that the 0D model has a very small influence on the flow situation in the opening phase of the intake ports. The passive scalar at 135 °CA also shows a good agreement in the comparison between the simulations in 3D-3D Fluent and in 0D-3D coupling methodology (Figure 40 and Figure 41).
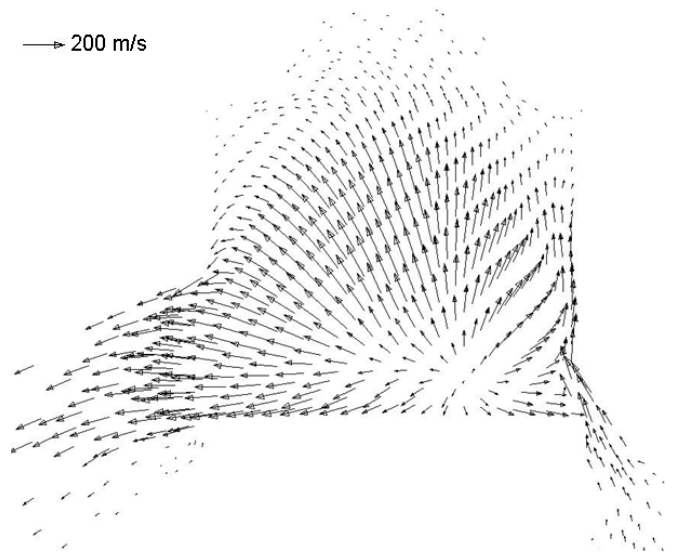
Figure 39: Velocity field at 135 °CA, 0D-3D coupling methodology
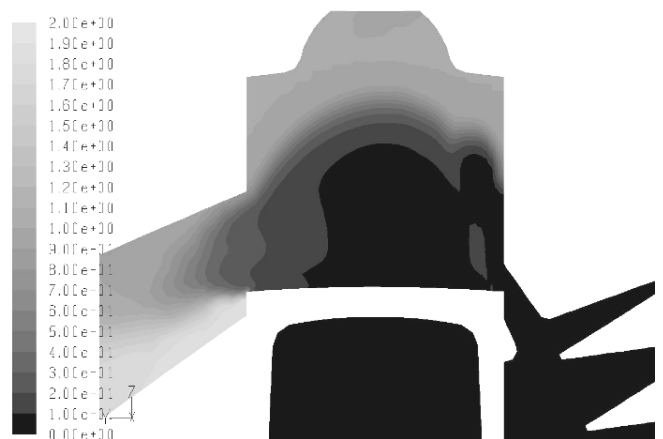
Figure 40: Passive scalar at 135 °CA, 3D-3D Fluent
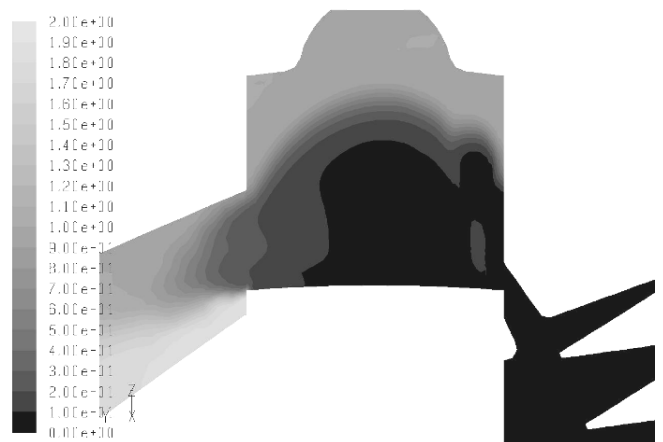
Figure 41: Passive scalar at 135 °CA, 0D-3D coupling methodology

SIMULATION OF THE COMPLETE ENGINE WITH 0D-3D, 1D-3D AND 3D-3D COUPLING METHODOLOGY – In this simulation the simultaneous working of the above mentioned models and coupling methodology is presented. The exhaust and the crank case 3D region were replaced with the corresponding fast-calculating models. The 3D-3D coupling methodology was used between the 3D regions of the cylinder, exhaust, and intake ports. Results of this simulation are compared with a conventional 3D-CFD calculation. The reduced number of 3D cells is approximately 60000 cells, i.e. 40%. This simulation includes overall nine couplings, one 1D-3D, three 0D-3D and five 3D-3D. The settings for the 0D and the 1D model are taken from the above validated cases.

Results after five cycles of the simulation with the 0D-1D-3D coupling methodology are presented in Figure 42- Figure 49 and are compared with the total 3D simulation.

Mass Flow: Figure 42 shows the comparison of mass flow in the exhaust (EXH 0 and EXH 0a). In the opening phase of the exhaust port a good agreement can be seen. After 150°CA a difference in both measurement faces is visible. The biggest difference emerges in extreme points of the curves, at approximately 170°CA and 190°CA with a deviation of 20% and 30% respectively. The trend of the mass flow shows a good agreement in the opening phase of intake ports (IN 1, IN 2 and IN 3). The biggest difference emerges in extreme points of curves at 200°CA with nearly 5% variation.
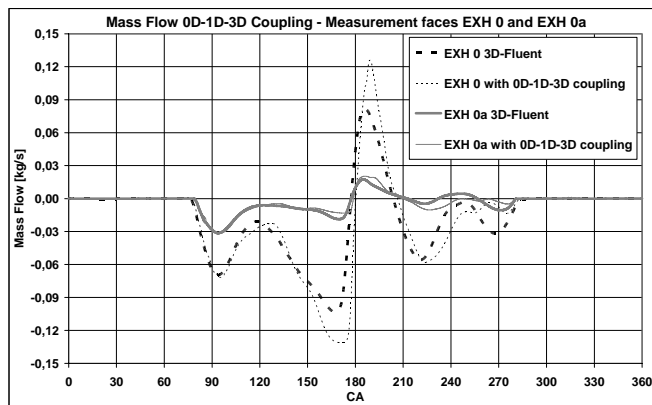
Figure 42: Mass flow 0D-1D-3D coupling EXH 0 & 0a

Pressure: Figure 44 shows the comparison of the pressure in measurement faces "EXH 0" and "EXH 0a" of the exhaust and Figure 45 in faces "IN 1", "IN 2" and "IN 3" of intake ports. The deviation can also be seen in extreme points of curves. In faces "EXH 0" and "EXH 0a" the biggest difference is at 320°CA with an entirely other trend. This trend can be seen even in the simulation with only the 1D model and is caused by the 1D code itself.
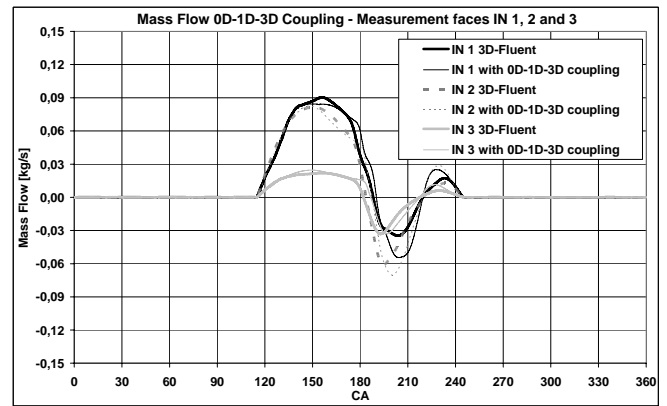
Figure 43: Mass Flow 0D-1D-3D Coupling IN 1, 2 & 3
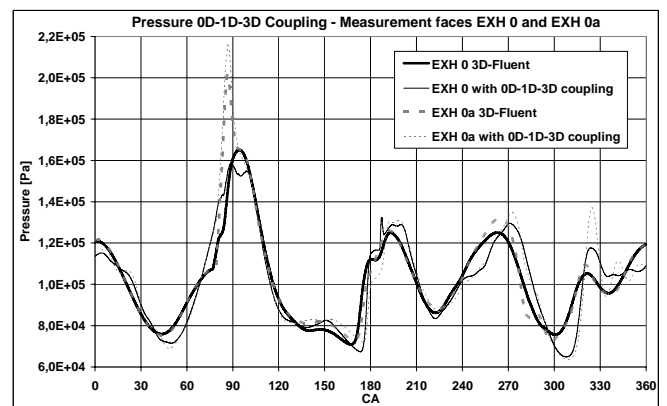
Figure 44: Pressure 0D-1D-3D coupling, EXH 0 & 0a
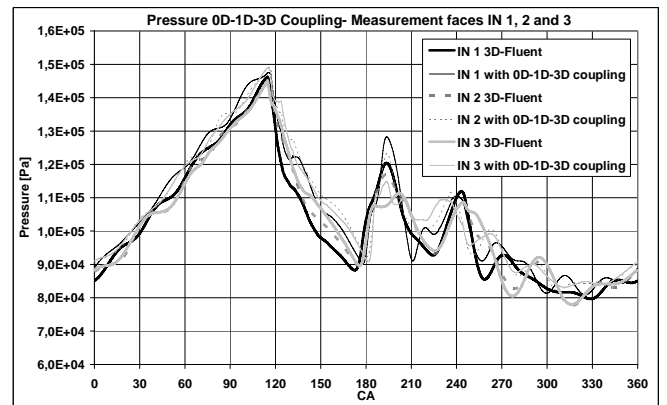
Figure 45: Pressure 0D-1D-3D coupling IN 1, 2 & 3

Temperature: Figure 46 and Figure 47 show the temperature in measurement faces "EXH 0" and "EXH 0a" of the exhaust and intake ports "IN 1", "IN 2" and "IN 3". The temperature trend in the exhaust shows a good correlation (Figure 46). In the measurement faces in the intake ports a similar situation appears as in the simulation with only 1D model of the exhaust.
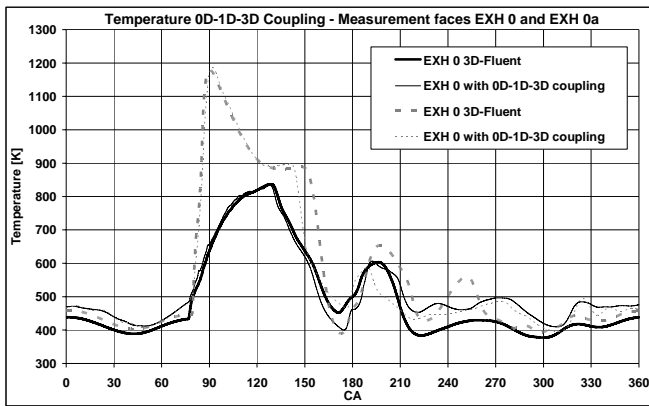
Figure 46: Temperature 0D-1D-3D coupling, EXH 0 & 0a
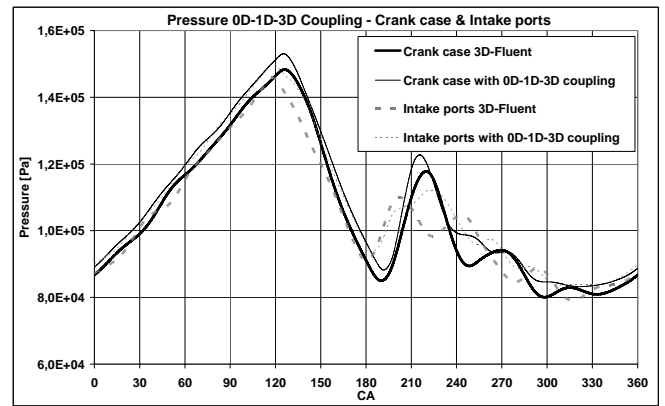
Figure 48: Pressure 0D-1D-3D coupling, crank case & intake ports
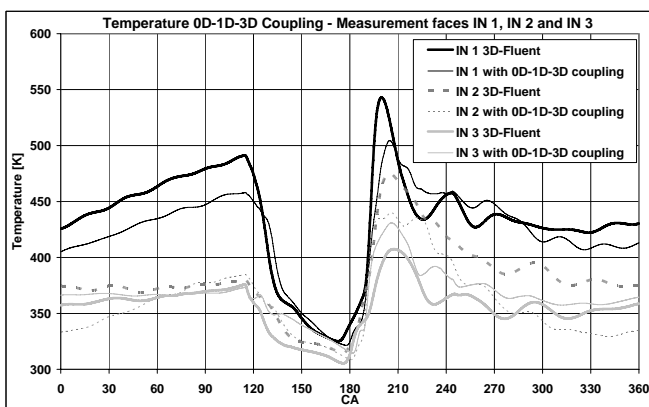
Figure 47: Temperature 0D-1D-3D coupling, IN 1, 2 & 3
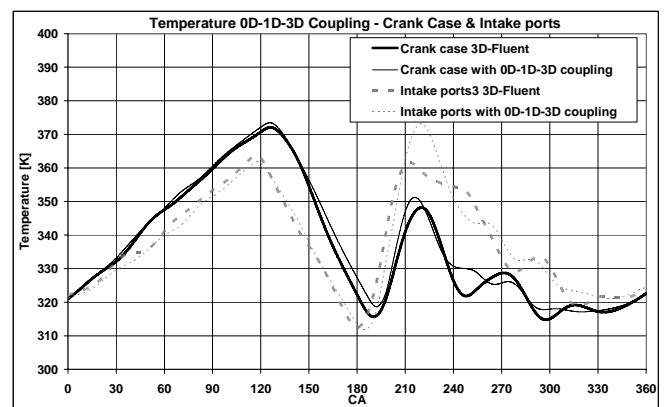
Figure 49: Temperature 0D-1D-3D coupling, crank case and intake ports

Crank case and Intake ports: The trend of the pressure in the crank case modeled with the 0D code shows a good agreement with the result of the 3D-calculation (Figure 48). The influence of the 0D model on the 3D volume of the intake ports can only be seen between 210°CA and 270°CA. The biggest difference occurs at 225°CA. The trend of the temperature in the crank case shows a good agreement between 0°CA and 180°CA (see Figure 49). A small deviation can only be seen after 180°CA. The temperature trend between 0°CA and 210°CA in the 3D region of the intake ports shows a good correlation. The biggest deviation is visible at 220°CA with approximately 11 K.

Figure 50 shows the velocity field at 195 °CA with the 0D-1D-3D coupling methodology. In comparison with the 3D-3D Fluent simulation (Figure 25) a good agreement in regard to the velocity vector direction can be seen. The difference in the velocity gradients in the region of the intake ports and the exhaust port is clearly visible. This difference can also be seen in Figure 42 at approximately 190°CA.
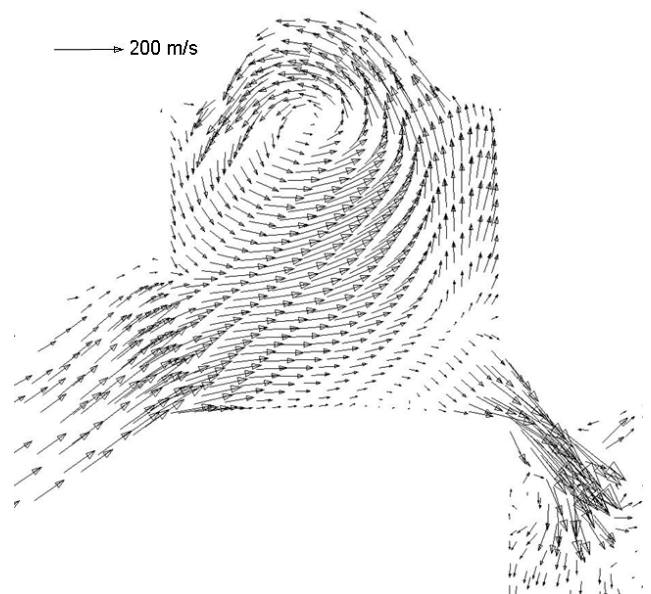
Figure 50: Velocity field at 195 °CA, 0D-1D-3D coupling methodology

CONCLUSION

This paper covers the discussion of the new coupling methodology, the 0D/1D models and their application on a real-geometry of the high-performance two-stroke engine. The coupling interface technology is the core for the establishment of a "Toolbox" for the predictive simulation of two stroke engines in the early development phase. The 0D and 1D models were developed especially for the requirements of the two stroke engine simulation with the CFD-Code FLUENT. All models were validated separately and compared with the conventional 3D CFD calculation. In the final simulation the simultaneous working of all above mentioned models and the coupling methodology is presented.
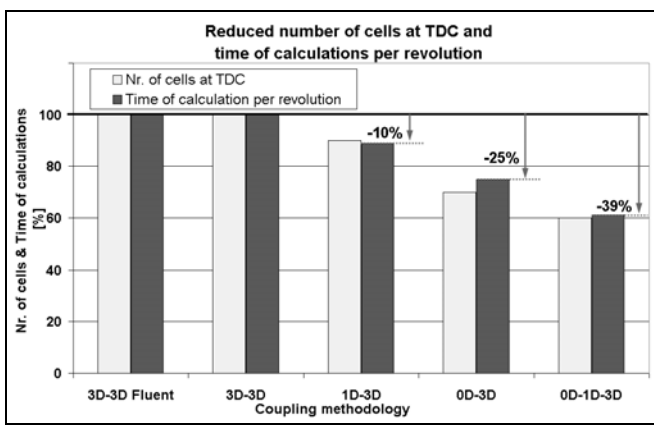
Figure 51: Reduced number of cells and time of calculation

The 3D-3D coupling methodology is the core of all other coupling methods, namely 0D-3D and 1D-3D coupling. This coupling does not have an influence on the computational time of simulation because the number of 3D cells has not been reduced (Figure 51). The results after five cycles of the simulation with the 3D-3D coupling methodology show a good agreement. The mass flow and the pressure plots show a good correlation over the complete revolution of 360°CA. In the temperature plots the difference is visible, especially in the 3D region of the intake ports. The difference can be explained by a preparation of the conserved variables for each section that are averaged over all cells and by the number of interface sections. The accurateness of results and the interface coupling itself predominantly depend on the number of interface sections.

The 1D-3D coupling method reduces the number of 3D cells and the computational time of calculation about 10% (Figure 51). The design of the exhaust geometry with the preparation in the 1D code does not require a lot of time. This advantage can be used for the development of the exhaust region and offers an array of information in the early development phase. The results of the simulation with the 1D-3D coupling methodology

show that this model and coupling have a very small influence on the 3D region of the intake ports. This advantage can be used for the development of the intake ports. A good agreement can be seen in the presented results, especially in plots of the mass flow and the pressure. The temperature plots show a small difference, especially in the 3D region of the exhaust port where the 1D code was coupled with the 3D region.

The 0D-3D coupling methodology offers the biggest potential for the reduction of regions with a high number of 3D cells. This methodology reduces the number of 3D cells in the investigated two stroke engine by 30% (at TDC) and the computational time of simulation per revolution by 25%. Furthermore, the moving 3D grid in the crank case is not modeled in this case. Therefore the time necessary for the calculation of the moving grid is reduced as well. Results of the simulation with the 0D-3D coupling methodology show a good agreement, especially in the region between 0°CA and 180°CA. The influence of the 0D model on the 3D region is only visible after 180°CA, especially regarding pressure and temperature in measurement faces of intake ports. The 0D model does not describe the design geometry, only the volume is defined. The condition of gas in the crank case is obtained by solving the First Law of Thermodynamics, where the momentum is neglected. Difference between inlet and outlet regions are not dissolved, as the 0D model consists of only one cell, which explains the deviation between the results. The advantage of this model can be especially used for the development of the exhaust port, because the influence of the 0D coupling on this region is hardly visible.

The combination of the 0D-3D and 1D-3D coupling methods reduces the number of 3D cells by 40% (measured at TDC) and offers the biggest potential for the reduction of the computational time. In this simulation the computational time was reduced by 39%. Results of the simultaneous use of 0D-1D-3D coupling methodologies show that the reduced number of 3D cells concurrently reduces the accurateness of the results. The difference of the results can be almost always seen in the extreme points of the curves. However, this combination can be used for the predictive simulation of two stroke engines in the early development phase, where an array of information about a new engine is required in a short calculation time.

All the calculations are compared with the conventional 3D CFD calculation of the scavenging process, i.e. without injection, mixture preparation and combustion. The fluid in the model is defined as air. Further enhancements of this software tool will be focused on the species transport in 0D and 1D codes as well as the species transport over the coupling faces into the 3D region and backwards. With these changes it will be possible to simulate a 2-stroke engine with injection, mixture preparation and combustion.

REFERENCES

[1] Rothbauer R.J., Margelik H.R., Aslam M.M., Almbauer A.R., Schmidt S.P., Glinsner K.: "Predictive Simulation Strategies for the 2-Stroke Scavenging Process with the Scope of the Development Process"; 20056552(JSAE), 2005-32-0099(SAE), 2005

[2] Rothbauer R.J., Almbauer A.R., Schmidt P.S., Margelik H.R., Glinsner K.: "A Multidimensional Interface for the Predictive CFD Simulation of the 2-Stroke Engine"; 20066559(JSAE), 2006-32-0059(SAE), 2006

[3] Rothbauer R.J., Grasberger G., Abidin Z., Almbauer A.R.: „Reed Valve, Crankcase and Exhaust Models Coupled to 3D Fluid Domains fort he Predictive CFD Simulation"; 20076530(JSAE), 2007-32-0030(SAE), 2007

[4] Schmidt S.P., Winkler F., Schoegl O., Pontoppidan M.: „Development of a Combustion Process for a High Performance 2-Stroke Engine with High Pressure Direct Injection"; 2004-01-2942(SAE), 2004

[5] G. Cunningham and R.J. Kee, J. Boyall: " CFD Prediction of Crankcase Flow Regimes in a Crankcase Scavenged Two-Stroke Engine"; 970361(SAE), 1997

[6] O. Chiavola: "MULTI-DIMENSIONAL CFD-TRANSMISSION MATRIX MODELLING OF IC ENGINE INTAKE AND EXHAUST SYSTEMS"; Journal of Sound and Vibration, 2002

[7] Rothbauer J. R. : "Methode zur Koppelung von bewegten 3D sowie 0/1D CFD Berechnungsgebieten"; Dissertation, Technische Universität Graz, 2007

[8] Schmidt S. : „Auslegung, thermodynamische Analyse and Entwicklung von Zweitakt-Brennverfahren mit Hochdruck-Direkteinspritzung"; Dissertation, Technische Universität Graz, 2005

[9] Toro E.: „Riemann Solvers and Numerical Methods for Fluid Dynamics"; Springer, ISBN 3-540-61676-4, 1997

[10] Blair G.P.: "Design and Simulation of Two-Stroke Engines"; Bd. 1. Edition. Society of Automotive Engineers, Warrendale, 1996

[11] ANSYS Fluent: "Fluent 6.3 User's Guide"; Fluent Inc, 2005

[12] ANSYS Fluent: "Gambit User's Guide"; Fluent Inc, 2005

[13] Adair R.P., Qvale E.B., Pearson J.T., "Instantaneous Heat Transfer to the Cylinder Wall in Reciprocating Compressors", Proceedings of the International Compressor Conference Purdue, USA, 1972

[14] Bryan J.F., Fleck R., Kee J.R., Thornhill D.: "The Evaluation of Discharge Coefficients in the Cylinders of High Performance Two-Stroke Engines", SAE 2003.32.0029, JSAE 20034329, 2003

[15] Chiatti G., Chiavola O.: "Multicode Prediction of the Influence of the Exhaust System on the Performance of a Turbocharged Engine", Journal of Engineering for Gas Turbines and Power, ASME, 2002

[16] ANSYS Fluent: "UDF Manual"; Fluent Inc, 2005

CONTACT

Dipl.-Ing. Dalibor Jajcevic
Christian Doppler Laboratory
for "Thermodynamics of Reciprocating Engines"
Graz University of Technology
Inffeldgasse 25C
8010 Graz-Austria
Phone: +43 316 873 4586
FAX: +43 316 873 8080
Email: jajcevic@vkmc.tu-graz.ac.at
Web: www.tugraz.at

DEFINITIONS, ACRONYMS, ABBREVIATIONS

0D:	zero-dimensional, zero dimensions
1D:	one-dimensional, one dimension
3D	three-dimensional, three dimensions
A:	flow area
CA:	crank angle
CFD:	computational fluid dynamics
e:	specific internal energy
E:	energy
EXH:	exhaust
F:	flux vector
h:	specific enthalpy
IN:	intake
m:	mass
Ma:	Mach number
p:	static pressure
Q:	heat release
rpm:	revolutions per minute
S:	source vector
t:	time
T:	static temperature
U:	state vector
u_i:	velocity i-direction
u:	velocity x-direction
v:	velocity y-direction
V:	volume
w:	velocity z-direction

5   Symmetry and time delayed boundary condition

The second method, which can be applied for the reduction of the computational domain, is the application of the cyclic/periodic boundary condition. The essential advantage of this method is that the data for the boundary conditions are deduced from the 3D simulation itself and therefore do not need to come from other software (such as 0D/1D calculations) or measurements. Generally, the basic idea of the above mentioned multidimensional simulation is a reduction of the dimension, e.g. from 3D to 1D/0D. A domain reduction can also be realized by employing symmetry conditions inside a technical problem, where the reduced domain still keeps a quasi 3D character. This can be explained by the fact that the application of a symmetry condition provides more information than a dimensional reduced calculation (e.g. 0D/1D), but still less than a complete 3D simulation.
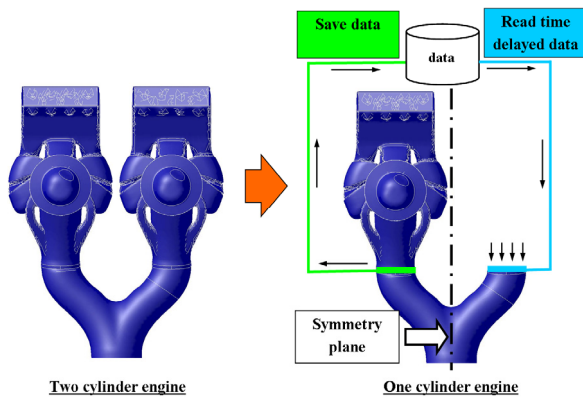
Figure 27:   Application of the symmetry and time delayed boundary condition

The basic idea of the symmetry and time delayed boundary condition introduced in this work is a reduction of the calculation domain by applying the symmetry condition with a minimal influence on the simulation results. An important advantage of the proposed method is the consistency of the fluxes of the individually conserved variables. It can be used for technical problems, where a flow pattern repeats in successive cycles, which additionally can be time delayed. The data do not need to be constant over the boundary face, which is usually the case in standard boundary conditions of all CFD applications as well as in 1D-3D coupling methodology. A good example for the application of this boundary condition is the simulation of a 2-cylinder 2-stroke engine. In this engine, the cylinders are coupled together in a so-called "two-into-one" exhaust system, see Figure 27 left side. Furthermore, the intake and the exhaust ports are open simultaneously over a long period of the cycle and the gas dynamic behaviour inside the exhaust system has a dominant influence on the scavenging process and on the mixture formation inside the cylinder, so that both cylinders must be taken into consideration in order to get accurate simulation results. Applying the new boundary condition, the domain of the second cylinder (including cylinder, intake ports and crank case) can be replaced.

Figure 27 (right) illustrates the application in a 2-cylinder 2-stroke engine simulation. In this case, cylinder 1 is completely calculated. For cylinder 2, the symmetric condition is used, so that it is replaced by the time delayed boundary condition. The boundary condition for the second cylinder is taken from the exhaust cylinder 1 domain and for each cell respectively. This means, that for each cell in the exhaust of cylinder 1 a symmetrically positioned cell in the domain of exhaust cylinder 2 is found and marked. Simultaneously, all cell properties are read and saved in an external output data file. Therewith, the correct boundary condition for each cell can be defined and the required flux can be calculated. For the flux calculation the time delayed data from the external data file are read for each cell respectively. In this work, the flux calculation occurs after the defined time delayed period. Explicitly, time delayed data

are available and the flux calculation can be carried out. The advantage of this boundary condition is that the requested data are only provided by the simulation of cylinder 1. Neither additional information about the variable profile, nor a 1D-model, nor measurement data for the replacement of the second cylinder are requested. This type of boundary condition can be used for time delayed as well as synchronous technical problems. An application of the new cyclic boundary condition for both cases is presented and discussed in the enclosed paper of a real world 2-cylinder 2-stroke engine simulation.

5.1 Paper III

A cyclic boundary condition for time delayed technical problems and its application for IC-engine simulation
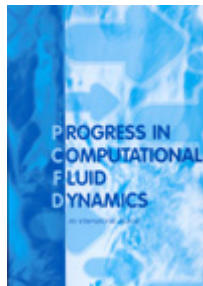
A cyclic boundary condition for time delayed technical problems and its application for IC-engine simulation

Dalibor Jajčević*

Graz University of Technology, Institute for Internal Combustion Engines and Thermodynamics,
Christian Doppler Laboratory for Thermodynamics of Reciprocating Engines,
Inffeldgasse 21 A, Graz, A-8010 Austria
Phone/Fax: +43 316 873 4586/+43316 873 8080
E-mail: jajcevic@ivt.tugraz.at
*Corresponding author

Raimund A. Almbauer

Graz University of Technology, Institute for Internal Combustion Engines and Thermodynamics,
Christian Doppler Laboratory for Thermodynamics of Reciprocating Engines,
Inffeldgasse 21 A, Graz, A-8010 Austria
Phone/Fax: +43 316 873 7583/+43 316 873 8080
E-mail: almbauer@ivt.tugraz.at

Wolfgang Lang

Graz University of Technology, Institute for Internal Combustion Engines and Thermodynamics,
Christian Doppler Laboratory for Thermodynamics of Reciprocating Engines,
Inffeldgasse 21 A, Graz, A-8010 Austria
Phone/Fax: +43 316 873 7583/+43 316 873 8080
E-mail: wolfgang.lang@ivt.tugraz.at

Stephan Schmidt

Graz University of Technology, Institute for Internal Combustion Engines and Thermodynamics,
Inffeldgasse 21 A, Graz, A-8010 Austria
Phone/Fax: +43 316 873 7591/+43 316 873 8099
E-mail: schmidt@ivt.tugraz.at

Abstract: The continuous improvement of numerical methods together with the increase of computer power allows the simulation of more and more complex technical problems even for large calculation domains. Growing calculation domains combined with the simulation of physically complex phenomena increase the simulation effort non-linearly and make them impracticable in the daily work of an engineer. A decrease of simulation time can be realized by the reduction of the calculation domain. In this paper, a new cyclic and time delayed boundary condition is introduced together with its application in the simulation of an IC-engine. The boundary conditions are calculated during the simulation and are set on the corresponding faces in the calculated domain. Furthermore, the data for the boundary condition is deducted from the simulation itself and therefore do not need to come from another software or measurements, what additionally reduces the pre-processing effort.

Keywords: simulation, CFD, boundary, condition, cyclic, time delayed, engine, two-stroke, exhaust, crankcase

Biographical notes: Dalibor Jajčević received his master degree in mechanical engineering in the year 2007. He is currently research assistant at the Christian Doppler Laboratory for Thermodynamics of Reciprocating Engines. His current research interests include computational fluid dynamics and simulation of IC-engine using multidimensional coupling methods between different CFD codes.

Raimund A. Almbauer is an associate professor at the Institute for Internal Combustion Engines and Thermodynamics at the University of Technology in Graz. He received his Phd 1991 and got his postdoctoral lecture qualification 2001. Since 2004 he is head of the Christian Doppler Laboratory for Thermodynamics of Reciprocating Engines. His main research task deals with thermodynamic simulation of reciprocating compressors and scavenging processes of two stroke engines.

Wolfgang Lang received his master degree in mechanical engineering and business economics in the year 2007. He is currently research assistant at the Christian Doppler Laboratory for Thermodynamics of Reciprocating Engines. His current research interests include computational fluid dynamics and multidimensional coupling methods between different CFD codes.

Stephan Schmidt received his PhD in Mechanical Engineering, University of Technology Graz in 2005. He is currently working as a senior scientist at the Institute for Internal Combustion Engines and Thermodynamics at Graz University of Technology. His special fields of works comprise engine design and simulation with special focus on a combustion process development.

1 Introduction

Computational Fluid Dynamics (CFD) solves the Navier-Stokes equations using computer technology in order to analyze the fluid flow. In general, CFD simulations consist of the three basic steps: pre-processing, solving and post-processing. In the pre-processing step, a geometrical flow model is created. This involves the use of various software tools for grid generation and the definition of boundary conditions as well as of fluid properties. Boundary conditions stem from a previous simulation (e.g. one-dimensional (1D)) or measurement data. The flow calculations take place in the solving step, where the conservation equations of mass, momentum, energy and species are solved. In the final step - post-processing - the simulation results are evaluated. Currently, different CFD software packages exist (such as FLUENT, AVL-Fire, STAR-CD, KIVA, CONVERGE CFD, OPENFOAM etc.), which offer the ability to simulate flows of gases and liquids using computer modelling. The computer modelling allows virtual prototyping of a technical system in order to evaluate the performance of a new design. CFD is a state of the art tool for the development of IC engine. It offers the successful assessment of new technologies, e.g. new fuel preparation methods, new combustion concepts and/or alternative fuels. Furthermore it supports the prototyping phase on the engine test bench. Additionally, these new technologies require high standards of knowledge and high testing efforts on the engine test bench. This knowledge can be partly acquired with the use of the CFD simulation.

The steady improvement of the numerical methods together with the increase of the computer power allows the simulation of more and more complex technical problems even for large calculation domains. The considered problems may involve complicated geometry, physically complex phenomena such as turbulence, phase change, chemical reactions, etc. Big calculation domains, which require the simulation of physically complex phenomena, increase the calculation time non-linearly and make them impracticable in the daily work of an engineer. The reduction of simulation time can be realized by the reduction of the calculation domain and/or by the simplification of the technical problem. The quality of the results depend on the completeness of the simulation of physical phenomena - potentially, simplifications lead to incorrect results. Furthermore, the numerical evaluation of all relevant phenomena is the main focus to gain a better understanding of the investigated technical problem. In order to save time, a part of the 3D domain can be replaced with corresponding boundary conditions, which usually stem from a previous 1D calculation. These data are also incomplete, cause an inaccuracy in the simulation and often lead to incorrect results. For instance, the constant boundary conditions for the outlet face of the internal combustion engine are usually defined with pressure and temperature or with mass flow and temperature. These data are generally approximated to be constant in space over the complete face, which influences the results. Moreover, the boundary conditions for the turbulence from a one dimensional (1D) model or from measurements are not available. Hence, the boundary conditions are placed far from the interesting domain; this directly increases the calculation time due to the increase of the calculation domain.

The new cyclic and time delayed boundary condition (further: J-BC) allows a reduction of the calculation domain and therewith the calculation duration with only a neglectable influence on the simulation result. The boundary condition is calculated during the simulation and is set on the corresponding face in the calculated domain. An important advantage of the proposed method is the consistency of the fluxes of the individual conserved variables. It can be used for technical problems, where a flow pattern repeats in successive cycles, which additionally can be time delayed. The data

do not need to be constant over the boundary face, which is usually the case in the standard boundary conditions of all CFD applications.

2 Technical problem description

The advantages of 2-stroke engines, high power and low weight, are in conflict to their disadvantages, high emissions and bad fuel economy. As these disadvantages are caused by mixture formation and the scavenging process, a solution of the problem can be analyzed using three-dimensional CFD (further: 3D CFD). The numerical investigation of the governing processes offers an array of information about the engine and provides a tool for the development of an improved engine. The investigation of a 2-cylinder 2-stroke engine requires the simulation of the complete geometry including both cylinders and the complete exhaust system (see Figure 1).

Figure 1: Design of a 2-cylinder 2-stoke engine

In this engine, the cylinders are coupled together in a so-called two-into-one exhaust system. Furthermore, the intake and the exhaust ports are open simultaneously over a long period of the cycle and the gas dynamic behaviour inside the exhaust system has a dominant influence on the scavenging process and on the mixture formation inside the cylinder. The consideration of only one cylinder causes a wrong gas dynamics inside the exhaust pipe and further leads to unrealistic simulation results. Hence, in order to get effective and significant results for the 2-cylinder 2-stroke engine, the simulation of the complete geometry with both cylinders and the entire unaltered exhaust pipe is required. E.g. (Zeng et al., 2004) uses the complete geometry of a 2-cylinder 2-stroke engine with both cylinders to simulate the in-cylinder flow and the gas dynamics inside the exhaust system. The main drawback is the necessity to calculate several revolutions until the gas dynamics behaviour inside the exhaust port achieves a cyclic steady condition. It includes the simulation of all processes of the 2-stroke engine such as fluid flow, heat transfer, fuel injection, mixture preparation, and finally combustion. Some of these processes only repeat in successive cycles, others are cumulating over several cycles. The simulation of the second cylinder almost doubles the calculation time, although it provides only little more information. Furthermore, bad initial conditions prevail for the combustion process during the first several revolutions. Typically, the incorrect results of the combustion process further lead to a wrong pressure difference between cylinder and exhaust port during the opening phase of the exhaust port. This induces a wrong pressure wave in the exhaust pipe and results in an incorrect scavenging process. In this case, the time of the calculation increases significantly, as it makes the simulation of additional revolutions necessary to fade out the wrong initial conditions. E.g. (Bozza et al., 2008) shows, that a converged solution is approached in about 10-12 cycles in the simulation of a single cylinder 2-stroke engine.

3 State of the art

The state of the art simulation of a symmetric 2-stroke engine is the simulation of only one or even a half of the cylinder, the exhaust, the intake ports and the crank case by the use of the conventional symmetry boundary condition, e.g. simulation of 2-stroke engine: (Jajcevic et al., 2008; Schmidt et al., 2004; Basshuysen, 2007; Schmidt et al., 2007; Chiatti and Chiavola, 2002; Pischinger et al., 2002). In case of an asymmetric design of the exhaust port, a conventional symmetry boundary condition cannot be used. Even if the exhaust port of a two-cylinder engine is symmetric, the simulation domain cannot be reduced to only one cylinder, as the influence of the second cylinder would be missing. A simulation of only one cylinder including the effects of the second cylinder can be realized by the use of a multidimensional simulation methodology. The 3D region of the second cylinder can be replaced by a fast-calculating zero/one dimensional (further: 0D/1D) model due to a so-called two-way coupling methodology where the different CFD models are synchronously simulating different regions, see Figure 2. E.g. (Jajcevic et al., 2008; Bozza et al., 2008) replace the 3D domain of the crank case and a part of the exhaust system by a 0D/1D code for the simulation of one cylinder 2-stroke engine. A similar simulation strategy can be realized using the conventional AVL BOOST-FIRE or FLUENT-GT Power coupling tools; see (Fluent, 2005a; AVL, 2006a; Li, 2002).

The drawback of the multidimensional simulation strategy - see (Jajcevic et al., 2008; AVL, 2006a; Bozza et al., 2008; AVL, 2006b; Li, 2002) - can be summarized in the following points:

1. An additional 0D/1D simulation is required, which increases the pre-processing and solving time of the CFD simulation.

2. Limitations using 0D/1D tools by the simulation of complex geometries and strong 3D physical effects occur, such as recirculation, turbulence, fuel
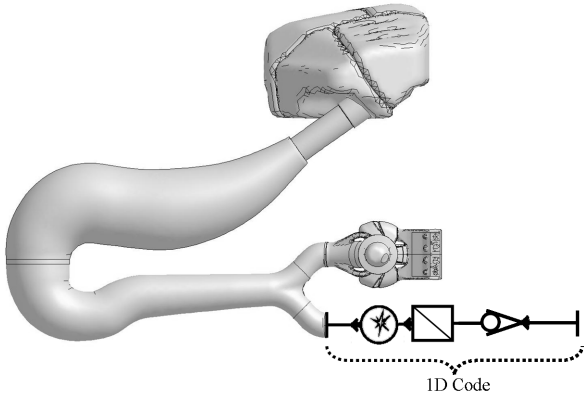
**Figure 2**: Multidimensional simulation strategy for a 2-cylinder 2-stroke engine

Figure 3: Application of rotational, translational, and anti-cyclical boundary conditions

injection process, mixture preparation, and combustion process.

3   The coupling position between 3D and 0D/1D domains depends on the flow situation and is thus limited.

4   Due to the coupling strategy, additional data loss can be caused, possibly leading to incorrect simulation results. These data are generally approximated to be constant in space over the complete coupling face.

In commercial CFD codes (Fluent, 2005a; AVL, 2006a; Amsden, 1993; Star-CD, 2006) the following boundary conditions can be found:

- Inlet/Outlet: pressure, velocity, mass flow

- Wall, periodic (cyclic) and pole: wall, symmetry, periodic, axis

The main focus of this work concerns periodic boundary conditions (further P-BC), which allow the simulation of the reduced domain in case that the physical geometry of the flow is symmetric and the solution has a periodically repeating nature. All P-BC are always used in pairs. The conventional CFD-codes (Fluent, 2005a; Star-CD, 2006) provide two types of P-BC, with and without pressure drop option. In dependence of the geometry and the technical problem, rotational or translational P-BC can be distinguished (see Figure 3). The rotational P-BC is used when the flow across two opposite planes are identical. A good example is an axis-symmetric cylinder flow with a swirl. The second translational P-BC can be used with and without the pressure drop function. For a technical problem with pressure drop, the boundary condition can be executed for fully-developed or stream-wise periodic flow, see (Fluent, 2005a). The fully-developed flow is a flow with a flow pattern repeating in successive cycles along the direction of the flow. The stream-wise flow includes the fully-developed flow in pipes and ducts and is applicable when the entrance
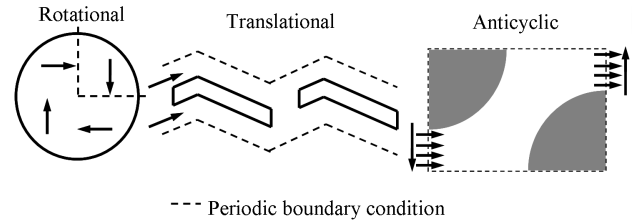
length is long enough. The application also depends on the Reynolds number and the geometry.

The conventional CFD code (Star-CD, 2006) allows a periodic boundary condition, defined as anticyclic, where the direction for variable matching is reversed. E.g. a 2D case of heat transfer from tube bundles in cross flow. A small segment of this anti-cyclical example is shown in Figure 3. In this case, two boundaries at which the flow is entering and leaving the calculating domain are matched in an anti-cyclical way by reversing one of the boundary local coordinate directions. The conventional periodic/cyclic boundary conditions, mentioned here, are not usable for the simulation of a 2-cylinder 2-stroke engine, because the time delayed option is missing.

4   Formulation and structure of J-BC

J-BC can be used for time delayed as well as not time delayed technical problems. The following example illustrates the application of J-BC in the simulation of two pipes (see Figure 4). In this case, Pipe 1 will be completely calculated. For Pipe 2, the mirror condition is used, so that only half of the pipe is calculated.

The boundary condition for Pipe 2 at the coupling face is taken from the Pipe 1 domain and for each cell respectively. This means, that for each cell in the Pipe 1 domain a mirrored cell in the Pipe 2 domain is found and marked (see Figure 4, Detail A). Therewith, the correct boundary condition for each cell is defined and the required flux can be calculated. In the case of a time delayed simulation, the flux calculation occurs after the defined time delayed period. Explicitly, time delayed data are available and flux calculation is possible after this period. The boundary condition code is written in the C programming language as a user defined function (UDF) and can dynamically be loaded with the FLUENT solver. The source code containing UDF is directly compiled in FLUENT and uses additional macros and functions that are supplied by FLUENT. A detailed description of the developed UDF can be found in (Fluent, 2005b). Figure 5 presents a flowchart of the new J-BC. The code consists of four main blocks   i.e. input data, read data, flux calculation and source preparation. The code is executed every time step and every iteration by the FLUENT solver. The block Input Data includes all required geometries and condition data which have to be defined

(a) Two pipes

(b) Detail A
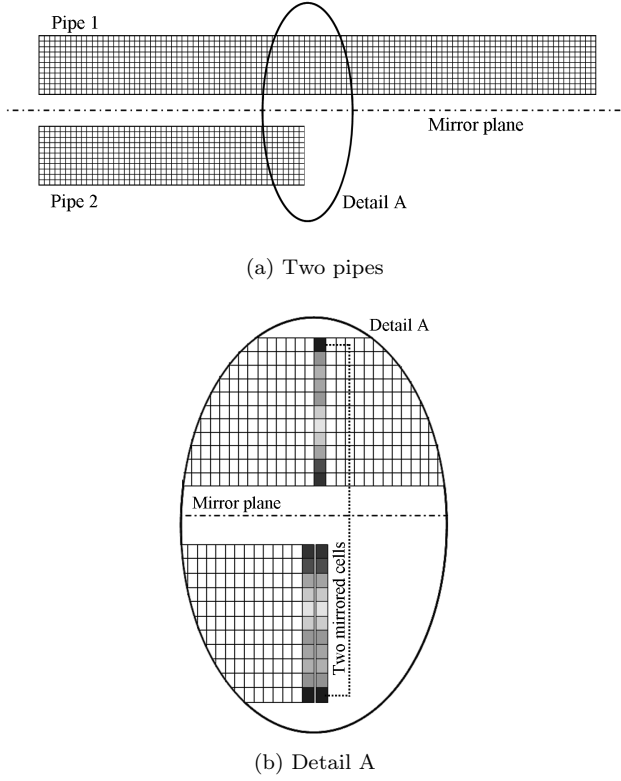
Figure 4: Application of J-BC for the simulation of two pipes
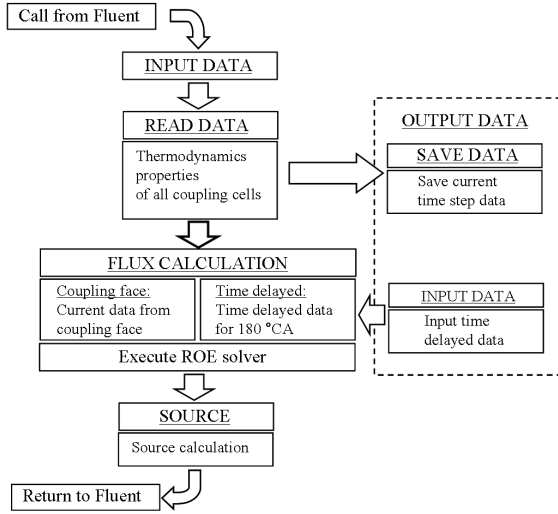
Figure 5: Flow chart

at the start of the simulation. For each 3D cell in the selected boundary face, thermodynamic properties and geometry data are read and saved (code READ DATA). These data cover static pressure, velocity in x-, y-, and z-direction, temperature, turbulent kinetic energy, turbulent dissipation rate, species mass fraction, material data, flow area, and cell volume. In this code part, the mirrored cells are found and marked with a coupling number and an ID number. In dependence on the mirror plane position, the velocity components are reversed by one of the boundary local coordinate

directions. The required time delayed data are saved every time step in an output data array and can be read at the start of the simulation as well. Therewith all required data for the flux calculation are available and are calculated separately for two coupled cells respectively (code FLUX CALCULATION). The fluxes are calculated by the Approximate Riemann Solver of Roe according to (Toro, 1997; Roe, 1981). Finally, the well-adjusted values are submitted to the CFD-code Fluent as a source term (code SOURCE). In previous investigations (Rothbauer et al., 2005, 2006; Rothbauer, 2007a; Rothbauer et al., 2007b; Jajcevic et al., 2008) the used coupling methodology and flux calculation have been presented and discussed in detail.

5 Flux and source calculation

J-BC can be used either in an own or a commercial CFD-Code. In both cases, it must enable the input of non-constant sources of mass, momentum, energy, turbulence quantities and species for each equation. These equations can be written in the general equation 1, where variable ϕ can stand for a variety of different quantities. In this equation, the four terms are visible: the transient term, the convection term, the diffusion term and the source term. Index i spans from one to three for the description of 3D flow situations.

$$\frac{\partial \rho \phi}{\partial t} + \frac{\partial \rho u_i \phi}{\partial x_i} = \frac{\partial}{\partial x_i} \left(\Gamma_\phi \frac{\partial \phi}{\partial x_i} \right) + S_\phi \qquad (1)$$

In case of a multi species problem, the dependent variable ϕ is the mass fraction of a chemical species and in case of turbulent flow, the dependent variable ϕ is used for the transport of turbulence quantities, e.g. turbulent kinetic energy k and dissipation rate ϵ in case of the standard $k - \epsilon$ turbulence model. For each of these variables the diffusion coefficient Γ_ϕ and the source term S_ϕ are given. In order to calculate the source term S_ϕ for each equation, the interface flux evaluation is required. In this work, the well-known Approximate Riemann solver is used, which was first presented in (Roe, 1981). It solves the Riemann problem between two cells, which contain two initial gas states at different pressures and densities separated by a contact discontinuity (see Figure 6). A detailed description of the employed solver can be found in literature (Rothbauer, 2007a; Toro, 1997; Roe, 1981; Sanz, 2007).

The one-dimensional partial differential Euler equations can be written in vector form as:

$$\frac{\partial U}{\partial t} + \frac{\partial F(U)}{\partial x} = 0 \qquad (2)$$

where,

$$U = \begin{pmatrix} u_1 \\ u_2 \\ u_3 \end{pmatrix} = \begin{pmatrix} \rho \\ \rho u \\ e \end{pmatrix} \qquad (3)$$
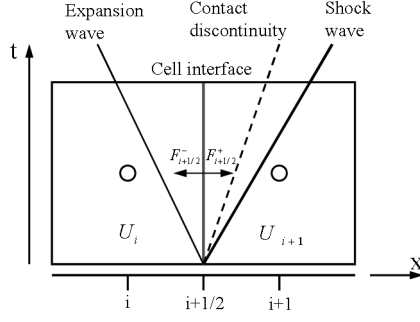
Figure 6: Schematic illustration of the Riemann problem between two cell

and

$$F = \begin{pmatrix} f_1 \\ f_2 \\ f_3 \end{pmatrix} = \begin{pmatrix} \rho u \\ \rho u^2 + p \\ u(e + p) \end{pmatrix} \tag{4}$$

The gas state is described with the vector of the conserved variables . Where ρ = density, p = static pressure, u = velocity in x-direction, and e is the total specific energy, related to the other variables by an equation of state, which - for a perfect gas - reads as follows:

$$e = \frac{p}{\gamma - 1} + \frac{\rho u^2}{2} \tag{5}$$

with γ = heat capacity ratio. Vector F in equation 6 represents the flux vector, which is required for the source calculation. The flux vector, at the cell interface position i+$\frac{1}{2}$, can be calculated from one of three following equations:

$$F^*_{i+1/2} = \frac{F_i + F_{i+1}}{2} - \frac{1}{2}|A|(U_{i+1} - U_i) \tag{6}$$

or

$$F^*_{i+1/2} = F_i + \left(R\frac{\Lambda - |\Lambda|}{2}L\right)_{i+1/2}(U_{i+1} - U_i) \tag{7}$$

or

$$F^*_{i+1/2} = F_{i+1} - \left(R\frac{\Lambda + |\Lambda|}{2}L\right)_{i+1/2}(U_{i+1} - U_i) \tag{8}$$

In equation 6, A represents the Jacobian matrix and can be written for the one-dimensional case as:

$$A = \frac{\partial F}{\partial U} = L^-\Lambda L \tag{9}$$

with

$$R = L^- \tag{10}$$

the Jacobian matrix A is given:

$$A^+ = R\Lambda^+L = R\frac{\Lambda + |\Lambda|}{2}L \tag{11}$$

respectively

$$A^- = R\Lambda^-L = R\frac{\Lambda - |\Lambda|}{2}L \tag{12}$$

The matrix $\Lambda^\pm$ is a diagonal matrix defined:

$$\Lambda^\pm = \begin{vmatrix} \dfrac{u \pm |u|}{2} & & \\ & \dfrac{(u + c) \pm |u + c|}{2} & \\ & & \dfrac{(u - c) \pm |u - c|}{2} \end{vmatrix} \tag{13}$$

The matrixes R and L are described as:

$$L = \begin{bmatrix} 1 - \dfrac{\gamma - 1}{2}M^2 & (\gamma - 1)\dfrac{u}{c^2} & -\dfrac{\gamma - 1}{c^2} \\ \dfrac{c}{\rho}\left(\dfrac{\gamma - 1}{2}M^2 - \dfrac{u}{c}\right) & \dfrac{1}{\rho} - \left(\dfrac{\gamma - 1}{\rho}\cdot\dfrac{u}{c}\right) & \dfrac{\gamma - 1}{\rho c} \\ \dfrac{c}{\rho}\left(\dfrac{\gamma - 1}{2}M^2 + \dfrac{u}{c}\right) & -\dfrac{1}{\rho} - \left(\dfrac{\gamma - 1}{\rho}\cdot\dfrac{u}{c}\right) & \dfrac{\gamma - 1}{\rho c} \end{bmatrix} \tag{14}$$

$$R = \begin{bmatrix} 1 & \dfrac{\rho}{2c} & \dfrac{\rho}{2c} \\ u & \dfrac{\rho}{2c}(u + c) & \dfrac{\rho}{2c}(u - c) \\ \dfrac{u^2}{2} & \dfrac{\rho}{2c}\left(\dfrac{c^2}{\gamma - 1} + \dfrac{u^2}{2} + uc\right) & \dfrac{\rho}{2c}\left(\dfrac{c^2}{\gamma - 1} + \dfrac{u^2}{2} - uc\right) \end{bmatrix} \tag{15}$$

with M = mach number and c = speed of sound. In order to calculate the variables at the cell interface position $i + \dfrac{1}{2}$ in the equations 13, 14, and 15, the density, the velocity, and the speed of sound are replaced by averaged weighted values. These particular mean values are defined by the square root of the densities (see equations 16):

$$R_{i+1/2} = \sqrt{\rho_{i+1}/\rho_i} \tag{16}$$

$$\bar{\bar{\rho}}_{i+1/2} = \sqrt{\rho_{i+1}/\rho_i} = R_{i+1/2}\cdot\rho_i \tag{17}$$

$$\bar{\bar{u}}_{i+1/2} = \frac{R_{i+1/2}\cdot u_{i+1} + u_i}{R_{i+1/2} + 1} \tag{18}$$

$$\bar{\bar{H}}_{i+1/2} = \frac{R_{i+1/2}\cdot H_{i+1} + H_i}{R_{i+1/2} + 1} \tag{19}$$

$$\bar{\bar{c}}_{i+1/2} = \sqrt{(\gamma - 1)\left(\bar{\bar{H}} - \frac{\bar{\bar{u}}^2}{2}\right)} \tag{20}$$

with the total enthalpy:

$$H = \frac{\gamma}{\gamma - 1}\frac{p}{\rho} + \frac{u^2}{2} \tag{21}$$

Therewith, all required data for the flux F calculation according to equation 4 are available and the source can be calculated:

Continuity source:

$$S_C = f_1 \tag{22}$$

Momentum source:

$$S_M = f_2 - p \cdot A \qquad (23)$$

Energy source:

$$S_E = f_3 \qquad (24)$$

Turbulent kinetic energy source :

$$S_k = f_1 \cdot k \qquad (25)$$

Turbulent dissipation rate source :

$$S_\epsilon = f_1 \cdot \epsilon \qquad (26)$$

Species source :

$$S_S = f_1 \cdot Y_i \qquad (27)$$

where Y_i = mass fraction of a chemical species and A = flow area.

6 Validation of J-BC

For the validation of J-BC, a simulation of two pipes is used (see Figure 7). Pipe 1 has a length of 1 meter, a diameter of 0.08 meter as well as two separate volumes. At the start of simulation, these volumes are initialized with a pressure of 10 bar and a temperature of 1000 K, and a pressure of 1 bar and a temperature of 300 K respectively. For Pipe 2, the mirror condition is used, so that only one half of the pipe with a length of 0.5 meter is calculated. At the start of simulation this pipe is initialized with a pressure of 1 bar and a temperature of 300 K. In both pipes, measurement planes are set with an evaluation of their averaged values. The evaluated data inside Pipe 1 are further used as reference values for the validation without the influence of the J-BC. These data are compared with evaluated values inside Pipe 2, which include the influence of the new boundary condition. The fluid in the model is defined as air with constant properties. The variation of density is calculated from the ideal gas law ($p = \rho R T$). Two simulations are used for the validation of J-BC, the first without and the second with the time delay option.
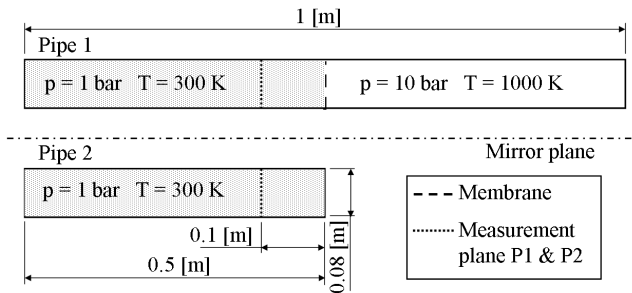
Figure 7: Validation model of two pipes

This simulation solves a particular problem, also called the Riemann problem. At the bursting of the membrane, at t = 0, the pressure discontinuity propagates to the left into the low-pressure gas and simultaneously an expansion wave propagates to the right into the high-pressure gas. In addition, a contact discontinuity separating the two gas regions propagates to the left in the tube. This is illustrated in Figure 6 for only two cells, which also show the characteristics and the discontinuities. Figure 8, Figure 9, and Figure 10 show the results of both simulations used for the validation. Evaluated data are pressure, mass flow and temperature. As explained before, reference values are the evaluated data on the measurement plane P1 inside Pipe 1. The curves of plane P2 can be distinguished for the results of two simulations, with and without time delay option. In case of a time delay, a time shift of 0.0003 seconds was set. A good agreement can be seen for the whole integration time of 0.02 seconds. This further confirms the accurateness of the used coupling methodology and time delayed boundary condition.
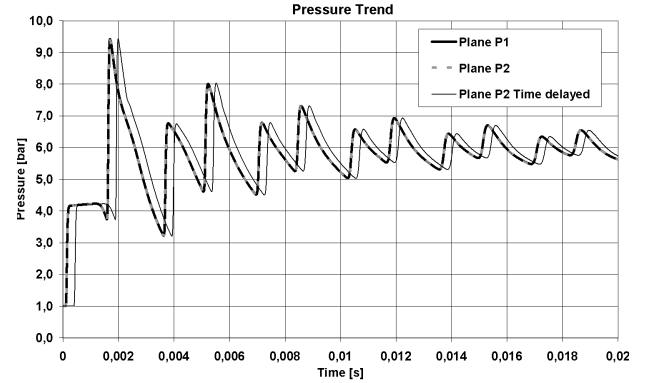
Figure 8: Pressure trend
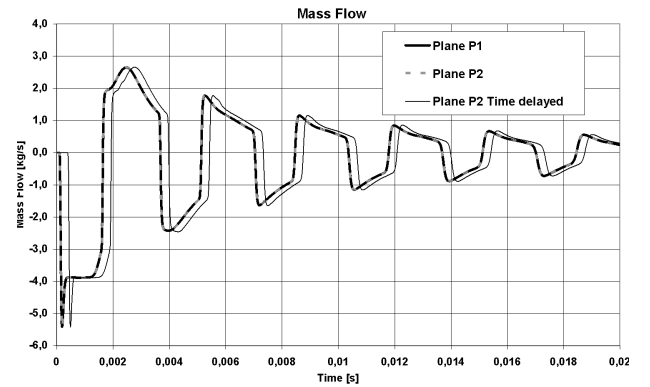
Figure 9: Mass flow
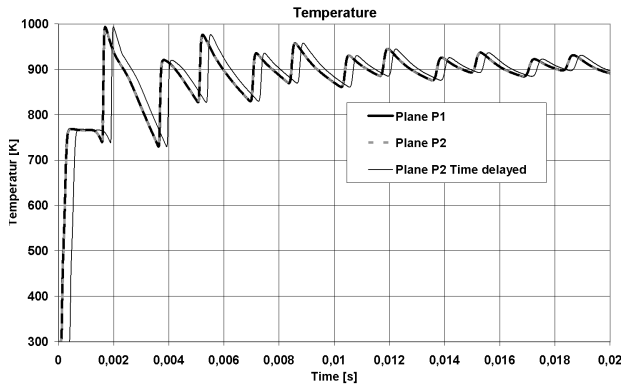
Figure 10: Temperature trend

7 Application of J-BC for IC-engine simulation

The selected engine for the simulation is a 2-cylinder 2-stroke engine from BRP-Powertrain with loop scavenging via five intake ports and a cylinder volume of approximately 300 cm. The engine can also be classified as a 2-cylinder 2-stroke engine with reed valve, crank case charge, Schnurle loop scavenging, variable exhaust port opening (RAVE Rotax Adjustable Variable Exhaust), tuned exhaust pipe, and gasoline direct injection (GDI). The intake ports are located symmetrically around the cylinder with the same opening time. A high-pressure injector into the cylinder directly injects the fuel during the scavenging process; early injection, homogeneous charge, see (Johnson and Braven, 2008; Harker et al., 2008; Basshuysen, 2007; Stanciu, 2005; Petermeier, 2001; Eichlseder et al., 2008). The simulation was conducted at only one engine speed of 7900 rpm and with wide-open throttle (WOT). This engine operating point was chosen because of the maximum torque value. The boundary and initial conditions were specified using data from the engine tests on a test bench and from simulation (Jajcevic et al., 2008; Schmidt et al., 2004; Jajcevic et al., 2009a,b). A reed valve model proposed by (Schmidt et al., 2007) was used in the simulation. The required data for the validation are calculated on predefined faces in the volume of the exhaust pipe. On these faces, the area-averaged pressure values are evaluated and compared with the total 3D simulation of both cylinders and the test bench results. For simulation purposes, the pressure-based solver is used with an implicit formulation for an unsteady flow. For the pressure-velocity coupling, the PISO scheme was chosen, as recommended for transient flow calculations. The variation of density is calculated from the ideal gas law ($p = \rho R T$). The standard $k - \epsilon$ turbulence model was used to model the turbulent flow. The standard values for the turbulent kinetic energy k and the dissipation rate ϵ were taken from the settings of (Fluent, 2005a). Further,

the standard wall function for the near wall modeling of the turbulent boundary layer was selected.
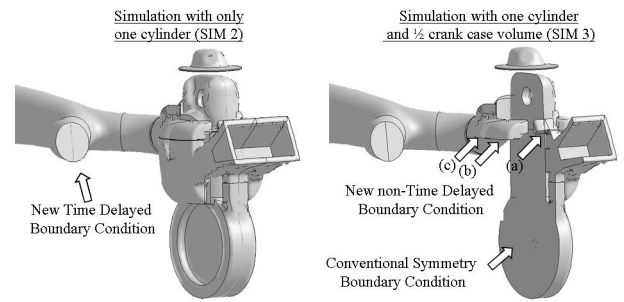
Figure 11: Application of J-BC for a 2-cylinder 2-stroke engine simulation

Figure 11 shows two different J-BC applications for the 2-cylinder 2-stroke engine simulation. Variant SIM 2 (left side) is a simulation, where the second cylinder is replaced by applying the new J-BC using time delayed data. Variant SIM 3 (right side) shows an example, where the J-BC is used for non-time delayed (synchronous) symmetric technical problems. Due to an asymmetrical flow situation inside the cylinder, the use of the conventional symmetry boundary condition is limited. In reality, this happens due to an unsymmetrical injector and/or spark position. Furthermore, when the pressure wave of the exhaust pipe re-enters the cylinder, it creates an asymmetrical situation, due to the close-by position of the junction to the cylinder. In this case, only a half of the crankcase and a part of the intake ports geometry using a conventional symmetric boundary condition was cut off. For the transition region a between symmetry and non-symmetry domains, and for two intake ports b and c (see Figure 11), the new J-BC without the time-delayed option is used.

	Test bench	SIM 1	SIM 2	SIM 3
Pressure trend exhaust pipe	X	X	X	X
Pressure, mass flow, and temperature trends intake ports	-	X	X	X
Equivalence ratio SOI (3D data)	-	X	X	X
Equivalence ratio around the spark plug	-	X	X	X
Fuel distribution inside the engine	-	X	X	X
Fuel evaporation inside the cylinder	-	X	X	X

Table 1 Matrix of used simulations and evaluated data for the validation of J-BC

Table 1 shows a matrix of simulations for the validation of J-BC. Simulation 2 (SIM 2) and Simulation 3 (SIM 3) are two calculations with used J-BC. The results of these simulations are compared with the results of the conventional simulation with both cylinders, i.e. Simulation 1 (SIM 1). Even with available measurement

data, these simulation results are compared with the test bench results. Furthermore, very important criteria for the validation of the new boundary condition are the flow situation inside the cylinder volume and the influence of the J-BC on the mixture preparation and the mixture quality. Hence, the mixture quality inside the cylinder volume at the time of ignition is evaluated and presented in this work. The evaluated data of Simulation 1, such as equivalence ratio and state conditions inside the intake ports, are further used as reference values for the validation of the J-BC.

(a) Exhaust system

(b) Intake ports
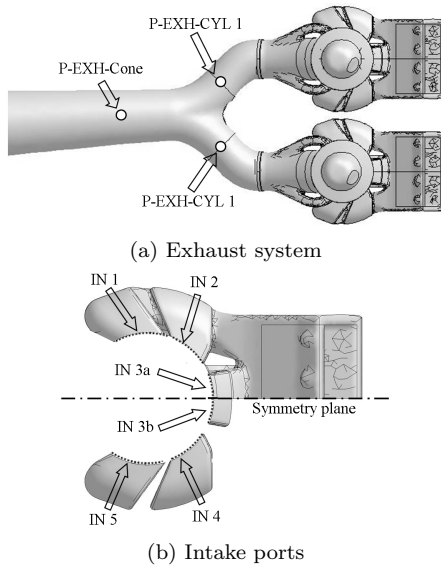
Figure 12: Measurement points in the exhaust (a) and intake (b) ports

Figure 12 (a) shows the measurement points in the exhaust port. The indicated pressure values (P-EXH-C1, P-EXH-C2 and P-EXH-Cone) are presented in the following chapter together with a comparison with the simulation results. For the validation of simulation SIM 3, the area averaged values pressure, mass flow and temperature are evaluated on the predefined faces IN 1, 2, 3a, 3b, 4 and 5 - see Figure 12 (b). Due to a symmetric situation inside the crankcase and the volumes of the intake ports, the trend of evaluated data in the two symmetrical faces should be identical. In this case, these faces are IN 1 & 5, IN 2 & 4, and IN 3a & 3b. All simulations apply the same solver settings and the same grid as well. The first phase of the simulation using the new J-BC concerns the scavenging process simulation without injection and combustion processes. In this phase, the cylinder volume is initialized with a pressure of approximately 12 bars and a temperature of 1788K at 70 °CA after TDC for each engine cycle. These data stem from test bench results. Furthermore, the species composition in the cylinder is initialized with an approximated rest gas concentration. A detailed description of the employed simulation strategy can be found in (Jajcevic et al., 2009b). The validation of the above described first steps is done with measurement

data, which mainly concern the pressure trends in the exhaust port. The next steps include the simulation of fuel injection inside the cylinder. During the first 180 °CA the boundary face properties are set as wall and the corresponding data are only saved. After 180 °CA, the time delayed data for the J-BC are available and provided at the correct position. The best piston position for the start of the simulation is the opening phase of the exhaust port of the first cylinder, as the second cylinder is already closed. With this piston start position, the influence of the second non-calculated cylinder on the gas dynamics behaviour inside the exhaust pipe during this first 180 °CA is minimized.
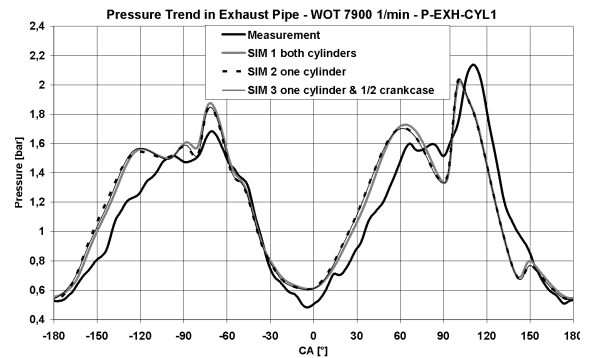
Figure 13: Pressure trend P-EXH-CYL 1
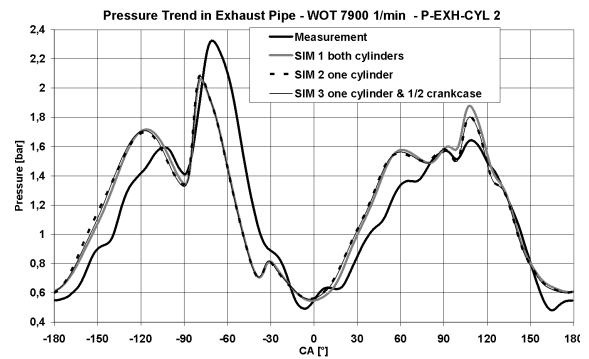
Figure 14: Pressure trend P-EXH-CYL 2

Figure 13, Figure 14, and Figure 15 show the pressure trend in the exhaust port in the measurement points P-EXH-C1, P-EXH-C2, and P-EXH-Cone, with a comparison of the simulation results with the measurement data. The simulation data are the results after five revolutions and are directly compared with the test bench results. Generally, the pressure trends show a good agreement over the complete revolution. The results also show that the second cylinder can be efficiently replaced due to a symmetry condition and the time delay using the new J-BC. It is furthermore
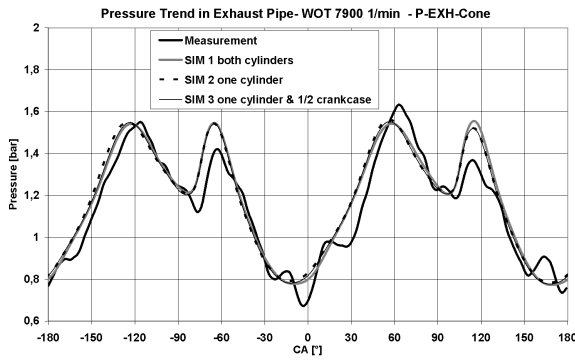
Figure 15: Pressure trend P-EXH-Cone
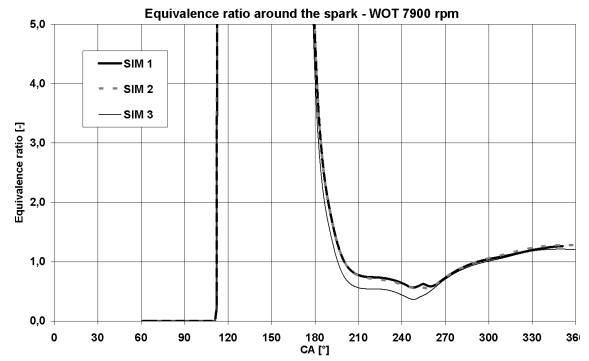
Figure 18: Equivalence ration around the spark
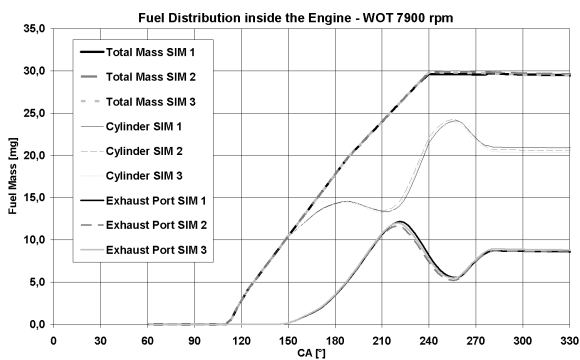
**Figure 16**: Fuel distribution inside the engine
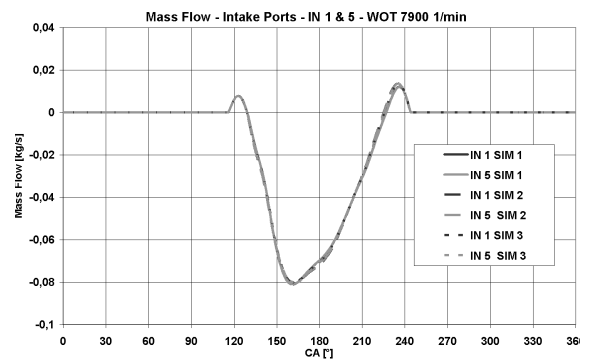
**Figure 19**: Mass flow intake ports IN 1&5
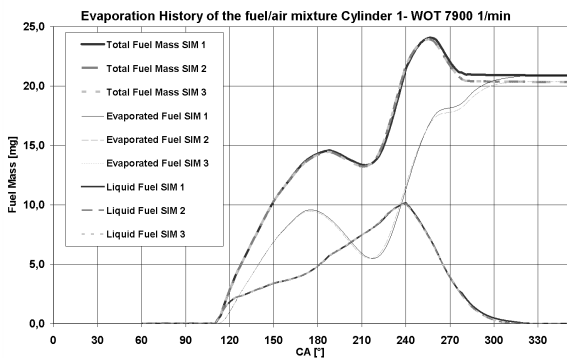

Figure 17: Evaporation history cylinder 1
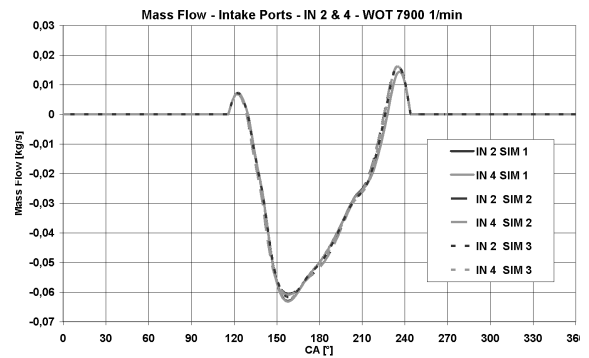
Figure 20: Mass flow intake ports IN 2&4

visible, that the calculation of half of the crankcase volume does not have any influence on the gas dynamics behaviour inside the exhaust system (see curves SIM 3). By a comparison of only measurement data, it is visible that a perfect symmetrical situation does not exist in the reality. This is caused by a different combustion processing and some variations of the pressure and temperature levels at exhaust port opening. For instance, a different combustion process and fluid temperatures cause a difference in the position and time dependant speed of sound distribution inside the exhaust system. This temperature difference between cylinder one and

two was 10 K on the test bench. Generally, a combustion process development for an IC-engine starts with a one cylinder test engine, e.g. (Schmidt et al., 2004). In this case a symmetrical situation is also assumed. Therewith, the presented boundary condition is well applicable for the development process of a new engine.

Figure 16 presents the fuel distribution inside the engine (liquid and evaporated fuel) for the first fuel injection and for the crank angle interval between TDC and 330 °CA. Start of injection occurs at approximately 110 °CA after TDC and lasts approximately 130 °CA. In the time span between 110 and 150 °CA the entire
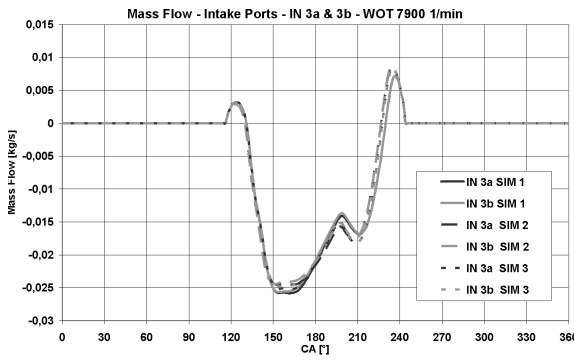
Figure 21: Mass flow intake ports IN 3a&3b
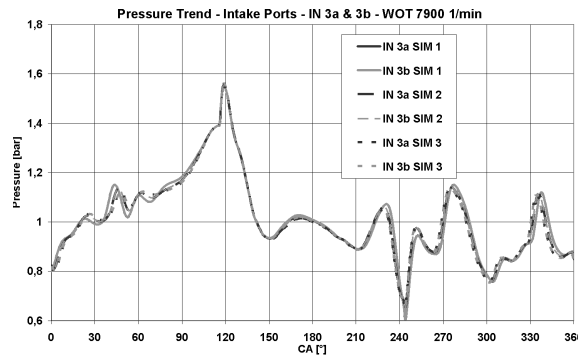
Figure 24: Pressure trend intake ports IN 3a&3b
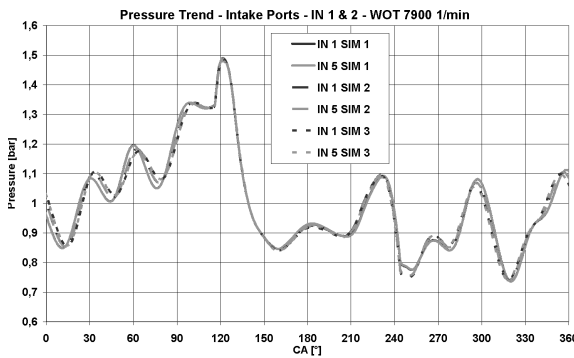
Figure 22: Pressure trend intake ports IN 1&2b
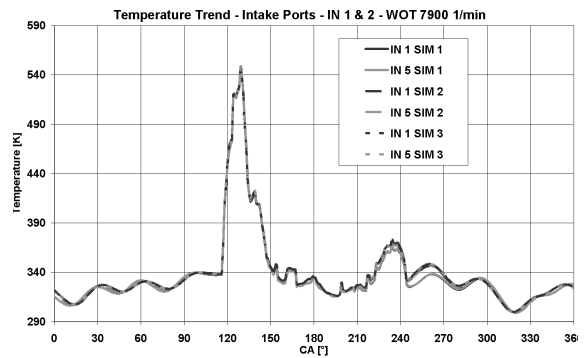
Figure 25: Temperature trend intake ports IN 1&2
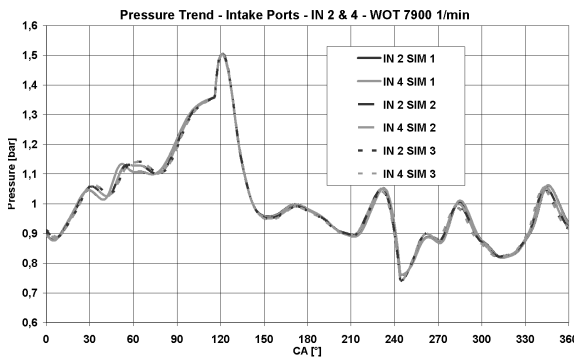
Figure 23: Pressure trend intake ports IN 2&4
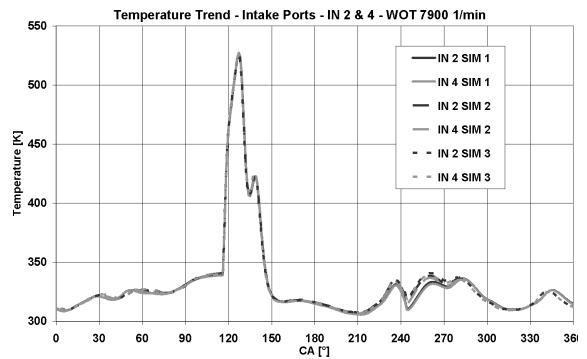
Figure 26: Temperature trend intake ports IN 2&4

fuel resides in the cylinder volume. After that, the first scavenging loss occurs and the fuel mass inside the exhaust volume increases. At approximately 220 °CA, the pressure wave returns and reduces the scavenging losses. Due to the closing phase of the exhaust port and the increasing pressure inside the cylinder a new fuel loss occurs and the fuel mass inside the exhaust pipe volume increases again. The very small deviation between the three simulations only has a minor influence on the required results for the industrial CFD simulation. These results also confirm that the replacement of the second cylinder by applying the new J-BC shows only a neglectable influence on the scavenging losses. This confirms the accurateness of used time delayed boundary

condition. Figure 17 shows the evaporation history of the fuel/air mixture in the volume of cylinder 1 after the first fuel injection. It can be seen, that the new J-BC does not have an influence on the fuel evaporation inside the cylinder (see curves Liquid fuel). Figure 18 shows the equivalence ratio trend over one revolution and around the spark. A good agreement can be seen between simulations SIM 1 and SIM 2. In the region between approximately 180 and 270 °CA, the result of simulation SIM 3 shows a deviation compared to the results of SIM 1 and SIM 2. This difference can be explained by the fact that a perfect symmetry situation inside the intake ports and the crankcase volume is assumed in SIM 3 with J-BC. In addition, J-BC causes a deviation inside the
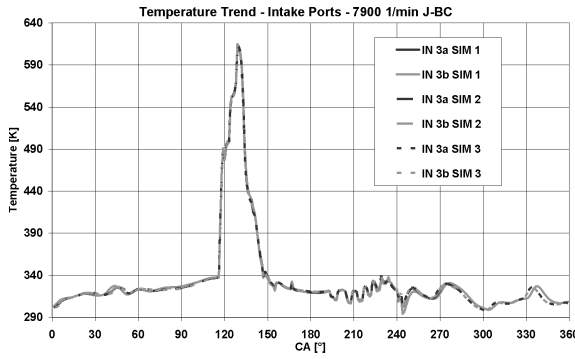
Figure 27: Temperature trend intake ports IN 3a&3b

cylinder in comparison with the simulations SIM 1 and SIM 2. For an industrial CFD application, the results after approximately 330 °CA (time of ignition) become very important keeping the deviation in an acceptable range.

Figure 19 up to Figure 27 show pressure, mass flow and temperature trends on the faces IN 1, 2, 3a, 3b, 4, and 5. These data are evaluated in order to verify an absolutely symmetrical situation inside the crankcase and volumes of the intake ports. Over a complete revolution, the simulation results (SIM 2 and SIM 3) using J-BC show a good agreement in comparison with the results of the simulation with both cylinders (SIM 1). This further confirms the accurateness of the used boundary condition.

Figure 28 shows the comparisons of the equivalence ratio at 345 °CA (time of ignition). The results of simulation SIM 1 serve as reference data for simulation SIM 2 and SIM 3 validation. The results of simulation SIM 2 (second cylinder is replaced) show a small deviation in comparison with reference simulation SIM 1. Simulation SIM 3 (with only one cylinder and half of the crankcase volume) shows bigger deviations in comparison with the reference simulation SIM 1, but still in an acceptable range for industrial CFD simulation. However, the SIM 3 simulation strategy can be used for the predictive simulation of 2-stroke engines in the early development phase, where an array of information about a new engine is required in a short calculation time, e.g. for different injector position and/or injection strategy investigations.

8   Conclusion

This paper covers the discussion of a methodology for the efficient simulation of a 2-cylinder 2-stroke high-performance engine using the new cyclic and time delayed boundary condition (J-BC). This boundary condition allows a reduction of the calculation domain and therewith of the calculation time. The boundary condition data are calculated during the simulation and are set on the corresponding face in the calculated domain. The essential advantage of the new boundary
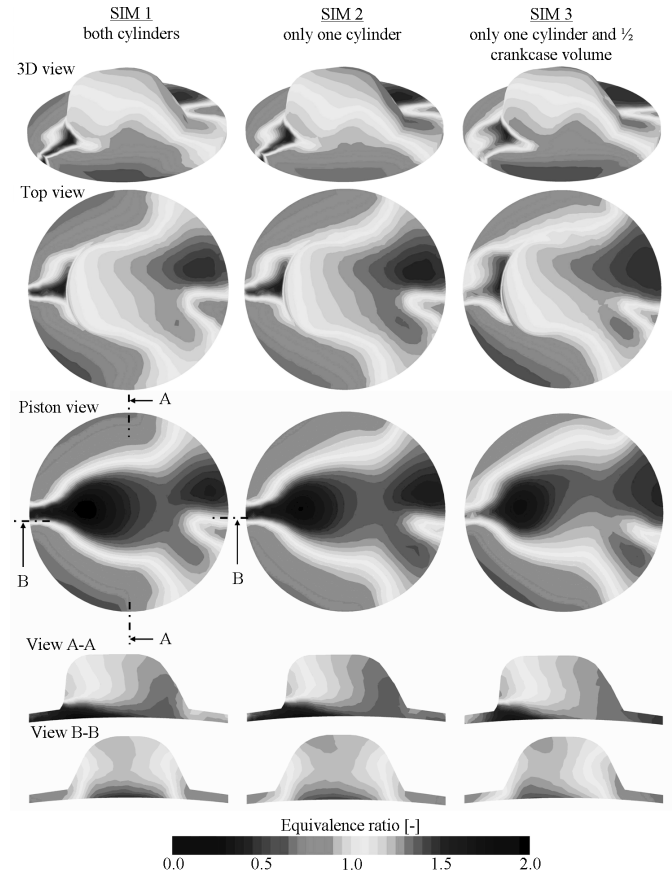
Figure 28: Equivalence ratio at 345 °CA, start of ignition

condition is the reduced simulation effort for cyclic and time delayed technical problems. For the IC-engine simulation, this means that the complete simulation of the 2-cylinder 2-stroke engine using the new J-BC can be carried out without the geometry of the second cylinder. In this case, the number of 3D cells is reduced by approximately 37% (simulation strategy SIM 2). A further reduction of the calculated domain, due to the simulation of only half of the crankcase volume and simultaneously without the second cylinder (simulation strategy SIM 3), allows a reduction of 3D cells by approximately 47%. This simulation strategy can be efficiently used for the predictive simulation of 2- stroke engines in the early development phase, e.g. for different injector position and/or injection strategy investigations, where an array of information about a new engine is required in a short calculation time. In comparison with the conventional boundary condition taken from 1D calculation, the data over the boundary face do not need to be constant. Additionally, 1D calculation or measurement data are obsolete. The requirement for the use of the J-BC is only a symmetric and/or time delayed flow situation. The presented results show a good agreement in comparison with the test bench results and the conventional simulation of the 2-cylinder 2-stoke engine with both cylinders.

References

Amsden A.A. (1993), 'A KIVA Program with Block-Structured Mesh for Complex Geometries', *Los Alamos National Laboratory*, USA.

AVL (2006a), 'AVL Boost 1D-3D Coupling', *AVL LIST GmbH*, Austria.

AVL (2006b), 'CFD Solver V8.5', *AVL LIST GmbH*, Austria.

Basshuysen R. (2007), 'Ottomotor mit Direkteinspritzung', *ATZ/MTZ-Fachbuch, Vieweg Germany*, ISBN 978-3-8348-0202-6.

Bozza F., Gimelli A., Andreassi L., Rocco V., Scarcelli R. (2008), '1D-3D Analysis of the Scavenging and Combustion Process in a Gasoline and Natural-Gas Fuelled Two-Stroke Engine', *SAE World Congress and Exhibition*, SAE Paper 2008-01-1087.

Chiatti G., Chiavola O. (2002), 'Scavenge Streams Analysis in High Speed 2T Gasoline Engine', *International Body Engineering Conference and Exhibition and Automotive and Transportation Technology Congress*, SAE Paper 2002-01-2180.

Eichlseder H., Klting M., Piok W.F. (2008), 'Grundlagen und Technologien des Ottomotors', *Springer-Wien-NewYork*, ISBN 978-3-211-25774-6.

Fluent (2005a), 'Fluent 6.3 Users Guide', *Fluent Inc.*, USA.

Fluent (2005a), 'UDF Manual', *Fluent Inc.*, USA.

Gambit (2005), 'UDF Manual', *Gambit Users Guide*, USA.

Harker N., Braven K.R.D., Johnson J., Findlay A. (2008), 'University of Idahos Clean Snowmobile Design Using a Direct-Injection Two-Stroke Engine', *Small Engine Technology Conference*, SAE Paper 2008-32-0031.

Jajcevic D., Almbauer R.A., Schmidt S. P., Glinser K. (2008), 'CFD Simulation of a Real World High-Performance Two Stroke Engine with Use of a Multidimensional Coupling Methodology', *Small Engine Technology Conference*, SAE Paper 2008-32-0042.

Jajcevic D., Almbauer R.A., Schmidt S. P., Glinser K. (2008), 'Simulation of Scavenging Process, Internal Mixture Preparation, and Combustion of a Gasoline Direct Injection Two-Cylinder Two-Stroke Engine', *Small Engine Technology Conference*, SAE Paper 2009-32-0046.

Jajcevic D., Almbauer R.A., Schmidt S. P., Glinser K. (2008), 'Simulation Strategy and Analysis of a Two-Cylinder Two Stroke Engine Using CFD Code Fluent', *EASC*, Munich.

Johnson J. and Braven K.R.D. (2008), 'Comparison of Homogeneous, Stratified and High-Squish Stratified Combustion in a Direct-Injected Two-Stroke Engine', *Small Engine Technology Conference*, SAE Paper 2008-32-0030.

Li, C. (2002), 'Coupled simulation between GT-Power and Fluent', *Master Thesis*, Lulea University of Technology.

Petermeier L. (2001), 'Simulation der Gemischbildung wandgefhrter Otto DE Brennverfahren unter besonderer Bercksichtigung der Strahl-Wandinteraktion', *Dissertation*, Graz University of Technology.

Pischinger R., Klell M., Sams T. (2002), 'Thermodynamik der Verbrennungskraftmaschine', *Springer-Verlag/Wien*, ISBN 3-211-83679-9.

Roe P.L. (1981), 'Approximate Riemann Solver, Parameter Vectors, and Difference Schemes', *Journal Comput. Phys.*, 43: 357-372.

Rothbauer R.J. (2007), 'Methode zur Kopplung von bewegten 3D sowie 0/1D CFD Berechnungsgebieten', *Dissertation*, Graz University of Technology.

Rothbauer R.J., Almbauer A.R., Schmidt P.S., Margelik H.R., Glinsner K. (2006), 'A Multidimensional Interface for the Predictive CFD Simulation of the 2-Stroke Engine', *Small Engine Technology Conference*, SAE Paper 2006-32-0059.

Rothbauer R.J., Grasberger G., Abidin Z., Almbauer A.R. (2007), 'Reed Valve, Crankcase and Exhaust Models Coupled to 3D Fluid Domains for the Predictive CFD Simulation', *Small Engine Technology Conference*, SAE Paper 2007-32-0030.

Rothbauer R.J., Margelik H.R., Aslam M.M., Almbauer A.R., Schmidt S.P., Glinsner K. (2005), 'Predictive Simulation Strategies for the 2-Stroke Scavenging Process with the Scope of the Development Process', *Small Engine Technology Conference*, SAE Paper 2005-32-0099.

Sanz W. (2007), 'Computational Fluid Dynamics', *Lecture script 319.082*, Institute for Thermal Turbomachinery and Machine Dynamics, Graz University of Technology.

Schmidt S., Schoegl O., Rothbauer R.J., Eichlseder H., Kirchberger R. (2007), 'An Integrated 3D CFD Simulation Methodology for the Optimization of the Mixture Preparation of 2-Stroke DI Engines', *Small Engine Technology Conference*, SAE Paper 2007-32-0029.

Schmidt S., Winkler F., Schoegl O., France M.M. (2004), 'Development of a Combustion Process for a High Performance 2-Stroke Engine with High Pressure Direct Injection', *Powertrain and Fluid Systems Conference*, SAE Paper 2004-01-2942.

Stanciu A.S. (2005), 'Gekoppelter Einsatz von Verfahren zur Berechnung von Einspritzhydraulik, Gemischbildung und Verbrennung von Ottomotoren mit Kraftstoff-Direkteinspritzung', *Dissertation*, TU Berlin.

Star-CD (2006), 'USER GUIDE STAR-CD VERSION 4.0', *CD adapco Group*, USA.

Toro E. (1997), 'Riemann Solvers and Numerical Methods for Fluid Dynamics', *Springer-Verlag Berlin Heidelberg New York*, ISBN 3-540-61676-4.

Zeng. Y., Strauss S., Lucier P., Craft T. (2004), 'Predicting and Optimizing Two-Stroke Engine Performance Using Multidimensional CFD', *Small Engine Technology Conference*, SAE Paper 2004-32-0039.

6 Methodology for an exhaust system simulation

The exhaust system of a 2-stroke engine has an important influence on the engine performance. It is designed in a way that at the desired operating point, the outflow pressure wave is reflected and arrives again at the cylinder at the correct time. This effect is generated with the following two specific parts of the exhaust system, a diffuser cone and a counter cone. Thus, the exhaust system supports the scavenging process inside the cylinder volume, due to a sucking effect of the fresh air from the crankcase volume through the cylinder into the exhaust system. Shortly before the exhaust port closing phase, the reflected pressure wave returns and pushes the fresh charge – lost due to the scavenging process itself – back into the cylinder volume. This process leads to a so-called "supercharging effect". In order to simulate a 2-stroke engine the timing of the discharge and the back loading waves must be very exactly predicted. This further means that the spatial and time dependent speed of sound of the exhaust gas has to be calculated correctly and requires an exact simulation of the transient energy flows through the exhaust system.

In a 2-stroke engine, the complete thermodynamic cycle is realized in only two piston movements (one revolution). The 2-stroke system increases the engine efficiency and often provides remarkable high specific power, but on the other hand, it needs a simultaneous exchange of exhaust gas with the fresh incoming charge inside the cylinder volume. In case of a GDI 2-stroke engine the fresh incoming charge is pure air. This leads to a reduction of the fuel concentration inside the exhaust system and the hydrocarbon emissions respectively. Nevertheless, at high engine speed and full load the fuel losses can rise up to 30%, due to an early fuel injection strategy, so that inside the exhaust system an ignitable mixture exists. However, a high exhaust gas temperature (for instance at 7900 rpm WOT about 900 K) can cause a self-ignition inside the exhaust system, so that an investigation applying the 3D CFD tool is a reasonable way.

In one of the previous studies of our Institute, Rothbauer et al. [107] investigated the effect of turbulence and fluid dynamics on the transient heat transfer of a discharged system. The authors investigated a separated exhaust system with 3D simulation techniques. The transient boundary conditions were taken from a 1D simulation and were set as a profile at the correspondent surface. The disadvantage of this method is that the inlet boundary condition is not complete, due to the missing of 3D data in a 1D simulation. Furthermore, the authors did not include the combustion process simulation inside the exhaust system, so that this aspect is missing as well. In some engine operating points, due to a high fuel concentration and fluid temperature inside the exhaust system, the exhaust system superheating is severe. For Rothbauer et al. [107] the post-combustion process could have caused this effect.

The main problem of an exhaust system simulation is that a calculation of many revolutions is required until steady condition considering the fluid flow as well as the heat transfer over the entire exhaust pipe wall and the post-combustion. In this case, the complete exhaust system is the domain of interest, so that both cylinders can be replaced by boundary conditions. In contrast to the state-of-the-art method, where the boundary conditions stem form a previous 1D calculation (e.g. Rothbauer et al. [107]), the symmetry and time delayed boundary condition of chapter 5 is applied. This new type of boundary condition allows an efficient simulation of only one cylinder without data losses and simultaneously accounting the effect of all cylin-

ders. A further development stage of this boundary condition allows a simulation with an isolated exhaust system, whereas all data already obtained in the 3D CFD simulation are available and are used. Furthermore, this strategy enables a relative easy re-coupling of the exhaust system with the cylinder and the crankcase, so that an investigation of the influence of the new exhaust system condition on the scavenging process and the mixture preparation can be carried out. A detailed description of the used simulation strategy and an analysis of the obtained results are presented in the enclosed paper.

6.1   Paper IV

Exhaust system simulation of a 2-cylinder 2-stroke engine including heat transfer effects

SAE *International*®

Exhaust System Simulation of a 2-Cylinder 2-Stroke Engine Including Heat Transfer Effects

Dalibor Jajcevic, Raimund Almbauer and Stephan Schmidt
Graz University of Technology

Karl Glinsner and Matthias Fitl
BRP-Powertrain GmbH & Co KG

ABSTRACT

The exhaust system design has an important influence on the charge mass and the composition of the charge inside the cylinder, due to its gas dynamic behavior. Therefore the exhaust system determines the characteristics of the indicated mean effective pressure as well. The knowledge of the heat transfer and the post-combustion process of fuel losses inside the exhaust system are important for the thermodynamic analysis of the working process. However, the simulation of the heat transfer over the exhaust pipe wall is time consuming, due to the demand for a transient simulation of many revolutions until a cyclic steady condition is reached. Therefore, the exhaust pipe wall temperature is set to constant in the conventional CFD simulation of 2-stroke engines. This paper covers the discussion of a simulation strategy for the exhaust system of a 2-cylinder 2-stroke engine until cyclic steady condition including the heat transfer over the exhaust pipe wall. The influence of the wall temperature on the gas dynamic behavior and the post-combustion process inside the exhaust pipe were investigated as well. Finally, test bench results of the fired engine were used for the validation of the simulation.

INTRODUCTION

The exhaust system of a 2-stoke engine has an importance influence on the engine performance. It is designed in such a way that at the desired operating point, the outflow pressure wave is reflected and arrives again at the cylinder at the correct time. This effect is generated with the following two specific parts of the exhaust system, a diffuser cone and a counter cone. Thus, the exhaust system supports the scavenging process inside the cylinder volume, due to a sucking effect of the fresh air from the crankcase volume through the cylinder into the exhaust system. Shortly before the exhaust port closing phase, the reflected pressure wave returns and pushes the fresh charge - lost due to scavenging process itself - back into the cylinder volume. This process leads to a so-called "supercharging effect". In order to simulate a 2-stroke engine the timing of the discharge and the back loading waves must be very exactly predicted. This further means that the spatial and time dependent speed of sound of the exhaust gas has to be calculated correctly and requires an exact simulation of the transient energy flows through the exhaust system.

CFD has been widely used to simulate the flow inside 2-stroke engines over the past twenty years and can be efficiently used for the investigation of the above mentioned effects. In a development process of a 4-stroke engine the investigation of the exhaust system is carried out in order to minimize cold-start emissions for catalyst-equipped gasoline cars. In the last decade several experimental and 1D simulation activities were carried out on this subject. Caton and Heywood [1] used the indicated pressure trends and the temperature measurements inside the exhaust system in order to validate a heat transfer model for 4-stroke exhaust system simulation. Konstantinidis et al. [2] and Kandylas and Stamatelos [3], considered the complex exhaust system geometry by the development of a special heat transfer model for 1D simulation. This model covers all exhaust pipe configurations, such as single wall, double wall with air gap, or isolation. Furthermore, authors also paid special attention to the 2-dimensional heat transfer with 2 connected flanges. The simulation results showed a good agreement with the

experiments. Zhang et al. [4] developed a model for the steady state temperature distribution calculation taking into account single and double wall configuration (with air gap isolated systems). Several 1D models for the heat transfer calculation in the exhaust system are presented and discussed in studies by Zhang et al. [4] and Chen [5]. All these investigations do not deal with 3D effects, due to the high computational effort for the large computational domain of exhaust systems. As the conventional 3D simulation of the exhaust system is time consuming, more efficient methods for the simulation of the 2-stroke exhaust system have been studied, see Rothbauer et al. [6], Eichlseder et al. [7], and Schmidt et al. [8].

In one of the previous investigation of our Institute Rothbauer et al. [9] investigated the effect of energy conservation, turbulence, and fluid dynamics on the transient heat transfer of a discharge system. The authors investigated a separated exhaust system applying 3D simulation techniques. The transient boundary conditions were taken from a 1D simulation and were set as a profile at the correspondent surface. The disadvantage of this method is that the inlet boundary condition is not complete, due to the missing of 3D data in a 1D simulation. Furthermore, the authors did not include the combustion process simulation inside the exhaust system, so that this aspect is missing as well. In some engine operating points, due to a high fuel concentration and fluid temperature inside the exhaust system, the exhaust system superheating is severe. For Rothbauer et al. [9] the post-combustion process could have caused this effect.

This paper covers the discussion of a 3D CFD- methodology for the exhaust system simulation of a 2-cylinder 2-stroke engine until steady conditions are reached including the heat transfer over the exhaust pipe wall. It starts with a complete engine simulation, including scavenging, fuel injection, mixture preparation and combustion process, until a steady cyclic condition inside the engine is reached. Then the simulation is continued with the separated exhaust system until a steady situation is gained regarding the heat transfer and the post-combustion effects. After that, the exhaust wall temperature profile and the new exhaust system condition are again implemented in the complete engine simulation and the influence on the gas dynamic behavior and the engine performance is investigated. The advantage of the presented strategy is that the cylinder volumes are replaced by the symmetry and time delayed boundary condition introduced by Jajcevic et al. [10]. This new boundary condition allows an efficient simulation of only one cylinder engine without data losses and simultaneously takes the effect of both cylinders into account. A further development of this boundary condition allows for a simulation of a separated exhaust system, where both cylinders are replaced by this method.

ENGINE DESIGN

The experimental engine is a 2-cylinder 2-stroke engine from BRP-Powertrain, applying loop scavenging via five intake ports. The displacement of each cylinder is approximately 300 cm^3. The engine can also be classified as a 2-stroke engine with reed valve controlled sucked air mass, crank case charge, Schnurle loop scavenging, variable exhaust port (RAVE - Rotax Adjustable Variable Exhaust), tuned exhaust pipe and high pressure gasoline direct injection (GDI). The intake ports are located symmetrically around the cylinder with the same opening time. The position of these ports causes the fresh charge to be directed upwards into the cylinder and to increase the efficiency of the scavenging process. The exhaust pipe entry consists of three ports, one main and two small ports. In order to reduce the scavenging losses and to widen the speed range for effective exhaust tuning, the RAVE system controls the exhaust port opening/ closing time. Furthermore its use and position depends on the engine speed (low engine speed = RAVE system closed, high engine speed = RAVE system open). Due to a well-tuned exhaust system the reflected pressure wave reduces the scavenging losses. It reaches the cylinder just before the piston closes the exhaust port and charges the lost fuel-air mixture back to the cylinder.

Figure 1 shows the design of the investigated 2-cylinder 2-stroke engine. For the purpose of this research work the complete exhaust system geometry - including the muffler geometry - was taken into account. The simulation was conducted for only one engine speed of 7900 rpm with wide-open throttle (WOT) and maximum torque value. Furthermore, the RAVE system is completely open, which induces the increased fuel losses during the scavenging phase. The losses stem from a long injection time and an early injection strategy.
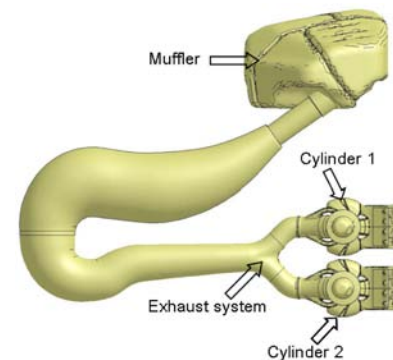

Figure 1. Design of the 2-cylinder 2-stoke engine

SIMULATION STRATEGY

In order to minimize the computational effort a simulation strategy was developed. This strategy consists of four steps,

which are presented in Figure 2. The first step is a scavenging process simulation; a calculation without the time consuming fuel injection and combustion process. At a selected piston position (before the exhaust port opens) the volume of the cylinder is initialized every cycle with the pressure, the temperature, and the according composition of the exhaust gases. This data can be taken from test bench or from previous simulation results. This strategy accelerates significantly the calculation time, as injection and combustion process simulations are missing. In addition, the gas dynamic behavior inside all parts of the engine achieves a steady condition within three or four revolutions, due to an unchanged initial condition inside the cylinder volume. An additional reduction of the computational effort is realized by the application of the time delayed boundary condition introduced by Jajcevic et al. [10]. The investigation of a 2-cylinder 2-stroke engine requires the simulation of the complete geometry including both cylinders and the complete exhaust port, because the simulation of only one cylinder causes an incorrect gas dynamic behavior inside the exhaust pipe and further leads to unrealistic results. Therefore, Jajcevic et al. [11] and Zeng et al. [12] use the complete geometry of a 2-cylinder 2-stroke engine with both cylinders to simulate the in-cylinder flow and the gas dynamics inside the exhaust pipe. However, in order to get effective and significant results for the 2-stroke 2-cylinder engine simulation in shorter calculation time, the second cylinder was replaced by the new time delayed boundary condition, which reduces the calculation time by approximately 50%.
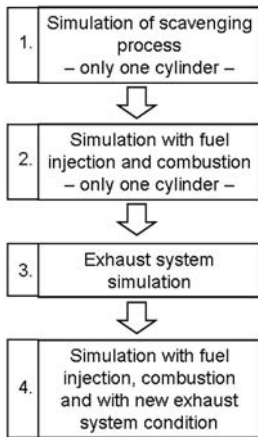
Figure 2. Strategy for exhaust system simulation

When the gas dynamic behavior calculation achieves a cyclic steady condition, regarding the indicated pressure trend inside the exhaust system, the crankcase volume, and the sucked fresh air mass, the second simulation phase covering the fuel injection and the combustion process can be carried out. After approximately three or four further revolutions with injection and combustion simulation, all processes inside the engine achieve a cyclic steady condition. Thus the inlet boundary condition at the entry to the exhaust system including time

dependent fluid temperature, mass flow, species concentrations etc. is available. The third simulation phase concerns the simulation of the exhaust system only. Therefore, the time delayed boundary condition was further developed for the application of an isolated exhaust system. This system simulation is run until steady conditions - concerning the heat transfer over the exhaust pipe walls, the wall temperature distribution and the fuel/oxidizer net-reaction rate inside the exhaust volume - are achieved. After this simulation, the wall temperature distribution and the cell data inside the complete exhaust system can be written as a file. Finally, the new exhaust system conditions can be re-implemented in the complete engine simulation, as the concluding step of the employed simulation strategy. The influence of the simulated exhaust system condition on the gas dynamic behavior and the engine performance will be investigated in this simulation phase as well.

SYMMETRY AND TIME DELAYED BOUNDARY CONDITION

This type of boundary condition can be used for time delayed as well as non time delayed technical problems. The following example illustrates its application in the simulation of a 2-cylinder 2-stroke engine. In this case, cylinder 1 is completely calculated. For the second cylinder, the symmetric condition is used, so that it is replaced by a time delayed boundary condition.
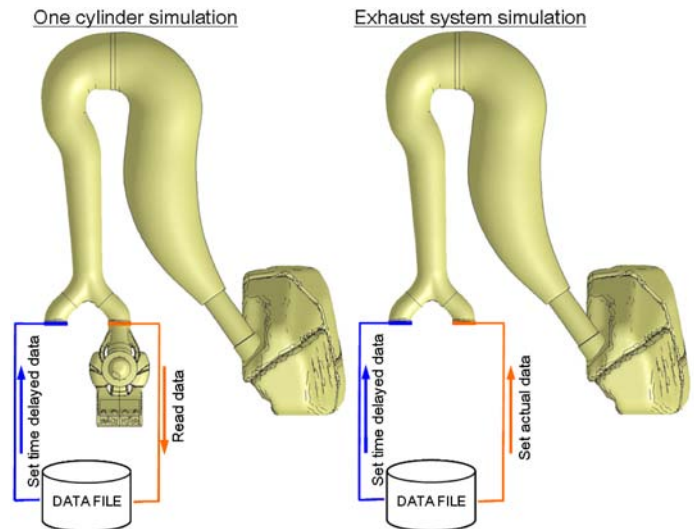
Figure 3. Application of symmetry and time delayed boundary condition

The boundary condition for the second cylinder is taken from the exhaust pipe of cylinder 1 for each cell respectively. This means, that for each cell in the exhaust cylinder 1 domain a symmetrically positioned cell in the domain of the exhaust of cylinder 2 is found and marked. Therewith, the correct boundary condition for each cell can be defined and the

required flux can be calculated. For the flux calculation, the time delayed data are read from an external data file for each cell respectively. In this case, the flux calculation occurs after the defined time delayed period. Explicitly, time delayed data are available and the according flux calculation is possible after this period. In the case of the isolated exhaust system calculation, both cylinders are replaced by the boundary condition. The required data are read from the external output data file. For cylinder 1 the data without delay are read and for cylinder 2 the 180 °CA time delayed data respectively. The advantage of this simulation method is the reduced calculation time taking into account all data for the boundary faces, such as velocity and species profiles, turbulence kinetic energy and dissipation etc. The disadvantage is that the exhaust system is still uncoupled with the cylinders 1 and 2, so that a change of the condition inside the exhaust system is not taken into account for the cylinder calculation. Explicitly, it is assumed that during the isolated exhaust system simulation a cyclic steady condition remains inside the cylinders. The boundary condition is written in the C programming language as a user defined function (UDF) and can dynamically be loaded with the Fluent solver. The source code containing UDFs is directly compiled in Fluent and uses additional macros and functions. A detail description about the UDFs can be found in Ansys [13] and [14].

SIMULATION SETTINGS

For the simulation, the pressure-based solver with an implicit formulation for unsteady flow is used. For the coupling of pressure and velocity the PISO scheme has been chosen, as recommended for transient flow calculations, see Ansys [13]. The variation of density is calculated with the Ideal Gas law ($p=\rho RT$). The standard k- ε turbulence model was used to model the influence of turbulence. The standard values for the parameters of turbulent kinetic energy k and the dissipation rate ε models were taken from Ansys [13]. Further, the standard wall function for the near wall modeling of the turbulent boundary layer was selected.

The spray model (discrete phase model, further DPM) was calibrated with experimental data from the injector test bench. These measurements included timing of the spray, spray angle and penetration of the injected fuel. Due to a high We-number and the simulation of a warm engine, the "wall-jet" model was chosen for the droplet-wall interaction simulation presented in this study. Details about the injector calibration and the used models can be found in previous investigations: [11], [16], as well as in Ansys [13].

In order to get fast simulation results, the minimum number of transported species and reactions was used. The applied finite-rate model is an approach based on the solution of transport equations for species mass fractions. The reaction rate that appears as a source term is calculated using Arrhenius rate expressions. The influence of the turbulent

flow and the interaction with the combustion is modeled using the eddy dissipation concept (EDC) proposed by Magnussen [13]. The kinetic chemical mechanism used in this study consists of only five main reactions, which was presented in a previous investigation [11]. Detailed kinetic chemical mechanisms demand a large number of species and therewith over hundred of reactions, which would cause a large increase of computational effort. Concurrently, the results of the simulation applying this mechanism offer an array of detailed information about the combustion. As the simulation of a 2-stroke engine has to cover several revolutions, the use of detailed mechanisms is impracticable and would consume too much of the computational resources.

In order to calculate the exhaust wall temperature the wall is modeled applying the Fluent "Thin-Wall" model with a wall thickness of 1 mm. Furthermore, the shell conduction model was used in order to compute heat conduction in the wall, in addition to the heat conduction across the wall, which is calculated when the energy equation is solved. For the heat transfer of the pipe to the surrounding environment the convective heat transfer boundary condition was set. For this boundary condition the external heat transfer coefficient and the free stream temperature was defined. A detailed description of the used thermal boundary condition can be found in Ansys [13].
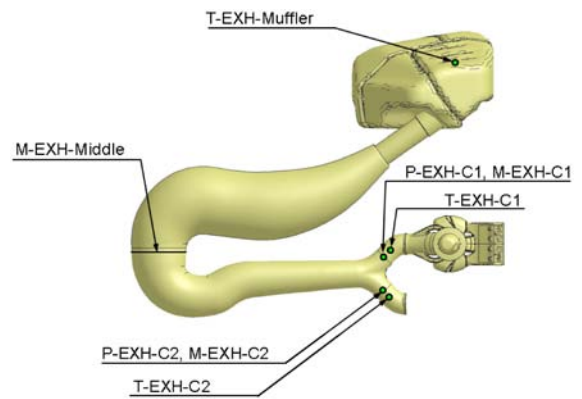
Figure 4. Measurement points in the exhaust system

Figure 4 shows the measurement points and faces inside the exhaust system used for the simulation validation. The indicated pressure values inside the exhaust system (P-EXH-C1, P-EXH-C2 and P-EXH-Cone) and the temperatures (T-EXH-C1, T-EXH-C2 and T-EXH-Muffler) are presented in this study together with the comparison to the simulation results.

SIMULATION OF THE SCAVENGING PROCESS

The first phase of the simulation strategy is a simulation of the scavenging process, without fuel injection and

combustion. Before the exhaust port opens, the volume of the cylinder is initialized every cycle with correct values of pressure, temperature, and the accordant composition of exhaust gases. This simulation is run for about 5 cycles until a cyclic steady condition inside the engine is achieved. This is the case when the pressure trends inside the exhaust system, the crankcase volume, and the sucked air mass do not change for the last two cycles. In addition, the pressure trends must show a good agreement with the test bench data. Furthermore, the DPM and the combustion model are switched off in this simulation phase, in order to reduce the simulation duration. Furthermore, the simulation is carried out with only a one cylinder calculation applying the symmetry and time delayed boundary condition.

Figure 5, Figure 6, and Figure 7 show a comparison of the pressure trends of the test bench at 7900 rpm WOT and the simulation results inside the exhaust pipe for three different measurement points, P-EXH-C1, P-EXH-C2, and P-EXH-Cone. The presented simulation results show a good prediction of the pressure trend inside the exhaust system in the case of the scavenging process simulation without combustion process.
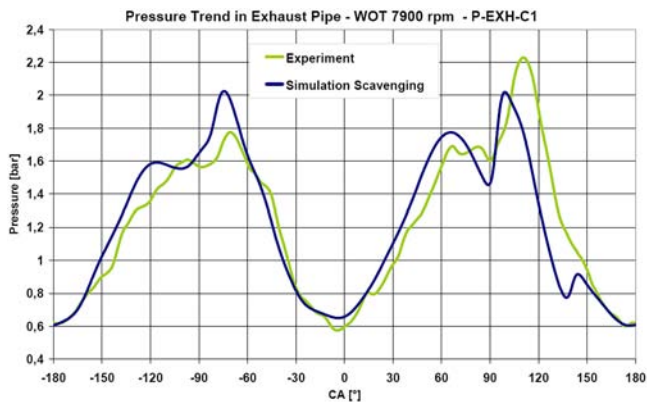
Figure 5. Pressure trend exhaust pipe, P-EXH-C1
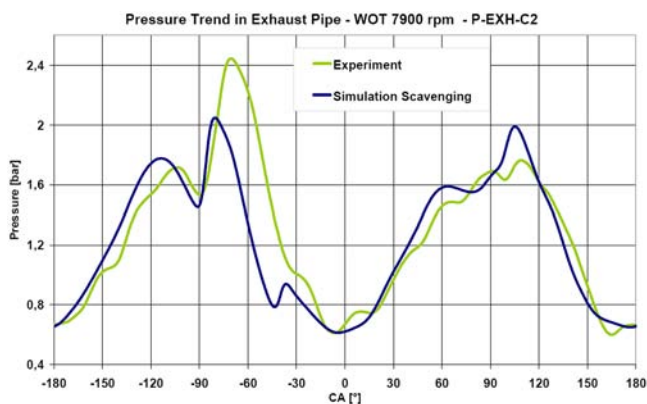
Figure 6. Pressure trend exhaust pipe, P-EXH-C2
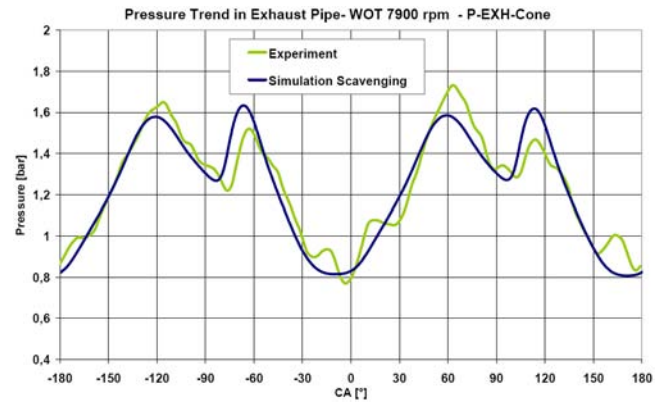
Figure 7. Pressure trend exhaust pipe, P-EXH-Cone

SIMULATION WITH FUEL INJECTION AND COMBUSTION PROCESS

After the gas dynamic simulation the calculation of fuel injection and combustion process can be started. This means that the first simulation is only carried out in order to get a good start condition inside the engine for this next simulation step. This simulation is run for the next four revolutions including fuel injection and the combustion process. Figure 8 shows the fuel distribution in different regions of the engine. The green curve shows the fuel mass in cylinder 1 over the crank angle, for four revolutions and four fuel injections respectively. The red curve represents the fuel mass inside the exhaust pipe and the blue curve the total mass of the injected fuel inside the calculation domain. The fuel mass inside the cylinder shows an almost periodical steady behavior without big changes. This confirms the correctness of the simulation strategy, e.g. the initialization of the cylinder volume with the corresponding condition values short before exhaust pipe opening leads to a fast convergence of the simulation. Concerning the second simulation phase, Figure 8 shows that already the first cycle results in the same fuel distribution inside the engine as the following do. This means that for an evaluation of different injection strategies in a development process already the first injection can be used for a suitable estimation of the fuel trapping efficiency (the fuel concentration inside the cylinder volume after exhaust port closure). The red curve presents the fuel mass inside the exhaust system and shows an increasing fuel concentration from cycle to cycle caused by the scavenging losses. Therefore, the fuel concentration (blue curve) inside the complete domain increases as well.
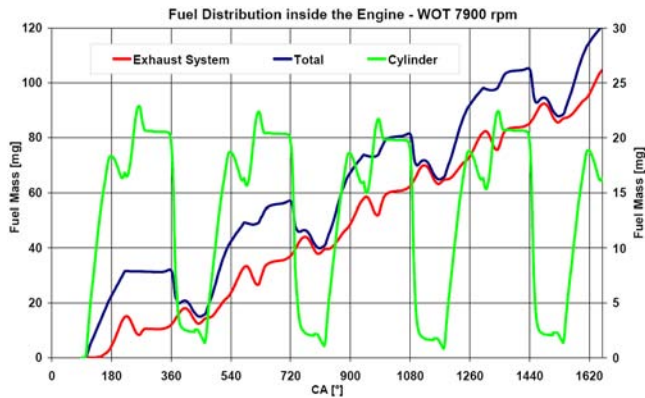
*Figure 8. Fuel distribution inside the engine*
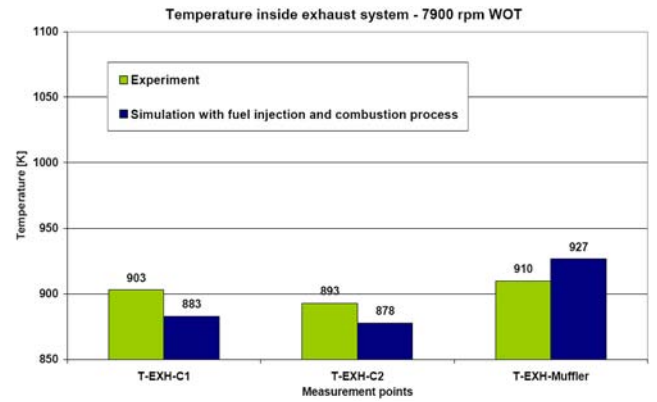
Figure 10. Temperature inside the exhaust system

In order to determine the convergence of the inlet condition inside the exhaust system, the fuel mass flow on the faces M-EXH-C1 and M-EXH-C2 is evaluated, (see Figure 9). It is clearly visible that after only four revolutions the scavenging losses and therewith the fuel mass flow achieve a cyclic steady condition. Furthermore, it can also be seen that on the measurement plane M-EXH-Middle the fuel mass does not change until the fourth revolution. On the plane M-EXH-Out (face at the end of the exhaust system) the value still remains zero. Anyway, in order to replace the cylinder domain with the symmetry and time delayed boundary condition a cyclic steady condition is only required for the measurement faces M-EXH-C1 and M-EXH-C2. Figure 10 shows a comparison of the mass flow averaged temperature inside the exhaust system to the measurement data. In the measurement points T-EXH-C1 and T-EXH-C2 a lower temperature was predicted in the simulation by 20 K and 15 K respectively. In the measurement point T-EXH-Muffler, the simulation temperature was 17 K higher than in the experiment.

Figure 11, Figure 12, and Figure 13 show a comparison of the pressure trends of the experiment and the simulation results inside the exhaust pipe, without and with fuel injection and combustion process (1st and 2nd simulation phase) for three different measurement points, P-EXH-C1, P-EXH-C2, and P-EXH-Cone. The presented simulation results show a good prediction of the pressure trend inside the exhaust system and a very small deviation between the two simulation results, representing the two simulation phases.
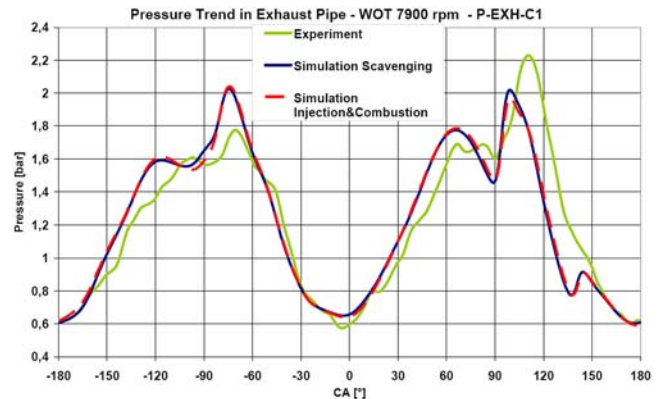
Figure 11. Pressure trend exhaust pipe, P-EXH-C1

Figure 9. Fuel mass flow in the exhaust system
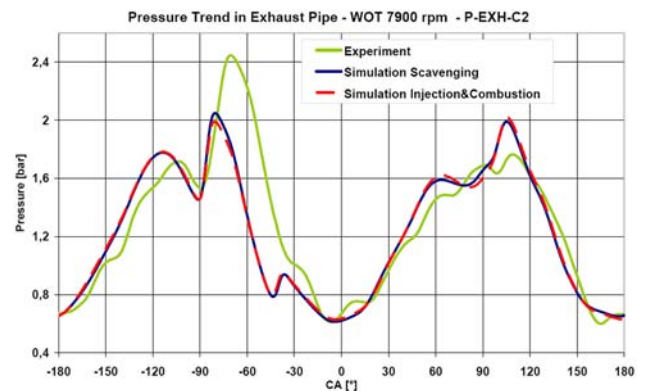
Figure 12. Pressure trend exhaust pipe, P-EXH-C2
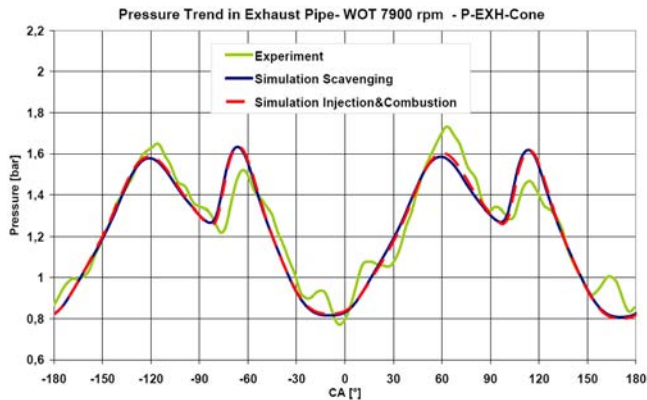
Figure 13. Pressure trend exhaust pipe, P-EXH-Cone

EXHAUST SYSTEM SIMULATION

The third phase of the applied simulation strategy concerns the isolated exhaust system. This means that the first two simulation phases are only carried out in order to get a good inlet condition for the exhaust system. In this case the required data for both exhaust pipe inlets are read from the external output data file. In order to be able to achieve a good depiction of the temperature distribution in the metal exhaust wall and simultaneously to be able to reduce the number of calculated cycles, the specific heat of the metal was changed stepwise from a reduced value of the specific heat capacity (cp/1000) to the correct value of cp. This means that a reduced specific heat capacity results in longer time steps for the simulation of the heating-up of the metal, compared to the time step of the fluid flow simulation. Nevertheless, this strategy significantly accelerates the exhaust wall heating-up and reduces the number of calculated cycles for a steady exhaust wall temperature calculation. The exhaust system was divided into four faces and cell zones, which are presented in Figure 14. On the face zones the area averaged temperature and in the cell zones the volume averaged fuel net reaction rate were evaluated in order to determine a steady condition. However, about 28 revolutions were calculated to make sure that the heat transfer and the reactions are stabilized. Furthermore, a simulation without species reactions was also carried out in order to determine the exhaust wall temperature in this case.
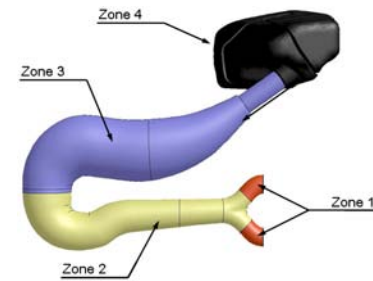
Figure 14. Exhaust system zones
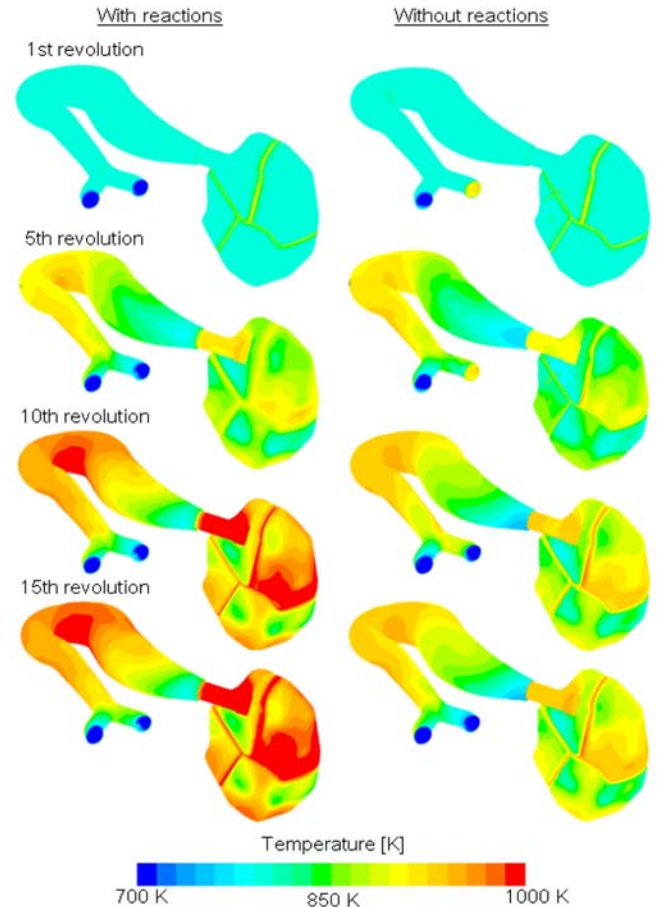
Figure 15. Exhaust wall temperature

Figure 15 shows the exhaust wall temperature from the start of the isolated exhaust system simulation until the 15th revolution and a comparison between the simulations with and without reactions inside the exhaust system. In both cases the metal exhaust wall was initialized at the start of the simulation with a constant temperature of 800 K. Already after 5 calculated revolutions an essential difference of the wall temperature is visible - in both cases with similar temperature contours. In the 10th revolution the influence of the post-combustion process with an increase of the wall temperature can already be seen. In both cases the simulations achieve a steady condition already at the 15th revolution; after that the changes of the wall temperature are

hardly visible. On the test bench, the exhaust wall superheating can take 20-30 seconds or longer. Due to a modification of the metal specific heat the exhaust wall heating in the simulation is significantly accelerated and thus makes the exhaust system simulation applicable in the development process of a new engine.

Figure 16 shows the fuel concentration inside the exhaust system for the simulation of the isolated exhaust system taking into account the post-combustion process. In the first 10 revolutions an increase of the fuel concentration can be seen. Taking into account the first 4 revolutions of the simulation with fuel injection and combustion process simulation (2nd simulation phase) and the 10 revolutions of the isolated exhaust system, it can be determined that the fuel mass is not completely transported through the exhaust system until the 15th revolution. After that a decrease of the fuel concentration is visible and after approximately the 17th revolution the fuel concentration achieves a steady condition.
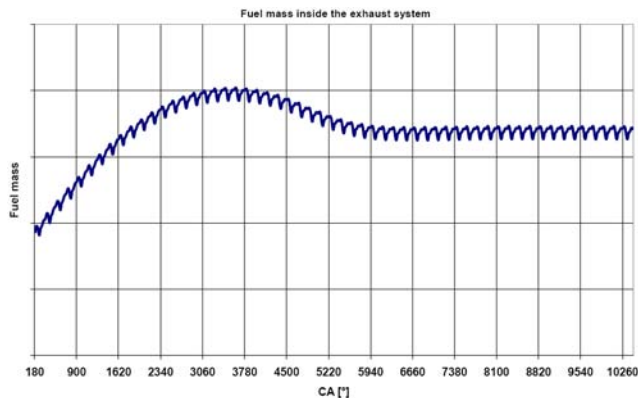
Figure 16. Fuel mass inside the exhaust system

A decrease of the fuel concentration inside the exhaust system between the 14th and the 15th revolution, presented in Figure 16, can be explained by an analysis of the fuel net reaction rate inside the exhaust system, see Figure 17. In the first 14 revolutions an increase in the reaction of the fuel can be seen. This effect is directly coupled with the increase of the exhaust wall temperature. An increase of the exhaust wall temperature leads to a reduction of the heat transfer of the exhaust gas over the exhaust wall and simultaneously to an increase of the fluid temperature. Further, the high fluid temperature accelerates the fuel reaction rate inside the exhaust system and causes once again an additional increase of the fluid temperature. However, after approximately the 17th revolution the heat transfer and the reactions are stabilized. As mentioned before, this superheating effect takes 20-30 seconds or longer with test bench configurations; whereas in simulation it is significantly accelerated due to modifications of the metal specific heat. A reduced specific heat increases the time step for the heating-up of the metal while maintaining the time step of the fluid flow simulation.
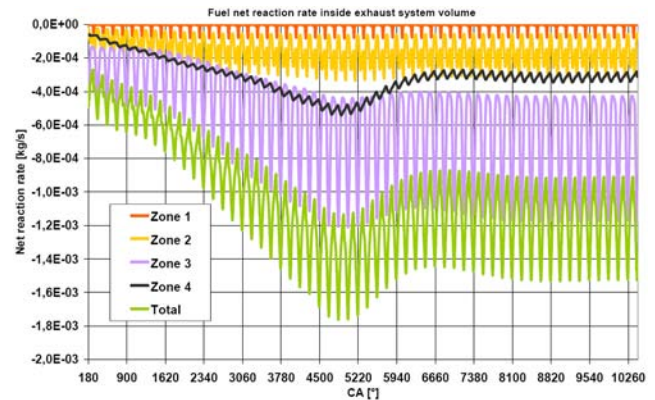

Figure 17. Fuel net reaction rate

The post-combustion process is different depending on the position in the exhaust system volume, see Figure 17 and Figure 18. It is clearly visible that about 57.4 % of the fuel reaction occurs in "Zone 3", 26.8 % in "Zone 4", 15 % in "Zone 2", and only less than 1 % in "Zone 1". These data were evaluated in a region with stabilized heat transfer and reactions (between the 22nd and the 28th revolution).
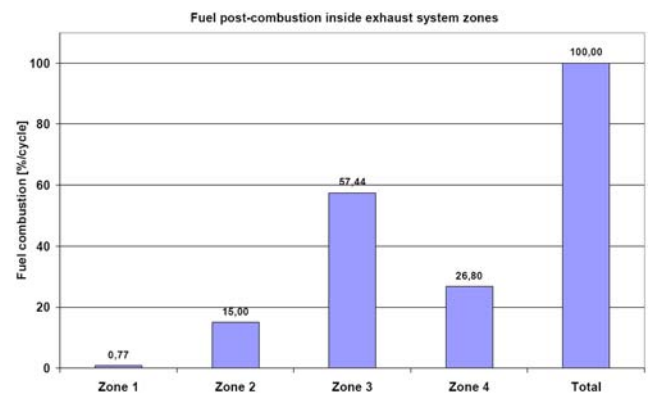

Figure 18. Fuel combustion inside exhaust system

Figure 19 shows a comparison of the mass flow averaged temperature inside the exhaust system for different simulation steps and the measurement data. It is clearly visible that the simulation with the isolated exhaust system, considering the post-combustion process, causes a temperature increase especially in the measurement point T-EXH-Muffler. This effect is caused by the post-combustion process inside the exhaust system itself. In the comparison with the measurement data, the simulation without the post-combustion process simulation shows a prediction of the exhaust temperature in an acceptable range. This can be explained by the fact that the test bench results also stem from a measurement without an exhaust system superheating. Actually, a superheating caused by a post-combustion process can occur leading immediately to exhaust system damage. The CFD-results show that the exhaust system superheating is caused by the post-combustion process inside the exhaust

system and in this case, the maximum fuel net reaction rate is situated in the exhaust system region "Zone 3" (see Figure 14, Figure 17, and Figure 18).
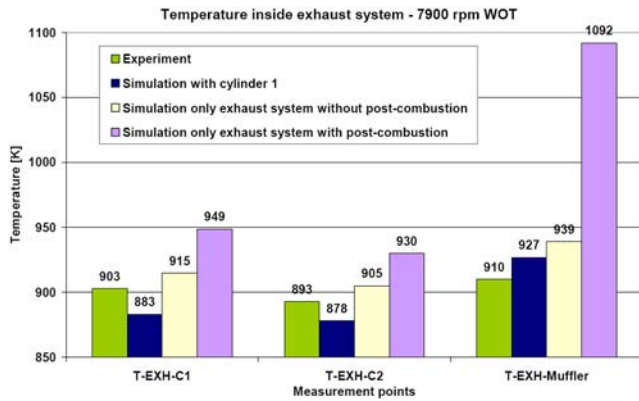

Figure 19. Temperature inside the exhaust system

SIMULATION WITH THE IMPROVED EXHAUST WALL TEMPERATURE

In order to investigate the influence of the exhaust wall temperature including the post-combustion process on the engine performance, the simulation with the new exhaust condition and wall temperature was carried out. The exhaust wall temperature was implemented as a profile. Furthermore, the 3D data from the isolated exhaust system simulation were mapped into the exhaust domain. With this method the new exhaust system condition is taken into account for the simulation with injection and combustion process, i.e. the last simulation phase.

Figure 20, Figure 21, and Figure 22 show a comparison of the pressure trends of the test bench and the simulation results inside the exhaust pipe for three different measurement points, P-EXH-C1, P-EXH-C2, and P-EXH-Cone. In all cases the simulation results "Simulation Injection & Combustion - New Exhaust Condition" show a difference in the timing of the pressure wave of about 10 °CA in the region between 0 and 60 °CA (pressure wave of cylinder 1, see Figure 20 and Figure 22) and in the region between −180 and −120 °CA (pressure wave of cylinder 2, see Figure 21 and Figure 22). This difference can be explained by the fact that a high fluid temperature - caused by the post-combustion process inside the exhaust system - changes the speed of sound and therewith the timing of the pressure wave as well.
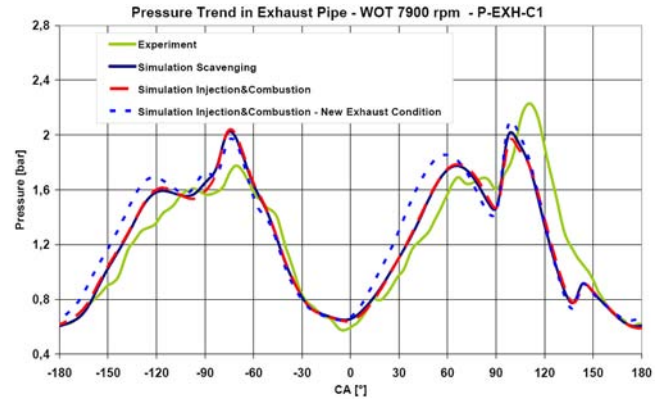
*Figure 20. Pressure trend exhaust pipe, P-EXH-C1*
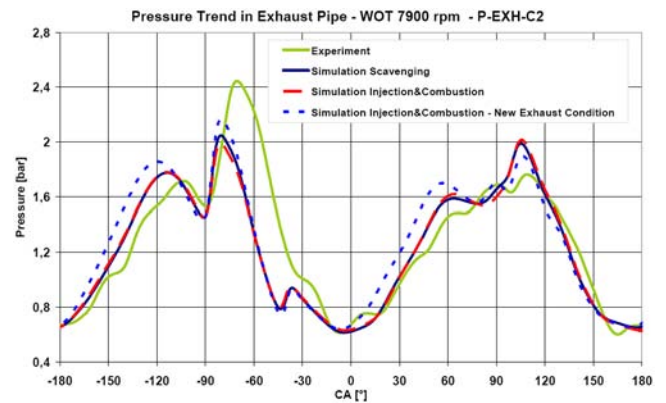
*Figure 21. Pressure trend exhaust pipe, P-EXH-C2*
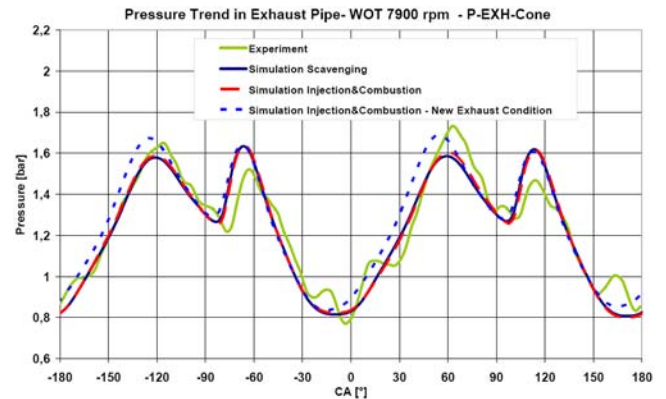
Figure 22. Pressure trend exhaust pipe, P-EXH-Cone

The influence of the changed pressure wave timing on the situation inside the cylinder volume is visible in Figure 23. In the region between −150 and −80 °CA a higher pressure level in the simulation with new exhaust condition can be seen. Furthermore, at −150 °CA it is visible that all ports are simultaneously opened (intake and exhaust ports). A higher pressure level before the intake ports close (further, IC close) causes a fluid motion from the cylinder to the crankcase volume. The fluid mass inside the crankcase volume is

increased as well as the pressure level. In the next revolution, the sucked fresh air mass will be automatically reduced, due to a self controlled reed valve system. In this study, the reed valve strategy proposed by Schmidt et al. [17] was used for the control of the sucked fresh air mass. The basic idea is to change the mass flow rate during the simulation depending on the pressure difference between the crank case volume and the section upstream the reed valve. This leads to a quasi self-control of the sucked air mass in the simulation. However, a self controlled sucking air mass model was implemented via UDFs. The simulation results with the new exhaust system condition show that a changed timing of the pressure wave of above 10 °CA causes a reduction of the sucked fresh air mass by about 11%. This reduced air mass will be directly reflected on the engine performances, e.g. loss of power. On the test bench, a superheating of the exhaust system also causes a loss of engine power and CFD simulation clearly shows the reason for this effect.
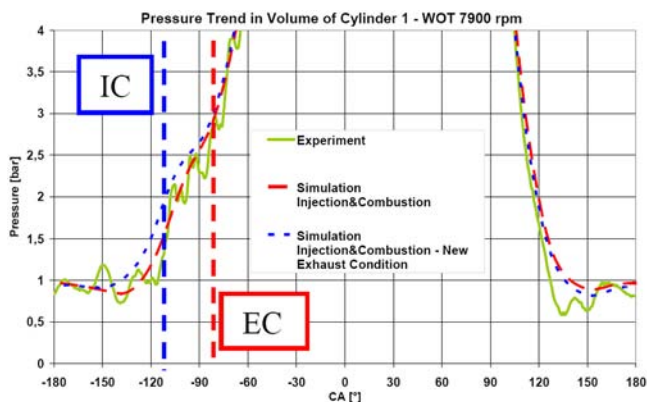
Figure 23. Pressure trend in volume of cylinder 1

CONCLUSION

This paper covers the discussion of a simulation methodology for the exhaust system of a 2-cylinder 2-stroke engine until steady condition considering the heat transfer over the exhaust pipe wall and the post-combustion effect inside the exhaust system. Starting with a complete engine simulation, including scavenging process, fuel injection, mixture preparation and combustion process simulation, the simulation with an isolated exhaust system was carried out. After that, the temperature profile and the new exhaust condition were taken for the complete engine simulation and the influence on the gas dynamic behavior and the engine performance was investigated. The advantage of the presented strategy is that the cylinder volumes are replaced by the symmetry and time delayed boundary condition introduced by Jajcevic et al. [10]. This new type of boundary condition allows an efficient simulation of the engine by the calculation of only one cylinder without data losses and simultaneously accounting for the effect of both cylinders. This simulation strategy also allows an isolated exhaust

system simulation in a short calculation time. Test bench results of the fired engine were used for the validation of the gas dynamic behavior and the temperature simulation inside the exhaust system. The simulation results presented in this study show a good prediction of the pressure trend inside the exhaust system in comparison with measurement data. The CFD-results also show that the exhaust system superheating is caused by the post-combustion process inside the exhaust system. An increase of the fluid and wall temperature, caused by the post-combustion process, changes the speed of sound and therewith the timing of the pressure wave as well. CFD simulation shows that these changes inside the exhaust system further lead to a reduction of the sucked fresh air mass by about 11%, which is directly reflected in the engine performance.

REFERENCES

1. Caton, J. A. and Heywood, J. B., "An experimental and analytical study of heat transfer in an engine exhaust port", International Journal Heat Mass Transfer, 1981

2. Konstantinidis, P. A., Koltsakis, G. C., Stamatelos, A. M. "Transient heat transfer modelling in automotive exhaust systems", Journal of Mechanical Engineering Science, ISSN 0954-4062 (Print) 2041-2983 (Online), 1997

3. Kandylas, I. and Stamatelos, A.: "Berechnung des Wärmeübergangs in Motorabgassystemen", MTZ Motortechnische Zeitschrift 59, 1998

4. Zhang, Y., Phaneuf, K., Hanson, R., and Showalter, N., "Computer Modeling on Exhaust System Heat Transfer," SAE Technical Paper 920262, 1992, doi:10.4271/920262.

5. Chen, D.K.S., "A Numerical Model for Thermal Problems in Exhaust Systems," SAE Technical Paper 931070, 1993, doi:10.4271/931070.

6. Rothbauer, R.J., Margelik, R.H., Aslam, M.M., Almbauer, R.A. et al., "Predictive Simulation Strategies for the 2-Stroke Scavenging Process within the Scope of the Development Process," SAE Technical Paper 2005-32-0099, 2005, doi: 10.4271/2005-32-0099.

7. Eichlseder, H, Schmidt, S. P., Rothbauer, R. J., "Entwicklungsmethodiken bei der Konzeptentwicklung neuartiger Brennverfahren", Internationales Symposium für Entwicklungsmethodik, S. 142-163, 2005

8. Schmidt, S., Winkler, F., Schoegl, O., and Pontoppidan, M., "Development of a Combustion Process for a High Performance 2-Stroke Engine with High Pressure Direct Injection," SAE Technical Paper 2004-01-2942, 2004, doi: 10.4271/2004-01-2942.

9. Rothbauer, R. J., Almbauer, R. A., Schmidt, S. P., Glinsner, K., "Effect of Energy Conversion, Turbulence and Fluid Dynamics on the Transient Heat Transfer and thus on the Scavenging of the Two Stroke Engine", Turbulence, Heat and Mass Transfer 5, Dubrovnik, 2006

10. Jajcevic, D., Almbauer, R.A., Schmidt, S.P., and Glinsner, K., "Symmetry and Time Delayed Boundary Condition for CFD Simulation and its Application in a Two-Cylinder Two-Stroke Engine," SAE Technical Paper 2009-32-0024, 2009, doi:10.4271/2009-32-0024.

11. Jajcevic, D., Almbauer, R.A., Schmidt, S.P., and Glinsner, K., "Simulation of Scavenging Process, Internal Mixture Preparation, and Combustion of a Gasoline Direct Injection Two-Cylinder Two-Stroke Engine," SAE Technical Paper 2009-32-0046, 2009, doi:10.4271/2009-32-0046.

12. Zeng, Y., Strauss, S., Lucier, P., and Craft, T., "Predicting and Optimizing Two-Stroke Engine Performance Using Multidimensional CFD," SAE Technical Paper 2004-32-0039, 2004, doi:10.4271/2004-32-0039.

13. ANSYS Fluent: "Fluent 6.3 User's Guide" Fluent Inc, 2005

14. ANSYS Fluent: "UDF Manual" Fluent Inc, 2005

15. Magnussen, B. F., "On the structure of turbulence and a generalized eddy dissipation concept for chemical reaction in turbulent flow", Aerospace Science Meeting, 1981

16. Jajcevic, D., Almbauer, R.A., Schmidt, S. P., Glinser, K., "Simulation Strategy and Analysis of a Two-Cylinder Two Stroke Engine Using CFD Code Fluent", European Automotive Simulation Conference (EASC), 2009

17. Schmidt, S., Schoegl, O., Rothbauer, R.J., Eichlseder, H. et al., "An Integrated 3D CFD Simulation Methodology for the Optimization of the Mixture Preparation of 2-Stroke DI Engines," SAE Technical Paper 2007-32-0029, 2007, doi: 10.4271/2007-32-0029.

CONTACT INFORMATION

Dipl.-Ing. Dalibor Jajcevic
Christian Doppler Laboratory for "Thermodynamics of Reciprocating Engines"
Graz University of Technology
Inffeldgasse 25C
8010 Graz-Austria
Phone: +43 316 873 4586
FAX: +43 316 873 8080
jajcevic@ivt.tugraz.at
www.tugraz.at

ACKNOWLEDGMENTS

DEFINITIONS/ABBREVIATIONS

1D
one-dimensional

3D
three-dimensional, three dimensions

CA
crank angle

CFD
computational fluid dynamics

cp
specific heat capacity

DPM
discrete phase model

EXH
exhaust

EC
exhaust close

EDC
eddy dissipation concept

IC
intake close

GDI
gasoline direct injection

M-EXH-C1
mass flow exhaust pipe cylinder 1 face

M-EXH-C2
mass flow exhaust pipe cylinder 2 face

M-EXH-Middle
mass flow exhaust pipe middle face

M-EXH-Out
mass flow exhaust pipe outlet face

P-EXH-C1

pressure trend exhaust pipe cylinder 1

P-EXH-C2

pressure trend exhaust pipe cylinder 2

P-EXH-Cone

pressure trend exhaust pipe cone

RAVE

Rotax Adjustable Variable Exhaust

rpm

revolutions per minute

T-EXH-C1

temperature exhaust pipe cylinder 1

T-EXH-C2

temperature exhaust pipe cylinder 2

T-EXH-Cone

temperature exhaust pipe cone

UDF

user defined function

We

Weber number

WOT

wide open throttle

SAE International

7 Reed valve simulation

Due to a very simple working principle the reed valve is widely used for the control of fresh charge into the crankcase of a 2-stroke engine. The simplest way to replace a reed valve system in a 3D CFD simulation is a mass flow profile from a previous 1D calculation. The disadvantage of this method is that the boundary conditions are cyclic constant and the exchange and the transfer of information between 3D domain and the region upstream the reed valve is missing. To overcome this disadvantage an adaptive boundary condition can be applied. The basic idea is to change the mass flow during the simulation depending on the pressure difference between the crank case and the section upstream the reed valve. This leads to a quasi self-control of the sucked mass and solves the above-mentioned problem. Probably the simplest way is the method proposed by Schmidt et al. [108]. The aim is that the mass flow is calculated in dependence of the pressure difference applying the following mass flow equation:

$$\dot{m} = c_{area} \cdot A_{flow} \cdot \rho_{out} \cdot \sqrt{\frac{2 \cdot p_{out}}{\rho_{out}} \cdot \sqrt{\left(\frac{\gamma}{\gamma - 1} \left[\left(\frac{p_{in}}{p_{out}} \right)^{\frac{2}{\gamma}} - \left(\frac{p_{in}}{p_{out}} \right)^{\frac{\gamma+1}{\gamma}} \right] \right)}} \qquad (7.1)$$

Where, c_{area} is a correction factor, A_{flow} is the flow area, ρ_{out} is the density outside, p_{in} is the pressure in the crank case, p_{out} is the pressure outside, and γ is the ratio of specific heat. The correction factor c_{area} is the ratio between the actual flow area and the theoretical flow area and can be obtained as follows:

$$c_{area} = \frac{A_{flow}}{A_{theo}} = \frac{h_{valvelift(\Delta p)} \cdot b_{width} \cdot c_{sideflow}}{A_{theo}} \qquad (7.2)$$

Where A_{theo} is the theoretical flow area, $h_{valvelift(\Delta p)}$ is the height of the valve lift in dependence on the pressure difference obtained from the test bench data (see Schmidt et al. [108]), b_{width} is th e width of the valve, and $c_{sideflow}$ is the side flow coefficient. The disadvantages of this method are the missing of the reed valve dynamics and that the height of the valve lift must be obtained experimentally. In order to avoid these disadvantages, the reed valve lift can be obtained in dependence on the pressure difference applying a mass-spring system introduced by Costagiola [109] or a 2D approach based on the beam theory proposed by Hinds and Blair [110] as well as a finite element approach based on beam elements proposed by Baudille and Biancolini [111]. Applying one of these approaches, the valve lift can be calculated in dependency on the pressure difference between the crankcase volume and the region upstream the reed valve. Nevertheless, a disadvantage is still remaining, the gas dynamic behaviour inside the intake duct is not considered. A constant outside pressure is defined, so that the sucked air mass rate must be provided from test bench measurements or a 1D simulation to be able to validate the simulation. In order to avoid the measurement, a calculation of the gas dynamics inside the intake duct, including the throttle and the air-box as well as the domain of the second cylinder, is needed. This can be realized by the application of either a multidimen-

sional simulation technique or of a complete 3D reed valve simulation including the complete engine geometry.

Figure 28 shows an application of the multidimensional simulation technique, where the complete intake duct as well as the second cylinder is calculated with the 1D code. In this simulation the gas dynamic behavior inside the inlet duct and the reed valve lift are obtained with a 0D/1D code. The data exchange between the 3D and the 1D domain can be realized with the described 1D-3D coupling methodology (see chapter 4.2). This simulation technique is already state-of-the-art and can for instance be realized by applying the commercial codes AVL Fire and Boost [104].
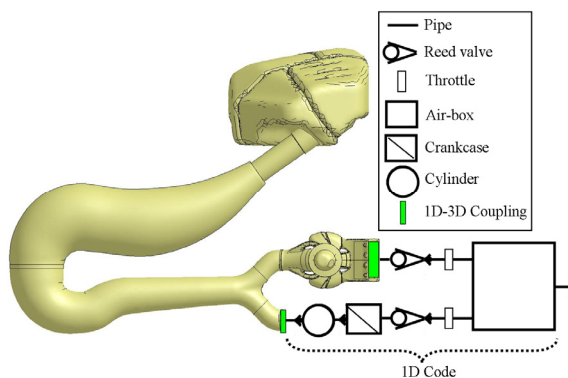
Figure 28: Application of the multidimensional simulation technique in a 2-cylinder 2-stroke engine
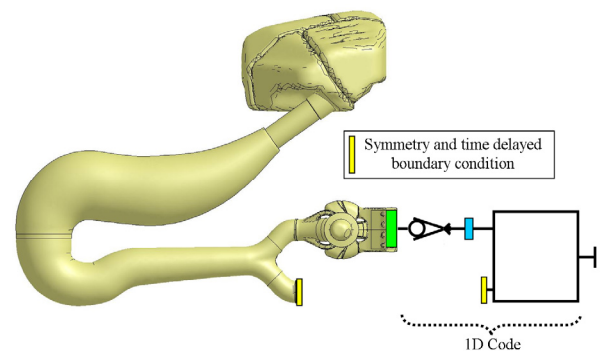
Figure 29: Application of the symmetry and time delayed boundary condition in combination with multidimensional simulation

The drawback of the simulation technique presented in Figure 28 is that the second cylinder must be modeled in order to get an accurate simulation of the gas dynamics upstream the reed valve of cylinder 1 as well as inside the exhaust system. Nevertheless, the information of the second cylinder is not needed. A possibility to reduce the computational effort is to replace the second cylinder completely by applying the symmetry and time delayed boundary condition introduced in chapters 5 and 6, see Figure 29. For the exhaust side of the second cylinder the 3D data from the exhaust manifold of cylinder 1 are used and for the intake side the data from the 1D code respectively.

Finally, the last method for the reed valve calculation, where the gas dynamics inside the intake duct is included, is a 3D reed valve simulation taking into account the complete 3D engine geometry, i.e. cylinder, crankcase, reed valve, intake duct, air-box and exhaust system. As the simulation of only one cylinder causes an incorrect gas dynamic behavior in the above mentioned domains and further leads to unrealistic results, the influence of both cylinders has to be taken into account. In order to reduce the calculation time, the second cylinder can also be replaced in this case by the symmetry and time delayed boundary condition. In this simulation additional problems appear, such as the need of a moving mesh strategy, opening and closing technique of reed valve etc. A detailed description of the used reed valve simulation strategy, where the complete 3D engine geometry and an application of the symmetry and time delayed boundary condition is included, is presented and discussed in the enclosed paper.

7.1   Paper V

Reed valve CFD simulation of a 2-stroke engine using a 2D model including the complete engine geometry

SAE *International*®

Included in:

SAE International™

Reed Valve CFD Simulation of a 2-Stroke Engine Using a 2D Model Including the Complete Engine Geometry

2010-32-0015
20109015
Published
09/28/2010

Dalibor Jajcevic, Raimund Almbauer and Stephan Schmidt
Graz University of Technology

Karl Glinsner and Matthias Fitl
BRP-Powertrain GmbH & Co KG

ABSTRACT

CFD has been widely used to predict the flow behavior inside 2-stroke engines over the past twenty years. Usually a mass flow profile or a simple 0D model is used for the inlet boundary condition, which replaces the complete intake geometry, such as reed valve, throttle, and air box geometries. For a CFD simulation which takes into account the exact reed valve geometry, a simulation of all above mentioned domains is required, as these domains are coupled together and thus interact. As the high speed of the engine affects the opening dynamic and closure of the reed valve, the transient data from the crank case volume and the section upstream the reed valve have an important influence on the reed petal dynamic and therewith on the sucked fresh air mass of the engine.

This paper covers a methodology for the transient CFD simulation of the reed petals of a 2-stroke engine by using a 2D model. It is a mathematical model, which describes the displacement and the dynamic behavior of a reed petal, applying a Fluid-Structure Interaction (FSI). This bending beam model of the petal is coupled with the commercial CFD Code Fluent via a user defined function. The used coupling and the mesh moving strategy is presented and discussed in detail. The 3D engine domain includes the complete engine geometry. The main focus lies on the requirements of a reed valve simulation for a 2-cylinder 2-stroke engine. Finally, test bench results of the fired engine were used for the validation of the gas dynamic behavior inside the engine.

INTRODUCTION

Due to a very simple working principle the reed valve is widely used for the control of fresh charge into the crankcase of a 2-stroke engine. Usually a variable mass flow profile or a simple 0D model is used for the inlet boundary condition of a CFD simulation of a 2-stroke engine. This boundary condition replaces the complete intake geometry, such as reed valve, throttle, and air box. For a CFD simulation with exact reed valve geometry also including the reed valve dynamic simulation, a simulation of all above mentioned domains is required, as these domains are coupled together and thus interact. This means that for the efficient simulation the transient data upstream the reed valve have an important influence on the reed petal dynamic and therewith on the engine performance. Figure 1 shows a typical configuration of the reed valve system with eight petals, investigated in this study.
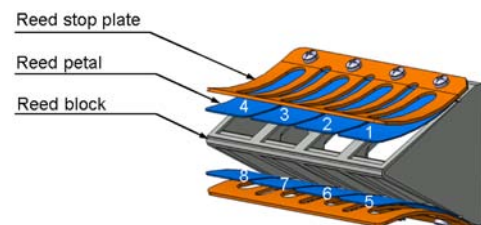
*Figure 1. Reed valve system of a 2-stroke engine*

Numerous investigations modeled the reed petals using different techniques in the last years. In some of them, a 1D approach based on the mass-spring system was used, other methods were based on the 2D approach using the beam theory, and in others the reed petals were modeled as a plate. Earlier studies proposed by Hinds and Blair [1] and Blair et al. [2] show a 2 dimensional model based on the beam theory. The motion of the reed petal is modeled as a cantilever beam with displacement at any point along the beam length equal to the superposition of the first three modes of free vibration. A testing procedure was developed for the validation of this approach permitting to record the petal lift displacements with a high speed camera. Presented results showed good correlation with measurements. Blair et al. [2] expanded the earlier study to provide further investigation of the used model taking into account different petal materials. Further, this model was improved by Fleck et al. [3] and [4], considering the variable petal width. Furthermore, the authors developed a technique to measure the reed valve lift on a fired engine. These measurements were obtained for a range of speeds and reed types and the results showed a good correlation with the calculated reed lift. Mitianiec and Bogusz [5] improved Blair's model and showed an application of this model with the reed petal as a plate. The authors were also interested in improving the load condition and therefore performed a 3D CFD simulation to determine the pressure profile on the petal surface. The steady improvement of the numerical methods together with the increase of computer power allows the simulation of increasingly complex technical problems and geometries. Therefore, some researchers applied 3D simulations in the last decade to investigate flow process through the reed valve where fluid and structural codes are coupled together. Cunningham et al. [6] and [7] used Blair's model for the reed petal movement. The employed 3D model consists of simplified reed valve geometry, the crankcase, and the intake ports. The rest of the engine geometry was replaced by a boundary condition stemming from a 1D simulation. Baudille and Biancolini [8] started the reed valve modeling using a finite element approach based on beam elements coupled with a 1D engine simulation. Thereafter, Baudille et al. [9] developed a 3D code based on the theory of bending beam taking into account the contact model. Therewith the influence of the stop plate was included in the simulation as well. Angeletti et al. [10] used Baudille's 3D model for the reed valve optimization with regard to the contact model - the used CFD model only includes the reed valve geometry and a small part of the intake ports. The rest of the engine geometry was replaced by boundary conditions.

In this paper Blair's model is used for the reed petal simulation, which is coupled with the CFD Code via a user defined function. In comparison to other models, the model does not need a large programming and computational effort, due to a small number of input- and exchange-data between the codes. The reed valve geometry was completely included in the simulation without design simplifications; the engine geometry also included exhaust system, cylinder, crankcase, intake duct, throttle, and air-box geometries. Applying the above described models, the gas dynamic simulation inside the intake duct was carried out. The investigated engine is a 2-cylinder 2-stroke engine, which requires the simulation of the complete geometry including cylinders, exhaust system, and complete intake duct system. As the simulation of only one cylinder causes an incorrect gas dynamic behavior in the above mentioned domains and further leads to unrealistic results, the influence of both cylinders has to be taken into account. In order to reduce the calculation time the second cylinder was replaced by a new symmetry and time delayed boundary condition proposed by Jajcevic et al. [11]. This new boundary condition allows an efficient simulation of only one cylinder engine without data losses and simultaneously taking into account the effect of both cylinders. In order to validate the applied reed valve model and the new boundary condition, the simulations were conducted for two different engine speeds (7900 rpm wide open throttle - WOT and 6800 rpm low load - LL). Test bench results of the fired engine were used for the validation of the gas dynamic behavior simulation inside the engine.

2-STROKE ENGINE

The experimental engine is a 2-cylinder 2-stroke engine from the BRP-Powertrain Company, applying loop scavenging via five intake ports. The displacement of each cylinder is approximately 300 cm^3. The engine can be also classified as a 2-stroke engine with reed valve controlled sucked air mass, crank case charge, Schnurle loop scavenging, variable exhaust port (RAVE - Rotax Adjustable Variable Exhaust), tuned exhaust pipe and high pressure gasoline direct injection (GDI). The intake ports are located symmetrically around the cylinder with the same opening time. The exhaust port consists of three ports, one main and two small lateral ports. In order to reduce the scavenging losses and to widen the speed range for effective exhaust tuning, the RAVE system controls exhaust port opening/closing time. Furthermore its use and position depends on the engine speed (low engine speed = RAVE system closed, high engine speed = RAVE system open). Due to a well-tuned exhaust system the reflected pressure wave reduces the scavenging losses. The engine has two separated intake ducts as well as two separate throttles. These intake ducts are further connected to an air-box volume (see Figure 2).
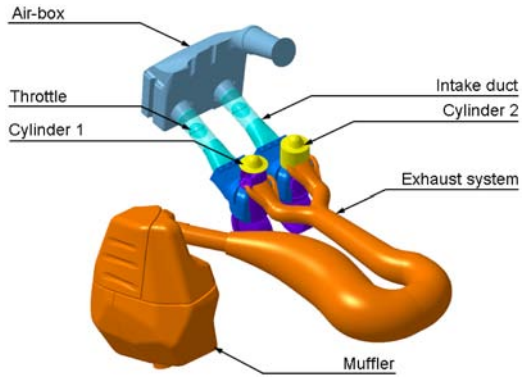
Figure 2. Flow geometry of the investigated engine

SIMULATION STRATEGY

As explained before, the investigation of a 2-cylinder 2-stroke engine requires the simulation of the complete geometry including cylinders, exhaust system, and the complete intake duct system. In this engine the cylinders are coupled together in a so-called "two-into-one" exhaust system. Furthermore, the intake and the exhaust ports are open simultaneously over a long period of the cycle and the gas dynamic behavior inside the exhaust port has a dominant influence on the scavenging process and on the mixture formation inside the cylinder. The simulation of only one cylinder causes an incorrect gas dynamic behavior inside the exhaust pipe and further leads to unrealistic results. For a simulation of the reed valve system the complete intake duct system simulation has to be considered, as the gas dynamic behavior inside the intake duct has an important influence on the reed valve behavior, so that for a correct simulation the transient behavior upstream the reed valve is needed.

However, in order to get reasonable results, the simulation of the complete and unaltered geometry is required. Another possibility is the replacement of the second cylinder by a corresponding boundary condition. In order to reduce the calculation time in this study, the second cylinder was replaced by the new symmetry and time delayed boundary condition proposed by Jajcevic et al. [11], taking into account the symmetry condition inside the engine.

This type of boundary condition can be used for time delayed as well as not time delayed technical problems. Figure 3 illustrates the application in a 2-cylinder 2-stroke engine simulation. In this case, cylinder 1 is completely calculated. For cylinder 2, the symmetric condition is used, so that it is replaced by the time delayed boundary condition. The boundary condition for the second cylinder is taken from the exhaust/intake cylinder 1 domain and for each cell respectively. This means, that for each cell in the exhaust/intake of cylinder 1 a symmetrically positioned cell in the domain of exhaust/intake cylinder 2 is found and marked. Simultaneously, all cell properties are read and saved in an

external output data file. Therewith, the correct boundary condition for each cell can be defined and the required flux can be calculated. For the flux calculation the time delayed data from the external data file are read for each cell respectively. In this work, the flux calculation occurs after the defined time delayed period. Explicitly, time delayed data are available and flux calculation is possible after this period. The advantage of this boundary condition is that the requested data are only provided by the simulation of cylinder 1. Neither a further variable profile, nor a 1D-model, nor measurement data for the replacement of the second cylinder are requested.
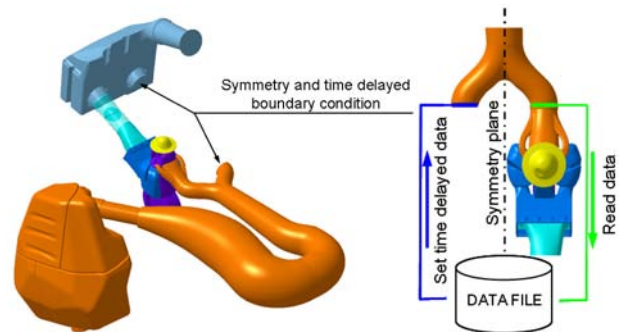
Figure 3. Application of the symmetry and time delayed boundary condition [11]

REED VALVE MODEL

The reed valve model code is written in the C programming language as a user defined function (UDF) and can dynamically be loaded with the Fluent solver. The source code containing the UDFs is directly compiled in Fluent and uses additional macros and functions that are supplied by Ansys [16]. Figure 4 presents the flowchart of the used model. The code consists of three main blocks - i.e. read data, reed valve model and transformation. The code is executed every time step by the Fluent solver. Using additional Fluent macros, the area averaged pressure on the upstream and downstream faces is read. After that the force is calculated from the pressure difference and the petal area. This force is further sent to the "Reed Valve Model" function. At the start of this function the new load condition is initialized and the beam lift position at time step n+1 can be calculated. The last step of the "Reed Valve Model" function is the calculation of the reed petal displacement along the reed length. The CFD code Ansys Fluent [12] uses a global Cartesian coordinate system for the flow calculation as well as a grid movement. In this work, a local coordinate system is used for the reed valve model (see Figure 5). Thus, an additional function for the coordinate transformation from local to the Cartesian coordinate system must be applied. Finally, the reed petal displacement can be submitted back to the Fluent solver and the node moving at time step n+1 can be evaluated.
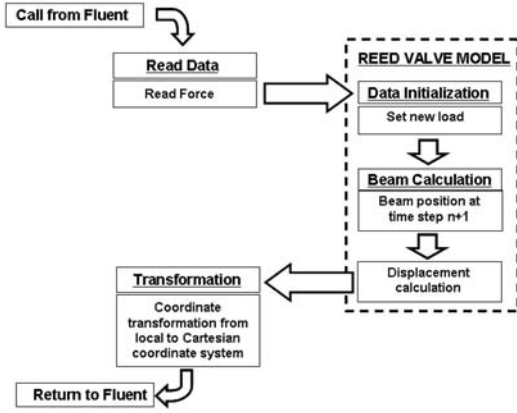
**Figure 4. Flow chart of the reed valve model**
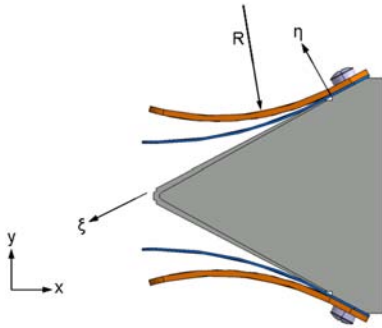
Figure 5. Local coordinate system for beam position calculation

In 1978 Hinds and Blair [1] published a 2D model based on the theory of transverse vibrations of a loaded beam. The authors deducted that the beam point motion can be described by following equation:

$$EI\frac{\partial^4\eta}{\partial\xi^4} + \rho A\frac{\partial^2\eta}{\partial t^2} = 0$$

(1)

where, E is the young modulus, I the moment of inertia, ρ the density, A the cross-sectional area, η the lift and ξ the position of calculated beam point. A solution of equation (1) has the following form:

$$\eta = \phi(\eta)\cdot e^{i\omega t}$$

(2)

with

$$\phi(\eta) = A\cos\lambda\eta + B\sin\lambda\eta + C\cosh\lambda\eta + D\sinh\lambda\eta$$

(3)

and

$$\lambda = \sqrt[4]{\frac{\rho A\omega^2}{EI}}$$

(4)

Considering the boundary condition for a cantilever beam, e.g. start and end point condition, following equation can be obtained:

$$1 + \cos\lambda l\cosh\lambda l = 0$$

(5)

Equation (5) is numerically solved and solutions of the first five roots of $\lambda_i l$ according to Hinds and Blair [1] are presented in Table 1.

Table 1. Solution of $\lambda_i l$ according to [1]

$\lambda_1 l$	$\lambda_2 l$	$\lambda_3 l$	$\lambda_4 l$	$\lambda_5 l$
1.875	4.694	7.555	10.996	14.137

The vibration frequency of each moving point is given by

$$f_i = \frac{\omega_i}{2\pi} = \frac{\lambda_i l}{2\pi}\sqrt{\frac{EI}{\rho A l^4}}$$

(6)

Applying the same transformation, equation (3) can be written:

$$\phi_i(\eta) = \cosh\lambda_i\eta - \cos\lambda_i\eta - $$
$$-\frac{\sinh\lambda_i l - \sin\lambda_i l}{\cosh\lambda_i l + \cos\lambda_i l}\left(\sinh\lambda_i\eta - \sin\lambda_i\eta\right)$$

(7)

The total displacement of each moving point is given by the following equations:

$$\eta(\xi,t) = \sum_{i=1}^{n}\phi_i(\eta)\cdot Z_i(t)$$

(8)

$Z_i(t)$ is obtained from:

$$\frac{d^2 Z_i}{dt^2} + 2\varsigma_i\omega_i\frac{dZ_i}{dt} + \omega_i^2 Z_i = \frac{F_i(t)}{m_i}$$

(9)

where ς_i is a damping factor, ω_i the vibration frequency, m_i the element mass, and F_i the force, which is dependant on the pressures upstream and downstream the reed petal and is set as a uniform forcing function. Fleck et al. [3] investigated various methods of calculating this forcing function and found that the best method was a simple uniform model, which considers that the pressure force is the same at any point on the reed petal. Equation (9) is solved by the four stage Runge-Kutta method according to Toro [14]. Zeng et al.

[15] used an alternative method, the first order accurate Euler-forward scheme, to solve this equation.

The movement of the reed petal is restricted - the petal maximum position is limited by the stop plate geometry and its minimum position by the reed block (see Figure 1). Therefore, the contact between the reed petal and the boundaries was taken into consideration. The main function of the stop plate is that it continuously reduces the free petal length during the opening phase. Therewith the elastic characteristic is automatically changed depending on the contact point position. E.g. Hinds and Blair [1] changed the effective free length by a contact between the reed petal and the stop plate. The new length is calculated from the distance between the contact point and the free reed end point. Fleck et al. [3] models this contact in a simple way by using the product of a coefficient of restitution and the time derivative of the principle coordinate in order to describe the rebound velocity of the reed from the reed stop. For the maximum petal position and a contact between the reed petal and the reed stop plate, it is assumed in this study that the reed lift at any point cannot be larger than the stop plate height. The reed stop plate geometry can be described with a circle function given by:

$$\eta_{max}(\xi) = \left| \sqrt{R^2 - (\xi - \xi_C)} - \eta_C \right|$$

(10)

where R is the radius of the stop plate curve and ξ_C and η_C the circle center position in the local coordinate system. With this function the stop plate is completely described along its length. If the reed lift is larger than the value of $\eta_{max}(\xi)$, the moving of all points in this region is stopped. In a next step, the max contact point position is found. For all beam points with a position smaller than the max contact point position the time derivative component of the principle coordinate is set to zero and the reed position is set to the position of the stop plate. For the beam points with a position larger than the max contact point position - the free length of the reed petal - the velocity component is multiplied by a coefficient c given by the following linear equation:

$$c = \frac{c_{max}}{N}(i - i_{max}), \quad i \geq i_{max}$$

(11)

where c_{max} is the max damping coefficient ($c_{max} = 0.7$ is used in this study), N the total number of the beam points, i the actual beam point and i_{max} the position of the max contact point.

The experimental verification of the simulation model is a necessary step to validate its correctness and is carried out with a Laser Doppler Vibrometer (further LDV). Nagy et al. [17] uses LDV for the valve lift measurement in hermetic piston compressors. An LDV instrument measures the velocity laser beam direction component of a moving reflective surface (see Figure 6). In the case of a moving surface - due to the Doppler Effect - the frequency of the reflected light compared to the source light is shifted. This frequency shift is evaluated by an interferometer and converted to a voltage signal. This signal is a function of the velocity of the moving surface. Finally, the reed valve lift can be obtained from the velocity function.
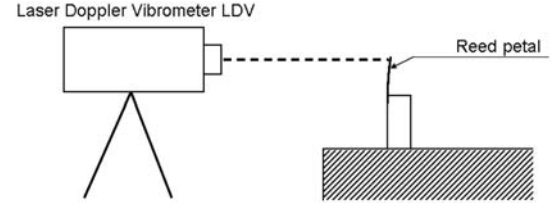

Figure 6. Laser Doppler Vibrometer - LDV

The start displacement of the reed petal at position $\xi = L$ is set to approximately 6.2 mm. The reed petal is disengaged and the free vibration of the cantilever beam can be measured.

Figure 7 shows the comparison between the measurement and simulation results in the case of a free cantilever beam vibration. A good prediction of the simulation model can be seen, which further confirms the accurateness of the reed valve model.
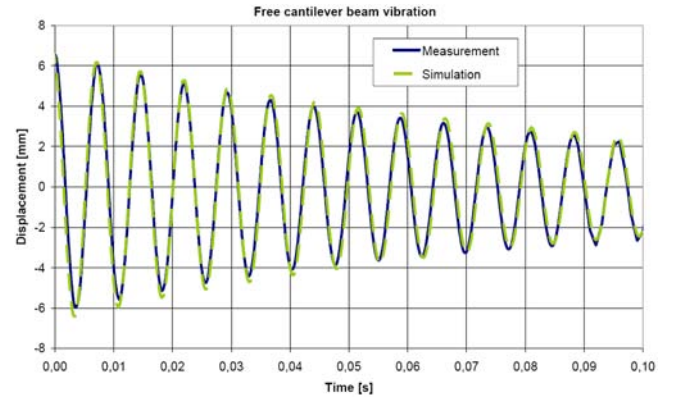

Figure 7. Free cantilever beam vibration

MOVING MESH STRATEGY

For the reed valve simulation a moving mesh is required and for this purpose the Fluent re-meshing method is used (see Ansys [12]). Fluent marks cells that violate the set "skewness" or size criteria and locally re-meshes the marked cells or faces. As soon as the new created cells or faces satisfy the skewness criterion, the mesh is locally updated with the new cells. For the efficient application of this meshing strategy the reed valve system is divided into two domains (see Figure 8). These two domains are completely

separated and their connection is realized by the use of the Fluent grid interface methodology.
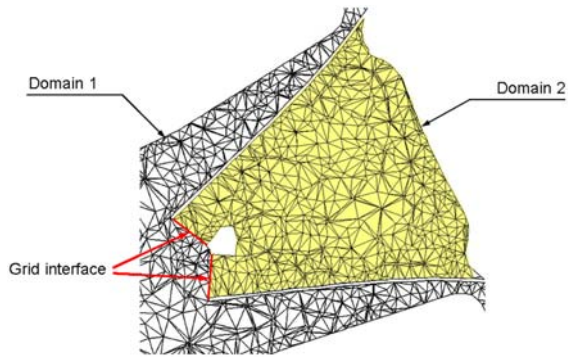
Figure 8. Reed valve mesh moving strategy

Figure 8 shows that the reed stop plate is not modeled. A modeling of this plate causes an additional problem for the re-meshing algorithm and can be time consuming. When the reed petal reaches its max position (the contact between the reed petal and the plate), the cells will be very small and the grid can cause a simulation abort. Therefore, and in order to minimize the computational effort, the reed stop plate was neglected and thus its influence on the flow situation. The contact between the reed petal and the plate was only included in the background - the reed valve model itself. The above mentioned problem also occurs in case of a closed reed petal (see Figure 9).
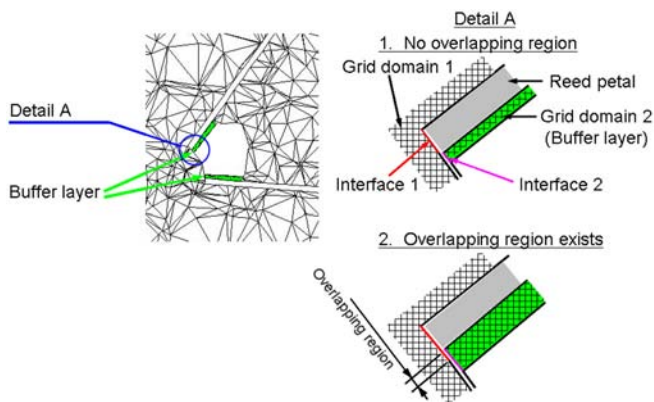

Figure 9. Strategy for reed valve closing phase

In this case, a buffer cell layer with very small cells is set between the reed petal and the reed block. A further problem when modeling the reed valve is the close/open phase of the reed valve system. E.g. Cunningham et al. [6] and [7] used an attachment boundary which provides a method of enabling or disabling the flow between two blocks with a common interface. The authors specified two coincident attachment boundary regions at the junction of the two blocks in the inlet duct. By attaching or detaching these regions, it is possible to enable or disable a flow across the interface. The 4-stroke

engine simulation of Ansys [12] provides a tool for the switch of the boundary - when the valve is closed the boundary is switched from an interface to a wall and contrariwise for the opening phase. As the opening and closing duration of the valve is constant in a 4-stroke engine simulation, it can be defined at the start of the simulation. By contrast, in a reed valve simulation of a 2-stroke engine the opening and closing phase is dependent on the pressure difference, so it cannot be defined at the start of the simulation. Therefore, Lang et al. [18] used an additional UDF code to control the flow across the interface by the switch of the boundary type depending on the valve position for a hermetic piston compressor simulation. All these additional boundary switches are not required when applying a smart simulation strategy. The face selections of the two coupled interfaces are selected in such a way that in the phase of a closed reed valve an overlapping region is omitted (see Figure 9, Detail A - No overlapping region). In the case of an open reed valve system, the overlapping region is automatically created due to its movement (see Figure 9, Detail A - Overlapping region exists). Applying this strategy, the boundary switches are obsolete.

The mesh and engine design rebuilding process is time consuming. A mesh change leads to a simulation re-run and often doubles the simulation duration. Therefore, it is very important that the simulation of all engine operating points can be carried out with only one mesh build-up. A good example is the throttle position, which depends on the engine operating point. This means that for the new position a mesh rebuild is required. In order to get a fast simulation result in the development process, the mesh rebuild is often inappropriate. Therefore, a simulation strategy was developed which allows simulations with only one mesh for all engine operating points and the throttle positions respectively.
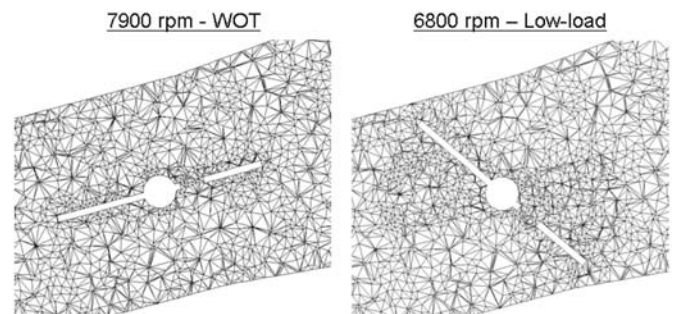
Figure 10. Throttle position dependent on engine operating points

Figure 10 shows two different throttle positions for the investigated engine operating points in this study. Using a rotational function, the throttle geometry will be moved around its axis to the right position during the simulation. This rotation function is implemented in Fluent via a user defined function and can be started on demand. The ideal

timing for the throttle moving is a closed reed valve system. Therewith, the correct throttle position in the simulation of the different engine operating points can be included without a mesh rebuild or a simulation case reset.

SIMULATION RESULTS

In order to get the gas dynamics in a shorter calculation time, the simulation was carried out without time consuming injection and combustion processes. At a selected position of the piston (before the exhaust port opens) the volume of the cylinder is initialized every cycle with the pressure, the temperature, and the accordant composition of the exhaust gases. This data can be taken from the test bench or from old simulation results. This simulation is run until a cyclic steady condition inside the engine is achieved. This is the case when the pressure trends inside the exhaust system and the crankcase volume and the sucked air mass do not differ between the last two last cycles. In addition, the pressure trends must show a good agreement with the test bench data. On the one hand, this strategy significantly accelerates the time of the calculation, as injection and combustion process simulations are missing. On the other hand, the gas dynamic behavior inside all parts of the engine achieves a steady condition within three or four revolutions. The boundary conditions and the simulation settings were specified using the data from the engine tests and from a preliminary investigation [19] and [20].

Figure 11 shows the measurement points and the faces inside the engine used for simulation validation. The indicated pressure values inside the exhaust system (P-EXH-C1, P-EXH-C2 and P-EXH-Cone), the crankcase volume (P-CC) and the intake duct (P-IN) are presented together with the comparison to simulation results. The sucked air mass of the engine (M-IN) is compared with the test bench results as well. These data are used for the gas dynamic behavior validation inside the engine and the reed petal behavior validation respectively.
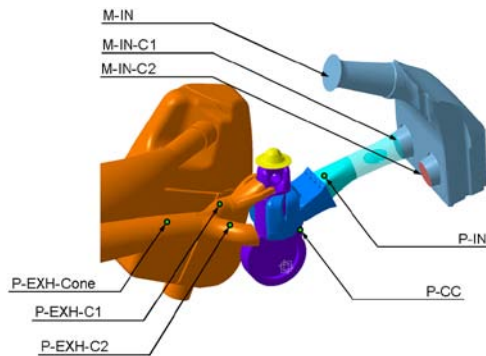

Figure 11. Measurement points inside the engine

In order to validate the reed valve model and the new symmetry and time delayed boundary condition by the simulation of different engine operating points, the calculations were conducted for two different engine speeds, 7900 rpm WOT and 6800 rpm LL. The results are evaluated with "very good" when the cyclic averaged relative deviation *RD* between the measurement and the simulation data in the measurement points ranges between 0 and 5% and with "good" between 5% and 10% respectively. The cyclic averaged relative deviation is calculated as follows:

$$RD = \frac{\sum_{i=1}^{n} \left| \left(\frac{x_{s_i}}{x_{m_i}} - 1 \right) \cdot 100 \right|}{n}$$

$$(12)$$

Where, n is the number of points inside a cycle, x_{s_i} are the simulation values and x_{m_i} are the measurement values.

7900 rpm - WOT

Figure 12, Figure 13, and Figure 14 show a comparison of the pressure trends of the test bench measurements at 7900 rpm WOT and the simulation results inside the exhaust pipe for three different measurement points, P-EXH-C1, P-EXH-C2, and P-EXH-Cone. The presented simulation results show a good prediction of the pressure trend inside the exhaust system with a relative deviation in the range between 6.1 and 9.7%, see Figure 17.

Figure 15 presents the pressure trend in the crank case volume P-CC and a comparison of the simulation, using the above described reed valve model, with the measurement data. Figure 16 shows the pressure trend upstream the reed valve system P-IN respectively. Both comparisons show a very good agreement, which further confirms the accurateness of the presented reed valve model. Furthermore, the symmetry and time delayed boundary condition, introduced by Jajcevic et al. [11], are used in order to replace the second cylinder. Figure 12, Figure 13, and Figure 14 show a good prediction of the pressure trend inside the exhaust system and Figure 16 inside the intake duct. These results also confirm the applicability of the symmetry and time delayed boundary condition for the simulation of a 2-cylinder engine.
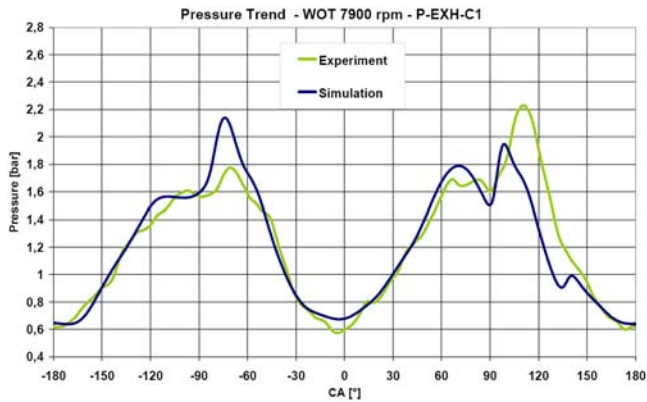
*Figure 12. Pressure trend exhaust pipe, 7900 rpm WOT, P-EXH-C1*
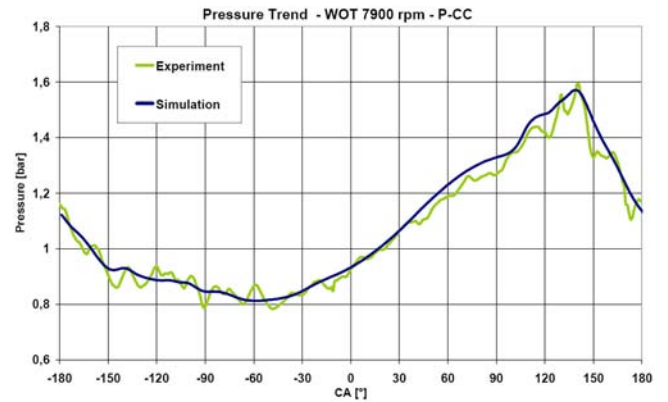
*Figure 15. Pressure trend crankcase, 7900 rpm WOT, P-CC*
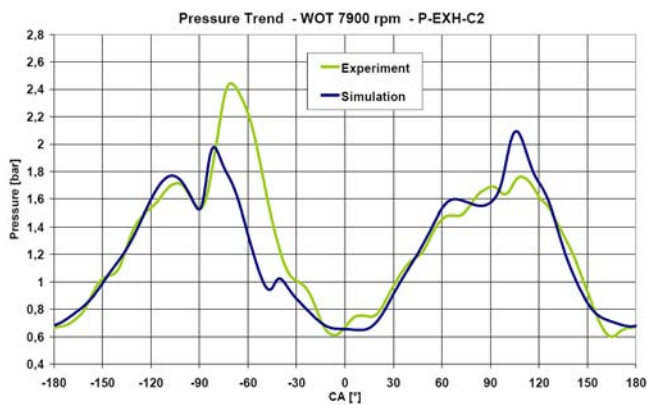
Figure 13. Pressure trend exhaust pipe, 7900 rpm WOT, P-EXH-C2
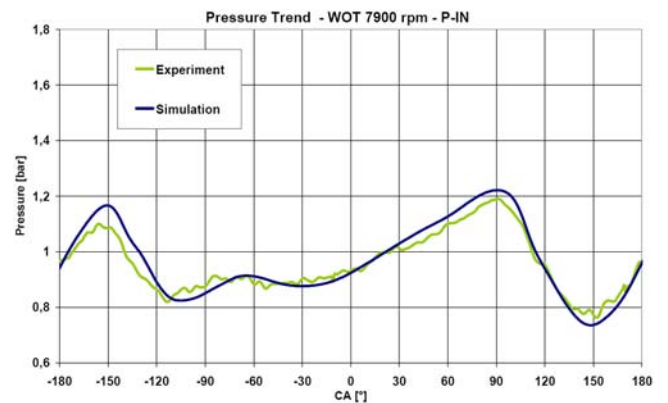

Figure 16. Pressure trend intake duct, 7900 rpm WOT, P-IN
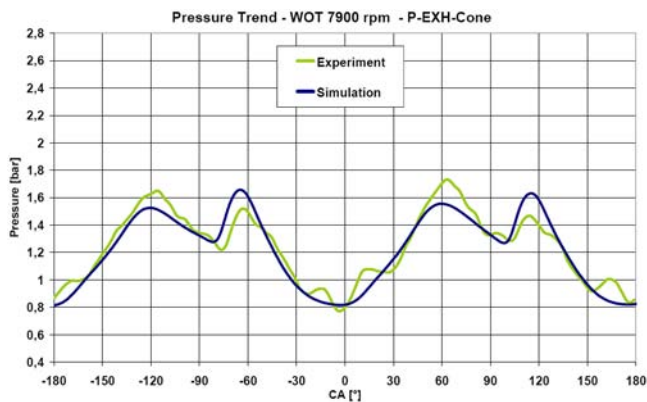
*Figure 14. Pressure trend exhaust pipe, 7900 rpm WOT P-EXH-Cone*
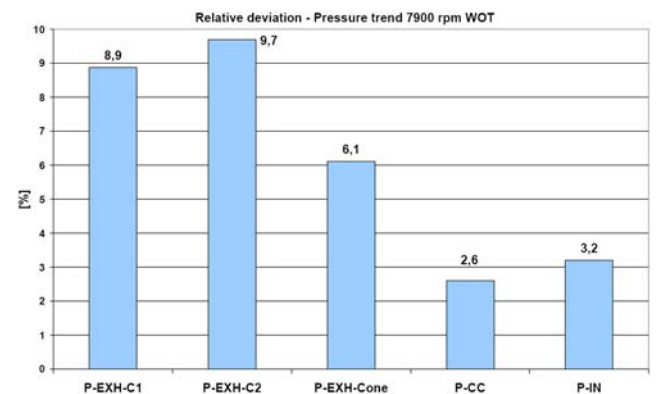
Figure 17. Pressure relative deviation, 7900 rpm WOT

Figure 18 displays the mass flow trend of the sucked fresh air for the complete engine (M-IN), for cylinder 1 (M-IN-1) and for cylinder 2 (M-IN-2). It is clearly visible that the second cylinder sucks the fresh air with a delay of 180° CA. This situation shows the application of the above mentioned boundary condition for the intake duct simulation. The sucked air mass amounted to 205 kg/h in the simulation and to 190 kg/h on the test bench (per cylinder and revolution).
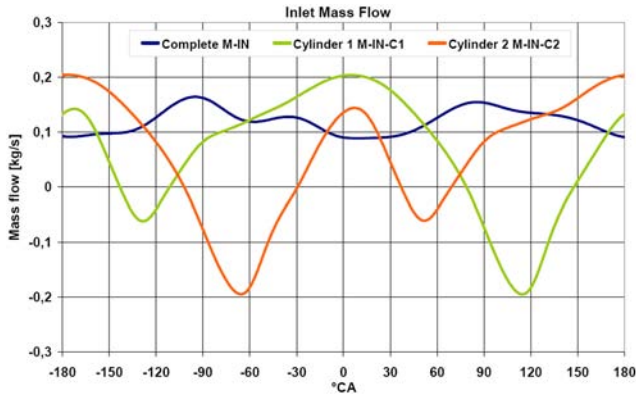
Figure 18. Simulation results of mass flow rate at 7900 rpm WOT, M-IN, M-IN-C1 and M-IN-C2
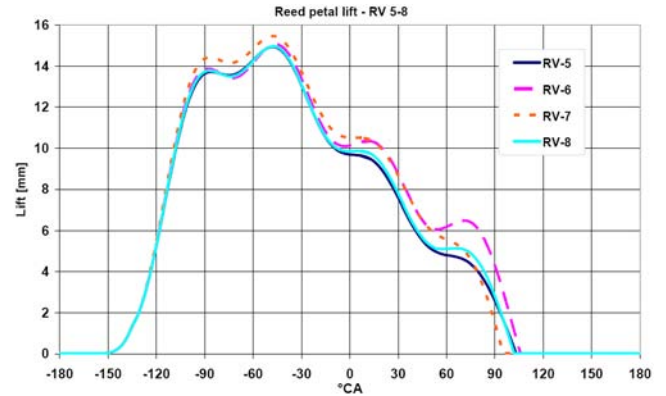
Figure 20. Reed petal lift 7900 rpm WOT, RV 5-8

Figure 19 and Figure 20 show the reed petal lift at position ξ = L, where L is the petal length. In the presented diagrams a very similar trend can be seen for the reed petals RV-2 and RV-3 (see Figure 19) and RV-6 and RV-7 (see Figure 20). These reed petals are positioned inside the reed valve system, see Figure 1. Their lift is clearly larger and thus several degrees crank angle later the closing phase of these petals occurs. In the case of the RV 5-8 (see Figure 20), all reed petals have approximately the same closing phase, but with distinctly different petal velocities.
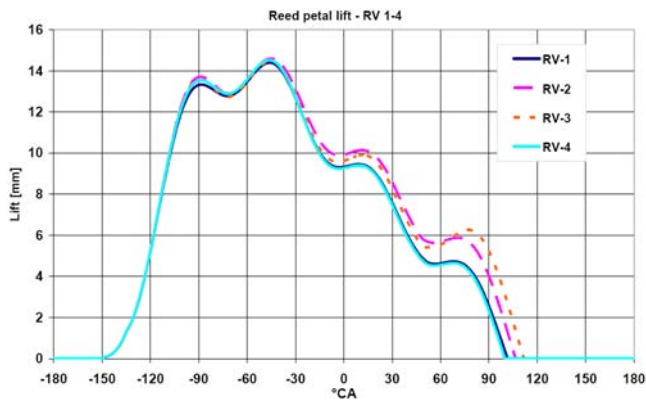
Figure 19. Reed petal lift 7900 rpm WOT, RV 1-4

6800 rpm - Low-Load (LL)

Figure 21, Figure 22, and Figure 23 give a comparison of the test bench pressure trends at 6800 rpm LL and the simulation results inside the exhaust pipe for three different measurement points, P-EXH-C1, P-EXH-C2, and P-EXH-Cone. The presented simulation results also show a very good prediction of the pressure trend for this engine operating point with a relative deviation smaller than 4.8% (see Figure 26), which further confirms the accurateness of the gas dynamic behavior simulation inside the exhaust system applying the new symmetry and time delayed boundary condition.

Figure 24 shows the pressure trend in the crank case volume P-CC at 6800 rpm LL and Figure 25 the pressure trend upstream the reed valve system P-IN respectively. Both comparisons conform very well with a relative deviation smaller than 1.8% (see Figure 26), which again confirms the accurateness of the presented reed valve model and the applicability of the symmetry and time delayed boundary condition for the gas dynamic behavior simulation inside the intake duct including the throttle geometry.
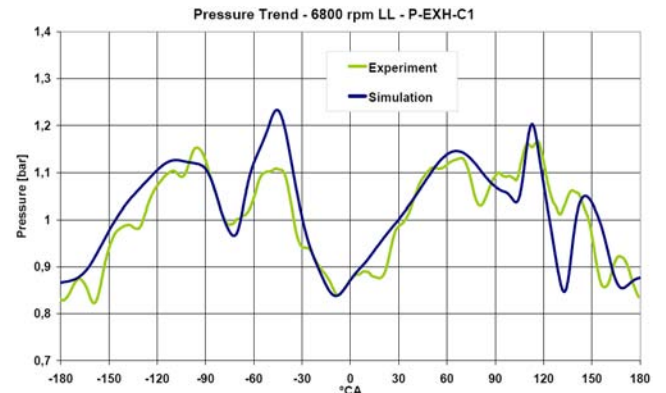
Figure 21. Pressure trend exhaust pipe, 6800 rpm LL, P-EXH-C1
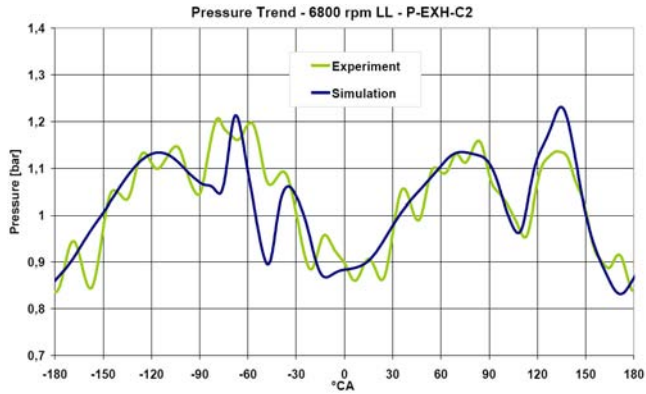
Figure 22. Pressure trend exhaust pipe, 6800 rpm LL, P-EXH-C2

Figure 23. Pressure trend exhaust pipe, 6800 rpm LL, P-EXH-Cone

Figure 24. Pressure trend crankcase, 6800 rpm LL, P-CC
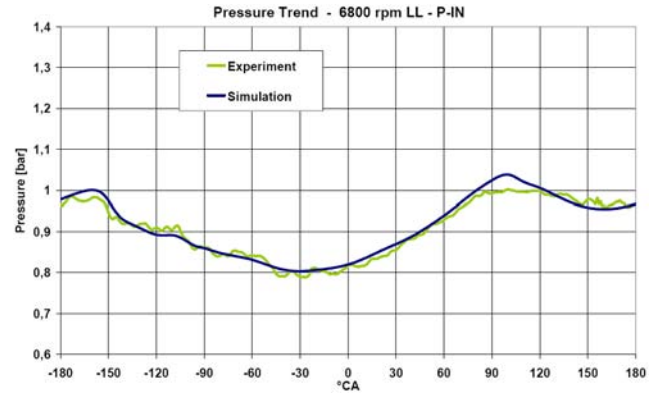
*Figure 25. Pressure trend intake duct, 6800 rpm LL, P-IN*
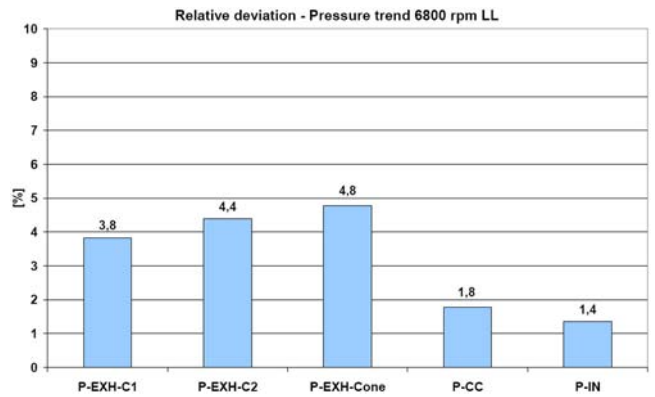
Figure 26. Pressure relative deviation, 6800 rpm LL

Figure 27 displays the mass flow trend of the sucked fresh air for the complete engine (M-IN), for cylinder 1 (M-IN-1) and cylinder 2 (M-IN-2). It is clearly visible that the 180 °CA time delayed situation can be coped with the application of the symmetry and time delayed boundary condition. The sucked air mass was 97 kg/h in the simulation and 85 kg/h on the test bench (per cylinder and revolution).
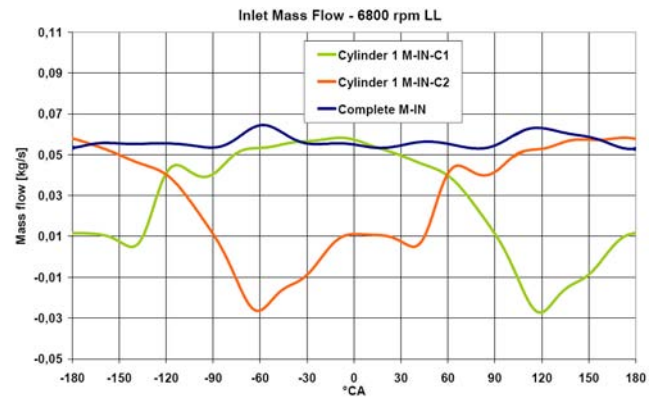
Figure 27. Simulation results of mass flow rate at 6800 rpm LL, M-IN, M-IN-C1 and M-IN-C2
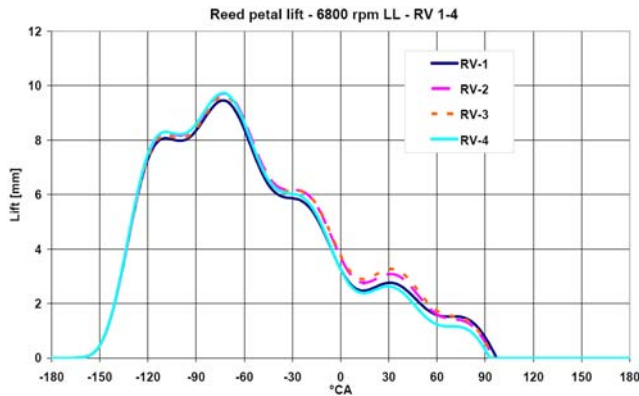
Figure 28. Reed petals lift 6800 rpm LL, RV 1-4
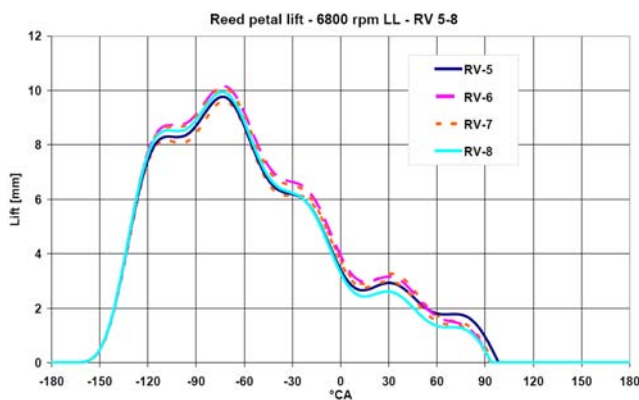
Figure 29. Reed petals lift 6800 rpm LL, RV 5-8

Figure 28 and Figure 29 present the reed petal lift at position $\xi = L$ and at 6800 rpm LL. The presented diagrams show a very similar trend and almost the same opening/closing phase for all reed petals.

Figure 30 displays the path lines of the flow through the intake duct and the reed valve system at 90 °CA before top dead center (BTDC) and for two investigated engine operating points. The path lines are colored by the velocity with the blue color representing 0 m/s and the red color 50 m/s and higher velocities. In these figures, the two different throttle positions are clearly visible together with their influence on the flow situation inside the intake duct. Furthermore, at the same piston position (90 °CA BTDC) different reed petal lifts can be seen at the two engine speeds.

CONCLUSION

This paper covers a methodology for the transient CFD simulation of the reed petals of a 2-cylinder 2-stroke engine by using Blair's 2D model and including the complete engine geometry. The reed valve geometry was completely integrated in the simulation without design modification with all eight reed petals and the engine geometry including the complete exhaust system, cylinder, crankcase, intake duct,

and air-box as well. The reed valve model is implemented in the conventional CFD code Fluent via a user defined function and is validated with the measurement data obtained by a Laser Doppler Vibrometer measurement technique.

For an efficient and stable simulation, a strategy for the moving mesh was developed and discussed in details. By the exploitation of the smart face selection in the simulation pre-processing phase, the reed petal opening and closing phase was modeled in such a way that an additional code and the boundary switch were redundant. By the application of the throttle moving strategy, neither a mesh re-build nor a case reset was needed. This means that any engine operating point simulation is effected with only one mesh build-up.

In order to reduce the calculation time, the second cylinder was replaced by the new symmetry and time delayed boundary condition introduced by Jajcevic et al. [11]. This new boundary condition allows an efficient simulation of only one cylinder without data losses and simultaneously considers the effect of the second cylinder. In this study, the calculation time was reduced by approximately 50%; compared to a simulation with both cylinders (taking into account the reduced number of 3D cells and the reduced number of the grid moving domains) The presented simulation techniques confirm the applicability of 3D simulation in the development process of a new engine, where a wide array of information is required in a short calculation time.

In order to validate the reed valve model and the new symmetry and time delayed boundary condition, the simulation of two different engine operating points were conducted (7900 rpm WOT and 6800 LL). The test bench results of the fired engine were used for the validation of the gas dynamic behavior simulation of the engine. The presented simulation results show a good correlation with the measurement data. The obtained reed petal lift results will further be used in the development process of a new engine for the analysis of the reed petals movement and their influence on the flow situation through the reed valve system taking into account different engine operating points as well as the throttle position. Especially with a fuel injection inside the crank case volume (see Winkler [21]), the flow through the reed valve system has a dominant influence on the mixture preparation and should be accurately included in the simulation.

7900 rpm – WOT – 90 °CA BTDC

6800 rpm – LL – 90 °CA BTDC

Velocity [m/s]

0   25   50
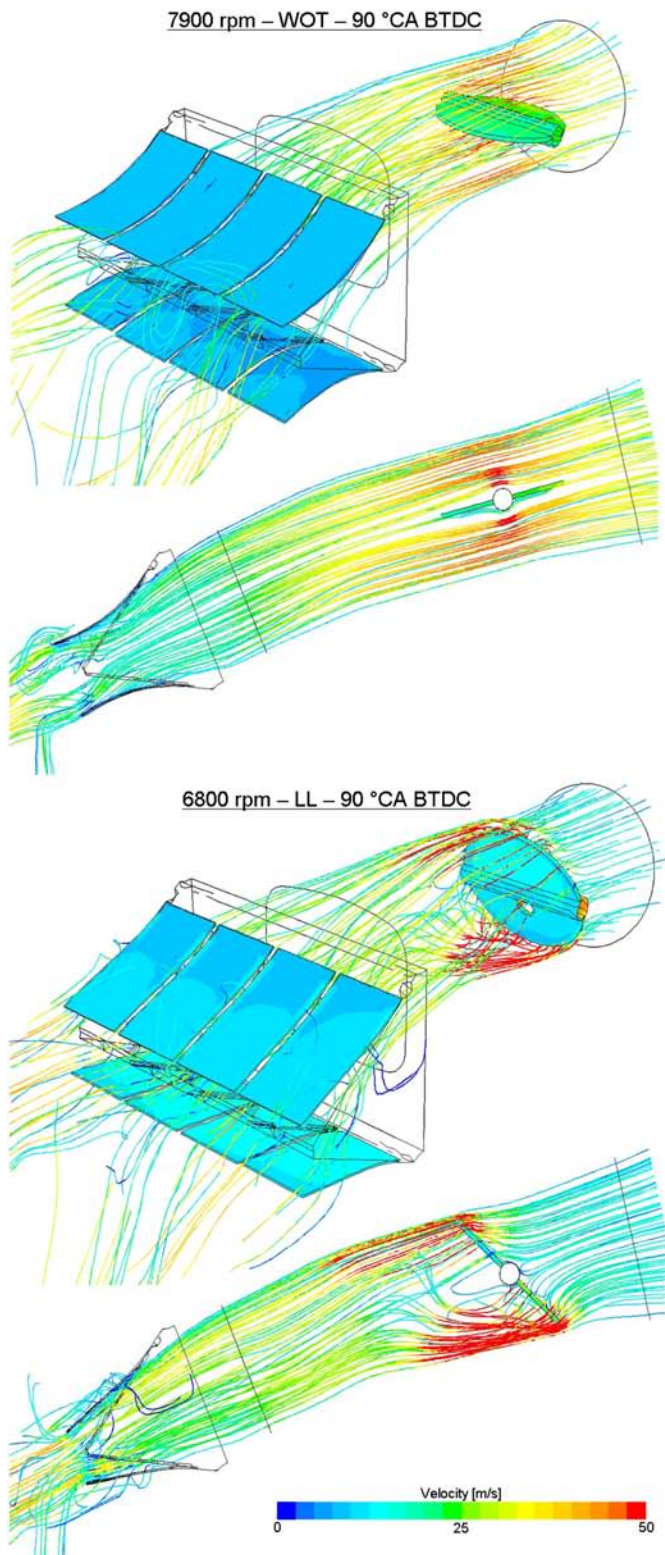
***Figure 30. Velocity field inside the intake duct at 90 °CA
before top dead center***

Further research work will focus on a comparison of the presented 3D simulation results and 0/1D calculations with the same boundary conditions - e.g. complete engine

geometry - in order to validate and investigate the presented simulation strategy. Furthermore, a comparison between 3D simulation results and the reed valve lift measurement on a fired engine including different engine operating points and loads is also recommended as a final validation level. The measurement technique was introduced by Fleck et al. [3] and [4] and it can be well applied for the validation process of the presented reed valve 3D CFD simulation strategy.

REFERENCES

1. Hinds, E.T. and Blair, G.P., "Unsteady Gas Flow Through Reed Valve Induction Systems," SAE Technical Paper 780766, 1978.

2. Blair, G.P., Hinds, E.T., and Fleck, R., "Predicting the Performance Characteristics of Two-Cycles Engines Fitted with Reed Induction Valves," SAE Technical Paper 790842, 1979.

3. Fleck, R., Blair, G.P., and Houston, R.A.R., "An Improved Model for Predicting Reed Valve Behaviour in Two-Stroke Cycles Engines," SAE Technical Paper 871654, 1987.

4. Fleck, R., Cartwright, A., and Thornhill, D., "Mathematical Modelling of Reed Valve Behaviour in High Speed Two-Stroke Engines," SAE Technical Paper 972738, 1997.

5. Mitianiec, W. and Bogusz, A., "Theoretical and Experimental Study of Gas Flow Through Reed Valve in a Two-Stroke Engine," SAE Technical Paper 961802, 1996.

6. Cunningham, G., Kee, R.J., and Boyall, J., "CFD Prediction of Crankcase Flow Regimes in a Crankcase Scavenged Two-Stroke Engine," SAE Technical Paper 970361, 1997.

7. Cunningham, G., Kee, R. J., Kenny, R. G., "Reed valve modelling in a computational fluid dynamics simulation of the two-stroke engine", Journal of Automobile Engineering, pages 37-45, ISSN 0954-4070 (Print) 2041-2991 (Online), 1999

8. Baudille, R., Biancolini, M. E., "Dynamic analysis of a two stroke engine reed valve", XXXI AIAS Congress, Parma-Italy, 2002

9. Baudille, R., Biancolini, M. E., Mottola, E., "Optimization of dynamic reed valve behaviour by material orientation", XXXIV AIAS Congres, Milano-Italy, 2005

10. Angeletti, A., Biancolini, M., Costa, E., Urbinati, M., "Optimisation of Reed Valves Dynamics by Means of Fluid Structure Interaction Modelling", 4th European Automotive Simulation Conference, Munich, 2009

11. Jajcevic, D., Almbauer, R.A., Schmidt, S.P., and Glinsner, K., "Symmetry and Time Delayed Boundary Condition for CFD Simulation and its Application in a Two-

Cylinder Two-Stroke Engine," SAE Technical Paper 2009-32-0024, 2009.

12. ANSYS Fluent: "Fluent 6.3 User's Guide"; Fluent Inc, 2005

13. ANSYS Fluent: "Gambit User's Guide"; Fluent Inc, 2005

14. Toro, E., "Riemann Solvers and Numerical Methods for Fluid Dynamics"; Springer, ISBN 3-540-61676-4, 1997

15. Zeng, Y., Strauss, S., Lucier, P., and Craft, T., "Predicting and Optimizing Two-Stroke Engine Performance Using Multidimensional CFD," SAE Technical Paper 2004-32-0039, 2004.

16. ANSYS Fluent: "UDF Manual"; Fluent Inc, 2005

17. Nagy, D., Almbauer, R.A., Lang, W., Burgstaller, A., "Valve lift measurement for the validation of a compressor simulation model", Proceedings of the International Compressor Conference at Purdue, 2008, West Lafayette, USA, Paper 1274

18. Lang, W., Almbauer, R.A., Nagy, D., 2009, "Comparison of two different approaches to model the suction valve dynamics of a hermetic reciprocating compressor", Proceedings of the 7th International Conference on Compressors and Coolants, Papiernicka, Slovak

19. Jajcevic, D., Almbauer, R.A., Schmidt, S. P., Glinser, K., "Simulation Strategy and Analysis of a Two-Cylinder Two Stroke Engine Using CFD Code Fluent", European Automotive Simulation Conference (EASC), 2009

20. Jajcevic, D., Almbauer, R.A., Schmidt, S.P., and Glinsner, K., "Simulation of Scavenging Process, Internal Mixture Preparation, and Combustion of a Gasoline Direct Injection Two-Cylinder Two-Stroke Engine," SAE Technical Paper 2009-32-0046, 2009.

21. Winkler, F., "Untersuchungen zur Reduktion von Spülverlusten bei kleinvolumigen Zweitaktmotoren", PhD thesis, Graz University of Technology, 2009

CONTACT INFORMATION

Dipl.-Ing. Dalibor Jajcevic
Christian Doppler Laboratory for "Thermodynamics of Reciprocating Engines"
Graz University of Technology
Inffeldgasse 25C
8010 Graz-Austria
Phone: +43 316 873 4586
FAX: +43 316 873 8080
jajcevic@ivt.tugraz.at
www.tugraz.at

ACKNOWLEDGMENTS

DEFINITIONS/ABBREVIATIONS

1D
  one-dimensional

3D
  three-dimensional, three dimensions

BTDC
  before top dead center

CA
  crank angle

CFD
  computational fluid dynamics

EXH
  exhaust

EC
  exhaust close

EO
  exhaust open

FSI
  Fluid-Structure Interaction

GDI
  gasoline direct injection

LDV
  Laser Doppler Vibrometer

LL
  low load

M-IN
  mass flow inlet

M-IN-C1
  mass flow inlet cylinder 1

M-IN-C2

mass flow inlet cylinder 2

P-IN

pressure trend inlet duct

P-CC

pressure trend crankcase volume

P-EXH-C1

pressure trend exhaust pipe cylinder 1

P-EXH-C2

pressure trend exhaust pipe cylinder 2

P-EXH-Cone

pressure trend exhaust pipe cone

RAVE

Rotax Adjustable Variable Exhaust

RD

relative deviation

RV 1-8

reed valve petal 1-8

rpm

revolutions per minute

UDF

user defined function

WOT

wide open throttle

SAE International

8   Summary, conclusion and outlook

Summary and conclusion

Computational Fluid Dynamics has become an essential tool in the design and development process of IC-engines. Due to increasing computer hardware performances and steady decreasing costs it is to expect that simulation technology becomes an unavoidable tool for the analysis of many technical problems. In the development process of an engine the simulation results are required in short calculation time, so that the application of the 3D simulation is still limited; primary due to a high effort in the pre-processing step and a long computational time. The goal of this work is to develop an efficient 3D CFD simulation strategy applicable in development process of a 2-stroke engine. The strategy includes an especially developed work flow as well as a new type of boundary condition, which allows a reduction of the computational domain with a negligible influence on the simulation results. Both aspects contribute to the reduction of computational time of an industrial relevant IC-engine simulation.

In chapter 2 the theoretical background of modern 2-stroke engines with GDI technology and of the CFD tool are introduced. This presents the basis for the IC-engine simulation as well as for a non-state-of-the-art application of the CFD tool in the development process. Beginning with 2-stroke engine theoretical background including the description of all processes inside the engine, the flow characterization and the governing equations of fluid flow and thermodynamics are discussed. Thereafter, the spray modeling technique is presented taking into account the requirement of a high pressure injection system for 2-stroke engines. Finally, the theoretical background of CFD tools completes chapter 2.

Chapter 3 describes the simulation strategy applied in this work which has been especially developed for a 2-cylidner 2-stroke engine simulation. In contrast to a 4-stroke engine simulation, the efficient and accurate simulation of a 2-stroke engine requires a calculation of more than one revolution in order to investigate the mixture preparation and combustion process. Therefore, a stepwise simulation strategy has been developed to accelerate the calculation process until a cyclic steady condition inside the engine is reached. Based on the experience obtained in this work the time of calculation until a cyclic steady condition is reached, can be reduced up to 50%. Furthermore, a detailed analysis of all simulation steps from the flow geometry build-up until the data evaluation has been carried out in order to exploit all possibilities for the reduction of the computational time. Several typical challenges in the development process are discussed; such as a variation of different engine geometries, investigation of intake ports opening/closing times, simulation of different engine operating points etc. Realizable solutions to prevent a return to the pre-processing step are also presented. Finally, chapter 3 is concluded with Paper I. An example of the spray design investigation of a GDI injector for a 2-cylinder 2-stroke engine including the simulation strategy is presented in this paper. Test bench results of the fired engine at four different engine operating points are used for the validation of the gas dynamic behaviour simulation. Essential advantages of the presented simulation strategy is that the gas dynamic behaviour simulation and therewith the scavenging process simulation can be carried out without the time consuming fuel injection and combustion process. Furthermore, the results show that the first fuel injection generates almost the same fuel distribution inside the engine as the following injections of the subsequent revolu-

tions, so that for the analysis of different injection strategies already the first injection can be used for a suitable evaluation.

Chapter 4 contains the discussion about the multidimensional coupling methodology. The basic idea is that a reduction of the computational domain leads to a decrease of 3D cells and therewith to a decrease of the computational time. The domain of smaller interest can be replaced by a fast calculating 0D/1D code, at which a data exchange between the domains is realized by applying the multidimensional coupling method. The basic investigation of the applied coupling method is presented in the work of Rothbauer [27]. A further improvement step in the accuracy as well as in the application of the coupling between 3D and 0D/1D domains in the real world 2-stroke engine simulation is also described. The results of a real world 2-stroke simulation applying the multidimensional coupling method are presented in Paper II. It is evident that the application of this method is strongly limited by the position of the coupling face. Explicitly, in a region with recirculation zones or zones of non-uniform flow profiles the application of this method can cause a decrease of simulation accuracy, as the 0D/1D code does not provide information about the flow profile. The data from the 0D/1D codes are generally approximated to be constant in space over the complete coupling interface. Therefore, the coupling face should be placed far from the interesting domain in order to avoid a negative influence on the 3D domain. Nevertheless, this directly increases the calculation time due to the increase of the calculation domain. The next challenge applying the multidimensional simulation is directly related to 0D/1D tools and their limitations concerning the simulation of complex geometries accompanied by strong 3D physical effects, such as recirculation, turbulence, fuel injection process, mixture preparation, and combustion. However, this limitation should be taken into consideration by the definition of the coupling position and the region which is replaced by 0D/1D codes. Due to the fact that the 3D-3D coupling methodology is already integrated in almost all CFD codes, the presented coupling method by Rothbauer [27] is not used in the development process of new engines. But it is applied for the coupling between 0D/1D and 3D domains as well as in the development of the new cyclic boundary condition presented in chapter 4. Nevertheless, the 3D-3D coupling methodology is the core of all other coupling methods and is successfully used in the development of symmetry and time delayed boundary condition.

In chapter 5 the new type of cyclic/periodic boundary condition is introduced. Its basic idea is a reduction of the calculation domain applying the symmetry condition with a minimal influence on the simulation results. The essential advantage of this method is that the data for the boundary conditions are deduced from the 3D simulation itself and therefore do not need to come from other software (such as 0D/1D calculations) or measurements. A further important advantage of the proposed method is the consistency of the fluxes of the individually conserved variables. It can be used for technical problems, where a flow pattern repeats in successive cycles, which additionally can be time delayed. The data do not need to be constant over the boundary face, which is usually the case in the standard boundary conditions of all CFD applications as well as in the 1D-3D coupling methodology. For IC-engine simulation, this means that the complete simulation of the 2-cylinder 2-stroke engine using the new boundary condition can be carried out without the geometry of the second cylinder taking into account the influence of the non-calculated domain. In Paper III the validation and the application of the boundary condition for time and non-time delayed technical problems is presented. The presented results show a good agreement in comparison with the test bench results and the conventional simulation of the 2-cylinder 2-stroke engine with both cylinders.

Chapter 6 covers the discussion of the simulation methodology for the exhaust system of a 2-cylinder 2-stroke engine until cyclic steady conditions are reached considering the heat trans-

fer over the exhaust pipe wall and the post-combustion effect inside the exhaust system. A further development stage of the symmetry and time delayed boundary condition allows for a simulation with an isolated exhaust system, where all data already obtained in the 3D CFD simulation are used. Furthermore, this strategy enables an easy re-coupling of the exhaust system back to the cylinder and the crankcase domain, so that an investigation of the new exhaust system condition on the scavenging process and the mixture preparation can be carried out. A detailed description of the used simulation strategy and an analysis of the obtained results are presented in Paper IV. The CFD-results show that the exhaust system superheating is caused by the post-combustion process inside the exhaust system. An increase of the fluid and wall temperature causes a change of the speed of sound and therewith the timing of the pressure wave as well. The results also show that these changes inside the exhaust system further lead to a reduction of the sucked fresh air mass by about 11% already in the forth revolution after the re-coupling of the exhaust system data. This will be directly reflected in the engine performance.

Chapter 7 treats an analysis of different simulation strategies including reed valve simulations. For an efficient simulation of the reed valve system the complete intake duct system simulation has to be considered, as the gas dynamic behaviour inside the intake duct has an important influence on the reed valve behaviour. So for a correct simulation the transient behaviour upstream the reed valve is needed. This can be realized by the application of either a multidimensional simulation technique or of a complete 3D reed valve simulation including complete engine geometry. Paper V covers a methodology for the transient CFD simulation of the reed petals of a 2-cylinder 2-stroke engine using Blair's 2D model and including the complete engine geometry. The reed valve geometry was completely integrated in the simulation without design modifications with all eight reed petals and the engine geometry including the exhaust system, cylinder, crankcase, intake duct, and air-box. For an efficient and stable simulation, a strategy for the moving mesh is developed and discussed in details. For the exploitation of the smart face selection in the simulation pre-processing phase the reed petal opening and closing phase was modeled in such a way that an additional code and the boundary switches were redundant. The application of a smart throttle moving strategy does not require a mesh rebuild or a case reset, so that a return to the pre-processing phase is avoided. This means that any engine operating point simulation is executed with only one mesh build-up. In order to reduce the calculation time, the second cylinder is replaced by the symmetry and time delayed boundary condition. In this study the calculation time was reduced by approximately 50% compared to a simulation with both cylinders (taking into account the reduced number of 3D cells and the reduced number of grid moving domains).

Outlook

Further applications of the new boundary condition

In this work, a newly developed symmetry and time delayed boundary condition is used for the 3D domains of a 2-cylinder 2-stroke IC-engine simulation with a symmetrical flow situation. The symmetry condition is applied in order to obtain the exact profile of all quantities, so that the data loss is reduced to a minimum. In the case of a non-symmetrical situation a dimension reduction from 3D to 1D can be applied, so that the boundary condition becomes equal to the conventional inlet/outlet with a uniform profile. The biggest potential for the reduction of the computational time offers the symmetry and time delayed boundary condition as the calculation of only one cylinder is needed and the influence of all cylinders can be taken into consideration. An investigation of more than a 2 cylinder engine with a non-

symmetrical situation applying the new cyclic/periodic boundary condition may be an interesting task and is recommended in further research works. In the case of a pure 0D/1D engine simulation all cylinders are also included. Applying the introduced boundary condition in this case, the pre-processing as well as the calculation time can be reduced, so that an investigation of the application of the new boundary condition for the pure 0D/1D simulation should also be carried out in near future research works.

LES/DES simulation of 2-stroke engine processes

For the validation of the gas dynamic behaviour the pressure trends inside the engine were used. Generally, simulation results show a good correlation with the measurement data in all four investigated engine operating points. Nevertheless, in some regions the deviation is visible, e.g. at 7900 rpm WOT short after opening phase of the exhaust port where the pressure level in the simulation is clearly lower than in the experiments. In all simulations presented in this work the RANS method was applied, which is characterised by time or ensemble averaging of flow variables. Due to a high level of turbulence in the region short after exhaust port, the RANS approach cannot capture all flow characteristics - only the essential ones can be described with this method. For more accurate results, the alternative methods such as LES or DES should be used, which directly solve the largest and energy carrying eddies. Today, the LES and the DES are increasingly popular approaches for industry relevant simulations (see Goryntsev et al. [114], Rezaei et al. [115], Moureau et al. [116], Banerjee et al. [117] etc.). Due to a high level of accuracy of LES and DES concepts for transient simulations a simulation of a 2-stroke engine scavenging process applying this technique may be an interesting task. Furthermore, in a previous investigation [112] of spray-fluid interaction the DES approach showed an improved simulation accuracy regarding droplet transport and distribution. Nevertheless, DES requires a more refined mesh than the RANS concept, but a coarser grid than the LES simulation, so that an increase of the simulation effort can be expected. This disadvantage limits the application of the DES concept in the development process of an engine which includes periphery parts. A solution for this limitation is a simulation applying the so-called "zooming" technique. The cylinder volume and a part of the intake and exhaust ports can only be considered in LES/DES simulations, whereas the rest can be replaced with boundary conditions. The LES and DES calculations are very sensitive to boundary conditions, so that more accurate boundary conditions in space and time are required. Once again, the symmetry and time delayed boundary condition could be the solution for this difficulty, which not only includes accurate data in space and time but also a consideration of all fluxes for each solved equation. In the investigation of an isolated exhaust system, presented in chapter 6, the boundary conditions are obtained from a 3D RANS simulation. The same method can also be applied for an isolated LES/DES simulation of a cylinder volume. In a first step, a RANS simulation, which includes a complete engine domain, must be carried out in order to get the required boundary data. This is concluded by the LES/DES simulation of an isolated cylinder volume, which <u>does</u> include the fuel injection as well as the combustion process simulation.

Validation of scavenging and mixture formation processes with LIF method

Petermeier [31] showed a method for the validation of scavenging and mixture formation processes applying a spectroscopic measurement method (Laser-Induced Fluorescence-LIF) in the case of a 4-stroke GDI engine. Eichlseder et al. [113] also presented some CFD validation examples of a 4-stroke engine with hydrogen (H_2) direct injection as well as a comparison of different turbulence models and the experimental data obtained with the LIF measure-

ment technique. Applying this measurement technique, a visualization of liquid and evaporated injected fuel in an operated engine is possible. LIF can also be used for the validation of the scavenging process inside a 2-stroke engine with gasoline direct injection and should be recommended in next research works.

<u>Influence of the scavenging and the mixture quality on the combustion process</u>

The main focus of the presented research work is related to the simulation of the scavenging and the mixture preparation process. Due to the high scavenging losses of a 2-stroke engine an investigation of these processes has been defined as prime goal. With the application of the presented simulation strategy, an investigation of the fuel injection as well as the scavenging losses without combustion process simulation was possible. Nevertheless, the influence of the scavenging and the mixture quality on the combustion process may be an interesting task and should also be investigated in near future research activities.

9 References

[1] Benson, R. S., Garg, R. D., Woollatt, D., "A numerical solution of unsteady flow problems", Int. J. Mech. Sci., Pergamon Pres Ltd., Vol. 6, page 117-144, 1964

[2] DeHaller, P., "Über eine graphische Methode in der Gasdynamik", Technische Rundschau Sulzer, Nr. 1, 1945

[3] Jenny, E., "Unidimensional Transient Flow with Consideration of Friction, Heat Transfer and Change of Section", Rev. Brown Boveri, Vol. 37, 1951

[4] Steifert, H., "Instationäre Strömungsvorgänge in Rohrleitungen an Verbrennungskraftmaschinen", Springer Verlag, 1962

[5] Blair, P. G. and Goulburn J. R., "An unsteady flow analysis of exhaust systems for multicylinder automobile engines", SAE Paper 700123, 1970

[6] Pope, S. B., "Turbulent Flows", Cambridge University Press, ISBN 0 521 59125 2, 2000

[7] Steiner, H., "Modeling and Numerical Simulation of complex technical flows", Habilitation Thesis, Graz University of Technology, 2006

[8] Basara, B., "Turbulence Modeling for Industrial CFD", Habilitation Thesis, Graz University of Technology, 2006

[9] Goryntsev D., Klein M., Sadiki A., Janicka J., "Grobstruktursimulation für einen DI-Ottomotor, Charakterisierung des Strömungs- und Mischungsfeldes", MTZ Fachzeitschrift 03/2009, 2009

[10] Rebhan M., Stokes J., Eatwell J., "Kombinierter Zweitakt- und Viertakt-Ottomotor für Downsizinganwendungen", 12. Tagung der Arbeitsprozess des Verbrennungsmotors, 2009

[11] Jajcevic D., "CFD simulation eines Hochleistungsmotors mit Benzindirekteinspritzung", Diploma thesis, Graz University of Technology, 2007

[12] Korman M., "Concepts and operational strategies for exhaust emission after treatment systems with impact on modern small capacity SI engines", Doctoral thesis, Graz University of Technology, 2007

[13] Trattner A., „Experimentelle Untersuchungen und thermodynamische Analyse eines Brennverfahrenskonzepts für 4-Takt Hochleistungsmotoren mit Direkteinspritzung", Diploma thesis, Graz University of Technology, 2009

[14]   Merker G., Schwarz C., Stiesch G., Otto F., "Verbrennungsmotoren, Simulation der Verbrennung und Schadstoffbildung", B. G. Teubner Verlag, ISBN-10 3-8351-0080-7, 2006

[15]   Pischinger R, Klell M., Sams T., "Thermodynamik der Verbrennungskraftmaschine", Springer-Verlag Wien, ISBN 3-211-83679-9, 2002

[16]   Raghunathan B. D. and Kenny R. G., "CFD Simulation and Validation of the Flow within a Motored Two-Stroke Engine", SAE Paper 970359, 1997

[17]   Cunningham G., Kee R. J., Boyall J., "CFD Prediction of Crankcase Flow Regimes in a Crankcase Scavenged Two-Stroke Engine", SAE Paper 970361, 1997

[18]   Corcione F. E., Rotondi R., Gentili R., Migliaccio M., "Modeling the Mixture Formation in a Small Direct-Injected Two-Stroke Spark-Ignition Engine", SAE Paper 970364, 1997

[19]   Meister G., "Strömungs- und Einspritzungsimulation in einem umkehrgespülten 125cc Zweitaktmotor", Diploma thesis, Graz University of Technology, 1999

[20]   Kirchberger R., "Abgasoptimierung durch Einsatz von luftunterstützter Direkteinspritzung beim Zweitakt-Kleinmotor", Doctoral thesis, Graz University of Technology, 2003

[21]   Schmidt S., "Auslegung, thermodynamische Analyse und Entwicklung von Zweitakt Brennverfahren mit Hochdruckdirekteinspritzung", Doctoral thesis, Graz University of Technology, 2005

[22]   Chiavola O., "Integrated modeling of internal combustion engine intake and exhaust systems", Proc Instn Mech Engrs IMechE, Vol. 215, Part A, Page 495-506, 2001

[23]   Chiatti G. and Chiavola O., "Scavenge Strems Analysis in High Speed 2T Gasoline Engine", SAE Paper 2002-01-2180, 2002

[24]   Riegler U. G. and Bargende M., "Direct Coupled 1D/3D-CFD-Computation (GT-Power/Star-CD) of the Flow in the Switch-Over Intake System of an 8-Cylinder SI Engine with External Exhaust Gas Recirculation", SAE Paper 2002-01-0901, 2002

[25]   Bozza F., Gimelli A., Andreassi L., Rocco V., Scarcelli R., "1D-3D Analysis of the Scavenging and Combustion Process in a Gasoline and Natural-Gas Fuelled Two-Stroke Engine", SAE Paper 2008-01-1087, 2008

[26]   Zeng Y., Strauss S., Lucier P, Craft T., "Prediction and Optimizing Two-Stroke Performance Using Multidimensional CFD", SAE Paper 2004-32-0039, 2004

[27]   Rothbauer R., "Methode zur Kopplung von bewegten 3D sowie 0/1D CFD Berechnungsgebieten", Doctoral thesis, Graz University of Technology, 2007

[28]   Blair, P. Gordon, "Design and Simulation of Two-Stroke Engines", Society of Automotive Engineers, ISBN 1-56091-685-0, 1996

[29]   DIN 1940 Hubkolbenmotoren, "Begriffe, Formlezeichen, Einheiten", Beuth Berlin, 1976

[30]   Kolmogorov, A. N., "The local structure of turbulence in incompressible flow for very large Reynolds number", Compt. Rend. ACD. SCI. URRS, 1941

[31]   Petermeier L., "Simulation der Gemischbildung wandgeführter Otto-DE Brennverfahren under besonderer Berücksichtung der Strahl-Wandinteraktion", Doctoral thesis, Graz University of Technology, 2001

[32]   Kundu K. P. and Cohen M. I., "Fluid Mechanics, Second Edition", Academic press, Elsevier Science (USA), Book Number: 0-12-1782514, 2002

[33]   Versteeg H. K. and Malalasekera W., "An introduction to computational fluid dynamics, The finite volume method", Prentice Hall, ISBN 0-582-21884-5, 1995

[34]   Navier, M., "Mémoires sur les lois du movements de fluids", Mem. De l' Acad. De Sci. 6, page 389-416, 1827

[35]   Stokes, G. G., "On the theories of internal friction of fluids in motion", Trans. Cambr. Phil. Soc. 8, page 287-305, 1845

[36]   Richard van Basshuysen, "Gasoline Engine with Direct Injection", Vieweg + Teubner, ISBN 978-3-8348-0670-3, 2009

[37]   Richard van Basshuysen and Fred Schäfer, "Handbuch Verbrennungsmotor", Vieweg ATZ/MTZ Fachbuch, ISBN 3-528-23933-6, 2005

[38]   Eichlseder H., Klüting M., Piock F. W., "Grundlagen und Technologien des Ottomotors", Springer-Verlag/Wien, ISBN 978-3-211-25774-6, 2008

[39]   Groth K., "Das Betriebsverhalten desschnellaufenden Zweitakt-Ottomotors mitEinspritzung und seine Entwicklungsmöglichkeiten", VDI-Verlag Düsseldorf, 1959

[40]   Plohberger, D., Miculic, L. A., "Der Zweitaktmotor mit innerer Gemischbildung", Vortrag bei 9. Internationalen Wiener Motorensymposium, F. B. VDI Reihe 12 Nr. 99. Düsseldorf: VDI-Verlag, 1988

[41]   Plohberger, D., Miculic, L. A., "Der Zweitaktmotor als PKW-Antriebskonzept- Anforderungen und Lösungsansätze", Vortrag beim 10. Internationalen Wiener Motorensymposium, F. B. VDI Reihe 12, Nr. 122. Düsseldorf: VDI-Verlag, 1989

[42]   Mitsubishi, "Mitsubishi Benzinmotor mit Direkteinspritzung", Technisches Dossier, 1995

[43]   Kaiser T. and Hoffmann A., "Einfluss der Zündkerzen auf das Entflammungsverhalten in modernen Motoren", MTZ 61, Nr. 10, page 656-663, 2000

[44]   Pecnik R., "Transitionsmodellierung in thermischen Turbomaschinen", Doctoral thesis, Graz University of Technology, 2007

[45]   Blazek, J., "Computational Fluid Dynamics: Principles and Applications", ELSEVIER SCIENCE, ISBN 0 08 0430090, 2001

[46]   Jiyuan T., Heng G. Y., Chaoqun L., "Computational Fluid Dynamics: A practical Approach", Butterworth-Heinemann, ISBN-10: 0750685638, 2008

[47]   Reynolds, O., "On the Dynamical Theory of Incompressible Viscous Fluids and the Determination of the Criterion", Philosophical Transactions of the Royal Society of London, Series A-186, page 123-164, 1895

[48]   Favre A., "Equations des gaz turbulents compressibles, part 1: formes generales", Journal de Mecanique, page 361-390, 1965

[49]   Favre A., "Equations des gaz turbulents compressibles, part 2: methode des vitesses moyennes; methode des vitesses moyennes ponderees par la masse volumique", Journal de Mecanique, page 391-421, 1965

[50]   Boussinesq J., "Théorie des ondes liquides périodiques", Mémoires présentés par divers savants à l'Académie des Sciences, Paris, 1872

[51]   Boussinesq J., "Essai sur la théorie des eaux courantes", Mémoires présentés par divers savants à l'Académie des Sciences, Paris, 1877

[52]   Fluent ANSYS, "Fluent 6.3 Users Guide", Fluent Inc., USA, 2005

[53]   Wilcox D. C., "Turbulence modeling for CFD", DCW Industries California, ISBN 1-928729-10-X, 2002

[54]   Craft T. J., Launder B. E., Suga K., "A non-linear eddy viscosity model including sensitivity to stress anisotropy", Proc. 10th Symp. on Turbulent Shear Flows, page 23.19-23.24, 1995

[55]   Basara B., "A nonlinear eddy-viscosity model based on an elliptic relaxation approach", IOP Publishing, Fluid Dynamics Reasearch, 2009

[56]   Launder B. E. and Spalding D. B., "Lectures in Mathematical Models of Turbulence" ,Academic Press, London, 1972

[57]   Henkes R. A. W. M., F. F. van der Flugt, and Hoogendoorn C. J., "Natural Convection Flow in a Square Cavity Calculated with Low-Reynolds-Number Turbulence Models" Int. J. Heat Mass Transfer, 34:1543-1557, 1991

165

[58]   Sarkar S. and Balakrishnan L., "Application of a Reynolds-Stress Turbulence Model to the Compressible Shear Layer", ICASE Report 90-18, NASA CR 182002, 1990

[59]   Dukowicz K. J., "A Particle-Fluid Numerical Model for Liquid Sprays", Journal of Computational Physics 35, page 229-253, 1980

[60]   Schiller L. and Naumann A. Z., "A drag coefficient correlation", VDI Zeitung 77, page 318-320, 1933

[61]   Liu A. B., Mather D., and Reitz R. D., "Modeling the Effects of Drop Drag and Breakup on Fuel Sprays", SAE Paper 930072, 1993

[62]   Ranz W. E. and Marshall W. R., "Jr. Evaporation from drops. Parts I & II", Chem. Eng. Progr., pages 141-6 and 173-80, 1952

[63]   Kuo K. K. Y., "Principles of Combustion", John Wiley and Sons, New York, 1986

[64]   Stanciu A. S., „Gekoppelter Einsatz von Verfahren zur Berechnung von Einspritzhydraulik, Gemischbildung und Verbrennung von Ottomotoren mit Kraftstoff-Direkteinspritzung", Doctoral thesis, Berlin University of Technology, 2005

[65]   Chu C. C., "One-Dimensional Transient Fluid Model for Fuel-Coolant Interaction Analysis", PhD Thesis, University of Wisconsin-Madison, 1986

[66]   Reitz R. D. and Diwakar J., "Effect of Drop Break-up on Fuel Sprays", SAE Paper 860469, 1986

[67]   Reitz R. D., "Mechanisms of Atomization Processes in High-Pressure Vaporizing Sprays", Atomization and Spray Technology, 3:309-337, 1987

[68]   Liu A. B. and Reitz R. D., "Modeling the Effects of Drop Drag and Break-up on Fuel-Sprays", SAE Paper 930072, 1993

[69]   O'Rourke P. J. and Amsden A. A., "The Tab Method for Numerical Calculation of Spray Droplet Break-up", SAE Paper 872089, 1987

[70]   Baritaud T., "Modeling Atomization and Break-up in High-Pressure Diesel Sprays", SAE Paper 970881, 1997

[71]   Huh K. Y. and Gosman A. D., "A Phenomenological Model of Diesel Spray Atomization", Proceedings of the International Conference on Multiphase Flows Japan, 1991

[72]   Patterson M. A. and Reitz R. D., "Modeling the Effects of Fuel Spray Characteristics on Diesel Engine Combustion and Emission", SAE Paper 980131, 1998

[73]   AVL Fire, "Spray Manual", AVL List GmbH Graz, Austria, 2004

[74]   Stanton D. W. and Rutland C. J., "Modeling Fuel Film Formation and Wall Interaction in Diesel Engines", SAE Paper 960628, 1996

[75]   O'Rourke P. J. and Amsden A. A., "A Spray-Wall Interaction Submodel for the KIVA-3 Wall Film Model", SAE Paper 2000-01-0271, 2000

[76]   O'Rourke P. J. and Amsden A. A., "A Particle Numerical Model for Wall Film Dynamics in Port-Fuel Injected Engines", SAE Paper 961961, 1996

[77]   Toro F. E., "Riemann Solvers and Numerical Methods for Fluid Dynamics", Springer-Verlag Berlin Heidelberg New York, ISBN 3-540-61676-4, 1997

[78]   Patankar V. S., "Numerical heat transfer and fluid flow", Series in comp. methods in mech. and therm. sciences, ISBN 0-07-048740-5, 1980

[79]   Anderson A. D., Tannehill C. J. and Pletcher H. R., "Computational Fluid Mechanics and Heat Transfer", Series in comp. methods in mech. and therm. sciences, ISBN 0-07-050328-1, 1984

[80]   McDonald P. W., "The Computation of Transonic Flow through Two-Dimensional Gas Turbine Cascades", ASME Paper, 71-GT-89, 1971

[81]   Trescher D., "Development of an Efficient 3–D CFD Software to Simulate and Visualize the Scavenging of a Two-Stroke Engine", Arch. Comput. Methods Eng., Springer Verlag, page 67-111, 2007

[82]   Van Leer B., "Flux Vector Splitting for the Euler Equations", 8th Int. Conf. on Numerical Methods in Fluid Dynamics, Springer Verlag, page 507-512, 1982

[83]   Liou M. S. and Steffen C. J., "A New Flux Splitting Scheme", Journal of Computational Physics, Vol. 107, page 23-39, 1993

[84]   Jameson A., "Positive Schemes and Shock Modelling for Compressible Flow", International Journal for Numerical Methods in Fluids, Vol. 20, page 743-776, 1995

[85]   Godunov S. K., "A Finite Difference Method for the Computation of Discontinuos Solutions of the Equation of Fluid Dynamics", Math. Sb. Vol. 47, page 357-393, 1959

[86]   Roe P. L., "Approximate Riemann solver, parameter vectors, and differences schemes", Journal Comput. Phys., Vol. 43, page 357-372, 1981

[87]   Sanz W., "Computational Fluid Dynamics", Lecture script 319.082, Institute for Thermal Turbomachinery and Machine Dynamics, Graz University of Technology, Austria, 2007

[88]   Harten A., "High Resolution Scheme for Hyperbolic Conservation Laws", Journal of Computational Physics, Vol. 49, page 357-393, 1983

[89]   Harten A., Engquist B., Osher S., Chakravarthy S., "Uniformly High Order Accurate Essentially Non-Oscillatory Schemes III", Journal of Computational Physics, Vol. 71, page 231-303, 1986

[90]   Roe P. L., "Discrete Models for the Numerical Analysis of Time-Dependent Multidimensional Gas Dynamics", Journal of Computational Physics, Vol. 63, page 458-476, 1986

[91]   Barth T. J. and Jespersen D. C., "The design and Application of Upwind Schemes on Unstructured Meshes", American Institute of Aeronautics and Astronautics, Paper 89-0366, 1989

[92]   Hirsch C., "Numerical Computation of Internal and External Flows: The Fundamentals of Computational Fluid Dynamics", Butterworth-Heinemann, ISBN-10: 0750665947, ISBN-13: 9780750665940, 2007

[93]   Tucker P., "Computation of unsteady flows", Kluwer Academic Publisher Group, ISBN 0-7923-7371-5, USA, 2001

[94]   Curtiss C. F. and Hirschfelder J. O., "Integration of Stiff Equations", Proc. Natl. Acad. Sci. U S A., Vol. 38(3), page 235–243, 1952

[95]   Fluent ANSYS, "UDF Manual", Fluent Inc, 2005

[96]   Kiva, "A KIVA-3 Program with Block-Structured Mesh for Complex Geometries", Los Alamos, 1993

[97]   AVL Fire, "CFD Solver V8.5", AVL LIST GmbH, Austria, 2006

[98]   Star-CD, "USER GUIDE STAR-CD VERSION 4.0", CD-adapco Group, 2006

[99]   Converge, "A Three-Dimensional Computational Fluid Dynamics Program for Transient or Steady State Flows with Complex Geometries", Convergent Science Inc., Middleton, USA, 2008

[100] OpenFOAM, "The Open Source CFD Toolbox, User Guide", Open source, Version 1.7.0, June, 2010

[101] Press H. W., Teukolsky A. S., Vetterling T. W. and Flannery P. B., " Numerical recipes, The art of Scientific Computing", Cambridge University Press, third edition, ISBN 978-0-521-88068-8, 2007

[102] Harten A. and Hyman J. M., "Self Adjusting Grid Methods for One-Dimensional Hyperbolic Conservation Laws", Journal of Computational Physics, Vol. 50, page 253-269, 1983

[103] Gambit ANSYS: "Gambit User's Guide"; Fluent Inc, 2005

[104] AVL Fire-Boost, "AVL Fire 1D coupling", AVL LIST GmbH, Austria, 2004

[105] Li C., "Coupled simulation between GT-Power and Fluent", Mater's Thesis, Lulea University of Technology, Sweden, 2002

[106] Rothbauer R. J., Grasberger G., Abidin Z., Almbauer A. R., "Reed Valve, Crankcase and Exhaust Models Coupled to 3D Fluid Domains fort he Predictive CFD Simulation", SAE Paper 2007-32-0030, 2007

[107] Rothbauer R. J., Almbauer R. A., Schmidt S. P., Glinsner K., "Effect of Energy Conversion, Turbulence and Fluid Dynamics on the Transient Heat Transfer and thus on the Scavenging of the Two Stroke Engine", Turbulence, Heat and Mass Transfer 5, Dubrovnik, 2006

[108] Schmidt S., Schoegl O., Rothbauer R. J., Eichlseder H., Kirchberger R., "An Integrated 3D CFD Simulation Methodology for the Optimization of the Mixture Preparation of 2-Stroke DI Engines", SAE Paper 2007-32-0029, 2007

[109] Costagiola M., "The theory of spring-loaded valves for reciprocating compressors", Journal of Applied Mechanics, page 415–420, 1950

[110] Hinds E. T. and Blair G. P., "Unsteady gas flow through reed valve induction systems", SAE Paper 780766, 1978

[111] Baudille R. and Biancolini M. E., "Dynamic analysis of a two stroke engine reed valve", XXXI AIAS Congress, Parma-Italy, 2002

[112] Abart M., Schmidt S., Schoegl O., Trattner A., Kirchberger R., Eichlseder H., Jajcevic D., "Basic Investigations on the Prediction of Spray-Wall and Spray-Fluid Interaction for a GDI Combustion Process", SAE Paper 2010-32-0030/20109030, 2010

[113] Eichlseder H., Heindl R., Kirchweger W., Messner D., "Comprehensive Development of Gaseous Fuelled IC Engines with Internal Mixture Formation", 11th European Automotive Congress, EAEC 2007

[114] Goryntsev D., Klein M., Sadiki A., Janicka J., "Grobstruktursimulation für einen DI-Ottomotor – Charakterisierung des Strömungs- und Mischungsfeldes", MTZ 03/2009, Jahrgang 70, 2009

[115] Rezaei R., Pischinger S., Ewald J., Adomeit P., "A New CFD Approach for Assessment of Swirl Flow Pattern in HSDI Diesel Engines", SAE Paper 2010-32-0037/20109037, 2010

[116] Moureau V., Barton I., Angelberger C., Poinsot T., "Towards Large Eddy Simulation in Internal-Combustion Engines: simulation of a compressed tumble flow", SAE Paper 2004-01-1995, 2004

[117]   Banerjee S., Liang T., Rutland C., Hu B., "Validation of an LES Multi Mode Combustion Model for Diesel Combustion", SAE Paper 2010-01-0361, 2010